

https://dspace.org/

The geological setting of uranium mineralisation in the Rössing Area, Namibia

Gray, Timothy M.

2015

https://hdl.handle.net/10539/32822

Gray, Timothy Mark (2015) The geological setting of uranium mineralisation in the Rossing area, Namibia, University of the Witwatersrand, Johannesburg, <http://hdl.handle.net/10539/32822>

Downloaded from a DSpace repository. https://dspace.org/

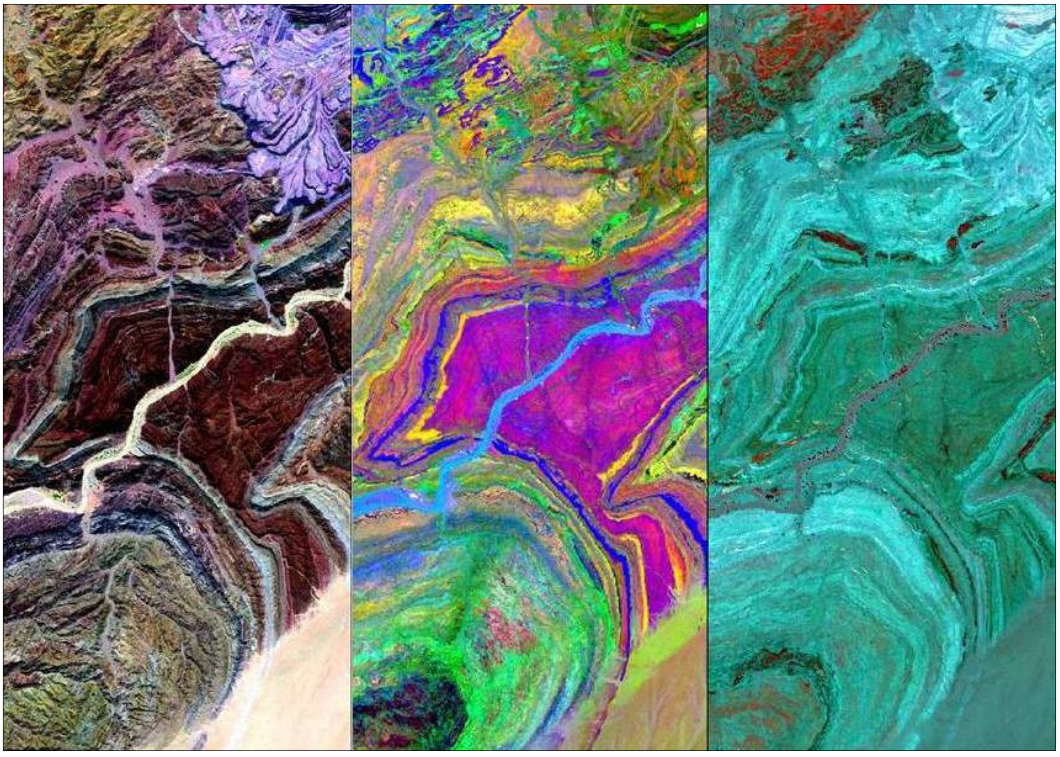
School of Geosciences, University of the Witwatersrand,
Ph.D. Thesis

The Geological Setting of Uranium Mineralisation in the Rössing Area, Namibia

Thesis submitted in association with geological mapping and data synthesis completed as part of the author's professional work with Rössing Uranium Ltd., for the fulfilment of requirements for the degree of Doctor of Philosophy, School of Geosciences, University of the Witwatersrand, Johannesburg.

Timothy M. Gray
August 2015

Student ID 511750



Cover figure: three processed images of HyMap airborne hyperspectral line mosaics over an identical area of the Lower Khan River and the southwest extremity of the Rössing Uranium Mine. Courtesy of Rössing Uranium Ltd., processing by A. Caballero.

Declaration

I declare that this thesis is my own, unaided work. It is being submitted for the fulfilment of requirements for the degree of Doctor of Philosophy at the University of the Witwatersrand, Johannesburg. It has not been previously submitted in association with any degree or examination to any other university. The map attached to this thesis in part represents a synthesis of work completed by others and this work is referenced wherever possible.

Signature of candidate:



_1st__ day of _____August_____ 2015

Acknowledgements

Thanks in particular are due to Professor Judith Kinnaird for both inviting me to submit this work as a postgraduate degree and for providing feedback throughout the writing of this text, for which I am also indebted to Paul Nex. Thanks are due to Graham Crook for providing the prerequisite Rössing Uranium Ltd. support to progress this project, and the current management of Rio Tinto Exploration and Rössing Uranium Ltd. for approving the final map and thesis.

At the outset of this project Justin Laberge (Rio Tinto Exploration) provided an invaluable introduction to the local area, whilst Justin's own mapping compilation of the SJ-SK area is embedded in the attached map. For their technical input throughout the mapping stage I would like to thank Luisa d'Andrea (Rio Tinto Exploration) for her support and discussion on remote sensing, Alasdaire Pope (Kennecott Exploration Company) for discussion on aspects of structural geology, John Hart (Rio Tinto Exploration) for support in airborne geophysical data processing, Branko Corner (consulting geophysicist) for additional discussion on geophysical data processing and interpretation, and the Rössing Uranium Ltd. geology team for their daily assistance and advice. The MapRoom in Windhoek provided an excellent service in digitising all hard copy maps and interpretations, whilst the Geological Survey of Namibia prepared all thin sections and polished blocks. All those who have previously worked in the Rössing area, particularly covering aspects of mapping and petrology, are gratefully acknowledged – their diligent work has been integral to much of this project.

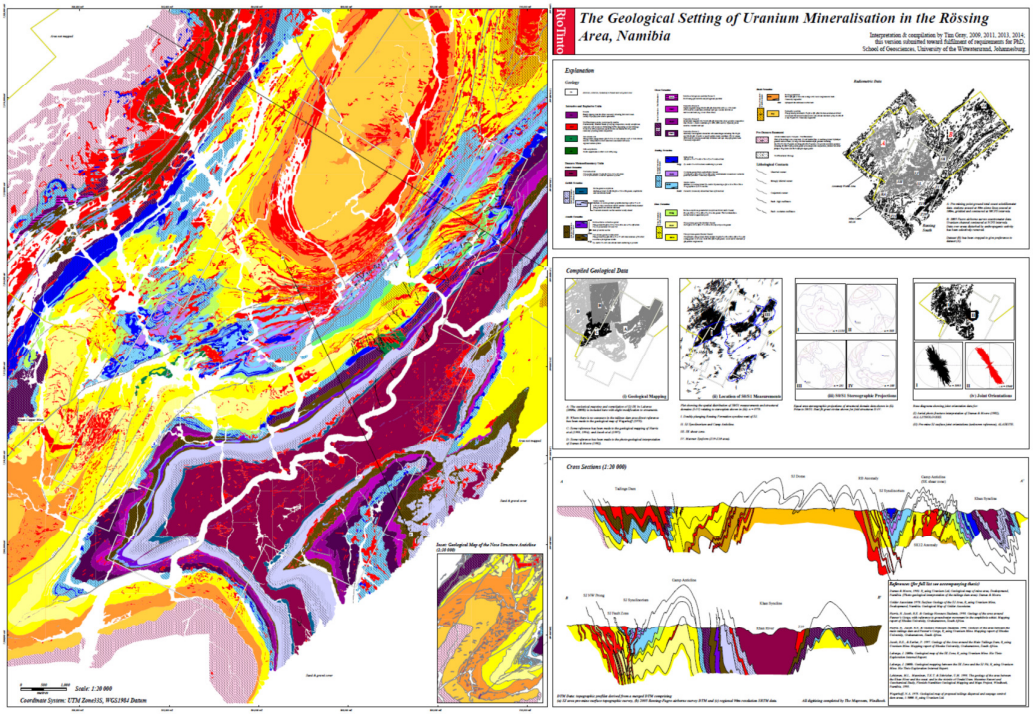
This work is dedicated to Thyon and Jasmine Gray who allowed me the time to complete this thesis during our years in China.

Abstract

The geology of the Rössing uranium mine area has been mapped and described through compilation and interpretation of all available data, underpinned by field traversing and sampling. The understanding of the stratigraphic and structural setting of granite-hosted uranium mineralisation in the wider Rössing area has in particular been refined. HyMap hyperspectral imagery significantly contributed to resolving the mapped geology in detail. Descriptions of the stratigraphic sequence have been compiled and augmented particularly within the upper parts of the Damaran stratigraphy. A three member diamictite-iron formation stratigraphy is constrained within the Chuos Formation whilst eight members are identified through the Arandis to Karibib Formation sequence. The detailed resolution of the stratigraphy has also resolved many aspects of the structural geology in the area. Pre-D_3 extension is expressed as a sheared basement-cover interface, major boudinage of stratigraphic units, and exploitation of such dilational zones by early alaskite intrusions. Within the F_2-F_4 fold phases identified across the area, major dome and basin and hook geometries result from F_2-F_3 fold interference. D_3 to D_4 deformation was progressive where the latter consisted of the development of early, minor north-northeast trending folds and left lateral faulting. Map relationships suggest this was followed by the formation of north-northeast oriented transtensional shear zones highly oblique to pre-D_4 litho-structural orientations and into which uranium-bearing granitic melts were focused. Alaskite generation is attributed to migmatisation and partial melting of potassic meta-psammites during lower granulite facies metamorphism. The sequence of alaskite intrusions is correlated with the scheme applied to the nearby Goanikontes uranium deposit with varying confidence. At Rössing SJ the intrusion of voluminous uranium-bearing alaskite melt material was especially facilitated by superimposition of a north-northeast trending shear zone upon both a major F_2-F_3 fold interference structure and a pre-existing D_4 fault zone. Uraniferous alaskites at the SH and SK ore bodies intrude peripheral F_3 fold structures superimposed on the F_2 folds. In the Z20-Z19-Z17 to Rössing South Zone 1 area, mineralised alaskites occur within the Rössing, Arandis and Karibib Formations, where doming of the Rössing South anticline is also demonstrated to be due to F_2-F_3 fold interference.

Executive Summary

This thesis and the appended 1:20 000 scale map describe the geological features of the Rössing mine area situated in the Erongo Region of coastal Namibia. The mapping product shown below is the result of data compilation from several decades of previous work complemented by additional fieldwork, data acquisition, processing and interpretation by the author together with the support cited within this text. A major factor towards satisfactorily resolving the geology of this complex area has been the availability of HyMap hyperspectral remote sensing data. In doing so the geological understanding of the area has been refined, in particular the stratigraphic and structural setting of granite-hosted uranium mineralisation encompassing the SH-SJ-SK and Z20-Z19-Z17 to Rössing South areas.



The principal project deliverable, a mapping compilation and geological interpretation of the area around the Rössing uranium mine – structural measurements, lithological contacts and radiometric contour data illustrated on the map included as Appendix II are not shown here for the purpose of clarity.

Data compiled from previous work and subject to additional processing included geological mapping at various scales (29 digitised maps), point structural measurements (>13,000 measurements), ground scintillometer data (25,000 digitised points), airborne magnetic and radiometric data and orthorectified aerial photography. Data interpretation was conducted at 1:10 000 scale over a suite of pre-processed HyMap hyperspectral imagery products and the above data layers,

and was underpinned by geological traversing and observations from >1000 ground points. Description of stratigraphic units was augmented by transmitted and reflected light petrography and infrared spectroscopy completed on 116 representative field and drill core samples. Refinements to the geological understanding of the Rössing area mineralisation borne out of this project are summarised below.

The U-Th-enriched Proterozoic Ababbis Metamorphic Complex (A.M.C.) basement is an undifferentiated map unit where metasedimentary (± metavolcanic) and orthogneiss lithologies are tentatively correlated with the Tsawisis Formation and Narubis Granitoid Complex respectively of the Abbabis Inlier described by Brandt (1987). The overlying Damaran-age (Neoproterozoic) metasedimentary Formations are in sheared and folded contact with the basement. Within the Damaran stratigraphy the Etusis Formation consists of two members where basal meta-arkoses inherit a radiometrically anomalous signature through derivation from an A.M.C. hinterland. A conformable sequence of Khan and Rössing Formation stratigraphy is laterally variable beyond the immediate SH-SJ-SK area where it is lithologically most heterogeneous, and where marble forming the base of Rössing Formation is variably dolomitised. Within the Chuos Formation three diamictite units are defined of which the upper unit passes laterally into a banded iron formation ± ferruginous quartzite member. The sequence through the Arandis to Karibib Formations is divided into eight members, all of which are correlated with regional geological survey mapping. The Karibib Formation contains a laterally continuous dolomitic marble member as well as calcitic marbles. Missing units within this sequence include the Ghaub Formation and suggest periods of non-deposition.

F_2-F_4 fold phases identified across the area are correlated with previous structural studies in the district. Significant pre-D_3 boudinage and extensional shear structures are deformed by D_3 or later structures. This includes the basement-cover contact and such extensional structures are extensively exploited by early alaskite intrusions. F_2-F_3 fold interference gives rise to type 1 dome and basin and type 3 hook geometries. Early D_4 deformation was predominantly ductile and progressive from D_3 deformation, however left lateral faulting with up to 1200 m displacement is also a common early D_4 feature. Map relations suggest that subsequent deformation during D_4 resulted in the development of north-northeast oriented transtensional zones into which uranium-bearing granitic melts were focused (see mineralisation below).

A brief review of metamorphic petrology broadly supports previous interpretations of M_1 and M_2 metamorphic pulses with peak lower granulite facies metamorphism reached during M_2 and continuing beyond D_3 deformation. Alaskite generation is attributed to migmatisation and partial melting of potassic meta-psammites during metamorphism. A replacive calc-silicate rock recognised in previous mapping is considered to have formed both early and late in the sequence of metamorphic events. Plutonism consists of dominantly sheeted alaskite intrusions which are correlated to the classification scheme of Nex (1997) for the nearby Goanikontes uranium deposit. Early garnet-bearing type B, type C and post-D_3 types D-E are readily distinguishable whilst earliest and latest types A and F are tentatively correlated. Subordinate early quartz diorite and late dolerite dykes also occur, the latter generally intruding F_3 fold axial zones.

Throughout the Rössing area syn-D_4 alaskite swarms are interpreted to have intruded into discrete north-northeast trending linear transtensional shear zones that formed highly oblique to pre-D_4 litho-structural orientations. This is particularly the case where such zones coincide with dilational F_2-F_3 fold interference structures and locally earliest D_4 strike slip faults. The SH-SJ-SK ore bodies were emplaced across the southeastern limb of the elongate F_2-F_3 SJ Dome fold interference structure. Intrusion of the most voluminous late alaskite intrusions at the SJ deposit was facilitated by the coincidence of one such interpreted shear zone with a northeast trending early D_4 fault zone occurring at the Khan-Rössing Formation contact. This fault zone was active immediately prior to alaskite intrusion and can be traced southwest through the Khan copper mine area, truncating the Nose Structure anticline. The SH uraniferous (refractory betafite-bearing) syenogranite plug is emplaced into a F_3 antiform superimposed on the F_2 Rössing synclinorium, whilst at SK an en echelon array of alaskites intrude the next F_2 anticline to the southeast and type 3 hook interference folding superimposed upon this. In the Z20-Z19-Z17 to Rössing South Zone 1 area, alaskite swarms have been emplaced across a large section of Damaran stratigraphy where mineralised alaskites only occur within the Rössing, Arandis and Karibib Formations. Doming of the Rössing South anticline presumably created dilational zones for subsequent alaskite emplacement and results from F_2-F_3 fold interference with final rotation to the present north-northeast orientation attributable to D_4 deformation. The interpretation of syn-D_4 uraniferous alaskite intrusion is consistent with previous work completed in the Rössing area (Corner, 1981, 1983; Anderson and Nash, 1997; Basson and Greenway, 2004). This project has particularly developed the understanding of the stratigraphy and pre-

mineral structural evolution of the area and the detailed structural evolution and timing of alaskite emplacement within the D_4 deformation episode. This project has provided Rössing Uranium Ltd. with a fundamental tool for the generation of uranium exploration targets. In particular through the course of this mapping the Z20 area was recognised as the northern extension to Rössing South Zone 1 and subsequent drill testing has added significant resources to the Rössing Uranium Ltd. uranium inventory.

Contents

Declaration *ii*

Acknowledgements *iii*

Abstract *iv*

Executive Summary *v*

List of Figures *xiii*

List of Tables *xvii*

Chapter 1: Introduction

1.1 Project Introduction and Objectives *1*

1.2 The Central Zone of the Pan-African Damara Belt *4*

1.2.1 Geological Setting and Tectonic Evolution *4*

1.2.2 Stratigraphy *10*

1.2.3 Structure *16*

1.2.4 Metamorphism *18*

1.2.5 Plutonism *21*

1.2.6 Mineralisation Associated with Pegmatites and Alaskites *25*

Chapter 2: Data Compilation and Interpretation

2.1 Introduction *31*

2.2 Geophysical Data *33*

2.2.1 Airborne Geophysical Data *33*

2.2.2 Ground Scintillometer Data *36*

2.3 Remote Sensing Data *36*

2.3.1 Remote Sensing Overview *37*

2.3.2 Landsat and Aster Imagery *40*

2.3.3 HyMap Hyperspectral Data *43*

2.3.4 Photogrammetry *47*

2.4 Digital Elevation Model *47*

2.5 Geological Mapping *48*

2.5.1 Previous Work *48*

2.5.2 This Work *51*

2.6 Data Interpretation *52*

2.7 Summary and Context for Subsequent Chapters *55*

Chapter 3: Stratigraphy

3.1 Introduction *57*

3.2 Summary of Previous Work in the Project Area *59*

3.3 The Abbabis Metamorphic Complex *59*

3.4 Damaran Metasediments *66*

3.4.1 Etusis Formation *66*

3.4.2 Khan Formation *70*

3.4.3 Rössing Formation *75*

3.4.4 Chuos Formation *81*

3.4.5 Arandis Formation *86*

3.4.6 Karibib Formation *88*

3.4.7 Kuiseb Formation *91*

3.5 Superficial Sediments *92*

3.6 Summary and Discussion *92*

Chapter 4: Structure

4.1 Introduction *97*

4.2 Previous Work in the Project Area *97*

4.3 This Work *102*

4.3.1 Planar and Lineation Structures *103*

4.3.2 Ductile Structures *104*

4.3.3 Brittle Structures *111*

4.4 Summary and Discussion *111*

Chapter 5: Metamorphism

5.1 Introduction *115*

5.2 Previous Work in the Project Area *115*

5.3 This Work *118*

5.3.1 Mineral Parageneses *118*

5.3.2 Skarn Development *123*

5.3.3 Calc-silicate Rock *123*

5.4 Summary and Discussion *125*

Chapter 6: Plutonism

6.1 Introduction *129*

6.2 Previous Work in the Project Area *129*

6.3 This Work *134*

6.3.1 Biotite Quartz Diorite *134*

6.3.2 Alaskite *135*

6.3.3 Dolerite *141*

6.4 Summary and Discussion *142*

Chapter 7: Mineralisation

7.1 Introduction *144*

7.2 Uranium *144*

7.2.1 Previous Work in the Project Area *144*

7.2.2 This Work *150*

7.3 Copper *154*

7.4 Summary and Discussion *155*

Chapter 8: Summary and Concluding Remarks

8.1 Project Summary *159*

8.2 Concluding Remarks *164*

References *165*

Appendices

Appendix I: Sample Details *184*

Appendix II: Geological Map of the Rössing Mine Lease Area 227

List of Figures

Figure 1.1. Satellite image showing the location of the Rössing mine and distribution of principal uranium mines, projects and prospects throughout the wider area *1*

Figure 1.2. Hyperspectral imagery showing the Rössing Uranium Ltd. ML28 mine area showing the location of the SJ, SK, SH and Z20-Rössing South uranium deposits *2*

Figure 1.3. Schematic map showing the location of the intracontinental Damara Belt and coastal Kaoko and Gariep belts within the Panafrican belts in Africa and South America *4*

Figure 1.4. Schematic tectonic map showing the tectonostratigraphic zones of the Damara Orogen *6*

Figure 1.5. Schematic geological map showing the distribution of main stratigraphic units of the Damara Supergroup *6*

Figure 1.6. North-south simplified structural profile of the Damaran Belt *8*

Figure 1.7. Schematic geological map showing the metamorphic zonation of the Damara Orogen *8*

Figure 1.8. Dome structures of the sCZ *11*

Figure 2.1. Compilation of geological mapping of the Rössing mine area *31*

Figure 2.2. Gridded heli-borne gradiometric magnetic data over the Rössing mine *34*

Figure 2.3. Radiometric data in the Rössing area *35*

Figure 2.4. Spectral characteristics of energy sources, atmospheric transmittance and remote sensing systems *37*

Figure 2.5. Plot of wavelength against reflectance showing spectral profiles for vegetation and dry soil, and bars representing various remote sensing sensors, vertically offset for comparison *39*

Figure 2.6. Selected laboratory mineral spectra showing diagnostic absorption and reflectance features *39*

Figure 2.7. An example of the ‘data-cube’ structure of hyperspectral imaging 40

Figure 2.8. Landsat 7 E.T.M.+ R.G.B. false colour composite of bands 7-4-2 of the Rössing Mine area *42*

Figure 2.9. Aster R.G.B. false colour composite bands 2-3-4, minimum noise fraction (M.N.F.) image of the wider Rössing area *42*

Figure 2.10. Processed area of 48 flight lines covering 3790 km^2 around the greater Rössing area *43*

Figure 2.11. Colour combination images of portions of HyMap survey data *44*

Figure 2.12. The minimum noise fraction (M.N.F.) transform applied to Rössing area HyMap data, bands 10-11-12 and 7-8-9 *45*

Figure 2.13. Mineral end-member images derived from the Rössing area HyMap data *46*

Figure 2.14. Iron oxide and hydroxide mineral end-member maps derived from Rössing area HyMap data *46*

Figure 2.15. Example of a portion of the ortho-rectified aerial photographic mosaic surveyed and produced by Southern Mapping Company for Rössing Uranium Ltd. in 2008 *47*

Figure 2.16. 1:250 000 Sheet 2214 of the Geological Survey of Namibia *48*

Figure 2.17. Geological map of the SJ-SK area *50*

Figure 2.18. Geological map of the SH area *50*

Figure 2.19. Photographs showing colour and geomorphological expression of major Damaran metasedimentary units in the area *51*

Figure 2.20. Interpretation at 1:10 000 scale of the project area *53*

Figure 2.21. Interpretation at 1:3500 scale of the geology in the SH area *54*

Figure 2.22. Interpretation at 1:20 000 scale of the Nose Structure anticline *54*

Figure 3.1. HyMap imagery band combination 108-26-2 covering the area south of the Khan River and corresponding map interpretation *62*

Figure 3.2. Red-weathering gneissic meta-arkose and gneisses of the A.M.C. northwest of the Rössing mine tailings area *64*

Figure 3.3. Mapped units of the Etusis Formation *69*

Figure 3.4. HyMap imagery band combination 10-11-12 with M.N.F. transform in the Panner Gorge area and lithological interpretation of the same area *72*

Figure 3.5. Mapped units of the Khan Formation *74*

Figure 3.6. Lithological variability of the Rössing Formation in the vicinity of the Rössing mine *76*

Figure 3.7. Hyperspectral end-member image showing the distribution of hematite-goethite and jarosite *78*

Figure 3.8. Hyperspectral carbonate end-member images showing examples of the distribution of calcite and dolomite in the Rössing and Karibib Formations *79*

Figure 3.9. Mapped units of the Rössing Formation *80*

Figure 3.10. HyMap imagery band combination 10-11-12 with M.N.F. transform in the area of the Blauer Heinrich syncline and lithological interpretation of the same area *83*

Figure 3.11. Mapped units of the Chuos Formation *85*

Figure 3.12. Lithologies of the Arandis Formation *88*

Figure 3.13. Lithologies of the Karibib Formation *90*

Figure 4.1. Selected structural elements in the Rössing area interpreted by previous workers *101*

Figure 4.2. Selected structural elements of the Rössing area incorporated from previous work with modifications and additional detail added from this mapping *102*

Figure 4.3. Examples of planar and lineation fabrics developed in the Damara succession *104*

Figure 4.4. Fold interference relationships in the SH-SJ-SK area as determined from compilation of structural data *106*

Figure 4.5. Lithological interpretation of the area northeast of the Z20 anomaly and Rössing South Zone 1 and structural interpretation *107*

Figure 4.6. Fold styles at outcrop scale *108*

Figure 4.7. Examples of structural attenuation in outcrop *109*

Figure 5.1. Diagram showing the paragenesis of selected minerals compiled from Nash (1971) *116*

Figure 5.2. Effects of metamorphism on units of the Damara succession *120*

Figure 5.3. Textures and mineral parageneses within metapelites in hand specimen and thin section *135*

Figure 5.4. Calc-silicate rock exhibiting characteristic quartz-tremolite-plagioclase mineralogy *124*

Figure 5.5. Diagram showing a revised mineral paragenesis after Nash (1971) with additional observations from this project *126*

Figure 5.6. Temperature pressure mineral stability plot showing the approximate position of peak metamorphic assemblages in the Rössing area *128*

Figure 6.1. Features of various types of intrusions *137*

Figure 6.2. Examples of textural and mineralogical variability in barren alaskites equated to the C type of Nex (1997) *138*

Figure 6.3. Examples of textural and mineralogical variability in uraniferous alaskites equated to the D and E types of Nex (1997) *140*

Figure 6.4. Dolerite samples from the SJ Dome and the hinge zone of the Blauer Heinrich syncline *141*

Figure 7.1. Location of radiometric anomalies within the Rössing mine lease ML28 shown on contoured radiometric data *145*

Figure 7.2. Summary geological map after the appended detailed map showing the geological setting of the SJ, SH and SK uraniferous alaskite bodies *151*

Figure 7.3. Simplified geological setting and major structures in the Z20-Z19-Z17 (and Rössing South Zone 1) area *153*

List of Tables

Table 1.1. Summary of stratigraphic and tectonothermal elements of the Central Zone of the Damaran Orogen *10*

Table 1.2. Lithostratigraphic units of the Damara Belt, Nosib Group *11*

Table 1.3. Lithostratigraphic units of the Damara Belt, Swakop Group *13*

Table 1.4. Summary of interpreted timing and P-T conditions of metamorphic events of the Central Zone *19*

Table 1.5. Damaran-age plutonic rocks of the Central Zone *23*

Table 1.6. Grade tonnage data of alaskite-hosted uranium deposits of the south Central Zone of the Damara Orogen *26*

Table 2.1. Data compiled throughout the course of the project with notes on application *32*

Table 2.2. Summary of rock samples taken from drill core and field localities *52*

Table 3.1. Detailed stratigraphy of the area around the Rössing Uranium Mine *58*

Table 3.2. Summary of the stratigraphy of the area around the Rössing Uranium Mine *57*

Table 3.3. Summary of mapping of the Ababbis Metamorphic Complex in the sCZ *60*

Table 4.1. Summary of deformation features of the Rössing and wider area from previous work *98*

Table 6.1. Sheeted leucogranite (alaskite) classification scheme of Nex (1997) and Nex et al. (2001a), modified after the latter to include the observations of other workers *132*

Chapter 1: Introduction

1.1 Project Introduction and Objectives

This thesis is submitted in conjunction with the attached geological map presented at a scale of 1:20 000 to fulfil requirements for the degree of Doctor of Philosophy with the School of Geosciences, University of the Witwatersrand, Johannesburg. Mapping and data compilation was completed during the author's secondment to Rio Tinto's majority-owned Rössing Uranium Ltd. during 2008-2009 and with Rio Tinto Exploration in 2010. Petrography and writing up was completed in the author's spare time from 2011 to 2014. The Rössing Mine Lease ML28 tenement is situated in the Namib Desert of the Erongo Region of coastal Namibia, approximately 60 km northeast of Swakopmund (Figure 1.1). Figure 1.2 illustrates the physiographic and mining-related features of the Rössing area and shows the extent of detailed geological mapping coverage around the SJ pit.

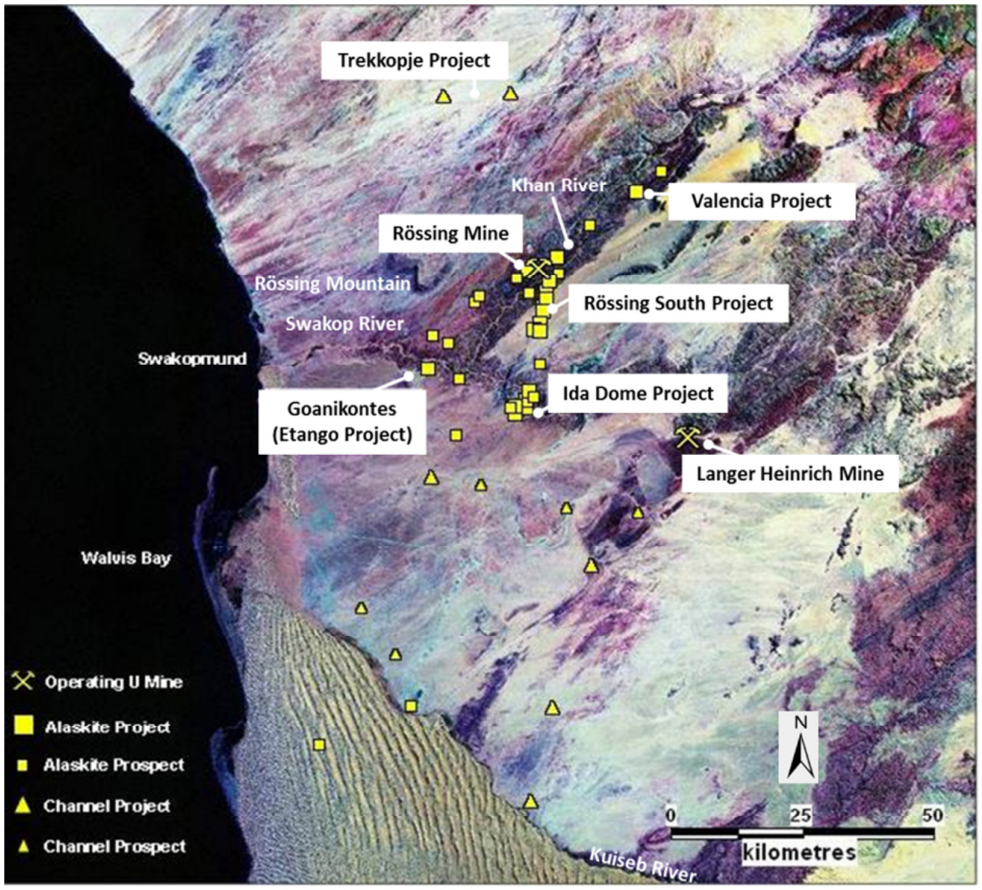


Figure 1.1. Satellite image showing the location of the Rössing Mine and distribution of principal uranium mines, projects and prospects throughout the wider area. Both alaskite- and channel-hosted deposits are shown; background image is a Landsat mosaic of bands 7-4-1.

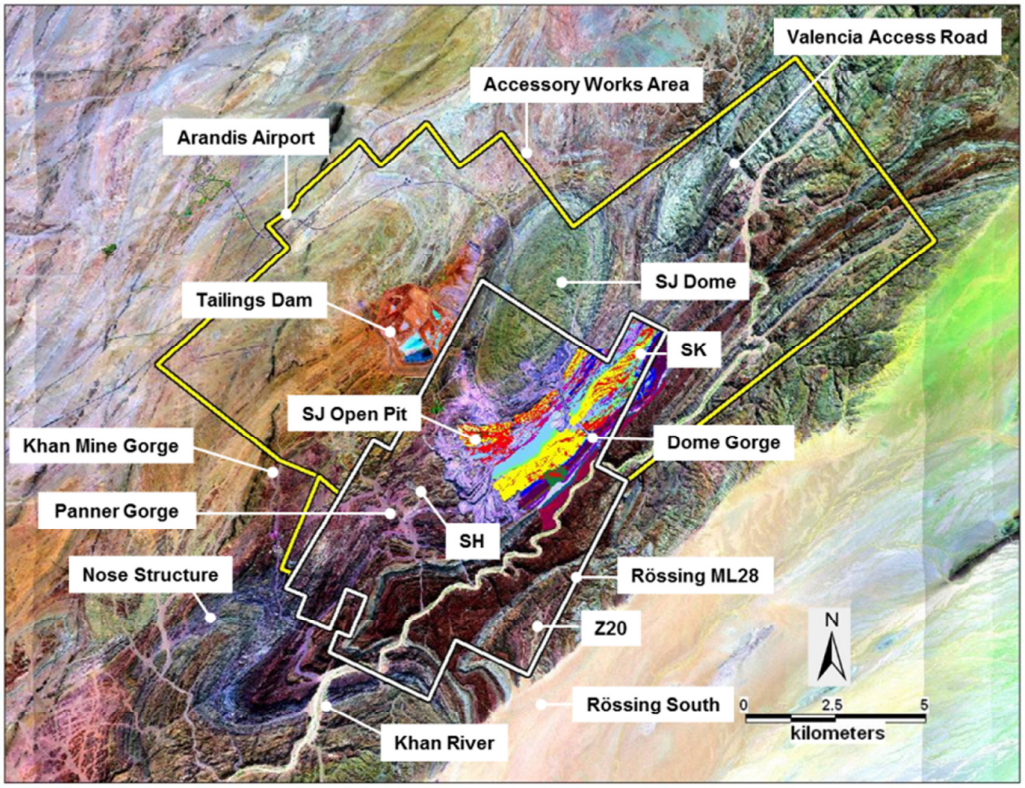


Figure 1.2. Hyperspectral imagery showing the Rössing Uranium Ltd. ML28 mine lease area (white border) and accessory works area (yellow border) showing the location of the SJ, SK, SH and Z20-Rössing South uranium deposits and extent of detailed geological mapping around the SJ open pit. The image is processed hyperspectral line data with RGB band combinations 108-26-2 (equivalent to Landsat bands 7-4-1). Some physiographic features referred to in the text are shown. Figure is centred on 506000 mE, 7516000 mN.

Rössing Uranium Ltd. commenced mining uranium ore from the SJ open pit in 1976 and presently supplies 4% of the world's uranium from alaskite[1]-hosted mineralisation. It is reported that 123,453 tonnes of uranium oxide had been produced from the mine operations by the end of 2012 (http://www.Rössing.com). The Rössing mine is the only producer of primary uranium ore from granitic rocks in the world and is an important contributor to the Namibian economy. The recently discovered Rössing South deposits are also under development (Swakop Uranium), whilst secondary uranium mineralisation relating to palaeo-drainages is mined at Langer Heinrich (Paladin Energy Ltd.) with development also underway at the Trekkopje deposits (Areva Inc.).

[1] The term 'alaskite' is used throughout this thesis and on the appended map in the sense defined by Spurr (1900): "*a holocrystalline granular plutonic rock characterised by essential alkali feldspars and quartz, and little or no dark component*". It is synonymous with the term 'sheeted leucogranite' applied regionally (e.g. Kinnaird and Nex, 2007). Whilst it is recognised that in the case of Rössing the term 'alaskite' covers a relatively wide spectrum of granitic rock compositions and textures, the author prefers this term as it avoids confusion with other regional units mapped as 'leucogranites'. Furthermore the intrusions are not ubiquitously sheeted.

The completed geological mapping covers some 175 km^2 around the periphery of existing detailed mapping of the SJ-SK areas, encompassing the mine lease and portions of the surrounding area. The primary purpose of the geological map is to provide Rössing Uranium Ltd. with a basis for uranium drill-target generation across ML28 and ultimately to extend the life of the business beyond the current life of mine through discovery of additional uranium resources. A major factor in the generation of this map beyond the compilation of previous work was the availability of HyMap hyperspectral remote sensing data, which was purchased, processed and interpreted during the course of this project. The combination of historical work with new data and observations means that the geology of this economically important area is resolved in significantly more detail than has hitherto been presented. This includes refinements to southern Central Zone Damaran stratigraphy, where the type locality of several formations falls within or near the project area. This project also advances the knowledge of the geological (principally stratigraphic and structural) setting of alaskite-hosted uranium mineralisation occurring throughout the area.

Chapter 1 of this thesis provides a summary of the geology and mineralisation of the Central Zone of the Damara Belt. Chapter 2 describes the data compiled and subsequently interpreted through the course of this project with specific focus on remotely sensed data. Chapters 3 through to 7 respectively review the stratigraphy, structure, metamorphism, plutonism and mineralisation in the project area. Each of these chapters distinguishes historical work from observations and interpretations made during this work. In Chapter 8 the main outcomes of the project are discussed.

1.2 The Central Zone of the Pan-African Damara Belt

1.2.1 Geological Setting and Tectonic Evolution

The Rössing area is situated in the southern Central Zone (sCZ) of the northeast-trending Damara Belt of the Neoproterozoic Damara Orogen (e.g. Basson and Greenway, 2004), one of a number of Pan-African orogenic belts occurring throughout the continent and adjoining parts of the South American continent (Figure 1.3). The Damara Orogen is a polydeformed and polymetamorphic orogenic belt comprising the coastal Kaoko and Gariep belts and the intracontinental Damara Belt meeting at a triple junction centred approximately at Swakopmund. The orogen records a 'Wilson Cycle' having evolved through phases of intracontinental rifting, spreading and subduction lasting from ~750 to 460 Ma, culminating in collisional orogenesis as part of the broader assembly of the Gondwana Supercontinent (Miller, 1983, 2008; Hminady *et al.* 1985; Stanistreet *et al.*, 1991; Prave, 1996; Hanson, 2003; Frimmel *et al.*, 2011).

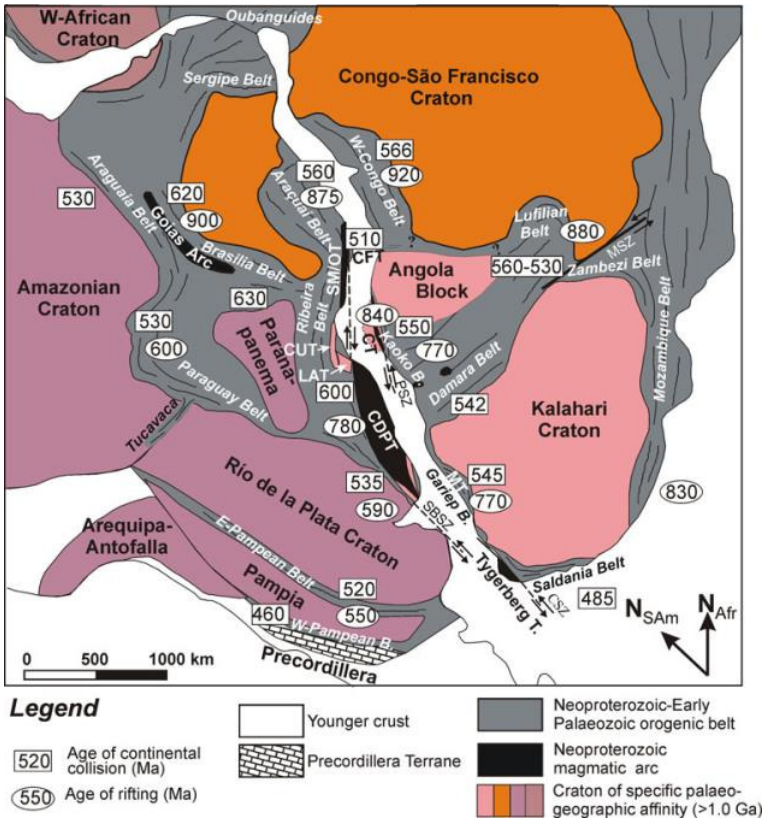


Figure 1.3. Schematic map showing the location of the intracontinental Damara Belt and coastal Kaoko and Gariep belts within the Panafrican belts in Africa and South America (John et al., 2003).

The intracontinental Damara Belt which is contiguous with the Kaoko Belt formed as a result of oblique, northeast-directed subduction of the Kalahari Craton beneath the Congo Craton (Miller, 2008). The Damara Belt is sub-divided into tectonostratigraphic zones based on contrasting depositional, structural, metamorphic, magmatic and temporal histories. These zones are the Northern Platform, Northern Margin, Northern, Central, Okahandja Lineament, Southern, Deep-Level Southern, and Southern Margin zones and the Southern Foreland shown in Figure 1.4, abbreviated respectively to NPZ, NMZ, NZ, CZ, OLZ, SZ, SMZ and SF (Clifford, 1967; Porada, 1979; Barnes and Sawyer, 1980; Miller, 1983, 2008). Zone boundaries are characterised by faults and/or lineaments with major aeromagnetic expressions, and on the same basis the CZ is divided into northern (nCZ) and southern (sCZ) parts (Miller, 1983).

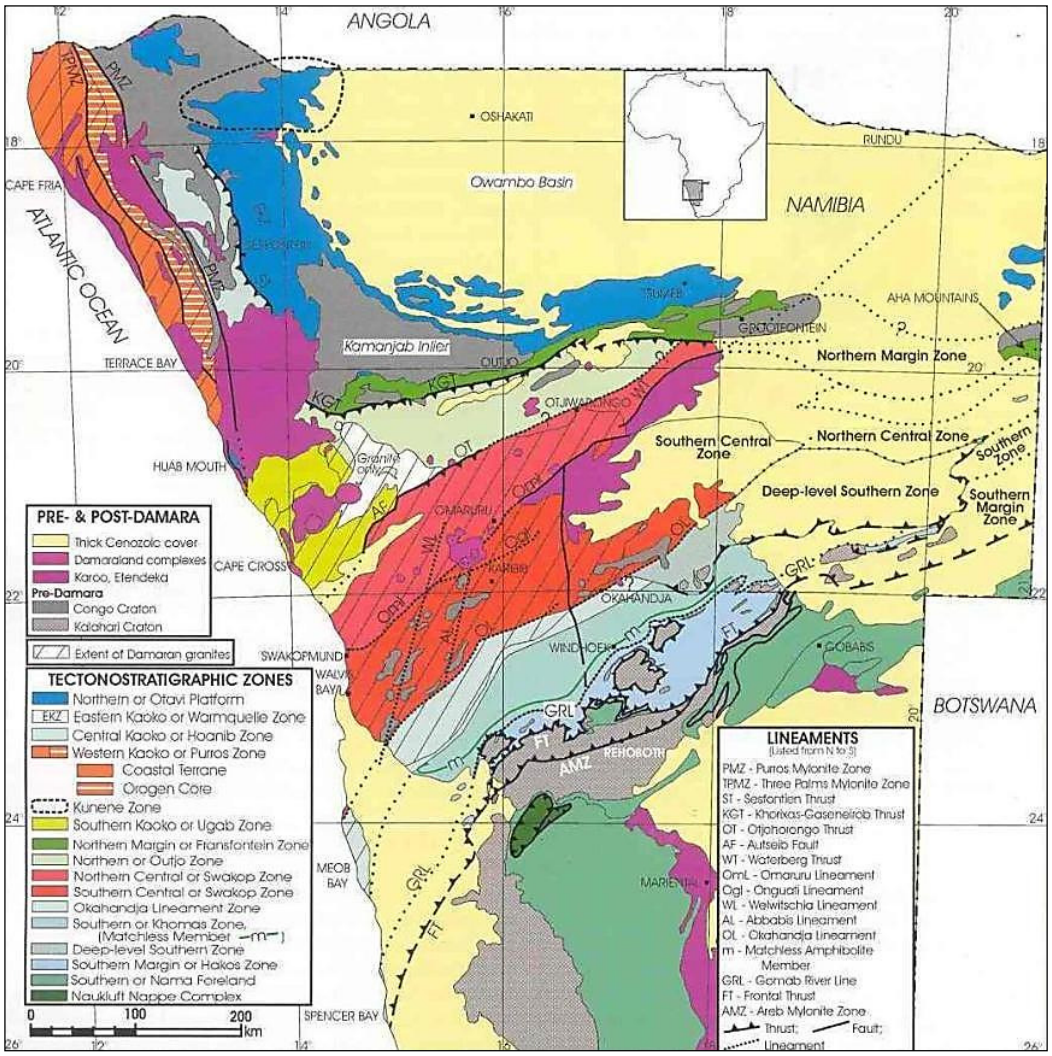


Figure 1.4. Schematic tectonic map showing the tectonostratigraphic zones of the Damara Orogen (from Miller, 2008 and references therein).

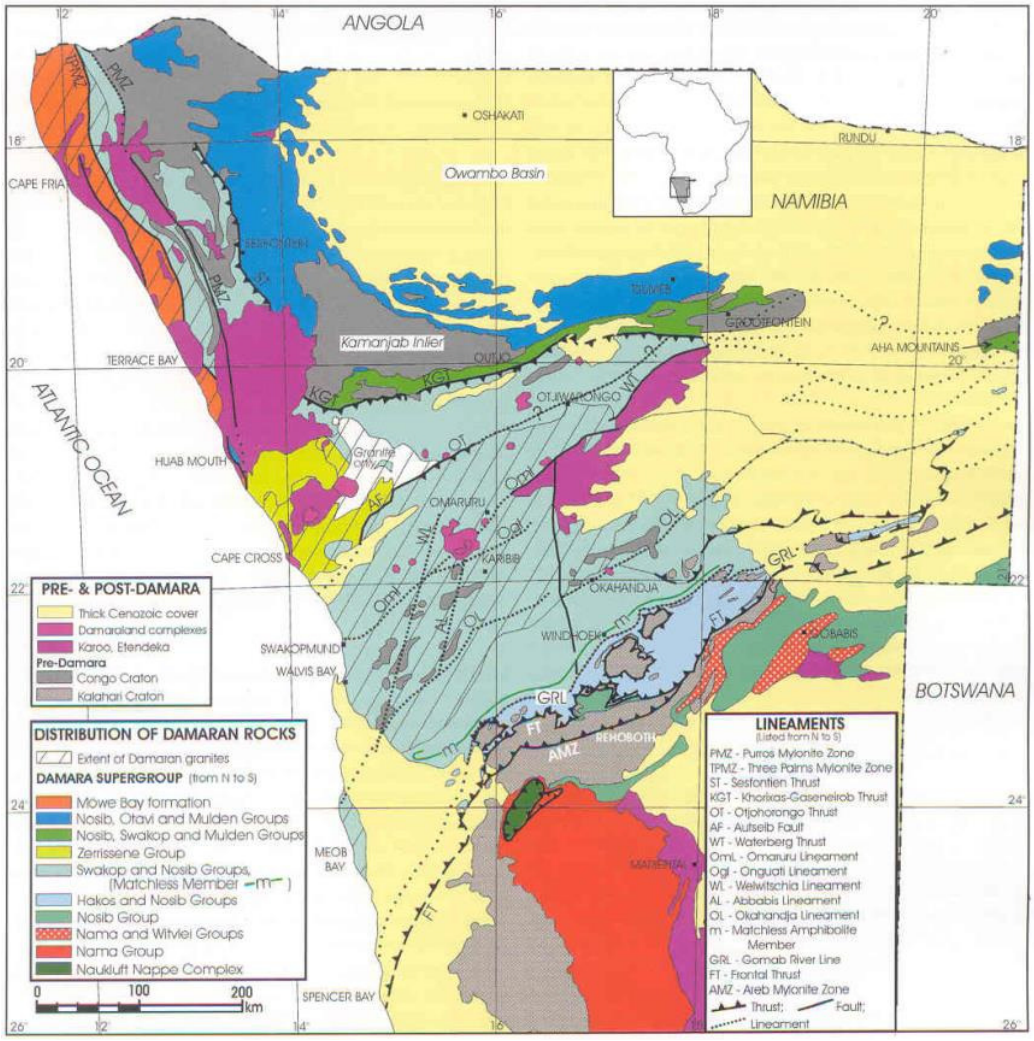


Figure 1.5. Schematic geological map showing the distribution of the main stratigraphic units of the Damara Supergroup (from Miller, 2008).

Major lithostratigraphic features of the Damara Belt include (i) Archaean to Proterozoic basement inliers, (ii) early rift-fill of the Nosib Group (iii) passive margin carbonates of the Otavi Group (iv) deeper water turbidites of the Swakop Group and (v) foreland basin molasse of the Mulden (northern Namibia) and upper Nama (Fish River Sub-Group, southern Namibia) Groups (e.g. Gray *et al.*, 2008; Miller, 2008; Figure 1.5). The Nosib and Swakop Groups constitute the Damaran-age (Neoproterozoic) metasedimentary sequence of the CZ.

Dating of volcanics indicates deposition of the Nosib Group commenced during rifting of the supercontinent Rodinia at *ca*. 750 Ma (e.g. Hoffman *et al.*, 1996; de Kock,

2001; Chapter 1.2.2). According to Miller (2008) deposition occurred in two northeast-trending grabens and on associated rift shoulders with the southern graben initially in the present location of the SZ and the northern graben extending across the NZ and northern half of the CZ. The southern graben subsequently drifted south through ocean spreading to underlie the SMZ. The grabens are interpreted by Miller (2008) to have evolved into two ocean basins, the north and south Outjo and Khomas seas respectively (a third north-south Adamaster Ocean is recorded by the Gariep and Kaoko Belts), where the sCZ occupied a central shelf region between the two. Laterally equivalent units deposited during spreading include the Otavi Group in the north and the Swakop Group in the central and south both of which host two 'Snowball Earth' glaciogenic deposits and associated cap carbonates (see Chapter 1.2.2; Miller, 2008). Submarine volcanism and sedimentary exhalative activity occurred throughout the evolution of the rifts. Whilst the northern graben (Outjo Sea) is interpreted as a failed rift, spreading and deepening of the southern Khomas Sea continued with the development of an active mid-ocean ridge corresponding to the Matchless Amphibolite Member of the Kuiseb Formation in the SZ (Barnes and Sawyer, 1980; Miller, 2008). Subsequent reversal of plate motions, subduction and eventual collision resulted in the accumulation of arc-related basin and molasse successions. Oblique subduction of the Kalahari beneath the Congo/Angola craton resulted in large-scale northeast over southwest transpressive deformation including the development of basement-cored nappes and sheath folds in the CZ and SMZ.

The fault- and shear-bounded zones of the Damara Belt show varying structural styles from north to south: the NZ is a craton-vergent fold and thrust belt, the CZ is granite-dominated with basement-cored domes between Damara sequence basins, the SZ is a wide zone of north-dipping shear-dominated fabrics and the SMZ comprises basement-cored fold nappes bordering the Kalahari Craton (Hoffmann, 2005, 2008; Figure 1.6). The southern part of the SZ and the SMZ constituted an accretionary prism (Miller, 2008). The presence of evaporite- and/or carbonate-bearing stratigraphy significantly influenced the late orogenic thrusts and fold nappes (e.g. Behr *et al*., 1983). In many cases thrust faults may represent reactivated normal faults associated with rifting (e.g. Henry *et al*., 1990). Four deformational episodes are generally distinguished in the CZ termed D_1-D_4 (Chapter 1.2.3).

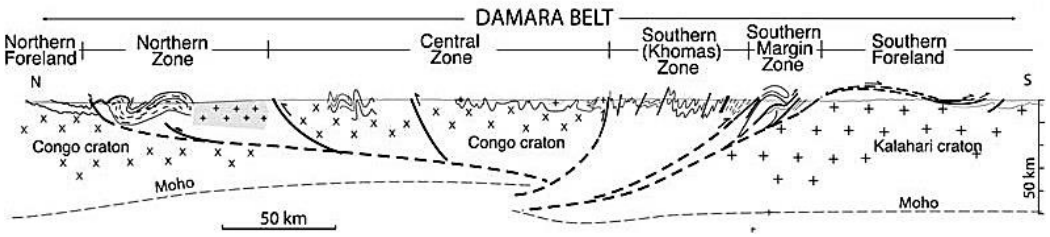


Figure 1.6. North-south simplified structural profile of the Damaran Belt (from Hoffmann, P.F., 2005., 2008, after Miller and Grote, 1988)

Paired metamorphic belts occur both in the Damara and Kaoko belts: low-temperature moderate-pressure kyanite facies assemblages occur on the subducting plates (SZ and SMZ of the Damara Belt) which are overridden by high-temperature low-pressure cordierite-sillimanite facies assemblages with associated syn- to post-tectonic granites (CZ of the Damara Belt; Kasch, 1983; Miller, 2008; Figure 1.7).

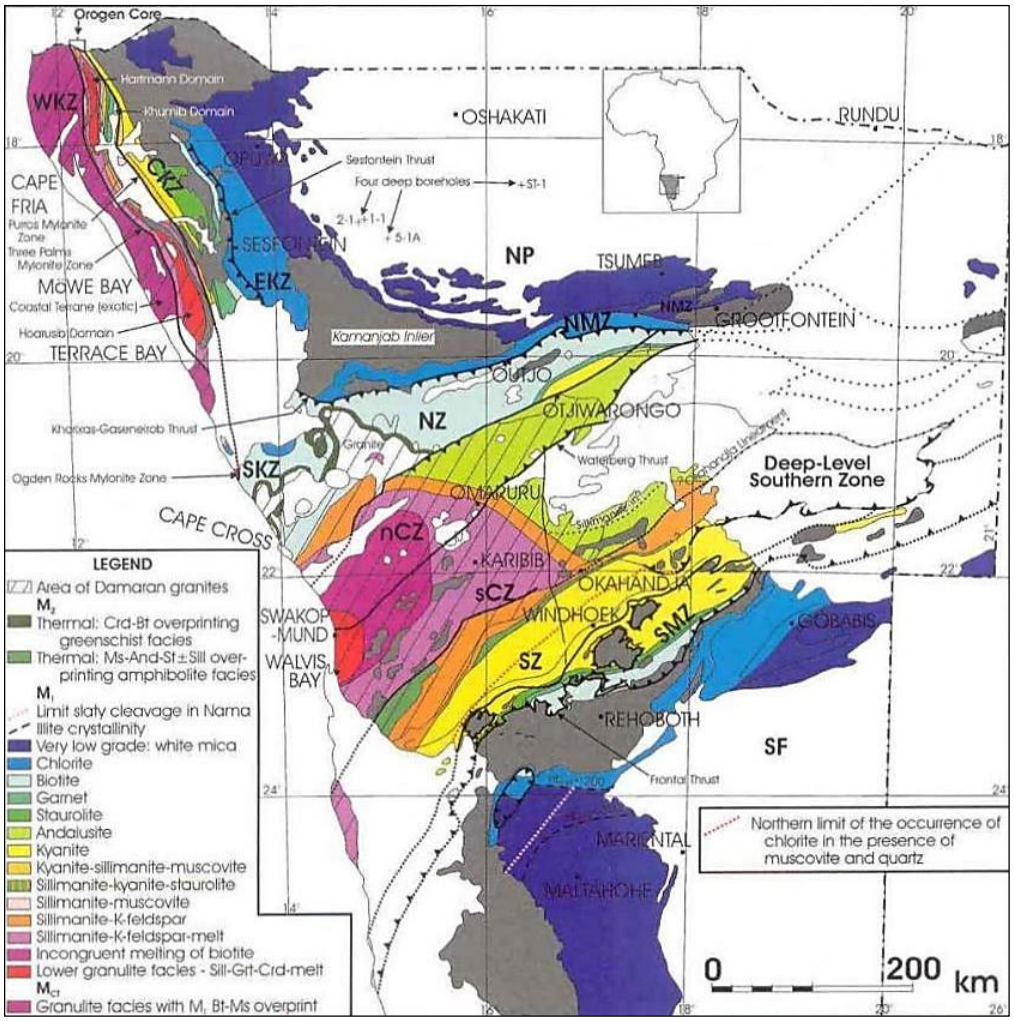


Figure 1.7. Schematic geological map showing the metamorphic zonation of the Damara Orogen based on metapelite assemblages (from Miller, 2008, and references therein).

Two metamorphic pulses[2] are variably recognised in the Damara Belt. Post-tectonic peak metamorphism at around 535 Ma (Briqueu *et al*., 1980; Miller, 2008) was followed by extensive partial melting of basement and cover rocks in the west of the CZ, products of which include the uranium and rare metal mineralisation associated with pegmatites. The Damaran Plutonic Suite is extensively developed in the CZ but also extends northwards as shown in Figure 1.7 (Miller, 2008). The intrusion of A-type granites between 495-486 Ma (McDermott *et al.* 2000) was followed by cooling and exhumation of the belt through 470 Ma (Gray *et al.* 2007).

The CZ and in particular the sCZ is characterised by dome structures with a northeast elongation and numerous syn- to post-tectonic granitic plutons (Miller, 1983, 2008). The nCZ exposes predominantly Swakop Group units and is magnetically very quiet, whereas the sCZ is characterised by exhumation of deeper levels with both pre-Damaran basement and Nosib-Swakop Group lithologies present. Miller (2008) interprets the nCZ (the southern part of the northern graben described above) as a thinned back arc zone where detachment of the subducting plate would have enabled hot mantle to intrude the base of the crust and provide the necessary heat for granite generation. The CZ is bound to the north by the Otjihorongo thrust whilst the northeast-trending Omaruru Lineament (Figure 1.5) marks the southern limit of Miller's northern graben and the boundary between the nCZ and sCZ, north of which Swakop Group rocks thicken rapidly (Miller, 2008). The southern boundary of the CZ is marked by a major crustal lineament, the Okahandja Lineament (Figure 1.5), which is considered to represent the southern boundary to the Congo Craton and forms the northern boundary of the original location of Miller's southern graben (Miller, 1979, 2008). Between these two major lineaments[3] a number of other lineaments are present, notably including the north-northeast-trending Welwitschia Lineament of Corner (1981; Figure 1.8) who postulated a relationship between this feature and the occurrence of alaskite-hosted uranium deposits in the sCZ (Chapter 1.2.6).

Table 1.1 presents a summary of stratigraphic and tectonothermal elements of the Central Zone after Longridge (2012). Details of the regional stratigraphy, structure,

[2] Many workers only describe one metamorphic pulse described here as M_2.

[3] In line with the comments of Corner (2008) a 'lineament' denotes a large-scale fault zone. Lineaments may also delineate linear zones of intrusive activity. The distinction between a lineament and a major regional fault is subjective. In the case of the Welwitschia Lineament this marks the onset of a change in structural style in the western CZ where younger NNE-orientated fold axes (D_4) are superimposed on the older NE-trending D_3 trend (Corner, 1981). According to Miller (2008) the Okahandja Lineament represents the southern margin on the Angola craton.

metamorphism, plutonism and mineralisation are presented in subsequent sections of this chapter.

Table 1.1. Summary of stratigraphic and tectonothermal elements of the Central Zone of the Damaran Orogen, modified from Longridge (2012) and Milani et al. (2014).

Age	Sedimentary & Plutonic Units	Deformation	Metamorphism
		D_4	
510-508 Ma	Uraniferous alaskite	D_3	
520-510 Ma	Grey granite, garnetiferous alaskites	D_2 (mid-crust, SW CZ)	M_2
540-535 Ma	Red granite		M_1
580-510 Ma	Goas Intrusive Suite & Salem-type granites	D_2 (shallow crust, NE CZ)	
750- <710 Ma	Deposition of Damara Supergroup		
1013 Ma	Basement amphibolites		
2 Ga	Abbabis Metamorphic Complex basement		

1.2.2 Stratigraphy

Abbabis Metamorphic Complex

The Palaeoproterozoic Abbabis Metamorphic Complex (A.M.C.) constitutes the oldest rocks in the region. A.M.C. inliers form the cores of numerous domes within the sCZ including the Abbabis and Ida Dome areas and the Palmenhorst and Hildenhof domes of the Khan Gorge Inlier, the northern extent of which is within the project area (Figure 1.8). The complex consists of poly-deformed and poly-metamorphosed metasedimentary rocks, paragneisses, orthogneisses, pegmatites and orthoamphibolites (Smith, 1965; Jacob *et al.*, 1978; Marlow, 1981). Stratigraphy within the A.M.C. is variable with schemes or descriptions including those of Gevers (1931), Smith (1965), and Lehtonen *et al.* (1993, 1996) for the wider sCZ, Brandt (1987) and Marlow (1981) for the Abbabis Inlier and Sawyer (1976, 1979), Bunting (1977), Downing (1982, 1983) for the area east of Swakopmund and Walvis Bay and Jacob (1974), and Barnes (1981) and Longridge (2012) for the Palmenhorst Dome (Khan Gorge Inlier) and Ida Dome. Details of these are elaborated upon in Chapter 3.2. In places the original character of lithologies is rendered difficult to recognise due to the effects of extensive partial melting and terms applied to these migmatites include red gneissic granite (Smith, 1965) and red granite gneiss (Jacob, 1974). Ages of ~2 Ga have consistently been obtained for Abbabis Complex gneisses and inherited cores in Damaran magmatic zircons (Jacob *et al.*, 1978; Kroner *et al.*, 1991; Jacob *et al.*, 2000; de Kock *et al.*, 2000; Tack *et al.*, 2002; Longridge *et al.*, 2008; Longridge, 2012). Intrusive components exhibiting U-Pb SHRIMP Grenvillian ages of 1038 ± 58 Ma obtained by Kroner *et al.*, (1991) may represent infolded Damaran lithologies (Longridge, 2012). Amphibolite intruding the A.M.C. in the Abbabis Inlier

has yielded a SHRIMP U-Pb age of 2027 ± 2.3 Ma (Longridge, 2012) however Damaran-age amphibolites have also been demonstrated to be present in the sCZ hence are not diagnostic of the A.M.C. (Longridge, 2012).

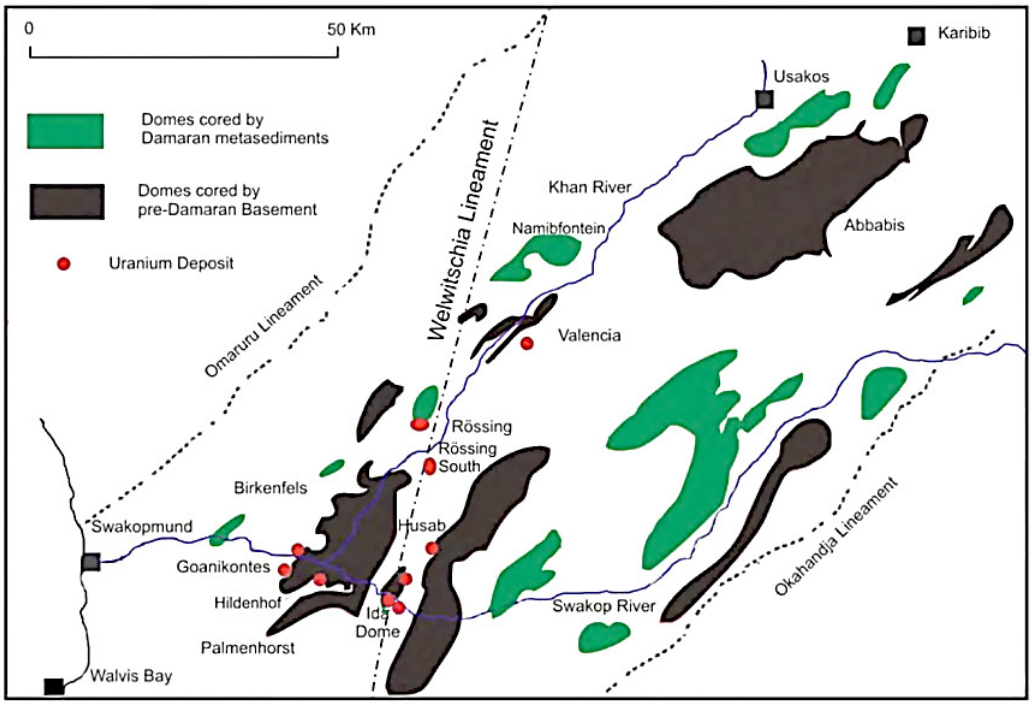


Figure 1.8. Dome structures of the sCZ cored by Damaran metasediments and pre-Damaran Abbabis Metamorphic Complex basement. The sCZ-bounding Omaruru and Okahandja lineaments are shown together with the Welwitschia Lineament of Corner (1981) and alaskite-hosted uranium deposits. From Mouillac et al., (1986) modified by Guy Freemantle, 2015.

Damara Metasediments – Nosib Group

The stratigraphic nomenclature of the Nosib Group is shown in Table 1.2.

Table 1.2. Lithostratigraphic units of the Damara Belt, Nosib Group. EKZ – Eastern Kaoko Zone; NP – Northern Platform; NZ – Northern Zone; nCZ – northern Central Zone; sCZ – Southern Central Zone; SZ – Southern Zone; SMZ – Southern Margin Zone; SF – Southern Foreland. From Miller (2008).

EKZ	NP	NZ	nCZ	sCZ	SZ	SMZ	SF
Unnamed	Upper Naauwpoort / Nabis	Upper / Lower Naauwpoort / Tsaun / Unnamed	Unnamed	Khan / Etusis		Duruchaus / Karntsas	Karntsas

Within the Nosib Group the Etusis Formation (>3000 m maximum thickness southwest of Karibib) consists of feldspathic quartzite with infrequent pelitic units and a locally developed basal conglomerate. Together with the Nabis Formation of the NP these lithologies are interpreted to have been deposited in a braided fluvial

environment within a northern graben and on a highly irregular A.M.C. unconformity surface (Jacob, 1974; Downing, 1983; Henry, 1992; Miller, 2008). In the nCZ, Nosib feldspathic quartzites form the cores of several domes in the area southwest of Otjiwarongo (Miller, 2008). In more distal or fluviodeltaic environments, rivers accumulated calcareous sediment producing the more calc-silicate-rich rocks of the overlying Khan Formation (maximum thickness ~1050 m; Downing, 1983; Henry, 1992; Miller, 2008). The type locality of the Khan Formation falls within the project area around the Khan River where the formation consists predominantly of clinopyroxene- and hornblende-bearing feldspathic quartzite (Nash, 1971; Jacob, 1974; Miller, 2008). Smith (1965) however notes that in the wider sCZ the formation may consist entirely of quartzite. Occupying a similar stratigraphic position to the Khan Formation is the Naauwpoort Formation of the NZ and NP consisting largely of ignimbrites that emanated from volcanic centres along the northern boundary fault of the northern graben. Temporally equivalent units within the Nosib Group of the southern graben occupying the SMZ and SF are the Kamtas and Duruchaus Formations, the latter a cyclic dolomite-pelite-evaporite lacustrine succession (Behr *et al*., 1983; Miller, 1974, 2008). Acid metavolcanics occur at the top of the Nosib Group immediately north of the Okahandja Lineament southwest of Karibib (Downing, 1982; de Kock, 1989) that Miller (2008) relates to the original location of the southern graben underlying the SZ. Nosib rift-related volcanics have been dated at 748 ± 3 Ma by Hofffman *et al*. (1994), 746 ± 2 Ma by Hoffman *et al*., (1996) and 752 ± 7 Ma by de Kock *et al*., (2000).

Damara Metasediments – Swakop Group

The stratigraphic nomenclature of the Swakop Group is shown in Table 1.3.

Table 1.3. Lithostratigraphic units of the Damara Belt, Swakop Group. CKZ – Central Kaoko Zone; NZ – Northern Zone; nCZ – northern Central Zone; sCZ – southern Central Zone; SZ – Southern Zone; Sg – Subgroup; Fm – Formation; Mb – Member. From Miller (2008).

CKZ		NZ		nCZ			sCZ			SZ			Age Ma
Sg	Fm	Sg	Fm	Sg	Fm	Mb	Sg	Fm	Mb	Sg	Fm	Mb	
													± 542
Syntectonic succession											Haub	Upper Hureb	
												Lower Hureb	
Pre-tectonic succession													
Navachab (old Khomas)	Kuiseb	Navachab (old Khomas)	Kuiseb	Navachab (old Khomas)	Kuiseb		Navachab (old Khomas)	Kuiseb		Khomas Complex	Kuiseb		
			Awa-huab mb										
	Gomatum		Karibib		Karibib	Arises River		Karibib	Onguati				
						Otjongeama		Tinkas			Tinkas, Klein Kuppe		
						Harmony			Quelle Kud-uleck				
	Diamictite?		Ghaub		Ghaub not yet identified			Ghaub	Daheim, Omusema, Lievental				635.5 ± 1.2
									Kachab				
	Needs remapping	Usakos	Okonguarri	Usakos	Arandis	Oberwasser	Usakos	Aran-dis	Oberwasser				
						Okawayo			Okawayo				
						Spes Bona			Spes Bona				
									Karub				
			Chuos		Chuos not yet identified			Chuos					
		Ugab	Orusewa	Ugab			Ugab	Rössing					746 ± 2
			Okotjize										

In the sCZ the Swakop Group consists of the Ugab (Rössing Formation), Usakos (Chuos and Arandis Formations), and Navachab (Ghaub, Karibib, Tinkas and Kuiseb Formations) Subgroups. The units progressively overstep each other from northwest to southeast. The Chuos and overlying formations locally rest unconformably on the Nosib Group indicating a period of uplift and erosion apparent also from the gritty and quartzitic facies of the Rössing and Chuos Formations (Miller, 2008); a major unconformity representing a time interval of 110 Ma is also locally observable between the Chuos and Karibib Formations (Sawyer, 1981).

The laterally restricted Rössing Formation (maximum thickness 200 m) shows a highly variably lithological succession consisting of dominantly dolomitic marble with intercalated siliciclastic rocks or vice versa; upper carbonates are often absent possibly due to removal during Chuos glaciation (see below; Jacob et al., 1986; Henry, 1992; Miller, 2008). Deposition of the Rössing Formation is interpreted to

have taken place on an epicontinental carbonate ramp subject to periodic siliciclastic influxes (Henry, 1992). The type locality of this formation is within the project area.

The Chuos Formation of the Usakos Subgroup is restricted to the sCZ and NZ and is the lower of two glacial horizons present across the Damara Orogen, the upper being the Ghaub Formation of the Navachab Subgroup showing the same general distribution (Hoffman and Prave, 1996; see below). In the sCZ, the Chuos Formation is best developed in the Trekkopje area and at the confluence of the Khan and Swakop rivers, and reaches 600 m thickness in the Khan Copper Mine area (Miller, 2008). The Chuos Formation in the sCZ is variable between tillite-dominated successions (mixtite and diamictite are terms also used), those with turbidites containing dropstones, successions with iron formation absent to dominant, and locally those with a minor dolomite component (Smith, 1965; Miller, 2008). Henry (1992) interprets the diamictites as reworked glaciomarine rocks mainly deposited by glacial debris flows. The Chuos Formation is correlated with the Grande Conglomerate of the Kundelungu System of DRC and Zambia where these units and other global examples represent a world-wide Sturtian glacial event at ~710 Ma by Hoffman (2005).

The Arandis Formation (up to 4000 m thickness in the nCZ), is the second unit of the Usakos Subgroup and is divided into the Spes Bona, Okawayo and Oberwasser Members (Badenhorst, 1992; Lehtonen *et al.*, 1993, 1995, 1996). The formation consists of dominantly marble and calc-silicate rock with the basal Karub Member locally forming a cap carbonate to the Chuos Formation. Again the type locality for this formation is in the Rössing area (Arandis town). Its distribution is restricted to the CZ however the turbidite succession of the Okonguarri Formation in the NZ is the lateral equivalent (Porada and Wittig, 1983; Hoffman *et al.*, 2004).

The Navachab Subgroup replaces older 'Khomas Subgroup' nomenclature where the latter unit originally included only the Kuiseb Formation (Miller, 2008, p13-150). Within the Navachab Subgroup of the sCZ the underlying Arandis Formation (or the Okonguarri Formation of the NZ) is locally separated from the Karibib Formation by the Ghaub Formation (the upper section of mapped Arandis Formation may actually represent the Ghaub Formation in some localities – see Miller, 2008 for discussion). Within the Ghaub Formation (<1500 m thickness) up to four members have been identified consisting of dropstones in thinly bedded siliciclastic rocks passing upwards into a variety of basic volcanics (Hoffmann *et al.*, 2004; Miller, 2008). This formation,

dated at 635.5 ± 1.2 Ma represents a second world-wide Marinoan glacial event and is correlated with the Petite Conglomerate of the Kundelungu System in the DRC (Hoffman *et al*., 2004). The Karibib Formation, present from the NZ across to the sCZ shows considerable facies changes, however within the sCZ broad zones can be correlated over tens of kilometres (Miller, 2008). In the nCZ and part way into the sCZ, the Karibib Formation (<1800 m) is subdivided into the Harmony Member, the Otjongeama Member, and the uppermost Arises River Member, of which all are marble- ± calc-silicate-dominated (Lehtonen *et al.* 1993, 1996). The upper two members of the nCZ Karibib Formation extend a little way into the sCZ where the formation is described as consisting essentially of different types of marble showing a large degree of lateral variation (Klein, 1980a). The Onguati Member (Badenhorst, 1992) is confined to the northern edge of sCZ and forms a local top to the formation. Henry (1992) interpreted deposition of the Karibib Formation in a shelf environment whilst the turbidites of the Tinkas Formation (<1000m thickness), straddling the Okahandja Lineament and not present in this study area, are lateral equivalents (Porada and Wittig, 1983; Miller, 2008). In the nCZ, the Kuiseb Formation schist (up to 5000 m thick) is pierced by numerous marble domes and granite plutons (Badenhorst, 1992; Miller, 2008). In the sCZ, this formation (locally >3000 m thick) consists largely of variably bedded biotite-schist occurring in irregularly shaped synforms of which many are almost filled with lopolithic bodies of Damaran granite (Miller, 2008). In the area of the Kranzberg syncline between Karibib and Usakos, Owen (2011) describes a four-unit coarsening-upward meta-turbidite stratigraphy. Kuiseb Formation sedimentation has been attributed to suppression of the Karibib shelf environment by a major fine-grained siliciclastic influx (Henry, 1992), to an accretionary prism environment (Kukla and Stanistreet, 1991) and to sedimentation during basin closure (Owen, 2011). Miller (1983) interpreted the Ghaub, Karibib and Kuiseb Formations as representing a change in sedimentary environment to a passive continental margin.

The only precise age obtained from the stratigraphy overlying the Chuos Formation in the CZ is a U-Pb single zircon from volcanic ash in the Ghaub Formation of the sCZ dated at 635.5 ± 1.2 Ma (Hoffman *et al*., 2004). The above geochronology dating the onset of rifting and deposition of the Nosib Group at ~750 Ma combined with the interpretation of the Chuos Formation as part of the world-wide Sturtian glacial event at ~710 Ma constrains the deposition of the Etusis, Khan and Rössing Formations to between around 750 and 710 Ma.

1.2.3 Structure

During its early evolution, the sCZ is interpreted to have occupied a horst region between two ocean basins and the nCZ the southern margin to the northernmost basin (Chapter 1.2.1). Oblique subduction-collision resulted in large-scale northeast over southwest transpressive deformation and formation of dome structures with a northeast elongation (Downing and Coward, 1981; Oliver, 1994; Miller, 2008). Gray *et al.* (2008) argue however that there is insufficient evidence for oblique movements. Kisters *et al.* (2004) propose that at shallow crustal levels orogen-normal shortening and crustal thickening was facilitated by folding and NE-directed thrusting whilst deeper levels of the CZ underwent pure shear deformation with lateral orogen-parallel stretch. Detachment of the downgoing slab in the back-arc region of the nCZ may have caused mantle upwelling and the necessary heat for the generation of voluminous syn- to post-orogenic plutonic activity (Miller, 2008). The present configuration of the nCZ is interpreted by Miller (2008) as a pop-up structure. The sCZ is bounded by the northern graben-bounding Omaruru Lineament to the north (this continues northeastward as the Cretaceous Waterberg Fault) and possibly southern graben-bounding Okahandja Lineament to the south, across which major downfaulting occurs to the southeast. North-northeast lineaments including the Welwitschia Lineament kink the otherwise northeast-dominant structural trend (Corner, 1981, 2008; Miller, 2008). The sCZ is interpreted as the root zone of the active continental margin of the overriding Congo Craton (Stanistreet, 1991; Miller, 2008).

In the Abbabis Metamorphic Complex any pre-Damaran age deformation has generally been overprinted by Damaran orogenesis, however in the Tumas and Abbabis inliers an earlier foliation has been noted (Smith, 1965; Bunting, 1977; Jacob *et al.*, 1983). Poli (1997) described pre-Damaran structures in the Abbabis Complex at the Nose Structure and Namibfontein-Vergenoeg Dome. Within the Damaran sequence the number of interpreted phases of deformation varies between different workers (e.g. Blaine, 1977; Jacob *et. al.*, 1983; Sawyer, 1981) however between these descriptions D_2- and D_3-related are evidenced with the acknowledgement that a poorly defined D_1 phase preceded these (Longridge, 2012).

In both the nCZ and sCZ earliest F_1 folds and S_1 foliation are refolded by coaxial F_2 recumbent folds with boudinaged limbs where in the sCZ the sense of vergence ranges from southeast- through south to southwest (Smith, 1965; Klein, 1980a and b; Haack *et al.*, 1980; de Kock, 1989; Downing and Coward, 1981, 1983). In the sCZ D_2

overprinting generally renders the identification and orientation of such F1 folds as speculative. However, the outcrop of the Khan Formation across Rössing Mountain, west of the project area, is interpreted to demarcate an F_1 fold axial trace (Smith, 1965; Miller, 2008). Infolding of basement (e.g. Jacob *et al*., 1983) and thrusting (Klein, 1980a; Downing and Coward, 1981) accompanied D_2 deformation throughout the CZ. D_2 in the southwestern CZ is expressed as kilometre-scale south- to southeast-verging folds and shear structures whilst in the Karibib area, it is characterised by northwest-verging folding and thrusting and lower metamorphic grade and probably occurred at higher crustal levels (Kisters *et al*., 2004; Longridge, 2012).

D_3 in the Central Zone is associated by most workers with the development of dome structures (Figure 1.8) where in the sCZ these are strongly northeast-trending and associated with upright- southeast-verging, moderately plunging generally coaxial (with F_2) folds which represent the dominant structural trend (e.g. Smith, 1965; Klein, 1980a; Sawyer, 1981; de Kock, 1989). These dome structures can be cored by lithologies of the Abbabis Metamorphic Complex, as in the Abbabis and Palmenhorst domes (e.g. Brandt, 1987; Longridge, 2012), by Damaran metasediments as in the Rössing SJ Dome (e.g. Oliver and Kinnaird, 1996), by Damaran granites as in the Namibfontein Dome (e.g. Poli and Oliver, 2001) or by two or more of these. The origin of the D_3 dome structures has been attributed to various processes acting either in isolation or in combination. Examples include dextral shearing and concomitant lateral shortening and dome rotation (Klein, 1980a) and diapiric upwelling of Karibib marbles (Miller, 2008) in the nCZ, and solid-state diapirism of basement gneisses or magmatic ballooning of intrusives (e.g. Sawyer, 1981; Kröner, 1984), single phase progressive or multiphase interference folding with or without a component of basement doming (e.g. Smith, 1965; Barnes, 1981; Jacob *et al*., 1983; Oliver, 1994) and metamorphic core complex development (Oliver, 1995) in the sCZ. Orogen-parallel mid-crustal extensional detachments resulting from orogen-normal constriction, are interpreted to have formed during D_3 at the basement-cover interface, evidenced by a metamorphic gap between basement and cover (Poli, 1997; Poli and Oliver, 2001).

The north-northeast-trending Welwitschia Lineament of Corner (1981; Figure 1.5) in the sCZ represents the regional expression of a poorly constrained D_4 episode of sinistral faulting and thrusting interpreted in the Rössing area from remotely sensed and geophysical data by Anderson and Nash (1997) and termed the 'Welwitschia

Trend' by Basson and Greenway (2004). Corner considered the lineament to occupy a 30 km wide zone with left-lateral (sinistral) strike-slip movement along the lineament as suggested by its truncation of the N-trending Okahandja Lineament. Oliver (1994) suggests sinistral movement along the Omaruru Lineament to have caused overturning of the southwestern and northwestern margins of domes.

The initiation of subduction of the SZ beneath the CZ and corresponding D_1 deformation north of the Okahandja Lineament is placed between 600-565 Ma (Miller, 2008). Miller (2008) places D_2 deformation in the sCZ between 565-546 Ma however syn-D_2 U-Pb intrusion and partial melt ages in the range 520-510 Ma obtained by Longridge (2012; Chapter 4) suggest younger ages consistent with the 514 ± 22 Ma age of Haack *et al*., (1980) for syn-D_2 early non-porphyritic granites and leucogranites in the northern Central Zone. D_2 deformation in the Karibib area may have been earlier as evidenced by the post-D_2 539 Ma age of the Rotekuppe Granite (Longridge, 2012). D_3 is placed at about 480-460 Ma and 542 Ma in the nCZ and sCZ respectively by Miller (2008). In the sCZ uraniferous alaskites are emplaced into the hinge zones of upright D_3 folds east of the Ida Dome and at the Rössing Mine (Nash, 1971; Longridge, 2012). Uraniferous alaskites from Goanikontes and Rössing have age data ranging 510-508 Ma (Chapter 1.2.5) suggesting a younger timing for D_3. The similar inferred ages for D_2 and D_3 suggests a single continuum of deformation (Longridge, 2012).

1.2.4 Metamorphism

Metamorphic zonation in the Damara Belt reflects a paired belt where low-temperature moderate-pressure kyanite facies assemblages occur on the subducting Kalahari plate in the SZ and SMZ proximal to the palaeocollisional zone and were overridden by high-temperature, low-pressure, cordierite-sillimanite facies assemblages associated with voluminous syn- to post-tectonic granites of the CZ, which formed the palaeo-active margin of the Congo plate (Kasch, 1983; Puhan, 1983; Miller, 2008; Figure 1.7). Metamorphic grade in the CZ has generally been interpreted to increase toward the coast where it reaches granulite facies (Puhan, 1983; Masberg *et al*., 1992; Goscombe *et al*., 2004; Figure 1.7). However, this is a simplistic model that is at least partly challenged by the observations of Buhn *et al.* (1995) where peak metamorphic conditions in the Otjosondu area northeast of Windhoek have been shown to be within error with those determined in the Goanikontes area (Nex *et al*., 2001a; Longridge, 2012). The main Damaran metamorphism has generally been considered to be post-tectonic (post-D_3) in age

and designated M_2 in recognition of an earlier event, however there is disagreement between studies on the relative timing of M_1 and M_2 in the CZ (Nash, 1971; Nex *et al*., 2001b; Miller, 2008; see Table 1.4 and text below). In the SMZ and SZ two distinct pulses are well constrained by mineral assemblages indicating M_2 pressures were up to 2 kbar lower than M_1 pressures (Kasch, 1983).

Within the Abbabis Metamorphic Complex the Damaran metamorphic overprint was such that any Abbabis age mineral assemblages may not be preserved (Miller, 2008). However Poli (1997) estimated P-T conditions in the Namibfontein Dome to be higher than in the Damaran cover, based on garnet-biotite thermometry. The documented presence of kyanite by Gevers (1931) in the Abbabis Inlier may support higher metamorphic grades in the basement, however such examples require further verification.

Table 1.4. Summary of interpreted timing and P-T conditions of metamorphic events of the Central Zone.

Author(s)	Methodology (location)	Age	P-T Conditions	Interpretation
Jung & Mezger (2003), Ward *et al.* (2008)	Garnet-cordierite metapelite mineral chemistry, U-Pb monazite & Sm-Nd garnet geochronology (lower Khan River) & mineral geochemistry of garnet-cordierite leucosomes in Kuiseb schists (Rössing area)	525-504 Ma	700-750 °C, ~5 kbar	Peak metamorphism
Longridge (2012)	U-Pb zircon & monazite geochronology of garnet-bearing leucogranites emplaced into and folded by F_2 structures & anatectic leucosomes (Palmenhorst Dome)	520-508 Ma		M_2 (syn-D_2)
Longridge (2012)	U-Pb geochronology of anatectic red granites (including Goanikontes) dated by Briqueu *et al.* (1980) & Longridge (2012)	539-534 Ma		M_1
Nex *et al* . (2001b)	Post granite emplacement garnet-biotite geochemistry (Goanikontes)	534-508 Ma	700 ± 50 °C, 4 ± 1 kbar	Late M_2 thermal overprint
Nex *et al.* (2001b)	Goanikontes anactectic red granite published U-Pb geochronology, petrography & mineral geochemistry of spinel-sillimanite-cordierite symplectites (Goanikontes)	Immediately post 534 ± 7 Ma	527 ± 112 °C, 4 ± 1 kbar	Early M_2 crustal decompression (post-D_3)
Nash (1971)	Petrography, phase equilibria		675-750 °C, 3-5 kbar	M_2 (syn-D_3)
Nash (1971), Jacob (1974), Downing (1982) Blaine (1977), Cuney (1980a), Sawyer (1981), Bühn *et al.* (1995), Miller (2008)	Petrography, phase equilibria (e.g. Nash, 1971), fluid inclusions (Cuney, 1980; Bühn *et al.* 1995)	>568 Ma (Miller, 2008)	660-700 °C, 5-8 kbar	M_1 (pre-D_3)

Early studies distinguished M_1 in the CZ where staurolite is observed to predate sillimanite (Nash, 1971; Jacob, 1974; Downing, 1982) and sillimanite knots are observed flattened in S_1 (Blaine, 1977; Sawyer, 1981). Maximum P-T conditions during M_1 metamorphism were estimated in the Rössing area by Nash (1971) as +700 °C and 6-8 kbar whilst M_1 peak pressures have been estimated at 5-8 kbar from fluid inclusion studies at Rössing and Otjosondu in the northeast CZ (respectively Cuney, 1980a and Bühn *et al*., 1995). The approximate timing of initiation of M_1 across the Damara Belt is inferred by Miller (2008) to be pre-565 Ma based on the established timing of D_1-D_2 and related deformation of interpreted M_1 index minerals.

Nex *et al.* (2001b) place early M_2 metamorphism as post-D_3 in the sCZ as recorded by the intrusion of an anatectic foliated red granite in the Goanikontes area dated at 534 ± 7 Ma (Briqueu *et al*., 1980; Miller, 2008). Thermobarometry of spinel symplectites interpreted to immediately post-date this event has determined P-T conditions of 527 ± 112 °C and 4 ± 1 kbar (Nex *et al*., 2001b). M_2 thermal overprinting and migmatisation in association with biotite breakdown and garnet growth at 700 ± 50 °C and 4 ± 1 kbar is related by these authors to post-534 ± 7 Ma, pre-508 ± 2 Ma granitoid emplacement. However the 534-508 Ma ages are interpreted by Longridge (2012) to date the early M_1 event due to the presence of syn-D_2 garnet-bearing leucogranites and shear zone-hosted anatectic leucosomes dated at 520-514 Ma and 511-508 Ma respectively in his study. The anatectic leucosomes are interpreted to result from partial melting of pelitic metasediments. Thermobarometry conducted by Ward *et al*. (2008) of garnet- and cordierite-bearing leucosomes within the Kuiseb Formation of the project area indicates granulite-facies peak conditions reached 750 °C and 5 kbar. This is consistent with results obtained by Jung and Mezger (2003) from unmigmatised garnet-cordierite metapelites in the lower Khan River area where thermobarometric data indicates P-T conditions of 700-750 °C and ~5 kbar between 525 ± 2 Ma and 504 ± 3 Ma; in the same study Sm-Nd garnet ages from migmatite restitic melanosomes of 518 ± 3 Ma lend further support to partial melting during M_2. Haack *et al*., (1980) considered peak metamorphism in the nCZ may have been late- to immediately post-D_2, however Jung *et al*. (1999) have shown that migmatisation associated with granitoid intrusion occurred around 500 Ma with P-T conditions of 700 °C at 4-5 kbar.

In summary of the above (see Table 1.4), an early M_1 event appears widely recognisable however there is considerable disagreement in the timing, mineral

paragenesis and hence P-T conditions reached during M_1 metamorphism. There is agreement that peak M_2 metamorphism at least spanned 520-504 Ma. Regardless as to the nomenclature of the metamorphic pulses, a pressure decrease in the CZ is apparent in the data and this is consistent with that seen in the SZ and SMZ (Kasch, 1983). Nex *et al.* (2001b) envisaged their late M_2 high temperature event as regional scale contact metamorphism resulting from voluminous granitoid intrusion. The associated extensive migmatisation occurred both in pre-Damara basement and in the metasedimentary cover with effects particularly pronounced in quartzofeldspathic units such as within the A.M.C. (for example in the Palmenhorst Dome) and Nosib Group but also within pelitic units such as the Kuiseb schist where migmatites have formed from both partial melting and injection of granite veins around intrusions (Jung *et al*., 1999; Miller 2008). Most lithologies within the CZ show a high degree of recrystallization and annealing resulting in polygonal granoblastic textures (Nex *et al*., 2001b).

1.2.5 Plutonism

Granitic rocks constitute >99% of the syn- to post-tectonic Damaran Plutonic Suite which covers more than 74,000 km^2 of the Damara Belt, dominating the palaeo-active margin of the CZ and extending northwards into the NZ. The Donkerhuk Granite forms a major post-orogenic batholith along the northern edge of the SZ directly in front of the leading edge of the Congo Craton (Miller, 2008). The granitic intrusions are weakly peraluminous with low abundances of high field strength elements and initial Sr isotope ratios indicating they are crustally derived (McDermott, 1986; McDermott *et al*., 1989, 1996).

Brandt (1985) classified this syn- to post-tectonic plutonic suite into five major groups which are shown in Table 1.5 with the addition of the Goas Intrusive Suite of Lehtonen *et al*., 1995 forming a less volumetrically significant basic suite of magmatism. According to Miller (2008) in the sCZ the sequence of intrusion is gabbro-diorite-porphyritic biotite granite-leucogranite, whilst in the nCZ there are two cycles of diorite-porphyritic biotite granite-leucogranite intrusion. Miller (2008) interprets that the locus of specific granite types is strongly controlled by stratigraphy.

The Salem type granites are a poorly-defined suite of pre-, syn- and post-tectonic granodiorites, granites and adamellites principally classified based on their porphyritic texture with published ages ranging 720-510 Ma (Kröner, 1982; Downing, 1982; Allsopp *et al*., 1983; Marlow, 1981, 1983; Hawksworth et al., 1983; Brandt,

1985; Johnson *et al*., 2006, Milani *et al*, 2014). The most abundant rock types are coarse-grained, porphyryitic biotite granites occurring as large plutons in synformal areas (Miller, 2008), however a large spectrum of compositions exist (Table 1.5). The Goas Intrusive Suite was named by Lehtonen *et al.* (1995) to diorites south of Karibib containing metagabbroic xenoliths. Goas magmatism has been shown to occur between 580 and 545 Ma (Table 1.5) and so may be contemporaneous with some of the younger Salem granites as suggested by descriptions of gradational contacts between the two suites (Sawyer, 1976; Jacob *et al*., 2000; Milani *et al*, 2014). Nd-Sm data indicates that the Goas Suite is sourced in ~2 Ga old crust with no juvenile component, whilst the Salem suite is sourced from Kibaran age crust rather than from Damaran sediments (J. Kinnaird, Pers. Comm. with permission from Rio Tinto Exploration). A SHRIMP U-Pb zircon age of 557.2 ± 7.4 Ma obtained from an amphibolite intruding Abbabis Metamorphic Complex gneisses in the Khan River area by Longridge (2012) also appears to represent Goas magmatism.

Brandt's (1985) distinction of red granites into homogeneous and inhomogeneous (gneissic) sub-types is not applied by all workers (e.g. Sawyer, 1976; Miller, 2008). The distribution of the inhomogeneous gneissic type in the western part of the CZ, confined to the Nosib Group or pre-Damaran basement (Table 1.5) may be suggestive emplacement of the same granite at lower crustal levels (Longridge, 2012), where it is considered to be the product of *in situ* partial melting of the host lithologies (e.g. Smith, 1965; Jacob, 1974). At Goanikontes and wider area of the Palmenhorst and Ida domes, red foliated granites (homogeneous red granite in the terminology of Brandt, 1985) are syenogranite in composition and predate grey, predominantly monzogranite (Nex *et al*., 2001a; Longridge, 2012) with respective ages determined by Briqueu *et al.* (1980) of 534 ± 7 Ma and 517 ± 7 Ma (Table 1.4). These are syn-D_2 granites and both are generally older than alaskites (Nex *et al*., 2001a; Longridge, 2012).

*Table 1.5. Damaran-age plutonic rocks of the Central Zone as grouped by Brandt (1985) with the addition of the Goas Intrusive Suite. *Leucogranite of Marlow (1981); **Red Gneissic Granite of Smith (1965), red granite-gneiss of Jacob (1974), red granite of Marlow (1981).*

Intrusive	Description	Geochronological Data
Alaskite (otherwise referred to as leucogranite, sheeted leucogranite, pegmatitic leucogranite)	Syn- to post-tectonic sheets at various stratigraphic levels, mainly confined to western part of CZ (Brandt, 1985); fine-grained aplite to pegmatitic (Smith, 1965; Marlow, 1981)	**508 ± 2** and **509 ± 1 Ma** (Briqueu *et al*., 1980; concordant monazite and uraninite respectively, alaskite from Goanikontes). **510 Ma** (Kröner, 1982; Rb-Sr whole rock, Rössing alaskite). **458 ± 8 Ma** (Hawksworth *et al*., 1983; Rb-Sr whole rock, Rössing uraniferous alaskite). **495 ± 12 Ma** (Hawksworth *et al*., 1983; Rb-Sr whole rock, Valencia uraniferous alaskite) **518 ± 2 Ma** (Kinny *et al.,* 1994; sphene, Khan Mine 'pegmatite') **520.3 ± 4.6** Ma (Longridge *et al*., 2012; SHRIMP U-Pb zircon, syn-D_2 garnet bearing Ida Dome alaskite). **526 ± 34** Ma (Longridge, 2012; SHRIMP U-Pb zircon, pre-D_3 Ida Dome alaskite possibly C-Type of Nex, 1997)
Post tectonic granites*	Post-tectonic, stocks or plutons, e.g. Donkerhuk, Gawib, Achas, Bloedkoppie & Kubas granites (Brandt, 1985); homogeneous, unfoliated, may be pegmatitic (Smith, 1965)	**505 ± 4 Ma** (Kukla *et al.*, 1991; Donkerhuk granite)
Red and grey homogeneous granites*	Syn-tectonic, no stratigraphic constraint (Brandt, 1985); Longridge (2012) suggests red granites predate D_2 grey granites syn-D_2 deformation	**534 ± 7** to **517 ± 7** Ma (Briqueu *et al.*, 1980; U-Pb, Goanikontes red granite). **542 ± 6** Ma (Tack *et al*. 2002; SHRIMP U-Pb, Ida Dome grey granite). **520.2 ± 4**.2 and **519.1 ± 4.2** Ma (Longridge *et al*., 2008; SHRIMP U-Pb zircon, grey granite); **535-540** Ma (Longridge, 2012; monazite and lower intercept zircon ages, Palmenhorst Dome red granite)
Red inhomogeneous granites**	Syn-tectonic, confined to western part of CZ with the Nosib Group or Abbabis basement (Brandt, 1985); red banded gneiss with metasedimentary xenoliths in anticlinal structures (Smith, 1965; Jacob, 1974); K-feldspar-rich with little ferrogmagnesian component (Marlow, 1981)	
Goas Intrusive Suite	Diorite with metagabbroic xenoliths (Lehtonen *et al.*, 1995); possible quartz diorite and diorite gneiss of Smith (1965) and calc-alkaline diorites of McDermott (1986); fine- to medium-grained, equigranular and foliated (Miller, 2008)	**564 ± 5** Ma, **546 ± 6** Ma (Jacob *et al.*, 2000), **558 ± 5 Ma** (de Kock *et al*., 2000), and **552 ± 1** Ma (Jung *et al.*, 2002), **557.2 ± 7.4** Ma (Longridge, 2012; SHRIMP U-Pb zircon, amphibolite dyke cross-cutting A.M.C. basement gneisses of Khan River), **580-545 Ma** (Milani *et al.,* 2014; LA-ICP-MS zircon U-Pb, Audawib and Neikhoes metagabbro, Gamikaub diorite, Oamikaub granodiorite and granite, Okongava diorite with Okatuwo dioritic enclaves, Mon Repos quartz-monzonite and Palmental monzonite)
Salem granites	Pre-, syn- to post-tectonic granites, varying grain size, porphyritic, grey (Brandt, 1985); mainly confined to synclines of Kuiseb Formation (Smith, 1965; Miller, 2008); non-porphyryitic gneissic granite (oldest), porphyryitic biotite granite and non-porphyritic leucogranite (oldest) of Jacob (1974); includes granodiorite and adamellite (Marlow, 1981)	**720-510** Ma including **549 ± 11 Ma** (Johnson *et al.,* 2006; LAM-ICP-MS U-Pb, syn-tectonic granite), **542-511 Ma** (Milani *et al.*; 2014, LA-SF-ICP-MS zircon U–Pb, NZ Salem-type granites).

Alaskite intrusions, generally intruded as sheets, may be barren or host primary and secondary uranium mineralisation (Chapter 1.2.6). They may be concordant or cross-cutting, sometimes composite bodies, with highly variable grain size and widths ranging up to >100 m. Intrusions may take the form of swarms of bodies concordant to the host metasediment gneissosity or bedding as at Rössing SJ (Berning *et al*., 1976), as cross-cutting en-echelon tension gash fills as at Rössing SK and Goanikontes (Laberge 2008a; Nex, 1997), or as small stock-like bodies as at Rössing SH and Valencia (Mestres-Ridge, 1991; Freemantle, 2012). The alaskites range in composition from granodiorite, through monzo- and syenogranite, to alkali feldspar granite and uranium mineralised bodies tend to be more alkalic (Kinnaird and Nex, 2007; Freemantle, 2012). Major element geochemical data compilation from various uranium deposits by Kinnaird and Nex (2007, and references therein) and Freemantle (2012) show the alaskites to be generally weakly metaluminous to peraluminous, whilst some major and trace element affinities are shared with A-type granites (Mestres-Ridge, 1992; Nex *et al*., 2001a) and S-type granites (Freemantle, 2012). The major element geochemistry and accessory mineralogy of alaskites is strongly influenced by the composition of the host lithologies (Freemantle, 2012). At Goanikontes, Nex (1997) classified the alaskites into six subtypes on the basis of structural and mineralogical characteristics where the latter three, including uranium-mineralised sub-types D-E are interpreted to post-date D_3 deformation (see Chapter 6.2). Freemantle (2012) subsequently extrapolated the same scheme to other deposits in the district including Valencia where five alaskite generations are identified. Freemantle (2012) observed that across a range of deposits mineralised alaskites tend to lack significant visible accessory phases.

Syn- to post-D_3 alaskite, grey granite (leucogranite) and syeno-monzogranite in the Ida Dome area, anatectic red granite in the Goanikontes area and the Rotekuppe Granite in the Navachab area have yielded ages ranging 542-519 Ma (Marlow, 1983; Tack *et al*., 2002; Briqueu *et al*., 1980; Jacob *et al*., 2000; Longridge, 2012). Whole rock Rb-Sr dating of alaskites at the Rössing uranium mine show two groups of ages at 510 Ma (Kröner, 1982) and 458 Ma (Hawksworth *et al*., 1983) with contrasting initial strontium ratios. The younger age group likely represents subsolidus re-equilibration (e.g. Miller, 2008) however Bowden *et al.* (1995) suggest either repeated pulses of intrusion and/or prolonged hydrothermal activity may have delayed closure of Rb-Sr mineral blocking temperatures. Longridge (2012) obtained a SHRIMP U-Pb age of 520.3 ± 4.6 Ma for a garnet-bearing alaskite at Ida Dome.

Briqueu *et al*. (1980) dated mineralised alaskites at Goanikontes (Etango Project, Figure 1.1) at 508-509 Ma (concordant monazite and uraninite).

The youngest intrusive rocks of the sCZ include the Cretaceous Henties Bay syenite and numerous northeast-trending dolerite and subordinate acidic dykes of Jurassic and Cretaceous age. These are related to continental fragmentation and the opening of the South Atlantic (Lehtonen *et al*., 1996; Trumbull *et al*., 2007).

1.2.6 Mineralisation Associated with Pegmatites and Alaskites

Syn- to post-tectonic pegmatite-hosted mineralisation in the CZ consists of lithium-beryllium-semi-precious stone pegmatites of the Karibib-Swakopmund-Omaruru area and tin pegmatites occurring in three northeast-trending belts in the nCZ: Sandamap-Erongo, Nainais-Kohero and Cape Cross-Uis (Uis Mine 60 Mt grading 0.13% Sn). Variably pegmatitic alaskite[4] intrusions host economic to sub-economic uranium mineralisation at Rössing, Rössing South (occurring under shallow overburden), Valencia, Ida Dome and Goanikontes (Etango Project; Figure 1.1). For detailed descriptions covering most of these deposits the reader is referred to Röesener and Schreuder (1994) and more recently Freemantle (2012). The alaskites were emplaced at deeper stratigraphic levels and more proximal to the palaeo-subduction zone than the tin-bearing pegmatites (Miller, 1992a, 1992b). Grade-tonnage information of the more important alaskite-hosted uranium deposits in the district at the time of writing is shown in Table 1.6 below.

The geology and controls of alaskite-hosted uranium mineralisation of the sCZ at Rössing and the nearby Valencia, Ida Dome and Goanikontes deposits were summarised by Kinnaird and Nex (2007) whilst the recently discovered Rössing South deposit has been described by Spivey *et al.* (2010). The work of Freemantle (2012) has further refined the petrological and geochemical characteristics of alaskite-hosted uranium across the district.

[4] 'Sheeted leucogranites' in the terminology of some workers - see footnote[1]. As per the comments of Nex *et al*. (2001a, p496 and references therein), the alaskites (or sheeted leucogranites) are not pegmatites *sensu stricto*, however the majority of intrusions are pegmatitic.

Table 1.6. Grade tonnage data of alaskite-hosted uranium deposits of the south Central Zone of the Damara Orogen, the location of which are shown in Figure 1.1. 1 – Rio Tinto 2013 Annual Report note that production to end 2012 was 123.5 Kt U_3O_8 (rossing.com) and this is shown for context; 2 - Spivey et al. (2010); 3 - bannermanresources.com; 4 – forsysmetals.com; 5 – Extract Resources 2008 press release; 6 – deepyellow.com. Note that all reserve and resource calculations apply a 100 ppm cut-off except Ongolo (250 ppm) and Rössing (not stated).

Deposit	Reserves		Resources						Total U_3O_8 (Kt)
	Total (Mt)	U_3O_8 (ppm)	Measured (Mt)	U_3O_8 (ppm)	Indicated (Mt)	U_3O_8 (ppm)	Inferred (Mt)	U_3O_8 (ppm)	
Rössing SJ[1]	148	320	9.4	260	122	230	12	200	**80** (+123)
Rössing Z20[1]	-	-	-	-	87	280	115	260	**54**
Rössing South Zone 1[2]	-	-	-	-	21	527	126	436	**66**
Rössing South Zone 2[2]	-	-	-	-	-	-	102	543	**55**
Etango (Goanikontes)[3]	-	-	62.7	205	273.5	200	45.7	202	**77**
Valencia[4]	-	-	18.6	172	140.2	158	15.3	163	**28**
Namibplass[4]	-	-	-	-	-	-	88	130	**11**
Ida Dome[5]	-	-	-	-	0.6	246	52.7	213	**11**
Ongolo[6]	-	-	7.7	395	9.5	372	12.4	387	**11**

Primary magmatic uranium mineralisation is dominantly as microscopic uraninite as at Rössing SJ (e.g. Beukes and Hiemstra, 1968) and Rössing South (Spivey *et al*., 2010), although locally the refractory pyrochlore-group mineral betafite may dominate as in the Rössing SH area (Herd, 1996). The highest primary uranium grades tend to be associated with biotite-rich zones as noted by various Rössing workers within alaskite and by Spivey *et al.* (2010) at Rössing South (up to 2000 ppm U_3O_8 in zones >50% coarse biotite). Primary uranium mineralisation is ubiquitously hosted by alaskites at Rössing whereas at Rössing South hydrothermal fluids exsolved from the intruding sheets may account for a component of mineralisation in country rock (Spivey *et al*., 2010). At Goanikontes, Nex *et al*. (2001a) report that where uranium or thorium levels are <20 ppm, the radiogenic elements occur in accessory monazite or zircon. Secondary uranium minerals at Rössing are dominantly betauranophane and/or uranophane and form a substantial component of the overall uranium budget (e.g. Kinnaird, 2005). However, Freemantle (2012) suggests coffinite to be the dominant secondary phase at Goanikontes and Valencia whilst at Rössing South this may be boltwoodite (Spivey et al., 2010). The formation of secondary uranium mineralisation has been attributed to both supergene (e.g. Bowden et al., 1995) and hypogene (e.g. Freemantle, 2012) processes. The latter is inferred by Freemantle (2012) given that uranyl-oxide hydrates do not readily mobilise uranium in meteoric fluids (Korzeb et al., 1997). However, mobilisation of uranium due to weathering processes appears clearly evidenced by the presence of a 100 m thick leached zone

in the upper part of the ore bodies at Rössing South where grades may be depleted by up to 40 percent (Spivey *et al*., 2010). At Goanikontes, halos of uranophane occur on magnetite grains (Freemantle, 2012). Further primary uranium mineralisation in the district locally occurs as skarns and skarn xenoliths at Valencia, Holland's Dome and Ida Dome and within fluorite veins in the Rössing South area (Freemantle, 2012).

Alteration in mineralised alaskites has been documented by various workers. Sodic (albite) alteration has been described in the Rössing area by Kerr (1990) and Mestres-Ridge (1994), and in the Goanikontes and Ida Dome areas by Freemantle (2012). The sodic alteration is generally described as albite overgrowths and late exsolution textures. Potassic alteration is also reported by Kerr (1990) and by Freemantle (2012) where the latter describes the presence of late fine-grained K-feldspar. Freemantle (2012) describes further alteration as consisting of silicification and quartz veining, introduction of fluorite, development of secondary uranium phases (see above) and intensive chloritisation of biotite. The presence of hydrothermal alteration is supported by fluid inclusion studies by Nex *et al*. (2001a) at Goanikontes and Nex *et al.* (2002) at Rössing SJ and presence of hydrothermal uraninite interpreted by Ryan (2010) at Rössing SJ (Chapter 7.2.1).

A number of key controls may exist in the localisation of uranium mineralisation in the alaskite sheets. A stratigraphic control is apparent in that all significant volumes of uraniferous alaskites have intruded close to the Khan-Rössing Formation boundary (Marlow, 1981; Jacob *et al*., 1986; Kinnaird and Nex, 2007) or within the Rössing Formation itself as at Rössing South (Spivey *et al*., 2010). In the case of Goanikontes where the Rössing Formation is partly missing, uraniferous alaskites intrude the contact zone of the Khan-Chuos Formations (e.g. Kinnaird and Nex, 2007). At Valencia, mineralised alaskite sheets intrude an attenuated Damaran sequence from the Etusis right through to the Kuiseb Formation (Freemantle, 2012) whilst at Rössing South, Zone 1 mineralised alaskite sheets occur within Chuos Formation hanging wall. There is no clear major or trace element geochemical control or thermometric fluid inclusion difference between mineralised and barren intrusions (Kinnaird and Nex, 2007) however the geochemistry of sheets may be influenced by the entrainment of host lithologies (Freemantle, 2012). A geochemical redox contrast exists between quartzofeldspathic iron oxide-bearing metasediments of the Khan Formation and quartzofeldspathic and carbonate-, graphite- and iron sulphide-bearing metasediments of the upper Khan Formation and Rössing Formation

(Marshall, 1973; Hiemstra, 1971; Cuney, 1980b; Kinnaird and Nex, 2007; Freemantle, 2012) that may facilitate reduction of U^{6+} uranyl complexes. At the Ida Dome, Corvino and Pretorius (2013) highlight the likely importance of both the presence of iron sulphides as a chemical trap where the bulk of uraniferous alaskite is hosted by sulphide-bearing biotite schist, combined with the structural geometry of the layers containing them. According to Kinnaird and Nex (2007) uranium deposition occurred as the alaskite magmas cross-cut this contact zone during metamorphism and release of CO_2, particularly where decarbonation of marbles increased CO_2 concentration in the vapour phase leading to magma boiling. The rheological characteristics of a thick marble-bearing sequence of Rössing Formation lithologies may, as suggested by many workers, strongly influence ponding of voluminous alaskite intrusions and it follows that the Karibib Formation likely plays a similar role where marble units in the Rössing Formation are poorly represented as at Rössing South (Spivey *et al*., 2010).

At Holland's Dome (southeast Ida Dome) alaskites intruded throughout the Khan Formation but are only mineralised with associated extensive skarn development at the contact with Rössing Formation marbles (Freemantle, 2012). Uraniferous skarns occur to a lesser extent at Hildenhof and Valencia (Freemantle, 2012).

The emplacement of mineralised sheets has been suggested to relate to the transition from ductile to brittle deformation (Basson and Greenway, 2004) whilst the structural setting of individual deposits differ widely (Freemantle, 2012). The timing of intrusion of mineralised alaskites has generally been interpreted as syn- to post-D_3 where these cut upright F_3 folds at Rössing (Nash, 1971) and at Ida Dome (Longridge, 2012), or dome structures interpreted to have formed during D_3 as at Goanikontes (Nex, 1997). However Basson and Greenway (2004) suggest uraniferous alaskite emplacement at Rössing was associated with north-northeast-orientated D_4 sinistral faulting and dome rotation that provided dilational sites (Anderson and Nash, 1997; Basson and Greenway, 2004; Chapter 1.2.3) where D_4 deformation is related to the regional Welwitschia Lineament of Corner (1981). According to Nex (1997), Nex *et al.* (2001a) and Nex *et al.* (2002) at Goanikontes and the Ida Dome (Figure 1.1) a high strain zone has provided an important control in the emplacement of post-D_3 mineralised alaskites. At Valencia uraniferous alaskites are emplaced into a Z-fold (Freemantle, 2012) where the north-northeast trending fold axial plane may represent a D_4 structure superimposed on the earlier Kuiseb syncline. At Rössing South uraniferous alaskites hosted by the Rössing Formation

are emplaced into a north-northeast trending, west-verging doubly-plunging (domed) Rössing South anticline cored by the Khan Formation where doming is attributed by Spivey *et al.* (2010) to be due to F_3-F_4 fold interference.

Of requisite importance for the generation of uranium-enriched magmas is the presence of upper amphibolite-granulite facies metamorphism (Andreoli *et al.,* 2006), the weakly peraluminous nature of which may increase uranium solubility in the melt (Cuney, 2009). The oblique erosional level of the Damara Orogen is also requisite to the exposure of this high grade metamorphic terrane (e.g. Freemantle, 2012). The ultimate source of such uranium-enriched magmas is unresolved, i.e. a basement source as suggested by Jacob *et al*. (2006) versus partial melting of either the Damaran cover or part of the Damaran Intrusive Suite. This distinction is complicated particularly due to the lower part of the Damaran succession and the basement being isotopically similar as the latter is derived from rapid weathering of the former (Kinnaird and Nex, 2007). At Goanikontes Nex *et al.* (2001a) point out that alaskite intrudes the pre-Damara basement (including uranium-mineralised E type) and only minor effects of partial melting are observable in the Damaran cover, and that the lithologically heterogeneous and anomalously radioactive basement represents a suitable source rock for granitoids and uranium mineralisation. The late uranium enrichment in the sequence of alaskite intrusion suggests a source lithology that has not experienced prior melt extraction otherwise uranium would have been removed at the onset of partial melting, and D_3-associated uplift could have provided a suitable section of uranium-anomalous basement (Jacob, 1978; Haack *et al*., 1983; Nex *et al*., 2001a).

At Goanikontes the close correlation between sheet type and uranium-thorium abundance, supported by linear trends in large ion lithophile plots led Nex *et al.* (2001a) to conclude that the distribution of radiogenic elements is primarily a magmatic feature rather than being due to substantial hydrothermal modification. This is consistent with the assertions of earlier workers in this area (e.g. Jacob, 1974; Bunting, 1977) and is further supported by geochronological data of Briqueu *et al.* (1980) where the U-Pb emplacement age of monazite in uraniferous alaskite at 509 ± 1 Ma is within error of a U-Pb age of 508 ± 2 Ma from uraninite (Table 1.3). Nex *et al*. (2001a) suggest this may not be the case at Rössing where hydrothermal modification may have added sufficient uranium to allow economically viable extraction.

Copper mineralisation may be spatially associated with pegmatitic alaskites, for example at the disused Ida Mine (Ida Dome) and at the Khan Copper Mine southwest of Rössing, where in the latter locality cupriferous 'pegmatites' form concordant bodies in the Khan Formation. Mineralisation is attributed in part to metasomatic processes by Miller (2008) at a pre-existing cupriferous horizon of the Khan Formation (see Chapter 7.3).

The sparse geochronological data suggests alaskite intrusion in the wider Rössing district spanned 520-510 Ma with the intrusion of uraniferous alaskites around 510-508 Ma, where younger Rb-Sr dates likely reflect sub-solidus cooling (Chapter 1.2.5 and Table 1.3). There are few precise ages of uraniferous alaskites as obtaining reliable geochronological ages using the U-Pb system is fraught with problems due to high uranium contents and the consequent metamict nature of zircons (e.g. Longridge, 2012).

Alaskite-hosted uranium mineralisation has been mined at the Rössing SJ open pit since 1976. In order to form the basis of future exploration across the Rössing Mine lease, a detailed mapping project was undertaken integrating historical data with remote sensing, geophysical and field mapping data. Details of the data collection and interpretation are presented in Chapter 2.

Chapter 2: Data Compilation and Interpretation

2.1 Introduction

Figure 2.1 below taken from the paper of Basson and Greenway (2004) provides a useful framework geological map and structural data compilation for the wider project area for the purpose of introducing this chapter. This map largely reflects the geological mapping resolution of the project area at the time the project was initiated.

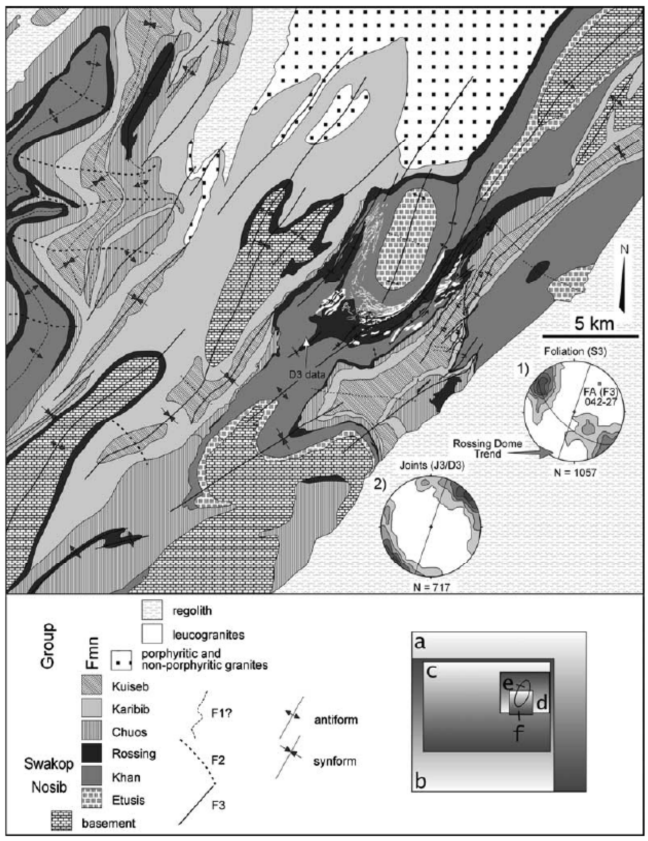


Figure 2.1. Compilation of geological mapping of the Rössing mine area encompassing the work of Basson and Greenway (2004), Smith (1965), Jacob (1974), Anderson and Nash (1997), Oliver and Kinnaird (1996) and Jacob and Kerber (1997); from Basson and Greenway (2004). Contoured equal area, best fit stereonets from Jacob and Kerber (1997) are: (1) S_3 data with best-fit F_3 fold axes of 042–27º; and (2) J_3 joint data, which defines a northwest–southeast trending joint set. The approximate source of this data is indicated as 'D_3 data' on the map – this data is included in this project compilation (see Chapter 2.5.1). Note that the Arandis Formation here is included in the Karibib Formation.

Geological mapping of the entire mine lease area around the Rössing mine had previously been at a regional scale, with segments of the mine lease mapped in detail. The mapping presented in this thesis is based on the compilation and analysis of numerous layers of exploration data. This includes 'historical' data such as

regional- and prospect-scale geological mapping, publications, Rössing Uranium Ltd. and Rio Tinto internal reports, and geophysical and remote sensing hard copy maps recovered from Rössing Uranium Ltd. archives. A major component of this project has been the interpretation of high resolution HyMap hyperspectral remote sensing data which was purchased and processed through the course of this project. Landsat ETM (as shown in Table 2.1), ASTER, 100 m line spacing aeromagnetic data and orthorectified aerial photo mosaics have also been incorporated. This chapter describes these datasets with special emphasis on HyMap hyperspectral imagery. Processing of the hyperspectral data was completed by a consulting specialist in conjunction with ground observations plus spectral analysis and petrography on 113 field and drill core samples. In addition to incorporation of the SJ-SK geological map of Golder Associates (1978) and Laberge (2008a; 2008b), 29 historical geological maps were digitised and incorporated into the attached map where mining activity precluded mapping of exposed geology. 3,773 S_0/S_1 measurements and 9,935 fracture measurements were digitised from previous work. Seventy one sheets of pre-mine development ground radiometric data consisting of 25,000 point scintillometer measurements were digitised and combined with airborne radiometric data to provide a radiometric contour overlay to the attached map. Table 2.1 summarises aspects of data compiled during this project.

Table 2.1. Data compiled throughout the course of the project with notes on application.

Data Type	Specifications	Year	Comments & Applications
HyMap hyperspectral data (lines from block B2)	2 km line spacing, 4.7 m spatial resolution, 126 bands covering 450-2500 µm	2005	Effective resolution of most lithology types but limits to ~1:20K map interpretations
Processed Landsat ETM & ASTER scenes	Max 15 m spatial resolution, 7 & 14 spectral bands respectively	Various depending on scene	Effective for regional lithological and structural discrimination particularly ASTER imagery
Ortho-rectified aerial photo mosaics (ortho-photos)	30 cm spatial resolution	2009	Some reference made to earlier photographic surveys; provide detailed lithological discrimination in natural colour
Airborne magnetics	100 m line spacing, 30 m nominal terrain clearance	2005	Principally referenced Total Magnetic Intensity and First Vertical Derivative grids for structural interpretation
Airborne radiometrics (spectrometer)			K, U & Th data, Th good indication of basement lithologies
Ground radiometrics (scintillometer)	30 m stations on 100 m line spacing or better; 71 sheets digitised	1970s	Definition of pre-mine surface radiometric anomalies where data available (as total count)
Digital Elevation Model	Pre-development SJ area topo survey merged with Fugro airborne data and SRTM data	Various	Used in generation of section profiles on appended map
Historical geological mapping	Various scales	1970s-present	29 map sheets digitised and >4000 structural measurements compiled
Geological mapping (this work)	Ground-truthing of remote sensing data	2010	>1000 mapping points
Sampling (this work)	113 rock samples from surface and drill core	2010	PIMA and TerraSpec analyses for comparison with remotely sensed spectral data and petrography in order to constrain and describe rock units

2.2 Geophysical Data

Detailed (non-regional) geophysical data incorporated into this project comprises both helicopter-surveyed magnetic and radiometric data and historical ground-surveyed scintillometer data.

2.2.1 Airborne Geophysical Data

In May 2005, Fugro were contracted by Rio Tinto Exploration to carry out a 2620 line km magnetic gradiometer and radiometric helicopter-borne survey of the Rössing Mine Lease ML28 and adjacent Accessory Works areas. The survey line spacing was 100 m with a mean planned terrain clearance of 20 m. The magnetic survey used a Midas^{TM}II geomagnetic mapping system employing two horizontally spaced Scintrex caesium vapour sensors with data acquisition at 0.1 seconds (approximately 5 m ground spacing) in conjunction with a CF1 caesium vapour base magnetometer (Fugro, 2005). The spacing of magnetic sensors in a magnetic gradiometry survey permits the measurement of either horizontal or vertical magnetic gradient which allows both for the removal of the regional gradient of the earth's magnetic field or diurnal variations, and the enhancement of the effect of near-surface magnetic sources (e.g. Sharma, 1987). The radiometric survey utilised a GPX256 Exploranium gamma ray detector collecting data every 1.0 second (approximately 50 m ground spacing). Derivatives of the data utilised in this project included Total Magnetic Intensity (T.M.I.) and First Vertical Derivative (1V.D.) grids for the magnetic data, and Total Count (T.C.), K, U, and Th grids and a K-U-Th ternary image for the radiometric data (Figures 2.2 and 2.3a; Fugro, 2005), gridded at quarter line spacing (25 m).

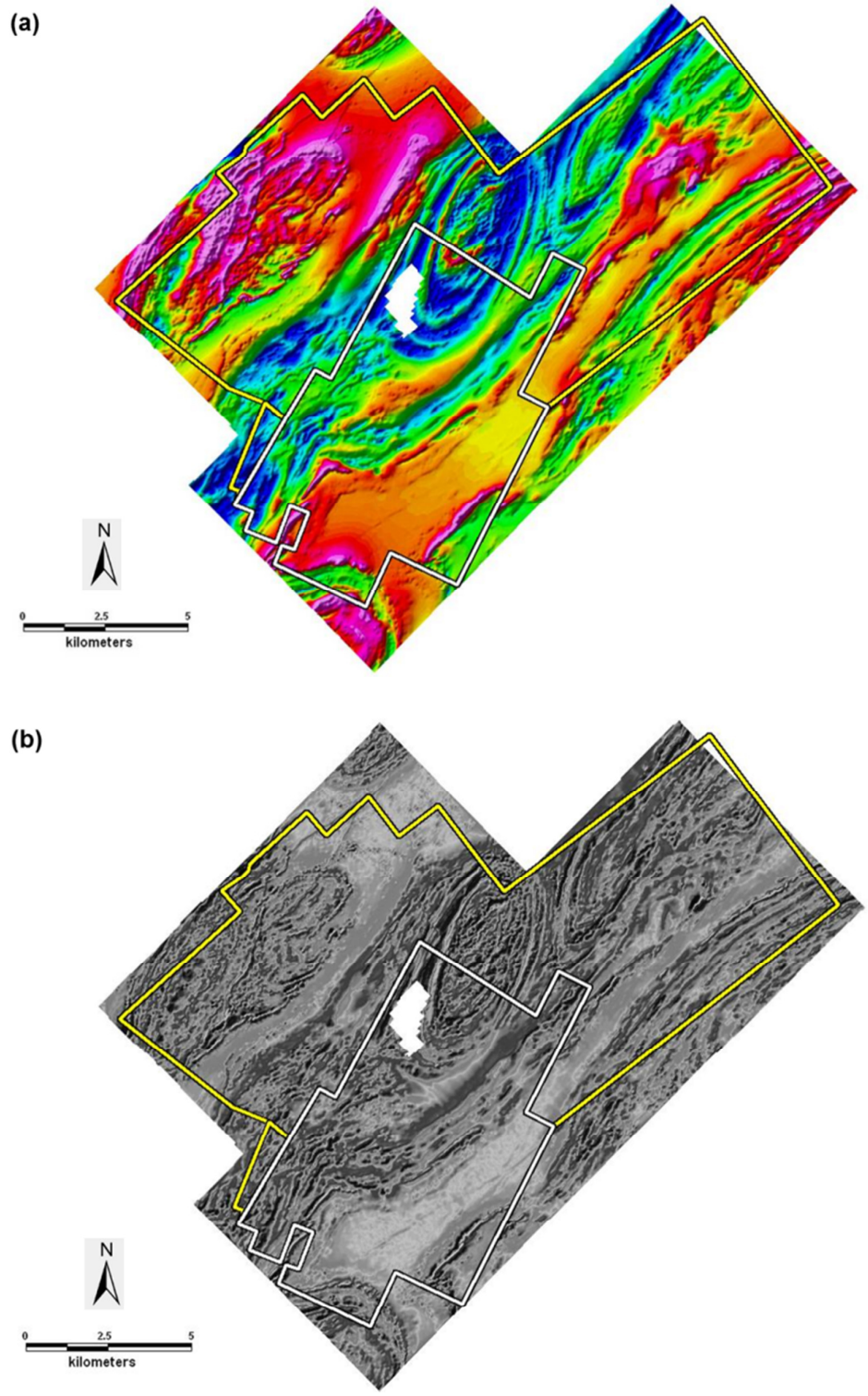


Figure 2.2. Gridded heli-borne gradiometric magnetic data over the Rössing mine lease (white border) and accessory works area (yellow border). (a) Total magnetic intensity reduced to pole (TMI RTP). (b) First vertical derivative of the TMI RTP. Gridded to 25 m and shaded with illumination from the northwest to highlight the principal structural trends. Figure is centred on 506000 mE, 7515000 mN.

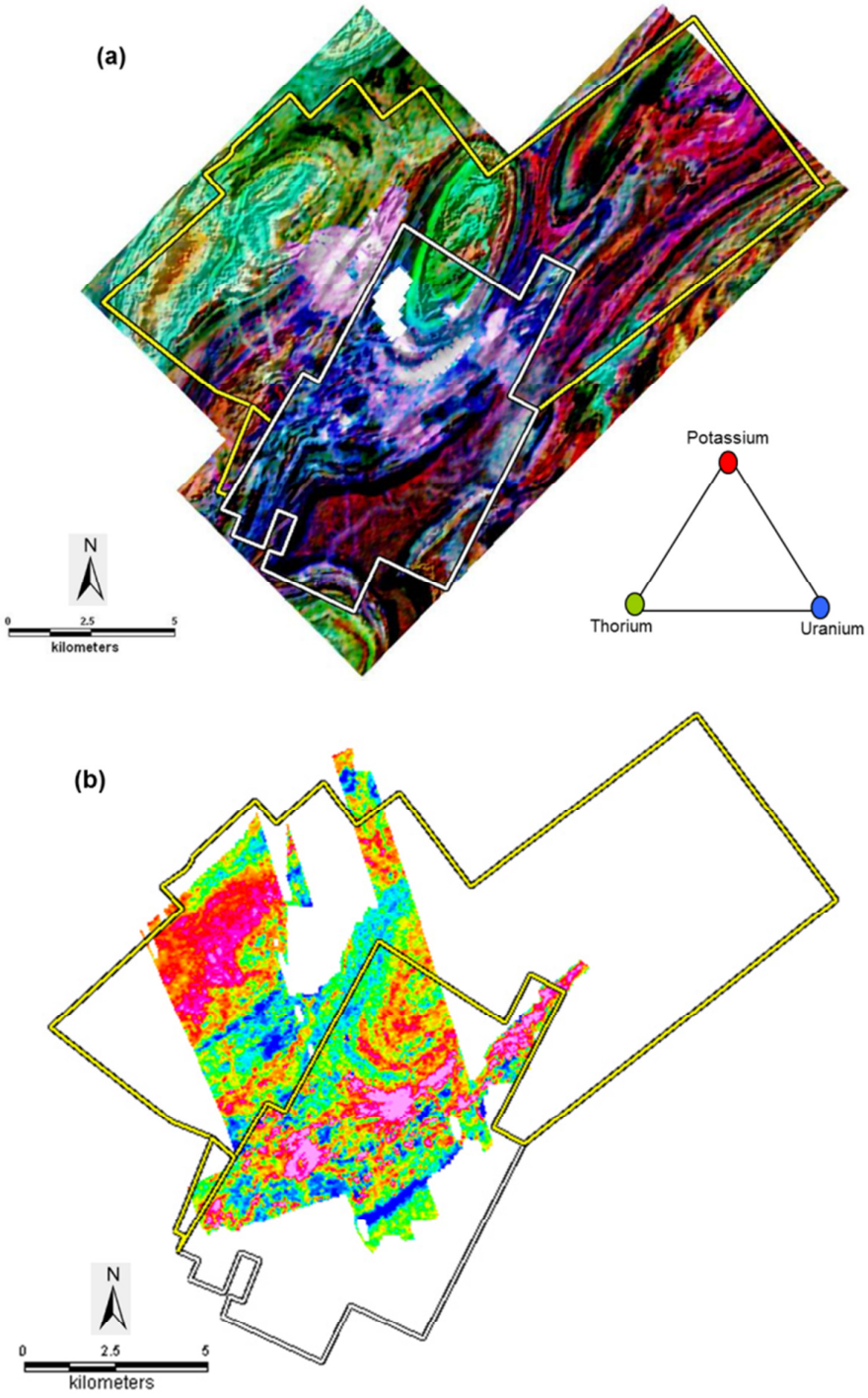


Figure 2.3. Radiometric data in the Rössing area. (a) Ternary image of heli-borne gamma ray spectrometer data. (b) Pre-mining ground scintillometer data, line spacing 100 m with stations spaced at 30 m data gridded to 20 m cell size (hot colours = higher count). Note the ground disturbance in the immediate vicinity of the mine (centre of the image) evident in (a) that masks the response of the sub-surface geology, whereas the total count data in (b) clearly shows the radiometric anomalies (hot colours) associated with the Rössing SJ ore body and surrounding uraniferous alaskites. Combined contoured data is shown on the attached map and on Figure 7.1. Figure is centred on 506000 mE, 7515000 mN.

The pre-delivery data processing workflow for both surveys is documented by Fugro (2005). This includes the levelling of data to a common altitude and the removal of the effects of variations in the earth's magnetic field (diurnal correction) from the magnetic data. The gridding techniques applied to the magnetic data aid interpretation. The first vertical derivative of the TMI provides sharper resolution of near-surface features, whilst the reduction to pole of aeromagnetic data removes the effect of the angle of inclination of the magnetising vector (e.g. Sharma, 1987). The primary application of the airborne magnetic data is the delineation of sub-desert cover stratigraphy and in the identification of faults. The airborne K-U-Th radiometric data is useful for the broad characterisation of stratigraphic packages and identification of uranium anomalies.

2.2.2 Ground Scintillometer Data

Seventy one hard copy maps of point ground scintillometer data dating back to the earliest exploration work at Rössing were located in department archives and digitised by an external company as part of the mapping project. This data covers a significant portion of the mapping area with ground stations spaced at 30 m along lines spaced at 100 m and consisting of greater than 25,000 point measurements. The total count (K+U+Th) data provides invaluable detail over areas disturbed by mining activities. This data was gridded (Figure 2.3b) and contoured using Geosoft's Oasis Montaj software to produce the contours in the SJ and SK areas as shown on the attached map. A polygon representing the area of the ground scintillometer data coverage was then used to clip (remove) the contoured airborne radiometric data where the ground data exists, due to the fact that the airborne data in the mine area is no longer representative of the surface geology radiometric response prior to mining. The ground scintillometer data in its entirety has not previously been digitally captured and imaged.

2.3 Remote Sensing Data

Remote sensing is the science of obtaining information about an object or area through the analysis of data acquired by a device that is not in contact with the subject under investigation (Lillesand *et al.*, 2008). Hence by definition airborne geophysical data is remotely sensed, however the term is here (and commonly elsewhere in the geological literature) applied to imagery data acquired either from satellite or aircraft platforms. Remote sensing data utilised throughout this project consists of both of these types of data and is dealt with in the sections below, following a brief overview of remote sensing science.

2.3.1 Remote Sensing Overview

Most remote sensing systems operate within the visible, infrared or microwave portions of the electromagnetic spectrum (Figure 2.4). 'Active' systems such as radar sensors supply their own source of energy to illuminate the subject area whilst 'passive' systems sense naturally available energy such as sunlight. All radiation detected by sensors passes through a path length of atmosphere which variously effects the intensity and spectral composition of the radiation sensed, depending on its length, the magnitude of the energy signal, the atmospheric conditions present and the wavelengths involved. Atmospheric 'scattering' is the unpredictable diffusion of radiation by particles in the atmosphere, whilst 'absorption' results in the loss of energy to atmospheric constituents. Atmospheric gases including water vapour tend to absorb electromagnetic energy in specific wavelength bands, whereby particularly transmissive wavelength ranges are termed 'atmospheric windows' (Figure 2.4). When selecting a remote sensor consideration must be given to the spectral sensitivity of the sensors available, the position of atmospheric windows in the spectral range in which one wishes to acquire data, and the source, magnitude and spectral composition of the energy available in these ranges. Furthermore, consideration must be given to the 'spatial resolution' of a remote sensor which refers to the degree of spatial detail that can be detected by the sensor. (Lillesand *et al.*, 2008).

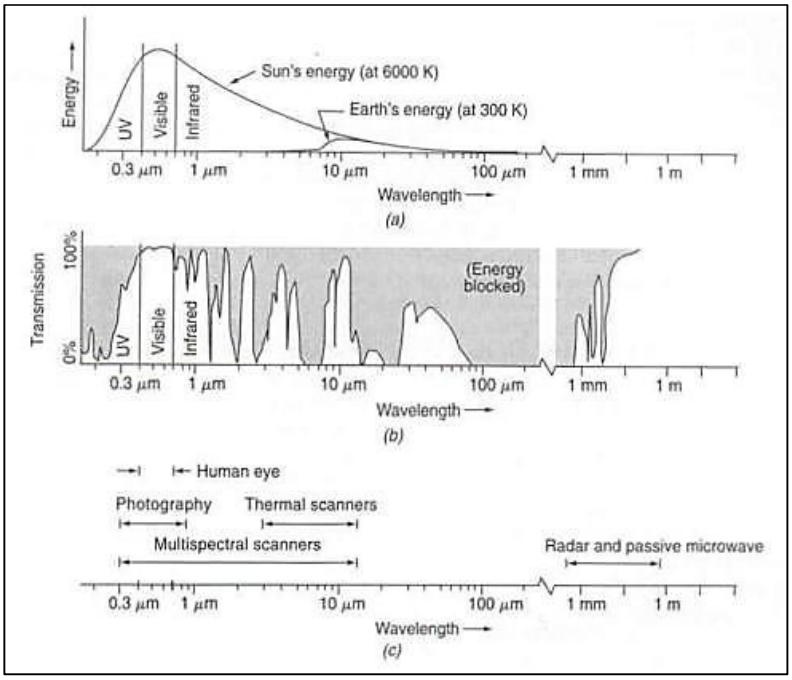


Figure 2.4. Spectral characteristics of (a) energy sources, (b) atmospheric transmittance, and (c) remote sensing systems (wavelength scale is logarithmic). From Lillesand et al. (2008).

Spectral reflectance and emittance curves produced from responses measured by remote sensors are referred to as 'spectral signatures' (see vegetation and dry soil reflectance profiles of Figure 2.5). In reality, these profiles should be considered as 'response patterns' as they may be distinctive but not necessarily unique (Lillesand *et al*., 2008).

Spectral data is now almost ubiquitously acquired as digital imagery rather than the traditional photographic film method. A digital image is composed of a two dimensional array of 'pixels' where the intensity of each pixel represents the radiance over the ground area corresponding to the pixel. The brightness or 'pixel value' of each pixel is referred to as the 'digital number' (D.N.). Imagery data may contain data from a single spectral band measured across a range of wavelengths (for example panchromatic film photography, Figure 2.5) or from multiple spectral bands whereby data is collected simultaneously in several spectral bands. In the case of the latter, each pixel in the 'multispectral' image will include multiple D.N.'s, one for each spectral band (Lillesand *et al*., 2008). Landsat T.M. and Aster imagery (Chapter 2.3.2) are both examples of multispectral imagery acquired from satellite platforms and the respective sensor band positions in the electromagnetic spectrum are illustrated in Figure 2.5. 'Hyperspectral' sensors (Chapter 2.3.3) acquire images in many narrow, contiguous bands throughout the visible (V.I.S.), near-infrared (N.I.R.), mid-infrared (M.I.R. otherwise referred to as short-wave infrared, S.W.I.R.) and thermal infrared (T.I.R.) portions of the spectrum for every pixel in the scene (Lillesand *et al*., 2008).

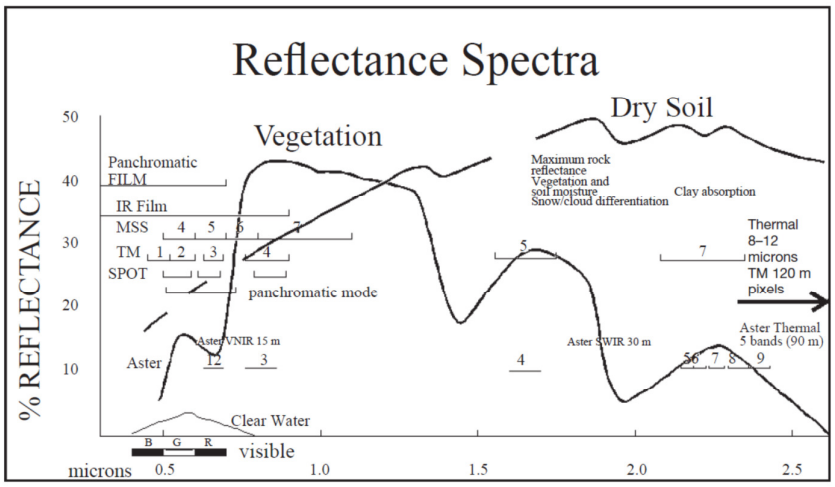


Figure 2.5. Plot of wavelength against reflectance showing spectral profiles for vegetation and dry soil, and bars representing various remote sensing sensors, vertically offset for comparison. From Bedell, (2004).

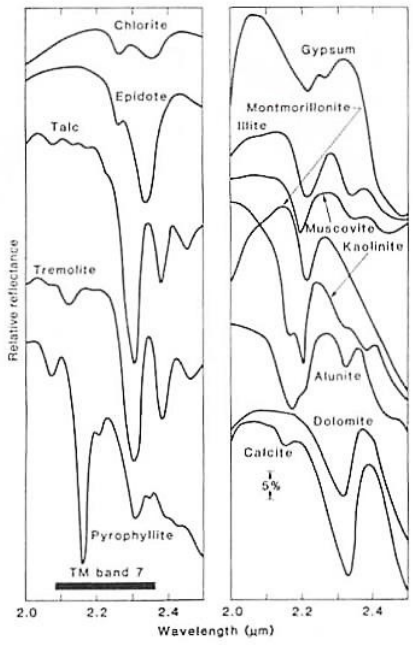


Figure 2.6. Selected laboratory mineral spectra showing diagnostic absorption and reflectance features. Spectra are arranged vertically for comparison. The bandwidth of band 7 of the Landsat T.M. sensor (see also Figure 2.4 and Chapter 2.3.2) is also shown and discussed in the text. Note the shift to the right in absorption features between calcite and dolomite which allows these minerals to be separated in hyperspectral imagery in the project area (see Figure 3.8). From Lillesand et al. (2008).

Hyperspectral sensors thus have a 'spectral resolution' which can discriminate absorption and reflection characteristics that are undetected within the relatively coarse bandwidths of multispectral scanners. This is illustrated in Figures 2.6 and

2.7: the Landsat T.M. band 7 obtains only one data point corresponding to the integrated response over a spectral band 0.27 µm wide, whilst a hyperspectral sensor can obtain many data points over this range using bands in the order of 0.01 µm wide (Lillesand *et al.*, 2008; Manolakis *et al.*, 2003). Examples of airborne hyperspectral sensors include AVIRIS, SpecTIR and HyMap, whilst Hyperion is a satellite-mounted sensor (Bedell, 2004).

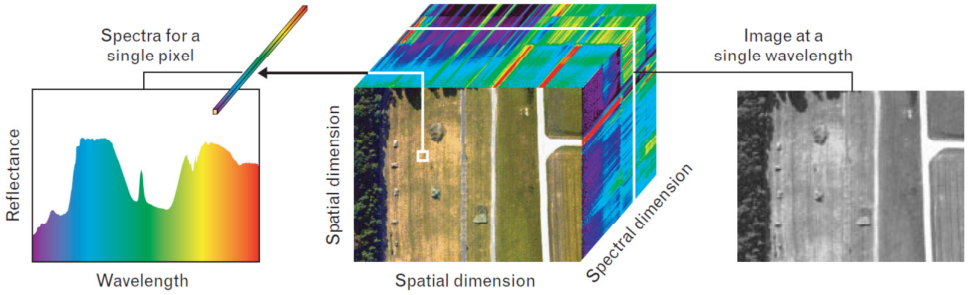


Figure 2.7. An example of the 'data-cube' (centre) structure of hyperspectral imaging illustrating the spatial and spectral nature of the data. The data cube can be visualised as a set of spectra for each individual pixel (left) or as a stack of images (right) for each single spectral channel. From Manolakis et al. (2003).

It is worth noting that even between the very few remote sensing systems presented here, there is an important trade-off between spectral and spatial resolution. With decreasing spectral bandwidth there exists a concomitant decrease in signal strength, whereby it may in cases be more appropriate to take a larger sample (use larger pixels with a better signal-to-noise ratio), with the disadvantage that larger pixels will have more mineral mixtures (Bedell, 2004).

2.3.2 Landsat and Aster Imagery

Initiated in 1967 N.A.S.A's Earth Resources Technology Satellites (E.R.T.S's) programme saw the launch of E.R.T.S. 1 on a Nimbus weather satellite platform in 1972. This represented the first unmanned satellite designed to acquire data about earth resources on a systematic, repetitive, medium resolution multispectral basis. In 1975 this was renamed as the 'Landsat' programme with six successful launches comprising Landsat-1 to -5 and Landsat-7. Landsat-6 suffered a launch failure. Five different types of sensors have been utilised in various combinations on these missions included the Thematic Mapper (T.M., missions 4 and 5; Figure 2.5) and Enhanced Thematic Mapper Plus (E.T.M. +, mission 7). The latter continues to collect data over six spectral bands in the VIS-N.I.R. to S.W.I.R. at 30 m spatial resolution, one 60 m band in the thermal infrared (T.I.R.) and one 15 m panchromatic band, however image acquisition has been greatly impacted by the failure of the

system's scan line corrector (S.L.C.) in 2003 (Lillesand *et al*., 2008). An example of a portion of a processed Landsat E.T.M. + image in the Rössing area is shown in Figure 2.8 as a R.G.B. 7-4-1 band combination.

The Advanced Spaceborne Thermal Emission and Reflection Radiometer (A.S.T.E.R. or Aster) is one of five remote sensing instruments aboard Terra, the flagship satellite of N.A.S.A.'s Earth Observing System (E.O.S.), launched in 1999. The Aster imaging instrument represents a cooperative effort between N.A.S.A. and the government of Japan and consists of three scanners capturing data across 14 bands in the VIS-N.I.R. (15 m spatial resolution), S.W.I.R. (30 m) and T.I.R. (90 m) providing continuous along-track stereo imagery (Lillesand *et al*., 2008). The five bands located in the S.W.I.R. overlap with the single Landsat T.M./E.T.M. band 7, allowing for the distinction between groups of clays, sulphates, carbonates and other minerals (Bedell, 2004; Figure 2.5). An example of a portion of a processed Aster image in the Rössing area is shown in Figure 2.9. Landsat and Aster imagery was used initially to define major units (formations) across the area prior to undertaking detailed interpretation of hyperspectral and aerial photographic data.

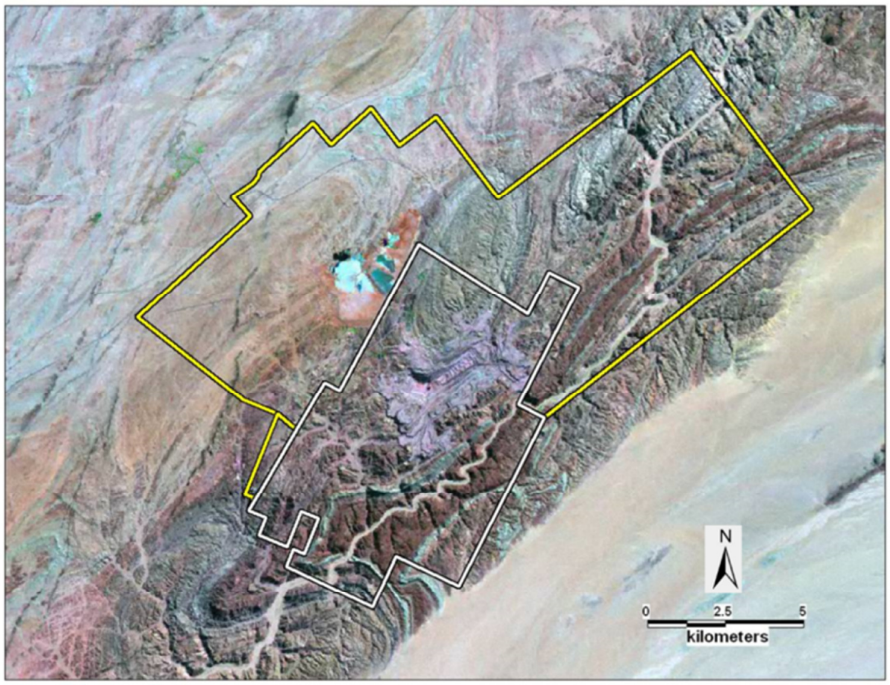


Figure 2.8. Landsat 7 E.T.M.+ R.G.B. false colour composite of bands 7-4-2 of the Rössing Mine area. Mine lease ML28 is shown in white, accessory works area in yellow. Image prepared by A. Caballero. Figure is centred on 506000 mE, 7515000 mN.

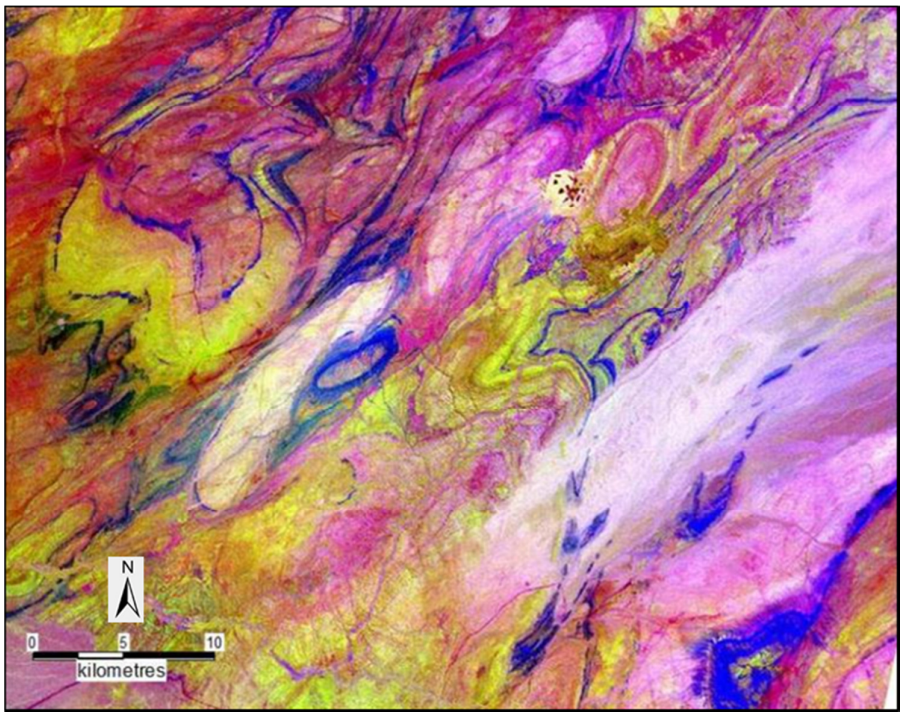


Figure 2.9. Aster R.G.B. false colour composite bands 2-3-4, minimum noise fraction (M.N.F.) decorellation method (see Chapter 2.3.3). The image covers the wider Rössing area with marble units in deep blue highlighting the regional structural style. Rössing Mountain is located in the N.W. quadrant of the scene. Image prepared by A. Caballero. Figure is centred on 506000 mE, 7515000 mN.

2.3.3 HyMap Hyperspectral Data

The HyMap airborne imaging spectrometer was developed in the 1990's by Integrated Spectronics Ltd. for mineral exploration and HyMap data is provided by Hyvista Corporation. The HyMap system utilises four whiskbroom spectrometer units collecting 126 contiguous spectral bands between 0.45-25 µm (except in the atmospheric water vapour bands) in 15 to 20 nm band passes and ground instantaneous field of views (G.I.F.O.V.'s, corresponding to pixel spatial resolution) ranging 3-10 m. HyMap provides a signal to noise ratio of >500:1 (Taranik and Aslett, 2009; www.hyvista.com).

Hyvista was commissioned by the Geological Survey of Namibia to fly a hyperspectral survey over various part of Namibia in 2005, and Rössing Uranium Ltd. purchased 3790 km^2 of data over 48 flight lines from Blocks B2 and B3 (Figure 2.10). The survey was flown from a fixed wing aircraft at a height of 2800-3000 m, at a line spacing of 2 km, line swathe of 2.4 km producing a spatial resolution of 4.7 m (A. Caballero, pers. comm.).

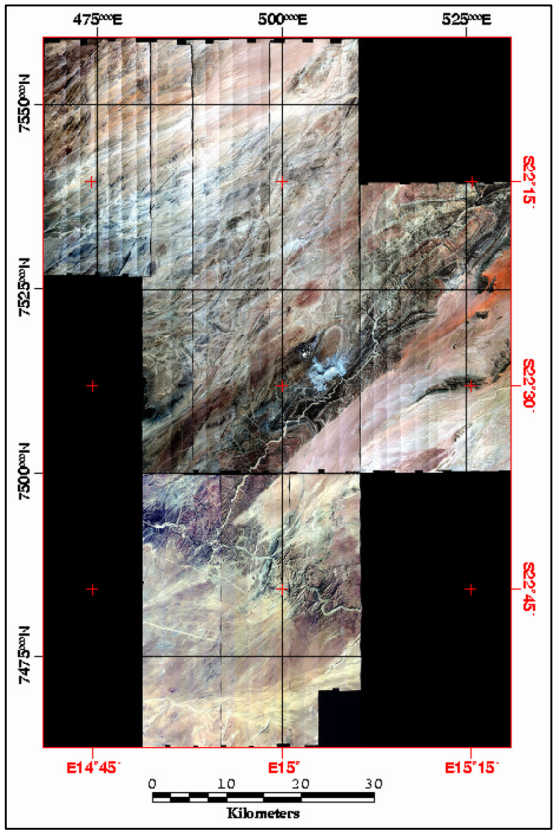


Figure 2.10. Processed area of 48 flight lines covering 3790 km^2 around the greater Rössing area. Hyperspectral RGB colour composite of bands 15-8-2 (Caballero, 2009).

The HyMap data was processed by Alejandro Caballero (Caballero, 2009) using the ENVI software package in consultation with the author as fieldwork was conducted. Pre-process of data received from HyVista included conversion of values from radiance to reflectance, dark current subtraction and atmospheric corrections (Caballero, 2009). Further pre-processing steps required included cross-track illumination and geometric corrections. The corrected flight lines were then mosaicked into groups of five to six lines to produce homogeneous image data which was then processed to produce the various band colour composite, minimum noise fraction (M.N.F.) and mineral maps shown and described below. Two colour combination images were produced as shown in Figure 2.11: a *real colour composite* using bands 15-8-2 (equivalent to Landsat RGB 3-2-1) and a *lithological contrast* image using bands 108-26-2 (equivalent to Landsat RGB 7-4-1; Caballero, 2009).

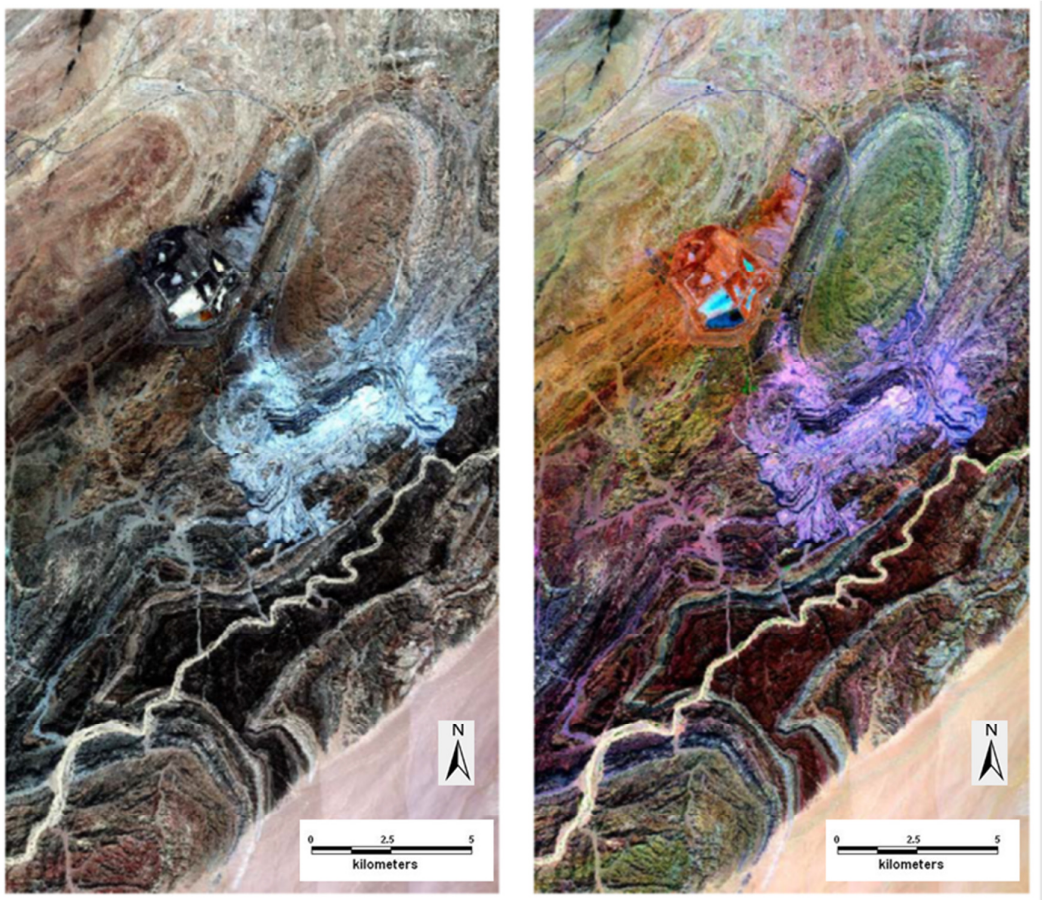


Figure 2.11. Colour combination images of portions of the HyMap survey data: left - real colour composite image bands 15-8-2 (equivalent to Landsat RGB 3-2-1); right - lithological contrast image using bands 108-26-2 (equivalent to Landsat RGB 7-4-1; from Caballero (2009). Figure is centred on 505000 mE, 7513000 mN.

The minimum noise fraction transform separates true signal from noise and was applied to the full spectral range (VIS, N.I.R., S.W.I.R), producing greater data dimensionality and discriminating individual lithologies to facilitate mapping (Caballero, 2009; Figure 2.12).

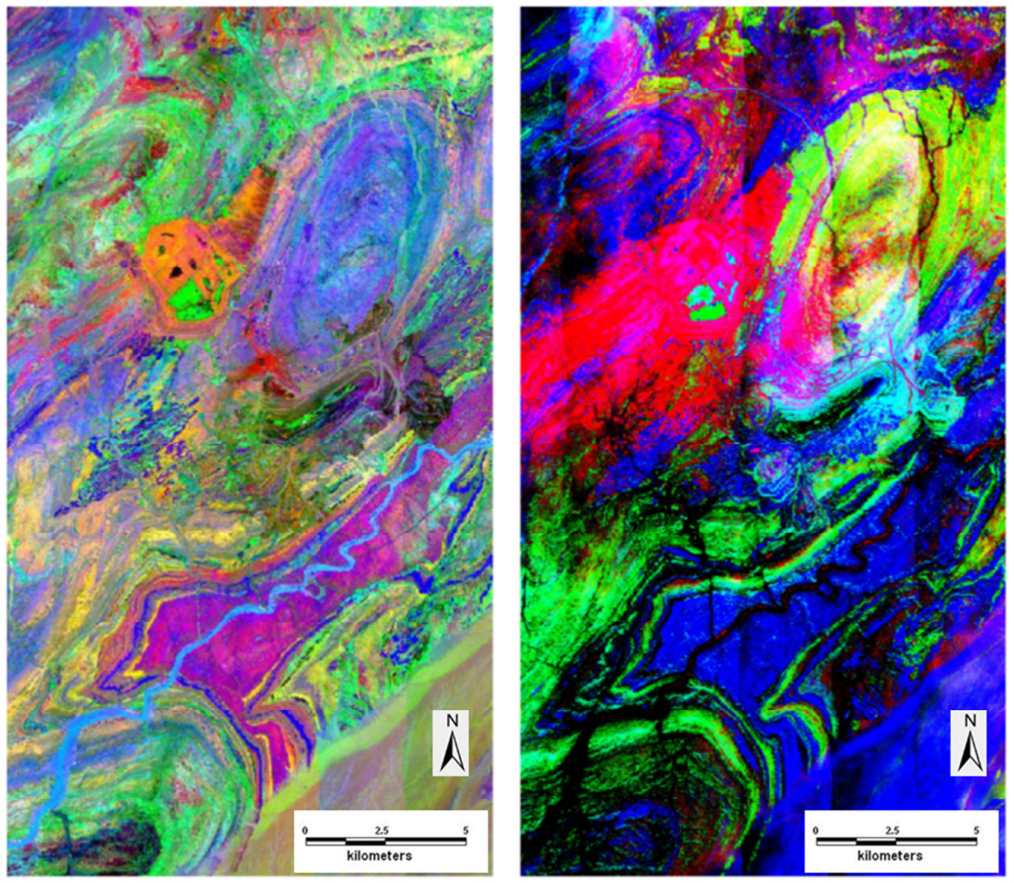


Figure 2.12. The minimum noise fraction (M.N.F.) transform applied to Rössing area HyMap data, bands 10-11-12 (left) and 7-8-9 (right); from Caballero (2009). See text for explanation. Figure is centred on 505000 mE, 7513000 mN.

Spectral analysis using a variety of software packages was carried out in conjunction with onsite P.I.M.A. analyses (see Chapter 2.5.2) in order to determine mineral species and mixtures of minerals present in the hyperspectral data. Minerals such as illite, epidote, chlorite, phlogopite, amphibole and calcite in the S.W.I.R. bands and hematite, goethite and jarosite in the VIS and N.I.R bands were readily identifiable using tools such as the Sequential Maximum Angle Convex Cone (S.M.A.C.C.) and Spectral Feature Fitting (S.F.F.). However in most cases as rock units tend to be mixtures of two or more minerals which are common to many other units, distinction of units are difficult with the exception of where pure calcite and dolomite occurs. Examples of end-member mineral images are shown in Figures 2.13 and 2.14 (Caballero, 2009).

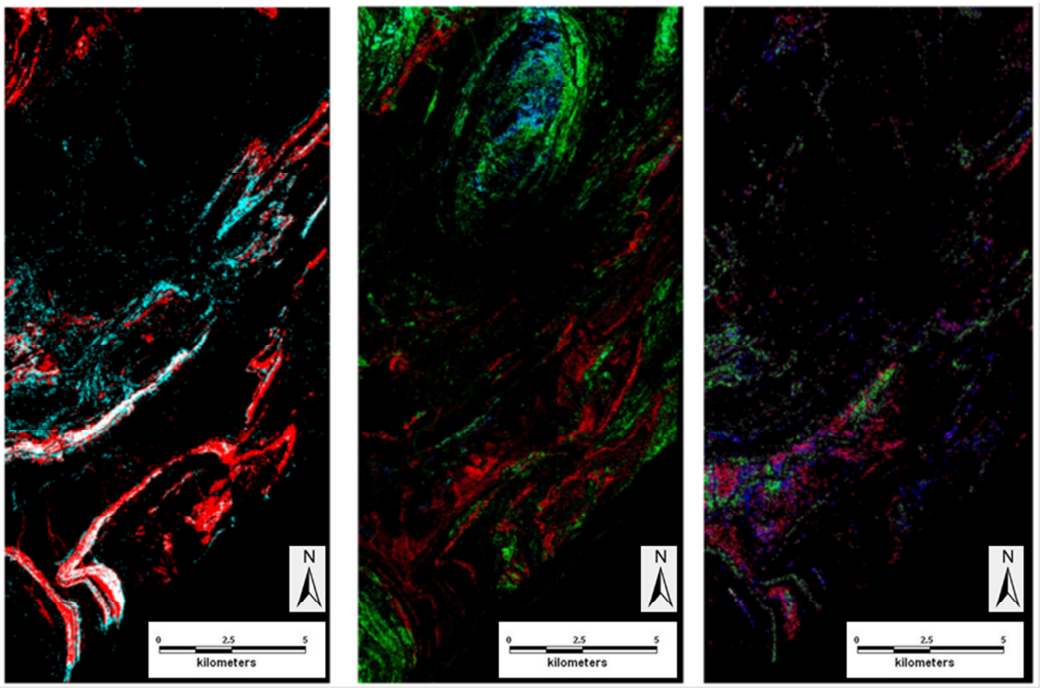


Figure 2.13. Mineral end-member images derived from the Rössing area HyMap data. Left – calcite (light blue) and dolomite (red); centre – illite composite consisting of montmorillonite (green) and a kaolinite-halloysite mixture (red); right – epidote-chlorite (from Caballero, 2009). Figure is centred on 505000 mE, 7511000 mN.

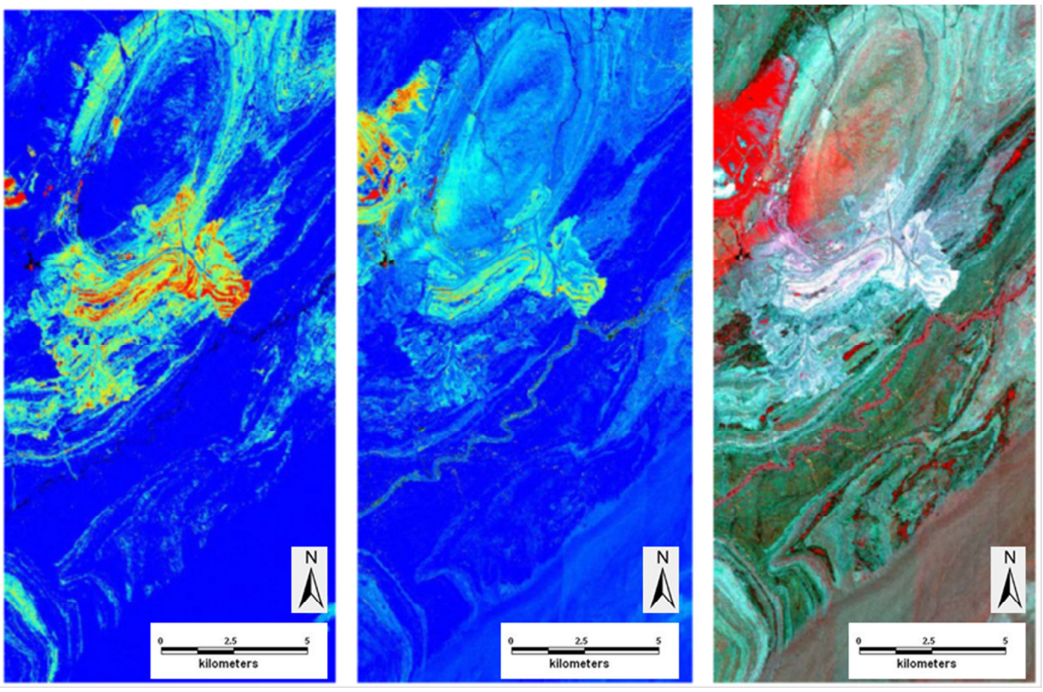


Figure 2.14. Iron oxide and hydroxide mineral end-member maps derived from Rössing area HyMap data. Left – goethite; centre – jarosite; right – goethite and hematite (blue-green) and jarosite (red). From Caballero (2009). Figure is centred on 505000 mE, 7511000 mN.

2.3.4 Photogrammetry

In 2008 Southern Mapping Company carried out an aerial photographic and Light Detecting and Ranging (L.I.D.A.R.) survey over 500 km^2 of the Rössing Mine Lease area. Orthorectified photo mosaics were produced from 15 cm spatial resolution digital photographs and formed the highest resolution base imagery for geological map interpretation throughout this project (Figure 2.15). In the construction of orthophotos, original image data are re-projected orthographically using elevation information to remove elevation effects from the original image (Lillesand *et al.*, 2008).



Figure 2.15. Example of a portion of the ortho-rectified aerial photographic mosaic surveyed and produced by Southern Mapping Company for Rössing Uranium Ltd. in 2008. The image has a 15 cm spatial resolution and covers the Blauer Heinrich Syncline area along the Khan River. A dolerite dyke cuts the hinge zone parallel to the fold axial plane. Note trees in the river bed for scale. Figure is centred on 501000 mE, 7508000 mN. The location of the Blauer Heinrich Syncline is shown in Figure 4.1.

2.4 Digital Elevation Model

A digitised pre-mining topographic survey of the SJ area was supplied to the author by the Rössing Mine Survey Department. A gridded version of this data was merged with a digital elevation model (D.E.M.) derived from the Fugro airborne geophysical survey (Chapter 2.2.1) of the Mine Lease, and with publicly available N.A.S.A. Shuttle Radar Topography Mission (S.R.T.M.) data of the surrounding area using

Geosoft's Oasis Montaj to provide a combined D.E.M. for production of the surface profiles shown on the cross sections on the appended map.

2.5 Geological Mapping

2.5.1 Previous Work

The most recent (and most detailed) published geological map of the area is the 1:250 000 Sheet 2214 of the Geological Survey of Namibia (Lehtonen *et al.* 1995), which also refers to the geological mapping at 1:125 000 of Smith (1965; Figure 2.16).

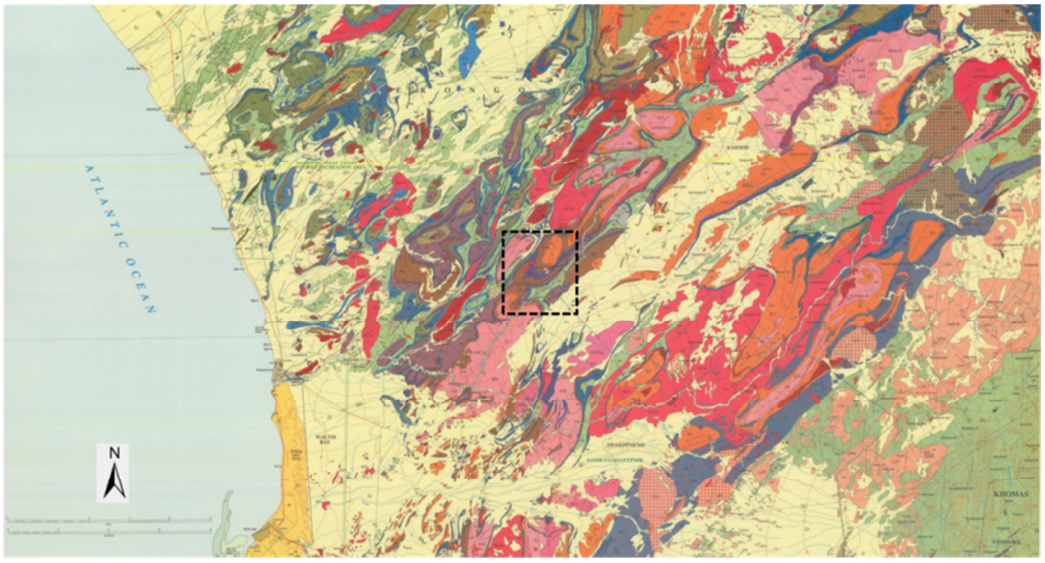


Figure 2.16. 1:250 000 Sheet 2214 of the Geological Survey of Namibia (Lehtonen et al. 1993, 1995, 1996), representing the most detailed geological mapping completed to date across the project area (indicated by the dashed rectangle). Figure is centred on 505000 mE, 7511000 mN.

Twenty nine geological map sheets (± structural data) covering the ML28 Mine Lease area were located in Rössing Uranium Ltd. archives and digitised by an external company as part of this project. Where possible this historical work is referenced (both within this section and on the appended map). A database of >4000 structural measurements was compiled from these sheets together with more recent structural mapping data of Laberge (2008a, 2008b) and data collected through the course of this project. Most historical mapping was used to guide interpretation of hyperspectral and remote sensing data however in places, such as the area now covered by the tailings dam, portions of maps have been reproduced where interpretation is not possible. The detailed geological mapping and compilation over the SJ-SK area of

Golder Associates (1978) and Laberge (2008a; 2008b) is also included on the appended map; the author claims no credit for this mapping and compilation work.

Mapping over the entire extent of the ML28 mine lease and surrounds has previously only been resolved by the excellent regional geological maps of Smith (1965) and Lehtonen *et al.* (1993, 1996). The most recent detailed geological mapping completed is that of Laberge (2008a, 2008b) in the areas of SK and south of SJ, complementing the original SJ map of Golder Associates (1978; Figure 2.17). Historical geological maps completed by Rio Tinto and Rössing Uranium Ltd geologists and students, held at the Rössing mine site in hard copy format are too numerous to list here. Mapping incorporated into this work beyond that described above that should be credited to other workers is the pre-tailings area mapping of Wegerhoff (1973) and Dames and Moore (1982), and that completed in the same area and in Panner Gorge by Rhodes University students (Harris *et al.*, 1993, 1994; Jacob and Kerber, 1997). Other mapping completed in the area but not synthesised into the attached map includes the map of the SH area by Mestres-Ridge (1992, Figure 2.18) and that of Poli (1997) of the Nose Structure of the Khan Mine Gorge and Khan River area. Mapping of regional radiometric anomalies, E.M. anomalies and the Khan Copper Mine area was also completed during exploration in the 1960-70s. Recently Longridge (2012) remapped the Palmenhorst Dome (Khan Gorge Inlier to the immediate south of the area and much discussion is drawn from this work in subsequent Chapters.

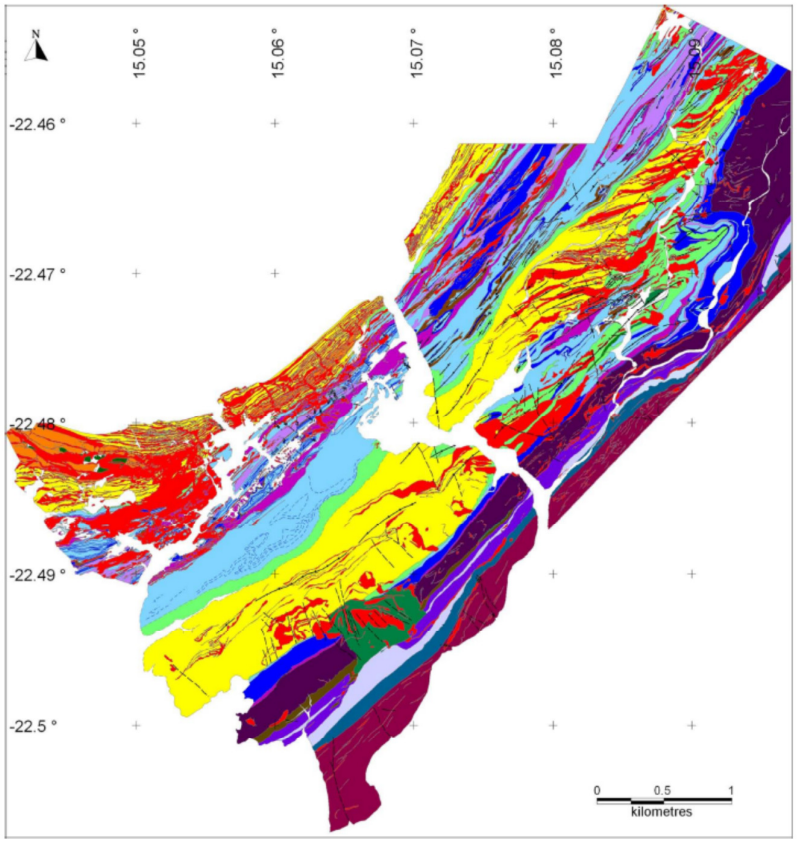


Figure 2.17. Geological map of the SJ-SK area comprising the original SJ geological map of Golder Associates (1978) and the geological mapping of Laberge (2008a, 2008b) in the SK and SJ south areas. Figure from Laberge (2008b). For explanation of colours see Appendix II.

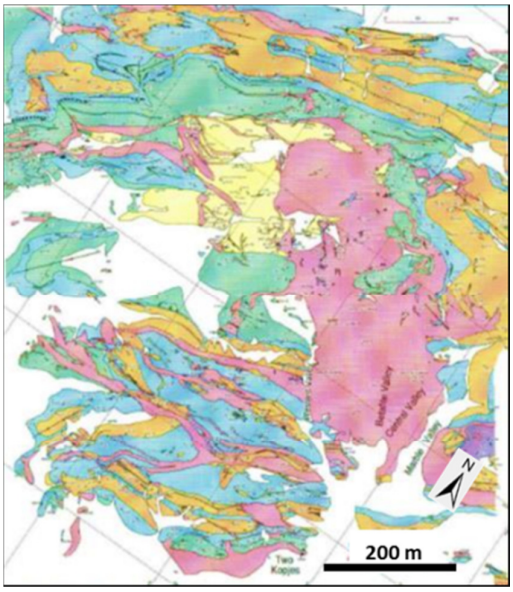


Figure 2.18. Geological map of the SH area of Mestres-Ridge (1992). For the location of the SH area see Figure 1.2. Figure is centred on 503000 mE, 7512000 mN.

2.5.2 This Work

Throughout the course of this project 51 days (or part days) were spent ground-truthing remote sensing data and recording the orientation of geological structures at >1000 mapping stations across the area. Particular attention was given to examining features of the hyperspectral imagery summarised in Chapter 2.3.3 by traversing stratigraphy across-strike, generally where it is best exposed in drainage systems. Observations were made regarding the colour and geomorphological expression of major rock units for comparison with aerial photographs (Figure 2.19). Geological units to be resolved by the mapping were chosen and coded. This fieldwork was made significantly easier by the use of a Trimble P.D.A. and Encom's Discover Mobile software upon which field positions were tracked via G.P.S. directly on remote sensing imagery and mapping stations could be rapidly recorded.

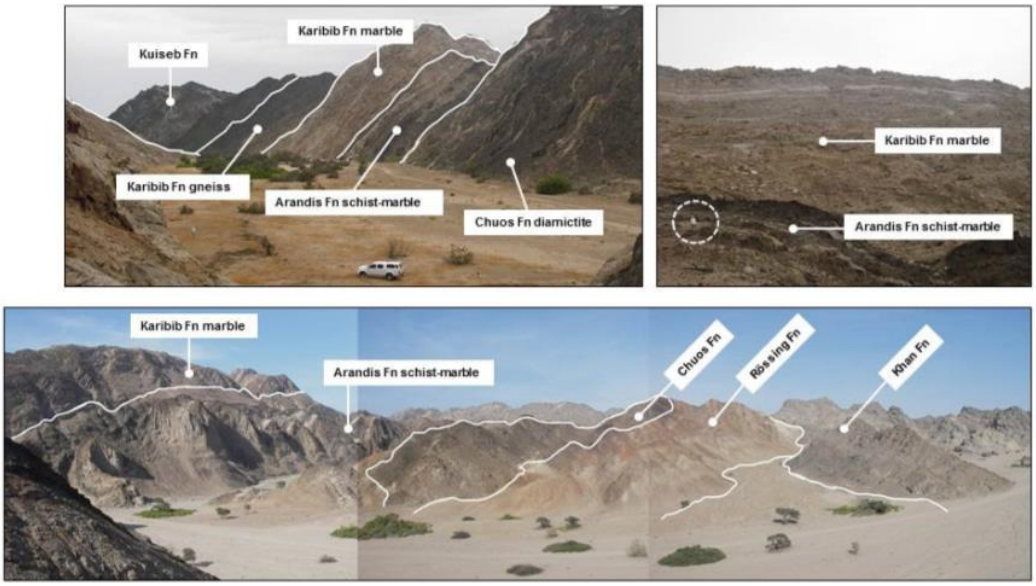


Figure 2.19. Photographs taken during field mapping showing colour and geomorphological expression of major Damaran metasedimentary units in the area. Top left – Chuos Formation and overlying units outcropping spectacularly in the Khan River area, view to the northeast; top right – distinctive outcrop morphology of Karibib Formation marbles and underlying stratigraphy (note Justin Laberge circled for scale), same locality as top left; bottom – section through the lower part of the Damaran stratigraphy as outcropping in the Panner Gorge area showing distinctive colour variations throughout the various formations, view to the west.

A total of 116 samples of representative lithologies throughout the stratigraphy were collected for the primary purpose of assigning accurate rock names to map units (Table 2.2). Whilst sampling was biased toward rock units less well constrained by previous mapping and/or fine-grained lithologies, the vast majority of map units defined were representatively sampled for reference.

Table 2.2. Summary of rock samples taken from drill core and field localities.

Unit	Number of samples	Unit (cont.)	Number of samples
Abbabis Metamorphic Complex	10	Karibib Fn	4
Etusis Fn	4	Kuiseb Fn	2
Khan Fn	24	Alaskite	36
Rössing Fn	17	Qtz diorite & dolerite	3
Chuos Fn	6	Other	3
Arandis Fn	7		
		Total	**116**

Thin sections and polished blocks were prepared by the Geological Survey of Namibia for microscopic examination under transmitted and reflected polarised light. Additional large polished blocks were prepared for photography. Spectral measurements of samples were collected by Luisa d'Andrea (Project Geophysicist, Rössing Uranium Ltd.) using a Portable Infrared Mineral Analyser (P.I.M.A.). A P.I.M.A. is a field portable spectrometer that operates in the S.W.I.R. (short wave infrared, see Chapter 2.3.1). This is a useful tool for rapid identification of minerals that have reflection and absorption characteristics within this range of the electromagnetic spectrum. In addition to the P.I.M.A. analyses, magnetic susceptibility and K-U-Th gamma ray spectrometer readings were also recorded in order to further characterise individual lithologies. Further spectral measurements were collected from these samples by the author using an A.S.D. TerraSpec spectrometer, a more modern infrared spectrometer that has an extended range of detection into the VIS-N.I.R. portion of the electromagnetic spectrum.

2.6 Data Interpretation

Six A1 geological map sheets at 1:10 000 scale were produced on transparent overlays by interpreting the data based on field definition and observation of rock units as shown in Figure 2.20. These lithological units are reviewed in Chapter 3. Reference to historical geological mapping (see Chapter 2.5.1) was required in areas where surface geology is now concealed, such as the mine tailings area and waste dumps west of the SJ pit. In particular the geology of the area under the waste dumps southwest of SJ is not well resolved which is purely a function of the quality of historical geological mapping available. Map features were interpreted in order of youngest to oldest (since younger features cross-cut older ones) primarily through reference to hyperspectral and aerial photograph imagery products described earlier in this chapter. In addition to the remotely sensed data, continuous reference was

made to geophysical data; in particular the basement-cover contact northwest of the tailings dam is particularly well delineated in the radiometric ternary image, whilst the top of the Chuos Formation can be easily traced where it is very magnetite rich on first vertical derivative magnetic images. Faults were interpreted in areas of obvious stratigraphic discontinuity, apparent either in geophysical or remote sensing data.

Subsequent modifications made to the first versions of the digitised 1:10 000 interpretations have included a more detailed interpretation at 1:3500 scale of the area around SH (Figure 2.21) and a re-interpretation of the Nose Structure area at 1:20 000 scale (Figure 2.22). These modifications were necessary in the SH area because the structural and lithological complexity present was such that this could not be resolved satisfactorily at 1:10 000 scale, whilst the Nose Structure area was more effectively resolved with reference to 2.5 m SPOT satellite imagery acquired subsequently to the main map interpretation.

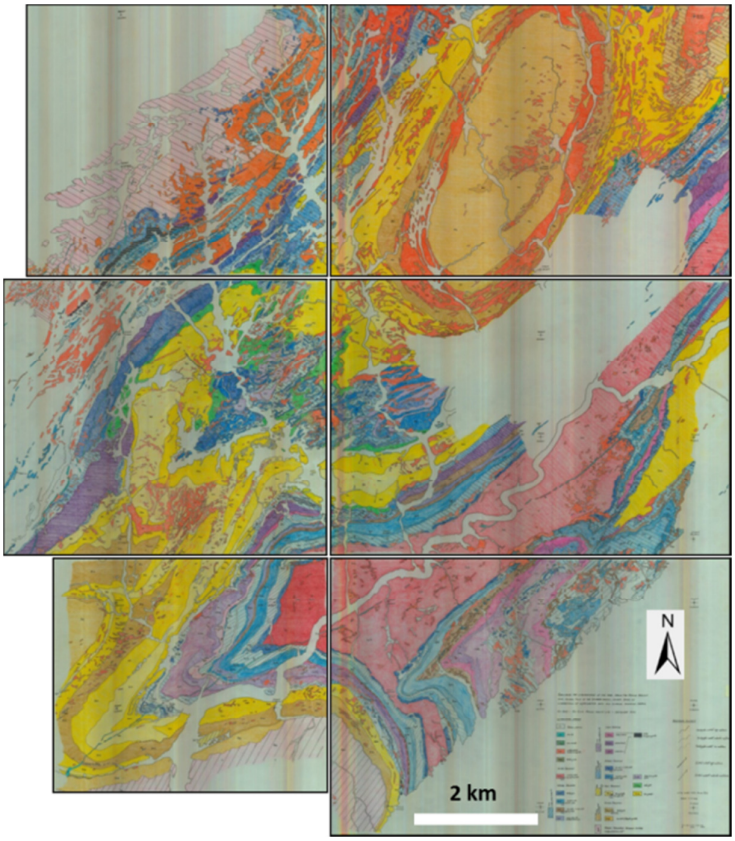


Figure 2.20. Interpretation at 1:10 000 scale of the project area. Note the hole in the interpretation is where detailed ground mapping exists (the SJ map of Golder Associates (1978) and the geological mapping of Laberge (2008a, 2008b) in the SK and SJ south areas described in Chapter 2.5.1. The Nose Structure portion of the bottom left sheet was subsequently re-interpreted as shown in Figure 2.22. See Appendix II for location and explanation of ornaments used.

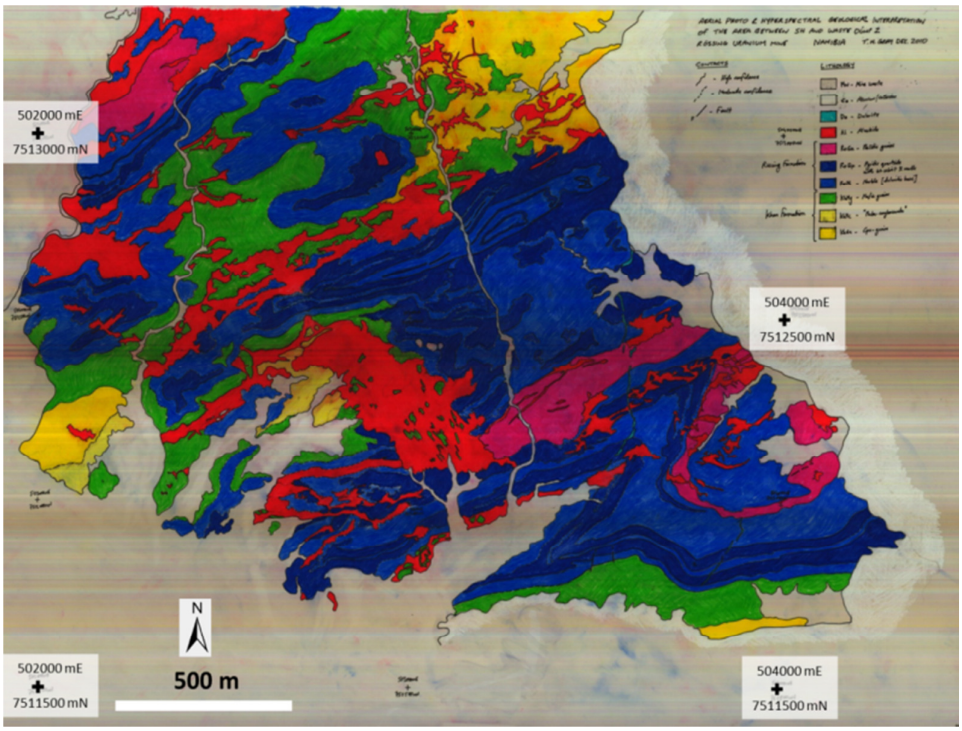


Figure 2.21. Interpretation at 1:3500 scale of the geology in the SH area. This interpretation was completed to better resolve the structural and stratigraphic detail of the area beyond that shown in the centre of Figure 2.20. The white shading on the interpretation indicates the extent of mine dumps. See appended map and legend for explanation of other ornaments used.

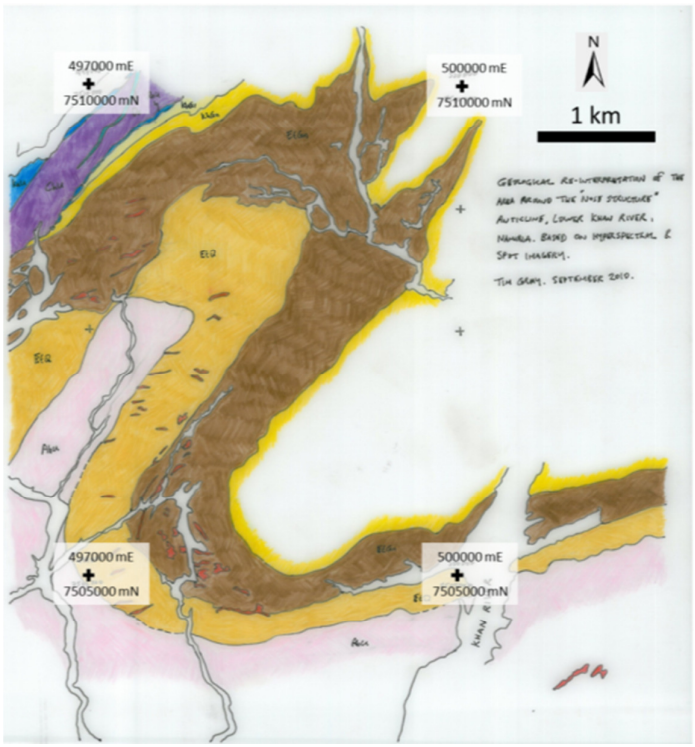


Figure 2.22. Interpretation at 1:20 000 scale of the Nose Structure anticline (Figure 1.2) utilising 2.5 m resolution SPOT imagery. See Appendix II for explanation of ornaments used.

2.7 Summary and Context for Subsequent Chapters

This chapter has described the data and interpretation methodology that has been utilised in the production of the attached geological map presented at 1:20 000 scale. The data consists of airborne and ground radiometric data, airborne magnetic data, remote sensing data at varied spectral and spatial resolution, historical geological mapping, digital elevation models, field data, and spectral and geophysical measurements taken from some 116 field samples collected by the author. Emphasis has been placed on the science and description of remote sensing data as these data layers have been fundamental to resolving the detailed geology of the area. The combination of such varied and high resolution data layers covering an area of generally exceptional outcrop and complex geology has facilitated the production of a detailed map interpretation that is anticipated will build on the geological understanding of the district.

Stratigraphic detail on the appended map has been resolved primarily through reference to the HyMap hyperspectral data purchased and processed as part of this project, and incorporation of previous mapping where this has not been possible. Additional detail of stratigraphy is obtained from aerial photography and examination of map units at outcrop and hand specimen scale. Airborne radiometric data has helped in the distinction of areas of basement outcrop. Constraint of mineralogy of individual units has been through microscopic review and infrared spectral analysis. The stratigraphy of the area is reviewed in the following chapter.

Many aspects of the structural geology of the area can be determined through map relationships presented on the appended map, together with the compilation of structural point measurements from generations of mapping investigations in the area including this project. Tracing stratigraphy on the map reveals the presence of complexly folded and faulted strata and in particular, details of fold interference structures that have not previously been resolved. The compilation and analysis of stereoplots of this data allows the orientation of major fold structures to be determined. The structural geology of the area is presented in Chapter 4.

A petrographic review of map unit samples, combined with field observations augments previous descriptions of metamorphism and plutonism in the area. Details of metamorphic and igneous petrology have largely been compiled from earlier work and, since this project has focused largely on the compilation and interpretation of

data rather than the generation of new data, this has not been an area of focus in this study. Metamorphism and plutonism are discussed in Chapters 5 and 6 respectively.

Ultimately the purpose of this project has been to provide Rössing Uranium Ltd. with an exploration tool for the discovery of further uranium resources in the area. The detailed geological interpretation of the mining lease combined with the digitisation of historical ground scintillometer surveys (and presentation with airborne spectrometer survey data) allows radiometric anomalies to be placed in geological context and drill targets to be generated. Compilation of numerous technical and academic reports of the Rössing area together with observations from this project permits a detailed review of uranium mineralisation in the Rössing area as presented in Chapter 7.

This project resolves details of stratigraphy, structure (to a lesser degree metamorphism and plutonism), and mineralisation in the Rössing area that present significant refinements to the geoscientific knowledge of the wider district. The project has directly assisted in the identification and definition of significant additional uranium resources in the Rössing Mine Lease where mineralisation can be geologically described in the context of the adjacent and recently discovered Rössing South deposits. Details are presented and discussed in subsequent chapters.

Chapter 3: Stratigraphy

3.1 Introduction

The metasedimentary stratigraphy of the Central Zone was introduced in Chapter 1.2.2. It was noted that the Palaeoproterozoic Abbabis Metamorphic Complex forms a basement to a Neoproterozoic (Damaran) metasedimentary succession deposited in an intracontinental rift setting that evolved through seafloor spreading and ultimately subduction and collisional orogenesis, polyphase deformation and high grade metamorphism.

The stratigraphy of the Rössing area largely reflects that introduced for the Central Zone as in Chapter 1.2.2 with the exception that the upper of two glaciogenic formations, the Ghaub Formation, is missing. The area is the type location for the Khan, Rössing and Arandis Formations. The Karibib Formation is present in place of the laterally equivalent Tinkas Formation that occurs to the south of the project area. Table 3.1 presents a detailed stratigraphy of the area around the Rössing Mine and includes map unit thicknesses taken either from previous work or estimated from field observations and the attached map. The author's observations on this table are italicised in order to distinguish these from previous work. The major basement and Damaran-age metasedimentary units are summarised in Table 3.2.

Table 3.2. Summary of the stratigraphy of the area around the Rössing Uranium Mine.

Group	Formation	Major Lithologies	Approximate Max. Thickness
Swakop	**Kuiseb**	Cordierite schist	>500 m
	Karibib	Calcitic and dolomitic marble, biotite gneiss	900 m
	Ghaub Formation missing		
	Arandis	Calc-silicate gneiss, biotite schist	500 m
	Chuos	Diamictite, iron formation	800 m
	Rössing	Marble, biotite-cordierite gneiss, meta-arkose	500 m
Nosib	**Khan**	Clinopyroxene gneiss and granofels, biotite gneiss	450 m
	Etusis	Meta-arkose and biotite gneiss	1000 m
Tectonised contact			

Undifferentiated **Abbabis Metamorphic Complex**: K-feldspar meta-arkose, intermediate to mafic gneiss, granitic gneiss

This chapter provides a detailed description of the stratigraphy of the *immediate* Rössing area, first as determined from previous work and secondly from the author's own observations. Where there is no known description of a stratigraphic unit or series of units within or near to the project area, examples are given from nearby areas.

3.2 Summary of Previous Work in the Project Area

The stratigraphy of the district has been established largely through the work of Smith (1965) and Jacob (1974) with modifications to this by Lehtonen *et al.* (1995). Depositional environments of the Damaran metasedimentary sequence were interpreted by Henry (1992). In the immediate Rössing area, Nash (1971) established a detailed stratigraphy of the upper Nosib and lower part of the Swakop Group which is the currently applied mine stratigraphy. Numerous mapping projects have been undertaken subsequent to the work of Nash (1971) that have all utilised the stratigraphic scheme established at, and prior to, that time and these are described in Chapter 2.5.1. With the exception of the 1:250 000 scale map of Lehtonen *et al.* (1995) these workers have not identified the Arandis Formation as a separate formation, but instead units within this formation are included in the lower part of the Karibib Formation.

3.3 The Abbabis Metamorphic Complex

Previous work

The Palaeoproterozoic Abbabis Metamorphic Complex as introduced in Chapter 1.2.2 consists of poly-deformed and poly-metamorphosed metasedimentary rocks, paragneisses, orthogneisses, pegmatites and orthoamphibolites (Smith, 1965; Jacob *et al*., 1978; Marlow, 1981) with various stratigraphic schemes described.

Lithologies assigned as undifferentiated Abbabis Metamorphic Complex (A.M.C.) by Smith (1965) and Lehtonen *et al.* (1993, 1995, 1996) are exposed in the periphery of the mapped area forming dome cores to the northwest of the Rössing tailings area and to the southwest in the Lower Khan River area (referred to as the Khan Gorge Inlier or Palmenhorst Dome). Mapping of the A.M.C. within the project area is limited to that of Smith (1965) who describes a spectacular porphyroblastic sillimanite-gneiss occurring structurally below augen gneiss in the Nose Structure area, and to that of Poli (1997) who mapped the structural geology of the Nose Structure area in detail.

The character of the A.M.C. in the larger vicinity of the project area is summarised from various workers in Table 3.3 below. Smith (1965) described the district-wide stratigraphy of the A.M.C. as consisting of a lower unit of quartzofeldspathic biotite augen gneiss, muscovite-rich pelitic quartzite and plagioclase-rich biotite gneiss, and an upper unit of dolomitic marble, calc-silicate rock and biotite-schist. More recent mapping of the Abbabis Inlier (Figure 1.8) particularly by Brandt (1987) shows this

area to consist of a lower quartzofeldspathic paragneiss with interbedded metasediments (Twasisis Formation), intruded by granitoids of the Narubis Granitoid Complex and overlain by a relatively thick sequence of metasediments and basic volcanics (Naob Formation). In the area of the Tumas Inlier, Swartbank and possibly that of the Rooikuiseb Anticlinorium to the northeast, the Tumas River Formation also consists of a lower paragneiss-dominated succession intruded by the Swartbank Orthogneiss and an upper mixed metasedimentary succession (the latter only in the Swartbank area; Sawyer 1976, 1979; Bunting, 1977; Downing, 1982).

Table 3.3. Summary of mapping of the Ababbis Metamorphic Complex in the sCZ. No correlation is directly inferred between each area, however there are some consistencies between units - in particularly between major lower and upper divisions.

Abbabis Inlier (Gevers, 1931; Smith, 1965; Marlow, 1981; Brandt, 1985, 1987; Lehtonen *et al* ., 1995)		**Tumas Inlier, Swartbank** (Sawyer, 1976, 1979; Bunting, 1977), possibly the **Rooikuiseb Anticlinorium** (Downing, 1982)			**Walvis Bay Sheet 2214** (& Lehtonen *et al.* (1995) & District-wide summary of Smith (1965)	**Palmenhorst Dome (Khan River Inlier) and Ida Dome** (Longridge 2012 remapping of Barnes, 1981 & Jacob, 1974)
Naob Formation	Amygdaloidal tholeiitic metabasalt-andesite altered to biotite-hornblende schist & cordierite-garnet-sillimanite-hornblende schist (400 m)	**Tumas River Formation**	Upper *(Swartbank Antiform only)*	Paragneiss, schist	Dolomitic marble, calc-silicate rock and biotite-schist and metavolcanics	
	Feldspathic quartzite, calc-silicate rock, marble (150-650 m)			Calc-silicate rock, paragneiss, schist,		
	Very dark to black schists, metabasite (300-750 m)			Basal marble, conglomerate		
Tsawisis Formation	Quartzofeldspathic (arkosic-quartzitic) augen paragneiss with local interbeds of quartzite, conglomerate, schist, metabasite, marble, intruded by Narubis Granitoid Complex including the Habis granodioritic orthogneiss		Lower	Banded (locally augen) paragneiss with local interbeds of quartzite, schist, calc-silicate rock, Intruded by the Swartbank Orthogneiss (syenogranite microcline-porphyroblastic augen gneiss)	Migmatitic, biotite-sillimanite-gneiss, augen gneiss, biotite schist/gneiss, quartzite and amphibolite intruded by microcline augen gneiss.	Quartzofeldspathic gneisses & augen gneiss tectonised to S- and L-tectonites, predominantly orthogneisses representing the Narubis Granitoid Complex of Brandt (1987, far left)

Remapping of the Palmenhorst Dome (Khan Gorge Inlier) and Ida Dome by Longridge (2012) after Smith (1965), Jacob (1974) and Barnes (1981) shows the A.M.C. in this area to consist entirely of quartzofeldspathic gneisses and augen gneiss displaying S- and L-tectonites with no overlying metasedimentary or volcanic units recognised. On the basis of field observations and major and trace element geochemistry the majority of these lithologies are interpreted as orthogneisses representing the Narubis Granitoid Complex of Brandt (1987), with a minor component of possible paragneiss (Longridge, 2012). Metasedimentary slivers within

granitoids intruding A.M.C. near the Nose Structure area (Figure 1.2) and on the southwestern margin of the project area that were previously interpreted by Poli (1997) as part of the Tsawisis Formation of Brandt (1987), were re-interpreted by Longridge (2012) as rafts of Damaran metasediments on the basis of the presence of a full sequence of the latter occurring directly to the east.

Given the above descriptions the division of the A.M.C. by Lehtonen *et al.* (1995) on the 1:250 000 Walvis Bay sheet of the Geological Survey of Namibia into a lower variable gneiss (paragneiss) unit intruded by orthogneiss, and an upper metasedimentary-volcanic unit seems an appropriate regional scale division. Presumably then the orthogneiss-dominant Palmenhorst Dome of Longridge (2012) likely represents the lower part of the known A.M.C. where the upper part was either eroded prior to the deposition of the overlying Damaran Supergroup, structurally removed, or not deposited at all.

Cross-cutting hornblende-feldspar amphibolite dykes are considered to be the youngest event in the A.M.C. (Smith, 1965; Steven, 1994; Barnes, 1981; Marlow, 1981) where Brandt (1987) considered these to be dolerite dykes metamorphosed during Damaran orogenesis. The presence of amphibolite dykes are not, however, contrary to the interpretation of Barnes (1981), ubiquitously diagnostic of the A.M.C. as demonstrated by the U-Pb dating of Damaran-age amphibolites in the A.M.C. of the Ida Dome (Longridge, 2012). Orthoamphibolites also occur in Damaran-age metasediments in the western part of the Rössing SJ mine (Golder Associates, 1978).

This Work

The A.M.C. is exposed in the extreme southwest and northwest of the mapped area as domed inliers. In this study only the northwest area (Arandis Airport and tailings dam area) was visited and sampled for petrography. The A.M.C. in both areas is mapped as an undifferentiated unit on the appended map.

The A.M.C. generally forms areas of subdued relief making map interpretation of lithologies more challenging due to the presence of a thin gravel cover. Whilst the A.M.C. shows lithological heterogeneity extensive areas of outcrop are usually easily distinguishable with reference to airborne radiometric data as prominent thorium-uranium highs, seen on the R.G.B. ternary grid in Figure 2.3a where the relative abundance of uranium (blue) and thorium (green) compared to potassium (red)

combine to produce a cyan colour delineating the presence of the A.M.C. Thorium levels may be highly elevated in this unit (commonly tens of parts per million as determined from handheld field spectrometer readings). Alaskites that are spatially associated with the A.M.C. also commonly contain significantly elevated thorium concentrations. This characteristic can be inherited by the overlying Etusis Formation meta-arkoses that are presumably at least in part derived by weathering of the A.M.C. From follow up of airborne radiometric anomalies in the periphery of the mapped area, the A.M.C. has been noted to host spatially extensive units that may contain up to 15 ppm uranium (as measured by field spectrometer); no voluminous alaskite swarms have been noted in the A.M.C even where it is often highly migmatised. Where the A.M.C. is well exposed in the mapped area (i.e. only in the southwest as the northeast part of the Khan Gorge Inlier or Palmenhorst Dome) it is also readily distinguishable on hyperspectral imagery band combination 108-26-2 (equivalent to Landsat 7-4-1) as shown in Figure 3.1 below.

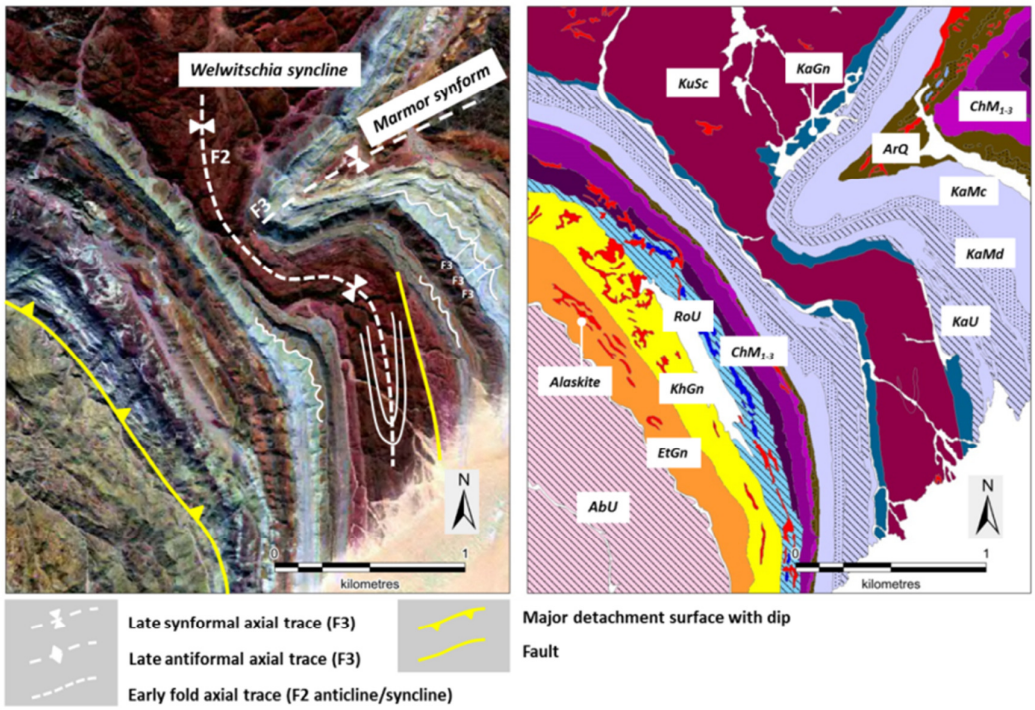


Figure 3.1. ***Left*** *- HyMap imagery band combination 108-26-2 (equivalent to Landsat 7-4-1) covering the area south of the Khan River and corresponding map interpretation. The image shows that this band combination can spectrally distinguish the entire mapped sequence at a formation-scale, and locally at a member-scale. Major structures (see Chapter 4) are shown on the hyperspectral image and include the fold axial trace of the major refolded Welwitschia syncline (Smith, 1965) and the sheared contact between the A.M.C. and overlying Damaran sequence. Highlighted satellite F_3 fold trends in Karibib Formation marbles show west vergence or M-type concentric folds. A north-northwest trending faulted contact is present between Kuiseb Formation schists and the top of the Karibib Formation observable in the bottom right of the image. Note the isoclinal north-south F_{1-2} similar fold within the hinge zone*

*of the Welwitschia syncline **Right** – lithological interpretation of the same area with map unit annotations as follows: AbU undifferentiated A.M.C.; EtGn Etusis Formation biotite gneiss; KhGn Khan Formation clinopyroxene gneiss; RoU undifferentiated Rössing Formation; ChM_{1-3} Chuos Formation diamictite units; ArQ Arandis Formation calc-silicate gneiss; KaMc Karibib Formation calcitic marble; KaMd Karibib Formation dolomitic marble; KaGn Karibib Formation biotite gneiss; KaU undifferentiated Karibib Formation; KuSc Kuiseb Formation cordierite schist. Figure is centred on 504000 mE, 7507000 mN.*

Field mapping and petrography has identified three major groups of lithologies occurring within the A.M.C to the northwest of the mine tailings area.

Meta-arkose (Figure 3.2a)

Samples RPS026, RPS027 and RPS028 were collected from the sheared contact zone between A.M.C. basement and Damara metasediments immediately northwest of the tailings area. They comprise well bedded fine- to medium-grained K-feldspar gneissic meta-arkoses. These arkoses could alternatively be assigned to one of the lower Damaran formations.

Mafic Gneisses (Figure 3.2b)

To the northwest of the basement-cover contact zone lithologies can be more confidently assigned to the A.M.C. and include epidote-chlorite-garnet-clinopyroxene-plagioclase gneiss, and magnetite-quartz-hornblende-plagioclase gneiss, (RPS029, RPS030, RPS031, and RPS032). Common features of these gneisses include a mafic composition, an abundance of magnetite and a retrograde epidote and chlorite assemblage after garnet and pyroxene respectively. Limited observable field relationships and petrography suggest these lithologies likely represent metamorphosed basic volcanics.

Granite and Felsic Gneisses (Figure 3.2c-e)

In the extreme northwest of the mapped area granitic lithologies including biotite-K-feldspar-plagioclase-quartz granite gneiss (RPS071) of monzogranitic composition and foliated red alkali feldspar biotite-granite (RSS071) appear to predominate; the latter is placed in the A.M.C. as no contact relationships have been defined, however this red granite may well be an intrusive of Damaran-age (see Table 1.5). To the east and spatially associated with the intermediate-mafic gneisses, biotite-plagioclase-K-feldspar-quartz augen gneiss occurs (RPS033) however contact relations are not exposed. No obvious compositional variation within the granite gneisses were observed in the field. These are therefore tentatively interpreted as orthogneisses.

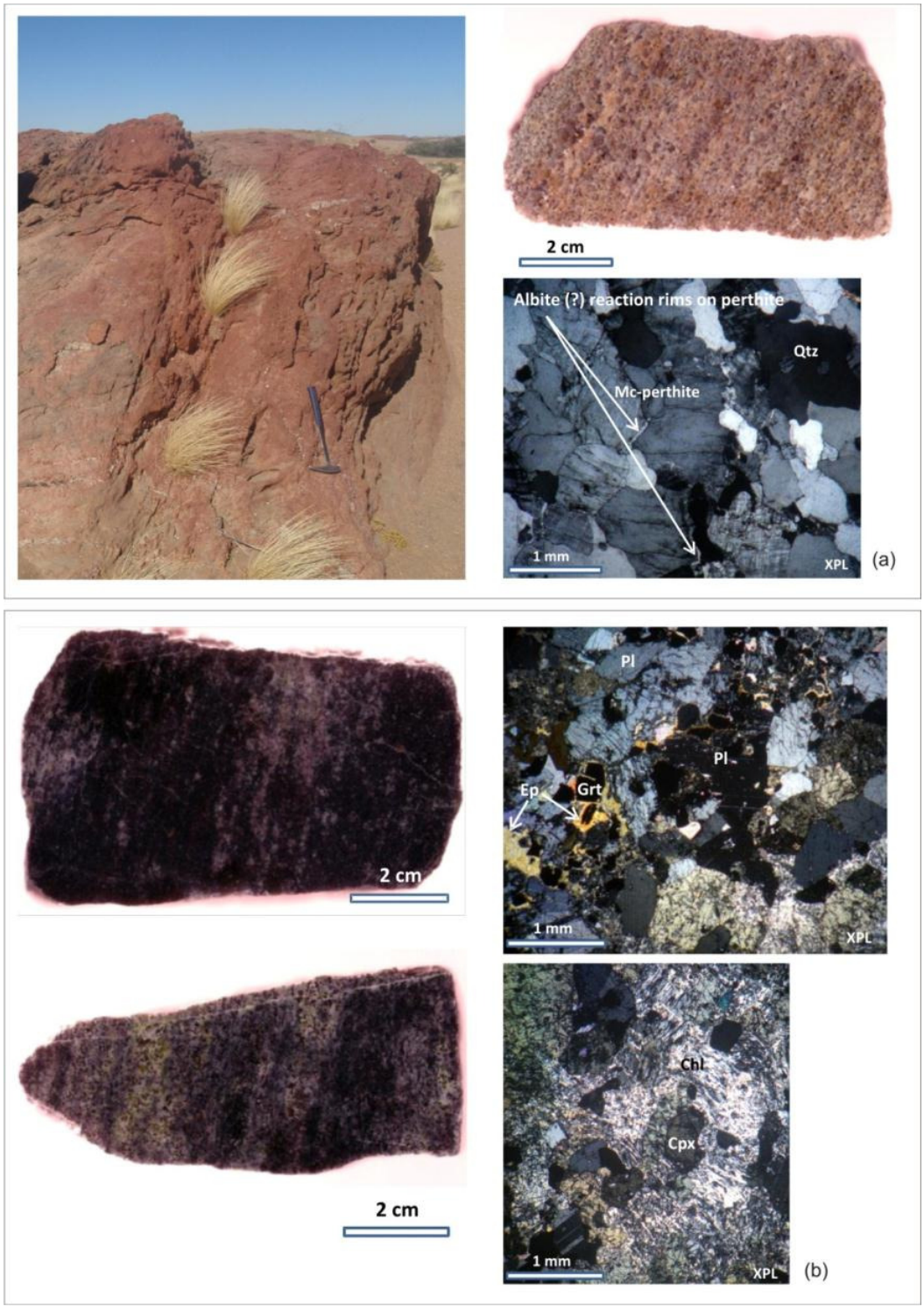


Figure 3.2. (a): Left – outcropping red-weathering gneissic meta-arkose of the A.M.C. northwest of the Rössing mine tailings area; top-right – meta-arkose RPS026; bottom-right – thin section of meta-arkose RPS026 showing characteristic decussate textures at microcline-perthite and quartz grain boundaries. (b): Intermediate to mafic gneisses of the A.M.C. from northwest of the tailings area; top-left – RPS029, bottom-left – RPS030, right – thin sections of RPS030 showing idiotropic textures, retrograde alteration of garnet to epidote and clinopyroxene to chlorite. PPL – plain polarised light, XPL – cross polarised light. For an explanation of mineral abbreviations refer to Appendix I.

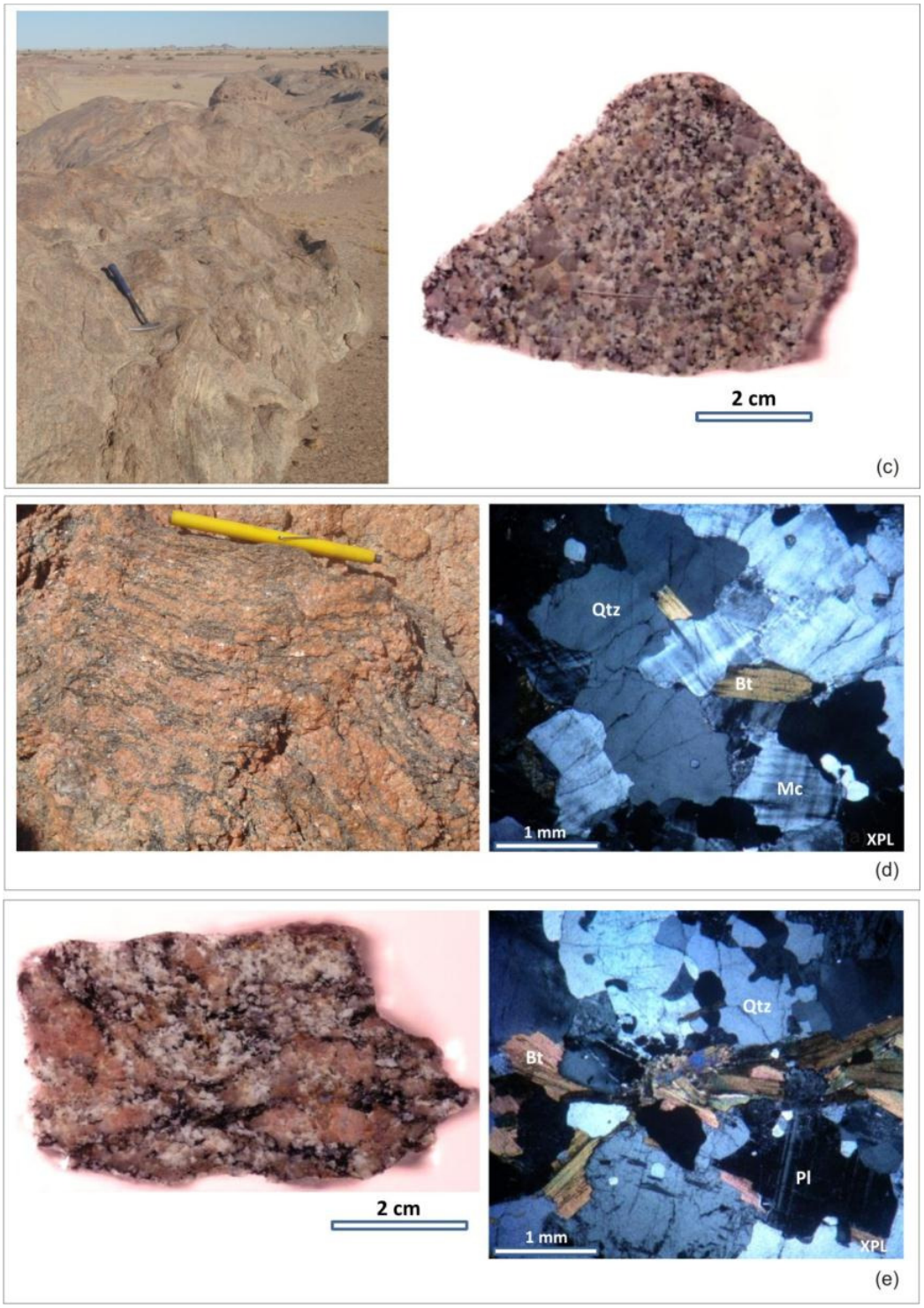


Figure 3.2 (Cont.). Granite and felsic gneisses of the A.M.C. (c) left – outcropping granite gneiss in the Arandis Airport area and, right - corresponding sample RPS071 (monzogranite); (d) left – outcropping foliated, biotite-bearing, red alkali feldspar granite in the Arandis Airport area and, right – corresponding thin section from RSS071; (e) left – augen gneiss sample RPS033 and, right – corresponding thin section. PPL – plain polarised light, XPL – cross polarised light. For an explanation of mineral abbreviations refer to Appendix I.

3.4 Damaran Metasediments

The Damaran-age metasedimentary sequence in the Rössing area is separated into an early rift fill comprising the Etusis and Khan Formations (Nosib Group) and a later deeper water succession represented by the Rössing, Chuos, Arandis, Karibib and Kuiseb Formations (Swakop Group). These units were introduced in Chapter 1.2.2. and characteristics of these formations within the mapping area are presented in Table 3.1.

3.4.1 Etusis Formation

Previous Work

The Etusis Formation in the sCZ is characterised by irregular packages of feldspathic quartzite with infrequent pelitic units deposited in a braided fluvial environment unconformably upon the Abbabis Metamorphic Complex, during rifting of the supercontinent Rodinia at ca. 750 Ma (Chapter 1 and references therein).

Southwest of Rössing in the Palmenhorst Dome area the lack of recognisable bedding in quartzites of the Etusis Formation obscures any clear contact with the A.M.C. (Longridge, 2012). According to Lehtonen *et al*., (1996) contact relations are complicated by increasing metamorphic grade downwards into rocks of the A.M.C., whilst the two units have a conformable foliation. Previously mapped as red gneissic granite of the A.M.C. by Smith (1965), the Rössing SJ Dome is assigned a four-unit Etusis Formation stratigraphy by Berning *et al.* (1976) and Berning (1986) that includes a basal feldspathic quartzite followed upwards by lower biotite gneiss, marker quartzite, and upper biotite gneiss. The tables depicting the stratigraphy in these respective papers appear to be erroneous as noted by Oliver and Kinnaird (1996), with only two principal units, a lower feldspathic quartzite and upper biotite gneiss actually described in the text of Berning *et al.* (1976). The upper biotite gneiss is noted to be invaded by alaskite on a massive scale.

In contrast to the above, the fourfold stratigraphy of Oliver and Kinnaird (1996) in the Rössing SJ Dome area consists of lower biotite-schist, lower meta-quartzite, upper biotite schist and upper meta-quartzite, and they place overlying biotite gneiss at the base of the Khan Formation. The schists are described as being composed of feldspar and biotite (± amphibole). Arkosic quartzites are flaggy centimetric- to metrically-bedded, exhibiting both graded and cross-bedding, the latter defined by the presence of heavy mineral laminae. These way-up criteria indicate that beds are not overturned. The arkosic quartzites commonly show migmatitic or agmatitic

textures in outcrop and at one locality a concordant 10 m thick mafic (epidote-diopside-hornblende-biotite) interbed occurs. Mylonitic textures in the contact zone between the upper biotite schist and upper quartzite are interpreted by Oliver and Kinnaird to represent the presence of a shear zone (Chapter 4.2).

Nash (1971) and Cuney (1980b) describe 'meta-arkose' of the Etusis Formation as fine-grained with plagioclase as the dominant feldspar, and 'migmatitic biotite-gneiss' as a calcite-biotite-plagioclase-K-feldspar-quartz gneiss. Both of these major rock types are typically fine-grained but show coarse migmatitic leucosomes, and both contain accessory magnetite and ilmenite as the most common opaque phases with frequent monazite and zircon. The microscopic texture of the quartzites is blastoclastic to granoblastic (Lehtonen *et al.*, 1996). The abundance of microcline feldspar in granitic gneisses has led some workers to interpret these as metamorphosed acid volcanic rocks (e.g. Blaine, 1977). An alternative explanation is that these lithologies may simply be volcanoclastic sediments derived from acid volcanics. Based on major element geochemistry, Cuney (1980b) interpreted one sample of Etusis quartzite to represent a metamorphosed albitised volcanic tuff. Many outcrops of Etusis Formation in the sCZ are noted to be typically wedge-shaped suggesting deposition in half-grabens (Miller, 2008). A basal conglomerate to the Etusis Formation that may be present elsewhere (e.g. Smith, 1965) has not been described in the project area.

Further afield from the project interbeds of biotite ± hornblende schist occur in the Etusis Formation of the lower Swakop River area (Jacob, 1974). In the Ida Dome area quartzite and meta-arkose grade upwards into biotite schist and to the east sillimanite schist and pelitic schist have been described (Longridge, 2012), whilst sillimanite ± biotite gneiss units occur on the northern margin of the Palmenhorst Dome (Marlow, 1981).

This Work

The Etusis Formation forms the lowermost unit of the Damara succession except where stratigraphically higher units appear to have been structurally juxtaposed presumably by shearing against A.M.C. basement lithologies in the area northwest of the mine tailings. The contact in the area of the Khan Gorge Inlier in the Khan River consists of a subtle transition from quartzofeldspathic gneiss of the A.M.C. through to a bedded meta-arkose of the Etusis Formation.

Mapping during this work identified a twofold member-scale stratigraphy of a lower meta-arkose unit and upper biotite gneiss. The name 'meta-arkose' is preferred here to 'feldspathic quartzite' as it is more indicative of the mineralogy. The meta-arkose shows rare submetric scale interbeds of conglomerate and forms the SJ Dome core which is then rimmed by the upper biotite gneiss member. The latter tends to form areas of lower relief, is intruded on a massive scale by early deformed alaskites, and is significantly more incised by drainage features due to its lower competency. Across the mapped area spectral contrasts between the two units are best exhibited by hyperspectral band combination 108-26-2 (equivalent to Landsat 7-4-1) as shown in Figures 1.2, 2.11 and 3.4. The meta-arkose and biotite gneiss units are described below.

Meta-arkose (Figure 3.3a)

Petrographic observations of the meta-arkose are limited to sample RSS051 taken from the Khan River valley in the extreme southwest of the mapped area, which shows plagioclase to be the only feldspar present. Late 'blebby-textured' quartz is a feature of this rock. An example of sporadic dark, lensoid calc-silicate interbeds on a metric scale occurring within the meta-arkose of the SJ Dome was sampled as RPS042 and consists of an assemblage of epidote-plagioclase-quartz-garnet. A similar example noted by Oliver and Kinnaird (1996) consists of epidote-diopside-hornblende-biotite. With reference to the radiometric ternary image of Figure 2.3a, the meta-arkoses forming the core of the SJ Dome are thorium-uranium-enriched exhibiting a similar radiometric signature to the A.M.C. Thorium enrichment within what is likely to be the same unit in the southeast extremity of the mapped area on the south side of the Khan River is also extremely pronounced. In places at the SJ Dome, sillimanite knots have been noted in the meta-arkose however this mineral was not noted in thin section.

Biotite Gneiss (Figure 3.3c)

Microscopic examination of a biotite gneiss sample from the SJ Dome (RSS011) determined an assemblage of ilmenite-phlogopite-plagioclase-microcline-quartz. Late 'blebby-textured' quartz is also feature of this rock. A sample of a conglomeratic interbed within the biotite gneiss taken from the Khan Mine Gorge (RSS042) is an ilmenite-quartz-tremolite-phlogopite microcline meta-conglomerate. Biotite gneiss on the SJ dome has been noted to contain magnetite porphyroblasts and sillimanite porphyroblasts at separate localities, and may be intensely migmatised, locally exhibiting agmatitic textures (Figure 5.2f).

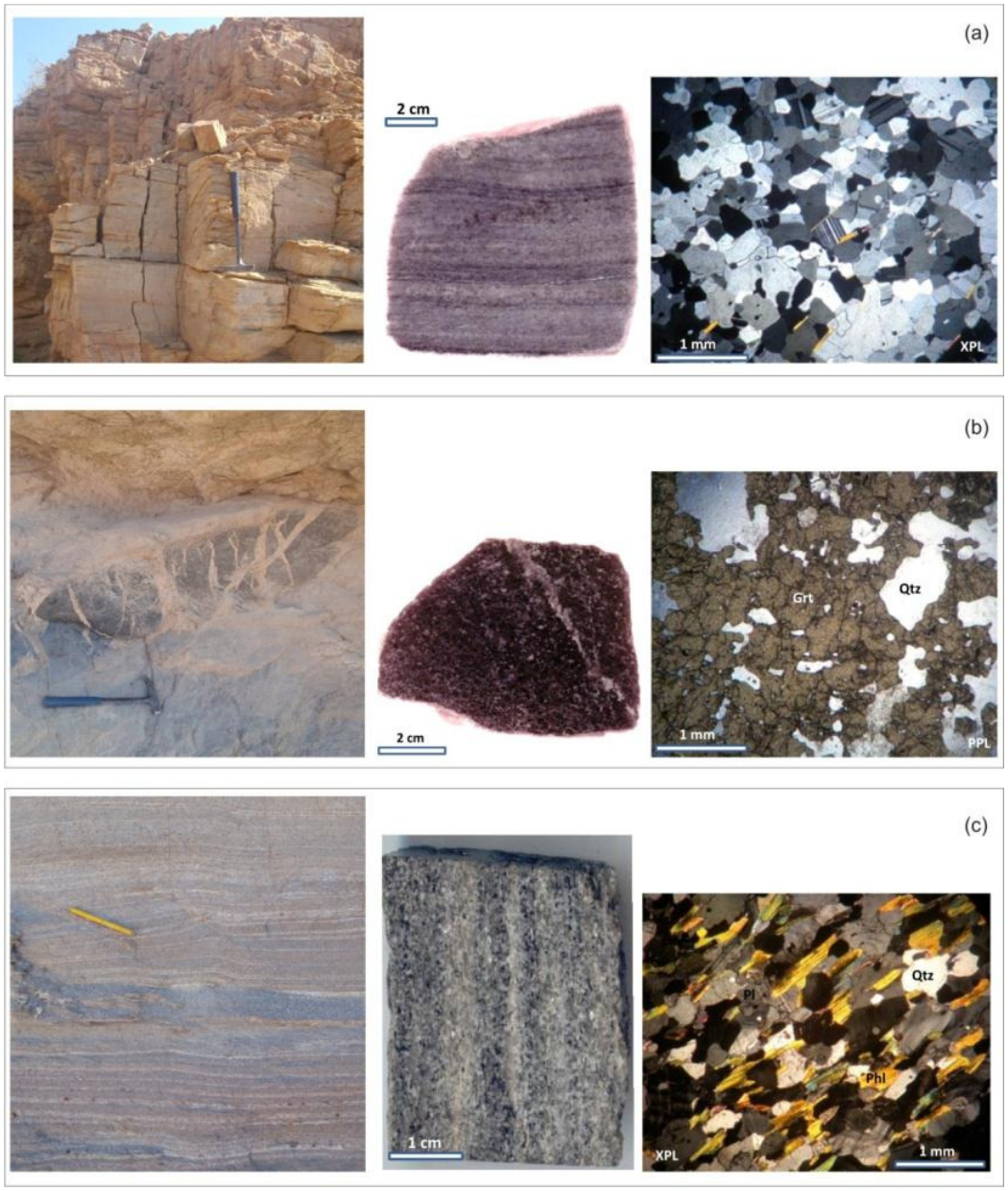


Figure 3.3. Mapped units of the Etusis Formation. (a): bedded meta-arkose outcropping on the SJ Dome (left), in hand specimen RSS051 (middle) showing heavy mineral-rich laminae, and exhibiting moderately developed granoblastic texture in a thin section of the same sample (right); (b): interbed of plagioclase-quartz-garnet calc-silicate in meta-arkose of the SJ Dome cut by alaskite (left), and in RPS042 hand specimen and thin section (middle, right); (c): outcrop of biotite gneiss on the SJ Dome showing the effects of shearing as tension gashes in the orientation of the swing magnet (left) and hand specimen and thin section of RSS011 (right), an ilmenite-phlogopite-plagioclase-microcline-quartz-gneiss. PPL – plain polarised light, XPL – cross polarised light. For an explanation of mineral abbreviations refer to Appendix I.

3.4.2 Khan Formation

Previous Work

The Khan Formation conformably overlies the Etusis Formation and consists of predominantly clinopyroxene- and hornblende-bearing feldspathic quartzite deposited in a fluviodeltaic environment (Nash, 1971; Jacob, 1974; Henry, 1992; Miller, 2008; Chapter 1.2.2). The type locality of the Khan Formation is in the Khan River within the mapping area where it shows cyclical repetition of more arenitic layers and sporadic, thin, pebble-conglomerate layers. Locally, arkosic quartzite is developed and at the top of the formation, biotite-gneiss and biotite-amphibole schist are locally present (Nash, 1971; Jacob, 1974; Miller, 2008). The presence of a calc-silicate-rich interlayer within the upper part of the Etusis quartzites (Lehtonen *et al.*, 1996) and interbeds of clinopyroxene-hornblende gneiss in Etusis Formation of the lower Swakop river area (Jacob, 1974), indicates a regional interfingering relationship between the Etusis and Khan Formations. In the Rössing area, clinopyroxene gneisses ('lower' and 'upper banded gneiss' of the Rössing Mine stratigraphy; 'calc-granulites' of Smith, 1965; 'basic gneisses' of Nash, 1971) of the Khan Formation are granoblastic, fine-grained, equigranular, thinly banded clinopyroxene-biotite-hornblende-K-feldspar-plagioclase-quartz gneisses. These exhibit alternating dark and pale green layers, respectively enriched in hornblende and clinopyroxene, with hornblende increasing upward at the expense of clinopyroxene with less marked banding in the upper unit. Opaque minerals, calcite, sphene, scapolite and apatite are common accessory phases (Nash, 1971, 1972). Higher strain zones are migmatitic where coarse-grained leucocratic segregations contain quartz-plagioclase ± biotite ± magnetite, whilst primary anhydrite can be common in accessory amounts but may constitute up to 20% of the rock volume in such zones (Nash, 1971, 1972; Cuney, 1980b; Basson and Greenway, 2004). Mafic restites consisting of pyroxene and amphibole within *in situ* migmatites in the Khan River section of the project area may also show increase in grain size in both concordant lenses and as irregular patches (Miller, 2008). Between the two 'banded' gneisses in the SJ area a migmatised clinopyroxene-garnet gneiss ('mottled gneiss' of the Rössing Mine stratigraphy) typified by aggregates of dark brown anhedra of calciferous garnet thickens to the west (Nash, 1971). Berning *et al.* (1976) note that to the east of SJ the mottled texture of the clinopyroxene-garnet gneiss gives way to a metamorphic banding, and that this unit, in contrast to the upper and lower banded gneiss, exhibits K-feldspar as being dominant over plagioclase. The uppermost unit of the Khan Formation in the SJ area, the 'amphibole schist' of Rössing Mine stratigraphy is a heterogeneous package of thinly-bedded amphibole-biotite-schist or gneiss, with

marble (or skarn) and amphibolite (hornblendite) bands with rare lenses of matrix supported conglomerate at its base (Laberge 2008a, 2008b; Nash, 1971). Biotite is the most abundant phase with colourless to pale green amphibole evident in thin section (Cuney, 1980b). Outside of the SJ-SK area Khan Formation lithologies are poorly described. However at SH, Mestres-Ridge (1992) mapped a 'basal conglomerate' in the Khan Formation consisting of exclusively quartz pebbles within a fine-grained silica matrix outcropping over an area of some 300 m by 100 m, and interpreted relict igneous textures in the 'amphibole schist' at the top of this formation. Further afield on the eastern margin of the Palmenhorst Dome, Longridge (2012) describes upper and lower clinopyroxene gneiss units separated by a sequence of cordierite gneiss followed by biotite ± quartz ± magnetite schist. The upper part of the Khan Formation is an important cupriferous horizon as described in Chapter 7.3.

This Work

Panner Gorge and the area to the immediately west (Figure 1.2) is considered the type area for examining the stratigraphy of the Khan Formation gneisses where the sequence of lithologies is more diverse and better exposed than elsewhere (Figure 2.19). Two clinopyroxene gneiss units ('banded gneiss' of Rössing Mine stratigraphy) in the lower part of the succession are separated by a clinopyroxene granofels ('mottled gneiss' of Rössing Mine stratigraphy). The gneiss and particularly the granofels units commonly show textures interpreted as resulting from partial melting. Textural features comprise either leucosomal tension gashes filled with coarse-grained quartz-feldspar or diopside-hornblende segregations which show a variety of post-formation deformation textures (Figure 4.7a, 4.7f, 5.2c). The biotite gneiss ('amphibole schist' of Rössing Mine stratigraphy) is only present in the area of the Rössing Mine (SK through SJ to SH areas) and it thins rapidly so that in the Panner Gorge area it is only intermittently present but is likely to underlie much of the alluvial cover present around the Rössing-Khan Formation contact. Away from Panner Gorge, to the southwest and the area around the SJ Dome, the stratigraphy of the Khan Formation is dominated by clinopyroxene gneiss.

The clinopyroxene gneisses and clinopyroxene granofels of the Khan Formation form a characteristic grey-green colour in outcrop whilst the biotite gneiss is much darker in colour and readily identifiable on aerial photography. The Khan Formation gneisses also form some of the most prominent topographic highs in the area, for example along the mine access road adjacent to the tailings dam, on the south side

of the SJ open pit, and in the Lower Khan River area. Optimum imagery for the purpose of separating the gneiss from granofels units is the Minimum Noise Fraction (M.N.F.) transform applied to the hyperspectral data as shown in Figure 3.4 below (see Chapter 2.3.3 and Figure 2.11). Details of the individual units of the Khan Formation are described below.

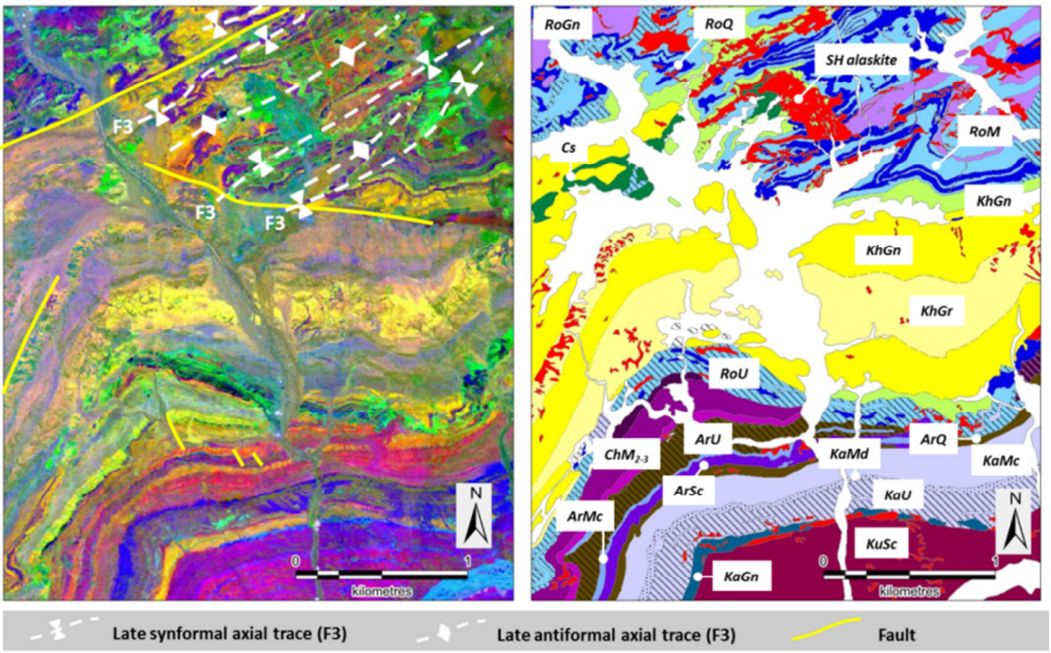


Figure 3.4. ***Left*** *- HyMap imagery band combination 10-11-12 with M.N.F. transform in the Panner Gorge area (see Figure 1.2). This image distinguishes virtually every mapped unit at member scale (right). Fold structures are dominantly F_3 synform-antiforms superimposed on the larger Rossing synclinorium F_2-F_3 fold interference structure (Chapter 4, Figure 4.2). Major faults are evident from map relations at the Khan-Rössing Formation contact zone with minor northwest-trending faults parallel to possible F_4 fold axial planes.* ***Right*** *– lithological interpretation of the same area with map unit annotations as follows: KhGn Khan Formation clinopyroxene gneiss; KhGr Khan Formation Granofels; KhMg Khan Formation Biotite Gneiss; RoM Rössing Formation marble; RoGn Rössing Formation cordierite gneiss; RoQ Rössing Formation feldspathic quartzite; RoU undifferentiated Rössing Formation; ChM_{2-3} Chuos Formation diamictite facies 2-3; ArMc Arandis Formation calcitic marble; ArSc Arandis Formation biotite schist; ArQ Arandis Formation calc-silicate gneiss; ArU undifferentiated Arandis Formation; KaMc Karibib Formation calcitic marble; KaMd Karibib Formation dolomitic marble; KaGn Karibib Formation biotite gneiss; KaU undifferentiated Karibib Formation; KuSc Kuiseb Formation schist; Cs cross-cutting calc-silicate replacement. The SH uraniferous alaskite plug intrudes an intensely (F_3) folded Khan-Rössing Formation contact hence is demonstrably post-D_3. Note that the Chuos Formation pinches out completely in the southern part of Panner Gorge. Figure is centred on 503000 mE, 7511000 mN.*

Clinopyroxene Gneiss (Figure 3.5a)

Samples of the clinopyroxene gneiss exhibit assemblages spanning biotite-diopside-quartz-plagioclase-K-feldspar, anhydrite-tremolite-plagioclase-quartz, ilmenite-diopside-quartz-tremolite-plagioclase, magnetite-quartz-plagioclase-tremolite-K-feldspar (RSS049, RPS025, RSS075, RSS078, and RPS029). Mineralogical species

and relative abundances of these are clearly variable and whilst clinopyroxene (as diopside) is the most common metamorphic index mineral, it is not ubiquitous. Fine-grained granoblastic textures are typical. The accessory iron oxide phase can be either ilmenite or magnetite, however from field observations, it is apparent that magnetite becomes increasingly more abundant upward and that the top of the upper clinopyroxene gneiss may be strongly magnetic. Typically less than 1 m thick quartz-pebble conglomerate beds occur in the upper clinopyroxene-gneiss unit in the southern section of Panner Gorge.

Clinopyroxene Granofels (Figure 3.5b)

This unit, termed the '*mottled gneiss*' in the mine stratigraphy, forms more rounded outcrops in comparison to the surrounding clinopyroxene gneisses. Samples, taken mostly from Panner Gorge but also SJ pit and SK drill core contain the assemblages plagioclase-K-feldspar-tremolite-quartz, ilmenite-hornblende-diopside-plagioclase-quartz, diopside-hornblende-plagioclase-quartz, feldspar-biotite-diopside-quartz, epidote-garnet-scapolite-quartz, diopside-biotite-quartz-plagioclase, quartz-diopside-hornblende-plagioclase, and tremolite-plagioclase-quartz (RPS017, RPS020, RPS021, RPS024, RSS050, RSS076, RSS077). Like the enclosing gneissic units, clinopyroxene as diopside is the most common metamorphic index mineral but is not always present. The 'mottled' texture exhibited by this unit is interpreted to represent a partial melting texture with ferromagnesian minerals forming restites and quartz-feldspar aggregates representing migmatitic leucosomes. The tendency for this unit to be more migmatitic in nature is probably due to its characteristically more siliceous composition than the enclosing gneisses.

Biotite Gneiss (Figure 3.5c)

Biotite gneiss (*'amphibole schist'* of the mine stratigraphy) forms the uppermost unit of the Khan Formation where it is present. It is thickest in the SJ-SH-SK area (Figure 1.2) and, owing to its high biotite content tends to be fissile and friable and poses stability problems on the south SJ pit wall. It is readily identifiable due to its black colour which may be black-green where appreciable amounts of diopside are also present. Assemblages include ilmenite-quartz-tremolite-biotite-feldspar, quartz-feldspar-biotite-hornblende, hornblende-quartz-biotite-plagioclase-K-feldspar, tremolite-biotite-K-feldspar and biotite-diopside-hornblende (RPS059, RPS072, RSS028, RSS079, RSS037, and RSS080). Biotite is common throughout whilst amphibole as tremolite or hornblende is common but not ubiquitous. Quartz commonly forms late leucosomes.



Figure 3.5. Mapped units of the Khan Formation. (a) outcropping clinopyroxene gneiss in the area northeast of SK (left), RSS049 from the junction of the Khan Mine Gorge and the Khan River (middle) and thin section of RSS078 from SK drill hole SK07D013 (right), a poikiloblastic ilmenite-diopside-quartz-tremolite-plagioclase gneiss; (b) outcrop of clinopyroxene granofels in Panner Gorge (left), RPS020 in hand specimen (middle) and thin section (right), also from Panner Gorge, an ilmenite-hornblende-diopside-plagioclase-quartz granofels; (c) outcropping biotite gneiss northeast of SK exhibiting dark biotite-amphibole-rich and green pyroxene-rich bands (left), and RPS072 from the same area in hand specimen (middle) and thin section (right), a quartz-feldspar-biotite-hornblende gneiss with quartz leucosomes. PPL – plain polarised light, XPL – cross polarised light. For an explanation of mineral abbreviations refer to Appendix I.

Thin centimetric beds of amphibolite (hornblendite) and/or marble are commonly found toward the contact with the overlying Rössing Formation.

3.4.3 Rössing Formation

Previous Work

The Rössing Formation is a laterally restricted mixed succession of carbonates and siliciclastics (Chapter 1.2.2). The extreme lithological variability of the Rössing Formation as noted by Smith (1965) in the vicinity of the Rössing mine is shown in Figure 3.6. Nash (1971) describes para-amphibolite of the uppermost Khan Formation conformably grading via marly interbeds into marble of the Rössing Formation, a similar observation to that of Nex (1997) at nearby Goanikontes. Smith (1965) and Jacob *et al*. (1986) interpret an unconformity at this horizon. In the Rössing SJ-SK area, the fivefold subdivision of the Rössing Formation of Nash (1971), consisting of lower and upper marble and gneiss units with an uppermost quartzite remains in current use in the mine stratigraphy. However, internally these units consist of multiple rock types. Nash recognised two marble parageneses independent of the upper and lower units: first a quartz-diopside-calcite marble and secondly, a pleonaste-phlogopite-chondrodite-forsterite-calcite marble. The lower marble is serpentine-marble with subordinate graphitic marble, with irregular intercalations of diopside-biotite granofels and pelitic schist. The upper marble is a serpentine or diopside-quartz marble with interbedded diopside-biotite granofels and cordierite-biotite gneiss, with a conglomerate at its base. Accessory minerals include sphene, pyrite, scapolite, plagioclase, epidote, tremolite and garnet (Nash, 1971; Cuney, 1980b; Smith, 1965).

Dolomite generally does not exceed 10% of marble rock volume. However, Smith (1965) notes samples where dolomite forms 80% of carbonate, and where calc-silicate bands are present these are principally composed of fine-grained quartz, scapolite, calcite and diopside. Thin beds of biotite schist intercalated with the marbles are strongly foliated, medium- to fine-grained quartzofeldspathic garnet-cordierite-biotite to porphyroblastic biotite-hornblende-scapolite-hedenbergite schist where porphryoblasts are generally randomly oriented.

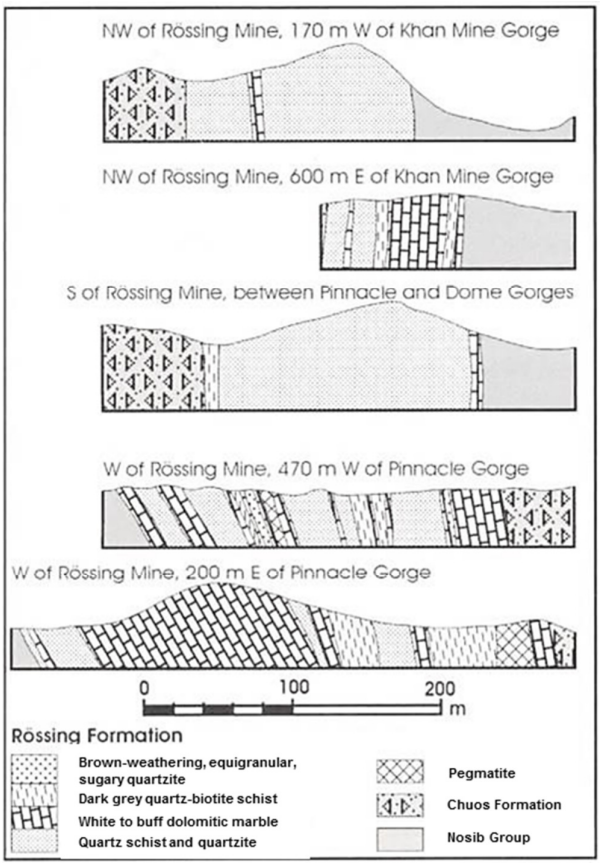


Figure 3.6. Lithological variability of the Rössing Formation in the vicinity of the Rössing mine. From Miller (2008) after Smith (1965). For locations see Figure 1.2; Pinnacle Gorge is assumed to be located between Panner Gorge and Rossing SJ.

The upper and lower gneiss units of the Rössing Formation in the SJ-SK area, variously described as 'cordierite-gneiss', 'semi-pelitic' or 'pelitic gneiss' and quartz-biotite schist show a general association of biotite-K-feldspar-cordierite-plagioclase-quartz ± sillimanite ± garnet (Smith, 1965; Nash, 1971; Laberge, 2008a, 2008b). The lower gneiss is a migmatised sillimanite-biotite-cordierite gneiss, locally garnet-bearing, grading upwards into biotite-hornblende schist. The upper gneiss is diopside-biotite ± scapolite gneiss with thin interbedded quartz grit and marble, grading upwards into cordierite-biotite gneiss. The characteristic migmatisation is expressed as quartzofeldspathic metatects up to several tens of centimetres long. Accessory minerals include apatite, zircon, pyrite, iron-titanium oxides and green spinel. Cordierite poikiloblasts are ubiquitously altered to pinite (Nash, 1971).

In the Rössing SJ-SK area, medium-grained, clean to pyritic quartzite with a gritty base forms the uppermost unit of the Rössing Formation (Nash, 1971; Laberge 2008a, 2008b). Elsewhere granular quartzite forms both distinct units and lateral

facies equivalents to marble members, containing microcline and/or plagioclase as subsidiary constituents with accessory zircon, apatite, biotite, muscovite and iron oxides. Pyritic quartzite weathers to a reddish-brown colour characteristic of the formation (Smith, 1965). Beyond the project area, the Rössing Formation is frequently missing from the Damaran succession (e.g. Smith, 1965). In the Ida Dome area in similarity to Rössing, the formation exhibits lower and upper marble units separated by calc-silicate and metapelites or, to the northwest of the Ida Dome, quartzite, where the upper marble unit is succeeded by quartzite, quartz-biotite schist and cordierite gneiss (Jacob, 1974; Longridge, 2012). According to Longridge (2012) to the southeast of the Ida Dome the formation is structurally repeated into packages up to 1 km thick and has likely been erroneously mapped as Karibib Formation by Lehtonen *et al.* (1995).

This Work

In similarity to the Khan Formation, the Rössing Formation stratigraphy established by Nash (1971) can only be applied to the immediate Rössing Mine area. Away from this area the formation rapidly thins and/or consists of a heterogeneous lithological package that exhibits marked lateral facies changes. In cases it appears to have been structurally removed through attenuation, as may be the case on the limbs of the Blauer Heinrich Syncline. Northwest of Panner Gorge the formation consists almost entirely of pyritic (± pyrrhotite) meta-arkose with minor marble. In the Z20 area the lithological assemblage is similar to that seen around the Rössing mine however, no detailed stratigraphy has been elucidated at the time of writing. In the Khan River south of SK no marble is present at all. This formation, due to its internally heterogeneous nature, is typically strongly deformed (Figure 4.6a).

The Rössing Formation is readily identifiable in the field by a typical red colour associated with the jarositic weathering of sulphide-bearing meta-arkose mixed with brown marbles. The marbles can also form ridges such as at SK and particularly where they are dolomitic. Biotite-cordierite gneiss forms distinctive dark outcrops that should not be confused with biotite gneiss of the Khan Formation on aerial photography. The top of the formation is characteristically a magnetic high on airborne magnetic data probably due to the presence of pyrrhotite as observed in meta-arkose (see below).

The typical red-brown colour of outcrops is readily observable on aerial photography, whilst on hyperspectral imagery marbles are easily identifiable on various processed

products (Figures 3.4, 3.8) and jarosite distribution can be used effectively to delineate pyritic or pyrrhotitic meta-arkose on iron oxide end-member images as shown in Figure 3.7 below. Details of the individual units of the Rössing Formation are described below.

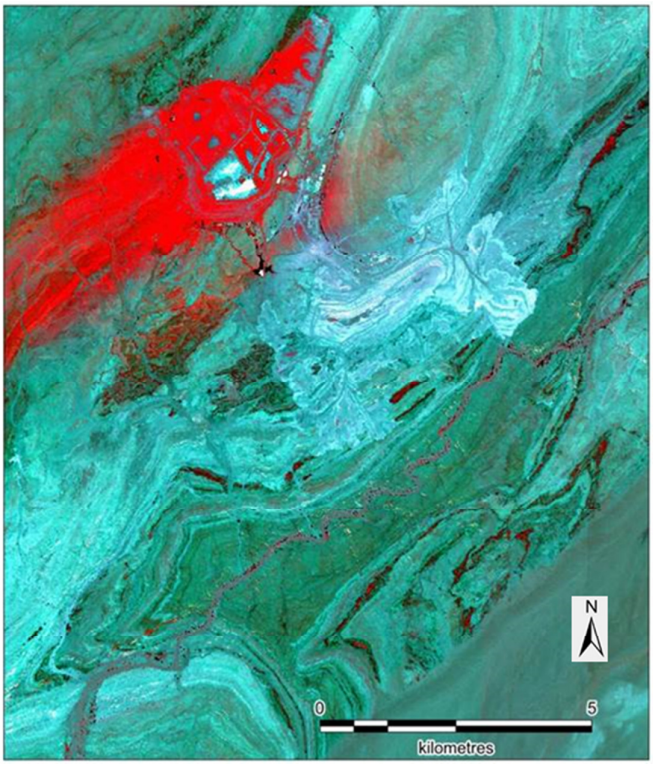


Figure 3.7. Hyperspectral end-member image showing the distribution of hematite-goethite (blue-green) and jarosite (red). Jarosite effectively maps the pyritic meta-arkose of the Rössing Formation and pyritic calc-silicate beds within the Arandis Formation. Jarosite forms through oxidation of pyrite and can be seen to be dispersed by wind to the southwest of the tailings area. Figure is centred on 505000 mE, 7511000 mN.

Marble (Figure 3.9a, 3.9b)

Calcitic versus dolomitic marbles can be distinguished easily on hyperspectral imagery due to a distinctive spectral shift in absorption features toward higher wavelengths in the latter (see Figure 2.6 for detail). In the case of the Rössing Formation, it can be seen with reference to Figure 3.8 that the lowermost marbles of this formation in the Panner Gorge area are commonly but not ubiquitously dolomitised. The carbonate species in field and core samples were also determined by reference to the collected P.I.M.A. spectra. Assemblages noted in thin section include pyrrhotite-tremolite-quartz-calcite, olivine-dolomite, pyrite-tremolite-calcite, graphite-scapolite-calcite, and calcite-serpentine (RSS081, RSS082, RSS045, RSS026, RSS084). Associated skarn assemblages sampled are calcite-wollastonite-scapolite-quartz (RSS038, upper reaches of Panner Gorge), phlogopite-chlorite-

calcite (RSS083, SK) and K-feldspar-quartz epidosite (RSS056, Khan River). 'Wollastonitised' marbles were noted in the field to be a very common feature in the Rössing Formation.

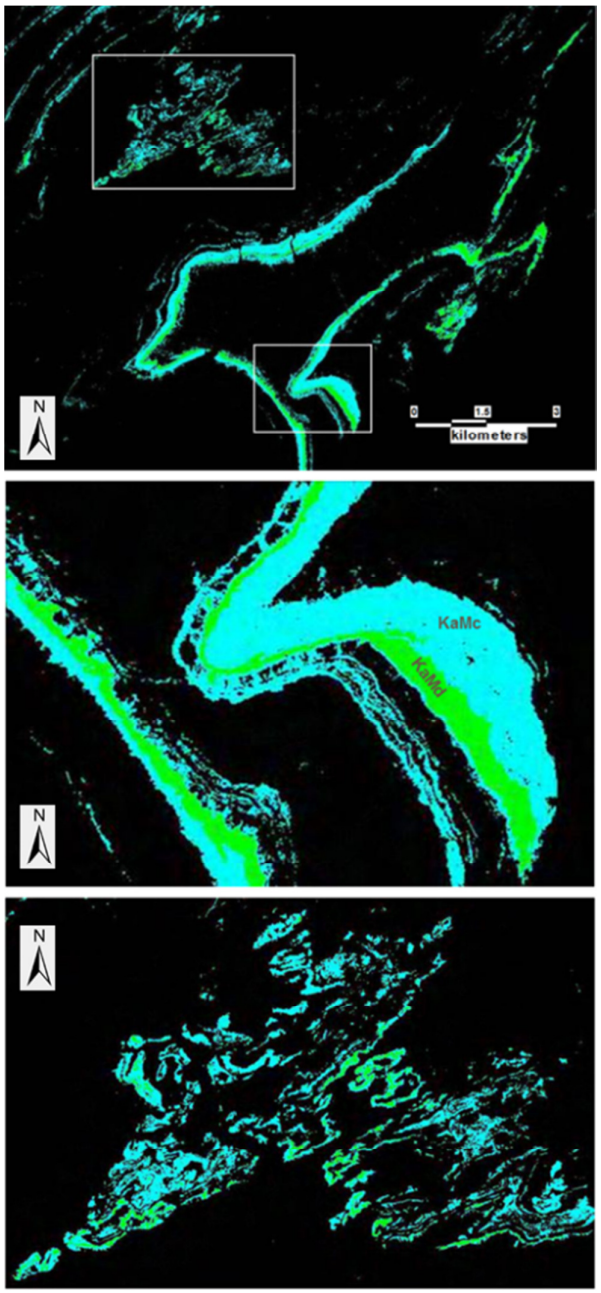


Figure 3.8. Hyperspectral carbonate end-member images showing examples of the distribution of calcite and dolomite in the Rössing and Karibib Formations. Upper image: overview of the areas shown in the lower two images; middle image: detail of the Karibib Formation marbles showing 1) a lower calcitic member (cyan, KaMc), 2) a middle dolomitic member (green, KaMd) and 3) an upper mixed calcitic marble-non-carbonate member; lower image: detail of calcite (cyan) versus dolomite (green) distribution in the general area of Panner Gorge and SH showing that the lower marble in the Rössing Formation is variably dolomitised. For location refer to Appendix II.

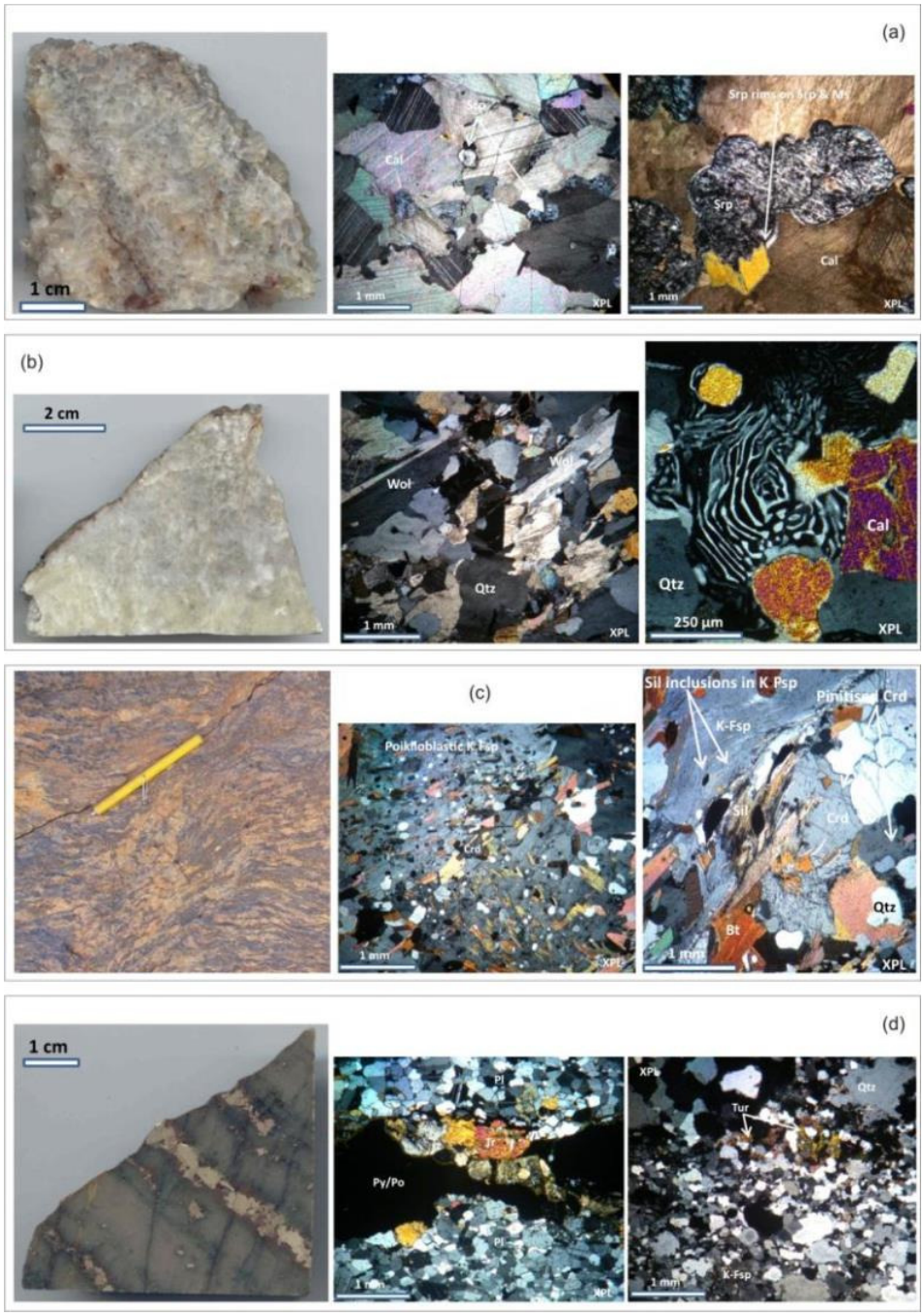


Figure 3.9. Mapped units of the Rössing Formation. (a) marble – graphitic, calcitic, scapolite-bearing marble RSS026 (left) and corresponding thin section (middle) from the SH area, and thin section of RSS084 (right), a serpentine calcitic marble from the SJ open pit; (b) RSS038 (left) and corresponding thin section (middle, right), representing wollastonite-scapolite-quartz skarn mineral development within the Rössing Formation marble; the central area of the right hand thin section photo shows a complex possible quartz-carbonate intergrowth texture; (c) cordierite gneiss outcrop (left) and thin section images of RSS086 from the SJ open pit (middle, right) showing poikiloblastic K-feldspar, pinitised cordierite and fibrous sillimanite; (d) pyrite-pyrrhotite bearing meta-arkose RSS087 from the SJ open pit (left), corresponding thin section (middle) and tourmaline bearing meta-arkose RSS047 from the hinge zone of the Blauer Heinrich Syncline (right). PPL – plain polarised light, XPL – cross polarised light. For an explanation of mineral abbreviations refer to Appendix I.

Cordierite Gneiss (Figure 3.9c)

Two samples of cordierite gneiss show the assemblages of garnet-biotite-quartz-cordierite and pyrite-sillimanite-cordierite-biotite-quartz-K-feldspar (RSS036 from Panner Gorge and RSS086 from SJ pit respectively. Based on textural relationships garnet is interpreted as pre-tectonic whilst cordierite is pinitised. In outcrop abundant quartz leucosomes are present and in thin section, late quartz growth is typical of both samples; both observations are interpreted to represent migmatitic (partial melting) textures.

Meta-arkose (Figure 3.9d)

All instances of this lithology which in the field appear to be fine-grained quartzites contain significant feldspar and are therefore meta-arkoses, usually containing significant pyrite ± pyrrhotite. Meta-arkose, which can form a substantially thick uppermost unit of the Rössing Formation, may in places be the dominant lithology of the formation, and/or is interbedded with other metasediments throughout the formation. Assemblages identified in thin section are pyrite-plagioclase-K-feldspar-quartz, tremolite-K-feldspar-quartz, muscovite-tourmaline-K-feldspar-quartz and pyrite-pyrrhotite-plagioclase-quartz (RSS027 from SH, RSS087 from SJ, RSS046 and RSS047 from the hinge zone of the Blauer Heinrich Syncline).

3.4.4 Chuos Formation

Previous Work

The Chuos Formation of the Usakos Subgroup is the lower of two glacial horizons present across the Damara Orogen consisting dominantly of tillite ± iron formation ± dolomite (Chapter 1.2.2). According to Jacob *et al.* (1986), Nex (1997) and Henry (1992) the Chuos Formation rests unconformably on the Rössing Formation. The Chuos Formation is not well documented in the project area but where it is documented the terms pebbly schist, tillite, and diamictite have apparently been used to describe the same lithology as per the following. In the SJ-SK area it is described by Laberge (2008a, 2008b) as a single lithology of pebbly schist, or matrix-supported meta-conglomerate. Clasts constitute 0-30% of the rock volume and include quartzite and various granitoids ranging commonly from several centimetres but locally up to 1 m in diameter, occurring within a medium-grained psammitic matrix with significant biotite and plagioclase. Lehtonen *et al.*, (1996) describe this formation as consisting of ‘mixtite’ exhibiting regional changes in clast size, morphology and frequency, with subordinate marble and iron formation beds. Smith (1965) describes the ‘Chuos tillite’

as exhibiting a more thinly-banded schistose nature toward the top of the succession. Miller (2008) notes that the matrix to 'diamictites' in the Rössing area is more calc-silicate rich than elsewhere, and that in the Khan River a single bed of dolomite and iron formation separately occur. Microscopically, matrix material is composed of quartz, feldspar, biotite and amphibole with locally abundant magnetite, ilmenite, tourmaline and epidote, whilst accessory minerals include calcite, zircon, apatite, sphene, garnet, staurolite and monazite (Smith, 1965; Cuney, 1980b). Around the Palmenhorst Dome, the Chuos Formation consists of quartz-biotite schist and diamictite with subordinate iron formation and cordierite-biotite-quartz ± garnet metapelites but on the southern margin of the dome only diamictite or quartz-biotite schist (in areas where there are no clasts) is present (Longridge, 2012).

This Work

The thickness of this unit is extremely variable in the project area, for example in Panner Gorge where it ranges from several hundred metres in thickness to being completely absent. No contact has been observed with the underlying Rössing Formation. Ground-truthing of hyperspectral imagery, particularly the 108-26-2 band combination and various M.N.F. transform band combinations has allowed the Chuos Formation to be subdivided into three units referred to as 'facies' 1 through to 3 on the appended geological map. This division requires refinement and further detailed description of the respective units, however a provisional scheme is set out here. The type area for examining these units is in the hinge zone of the Blauer Heinrich syncline and where the Khan River incises the southeast limb of this structure (Figure 3.10). Each facies consists predominantly of diamictite[5] which shows a progressive upward increase of ferro-aluminous minerals, with concomitant changes in clast size and abundance. The upward increase particularly in the abundance of iron may culminate in the presence of metamorphosed banded iron formation (itabirite) in facies 3. Hence the top of the Chuos Formation is a prominent magnetic high identifiable in regional scale magnetic data.

[5] Diamictite is a term applied to describe 'a type of sedimentary rock that consists of a wide range of lithified, non-sorted to poorly sorted, terrigenous sediment, i.e. sand or larger size particles that are suspended in a mud matrix' (http://en.wikipedia.org/wiki/Diamictite). The term tillite refers to a rock formed of till, a poorly sorted non-stratified material deposited directly by ice and divisible into basal till (carried at and deposited under the glacier base) and ablation till (material carried within or on the glacier and melted out of it). Till, also synonymous with moraine, is itself one sub-type of glacial drift, the other being stratified drift which is a well-sorted and layered material deposited by glacial meltwater (http://en.wikipedia.org/wiki/Till). The term diamictite is preferred here to that of tillite as there is no direct genetic connotation associated with the former.

The Chuos Formation is laterally non-persistent whereby the entire formation may be missing (Figure 3.4) or in places, such as east of Z20, facies 3 may rest directly on facies 1 or facies 2 and 3 may be missing. A notable additional feature of this formation is the potassic composition as indicated by the prevalence of K-feldspar. Details of the individual facies of the Chuos Formation are described below.

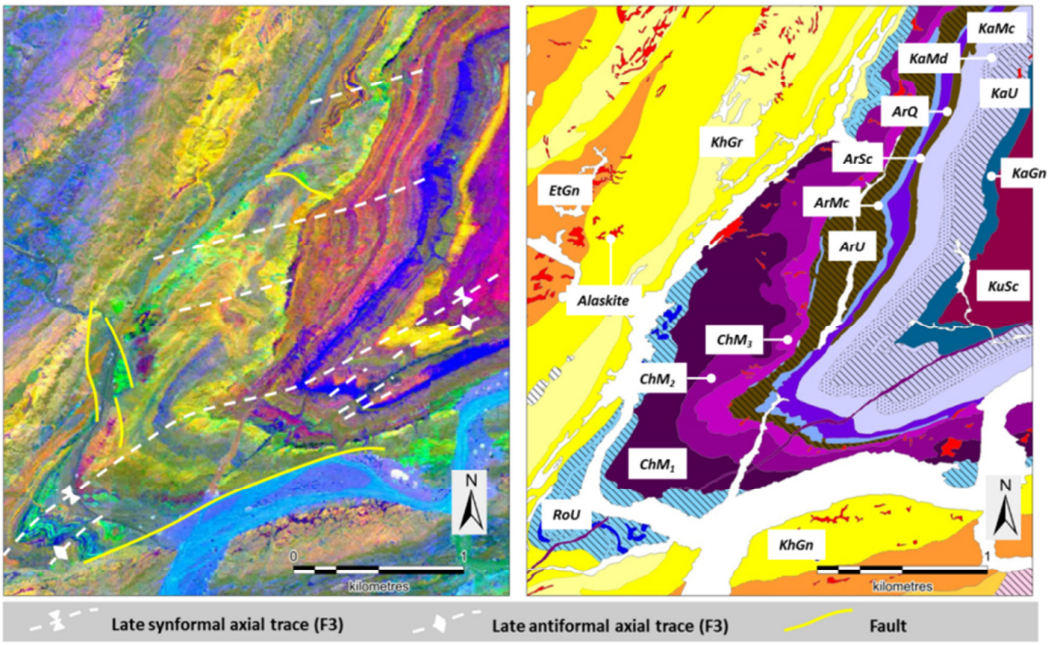


Figure 3.10. ***Left*** *- HyMap imagery band combination 10-11-12 with M.N.F. transform in the area of the Blauer Heinrich syncline. As per Figure 3.7 this image distinguishes most mapped units at member scale (right). In particular the three members of the Chuos Formation are visible, whilst a complete section of the Arandis and Karibib Formations are also present. Late fold (F_3) axial traces are shown.* ***Right*** *– lithological interpretation of the same area with map unit annotations as follows: EtU Etusis Formation biotite gneiss; KhGn Khan Formation clinopyroxene gneiss; KhGr Khan Formation Granofels; RoU undifferentiated Rössing Formation; ChM_{1-3} Chuos Formation diamictite facies 1-3; ArMc Arandis Formation calcitic marble; ArSc Arandis Formation biotite schist; ArQ Arandis Formation calc-silicate gneiss; ArU undifferentiated Arandis Formation; KaMc Karibib Formation calcitic marble; KaMd Karibib Formation dolomitic marble; KaGn Karibib Formation biotite gneiss; KaU undifferentiated Karibib Formation; KuSc Kuiseb Formation schist. Note that on the northern limb of the Blauer Heinrich syncline the Chuos Formation appears to show internal boudinage of units and that this probably predates the F_3 fold structures. Note also the late N-S oriented sinistral faults. Figure is centred on 501000 mE, 7508000 mN.*

Facies I (Figure 3.11a)

Facies I consists of diamictite which is generally non-magnetic (non magnetite-bearing) with assemblages sampled as phlogopite-plagioclase-quartz, K-feldspar-biotite-quartz (RSS052, RPS039). Granitic or quartz pebble clasts constitute 10% by volume (90% matrix), forming moderately schistose outcrops. Amphibole-quartz gneiss beds (RSS053) also occur in this unit.

Facies II (Figure 3.11b)

Facies II consists of moderately magnetic (magnetite-bearing) diamictite. Sample RSS040 shows the assemblage sillimanite-cordierite-biotite-K-feldspar-quartz. This is of more granitic composition than facies 1 and clasts constitute up to 40% (60% matrix). It typically forms massive (i.e. structureless), rounded outcrops.

Facies III (Figure 3.11c, 3.11d)

Facies III consists of highly magnetic diamictite with around 15% clasts (85% matrix), forming moderately schistose outcrops. Sample RPS041 consists of magnetite-hornblende-biotite-K-feldspar-quartz. Magnetite porphyroblasts are commonly >1 cm in diameter. Locally iron formation (± dolomitic marble) is present as metric-scale beds within the diamictite (e.g. Lower Khan River) or may constitute the entire formation (Chuos Formation between Arandis Airport and Panner Gorge). RPS068, from the latter locality, is a biotite-garnet-magnetite-quartz iron formation.



Figure 3.11. Mapped units of the Chuos Formation, in each case shows outcrop (left), hand specimen (middle) and corresponding thin section (right). (a) Facies 1, RPS031 K-feldspar-biotite-quartz diamictite; (b) Facies 2, RPS040 sillimanite-cordierite-biotite-K-feldspar-quartz diamictite; (c) Facies 3, RPS041 magnetite-hornblende-biotite-K-feldspar-quartz diamictite; (d) Facies 3, sample RPS068 biotite-garnet-magnetite-quartz iron formation outcropping between Arandis Airport and Panner Gorge. PPL – plain polarised light, XPL – cross polarised light. For an explanation of mineral abbreviations refer to Appendix I.

3.4.5 Arandis Formation

Previous Work

The Arandis Formation has been divided into four members dominated by marble and calc-silicate rock (Chapter 1.2.2). No previous detailed geological mapping within the project area shows the presence of this formation due to these lithologies having being included in the Karibib Formation (or the Chuos Formation in the wider CZ), a common problem commented on by Miller (2008, 2, p13-142).

Lehtonen *et al.* (1993, 1995, 1996) describe a 600 m thick schist- calc-silicate - marble sequence occurring continuously between the lower Khan River and the coast, forming a conformable unit between the Chuos and Karibib Formations which has regionally been sub-divided into further formations by other workers (e.g. Brandt, 1985). The formation thickens to almost 4000 m in the nCZ (Miller, 2008). Lehtonen *et al.* (1993, 1995, 1996) assign member status to lithological variability within this formation where the type exposure occurs on the periphery of this mapping area around the town of Arandis. The sCZ members are as follows (see Table 3.1): (i) the basal Karub Member, is a marble up to 60 m thick with interbedded calc-silicate and schist forming the cap carbonate to the Chuos Formation, *(ii)* The Spes Bona Member, 30-120 m thick, comprising dark-grey foliated biotite-schist, *(iii)* the Okawayo Member consisting of 2-20 m thick marble with thinly banded, alternating marble- calc-silicate rock, and *(iv)* the Oberwasser Member,10-50 m thick, consisting of foliated dark-grey, locally garnet-bearing biotite-schist.

South of the SJ pit, Laberge (2008b) mapped two units within the lower Karibib Formation: a discontinuous medium-grained interbedded quartzite and psammitic schist unit is overlain by a continuous unit of semi-pelitic cordierite-biotite-schist which forms the base of this formation where the quartzite-schist is absent. Compositional layering in the semi-pelitic schist occurs as common bands several centimetres thick with up to 20% cordierite porphyroblasts up to 1 cm in size, and as 2-10 cm thick quartzite bands. These units are considered to be the Karub and Spes Bona Members respectively; they are further described below and in Table 3.1 and are included within the Arandis Formation.

This Work

As per the descriptions of Lehtonen *et al*. (1993, 1995, 1996) the Arandis Formation in the mapping area consists of varying amounts of calc-silicate rock (here described as calc-silicate gneiss due to the pronounced banding exhibited), biotite schist and to

a lesser extent marble. Calc-silicate gneiss and biotite schist samples were taken during traversing for petrographic review and these are described below. Subsequent map interpretation of the distribution of these rock types permitted the distinction of the first three members of the Arandis Formation described by Lehtonen *et al*. (1993, 1995, 1996) as shown in Table 3.1. Calc-silicate gneiss at the base of the Arandis Formation is interpreted as the Karub Member and may be the only member present. On the north side of the Khan River two calc-silicate gneiss units, the upper correlated with the Okawoyo Member and the lower the Spes Bona Member enclose biotite schist of the Spes Bona Member. The latter can also rest directly on the underlying Chuos Formation, for example in the hinge zone of the Blauer Heinrich syncline. The Karub Member may be represented by a heterogeneous undifferentiated package of calc-silicate gneiss laterally passing laterally into a mixed undifferentiated metrically interbedded calc-silicate-marble-schist-meta-arkose package. Details of individual samples from the Arandis Formation are described below.

Calc-silicate Gneiss (Figure 3.12a)

The type locality of the calc-silicate gneiss is in the Z19 area on the south side of the Khan River where the unit can be seen to include marble and diamictite units. The most distinguishing feature of this unit which makes it immediately identifiable on iron oxide hyperspectral imagery (Figure 4.6) is the presence of iron as pyrrhotite, oxidising at surface to jarosite. Assemblages present in samples from the Z19 area include pyrrhotite-tremolite-scapolite-quartz-hornblende, scapolite-quartz-hornblende and quartz-tremolite (Rio Tinto Exploration samples 20008978 to -80 and 20008992). RPS001 is a hornblende-tremolite-scapolite skarn occurring in the same unit.

Biotite Schist (Figure 3.12b)

In contrast to the jarositic ferruginous lithologies of the calc-silicate gneiss this biotite schist, which can occur within the calc-silicate gneiss as the Okawoyo Member, is a fresh looking lithology with assemblages including garnet-biotite-quartz (RPS011, bottom of Panner Gorge) and sillimanite-plagioclase-biotite-quartz-cordierite schist (RSS060). Garnet and/or cordierite can generally be observed in the unit in the field and in hand specimen, and in thin section can be seen to be pre- to syn-tectonic. Sillimanite shows late growth.

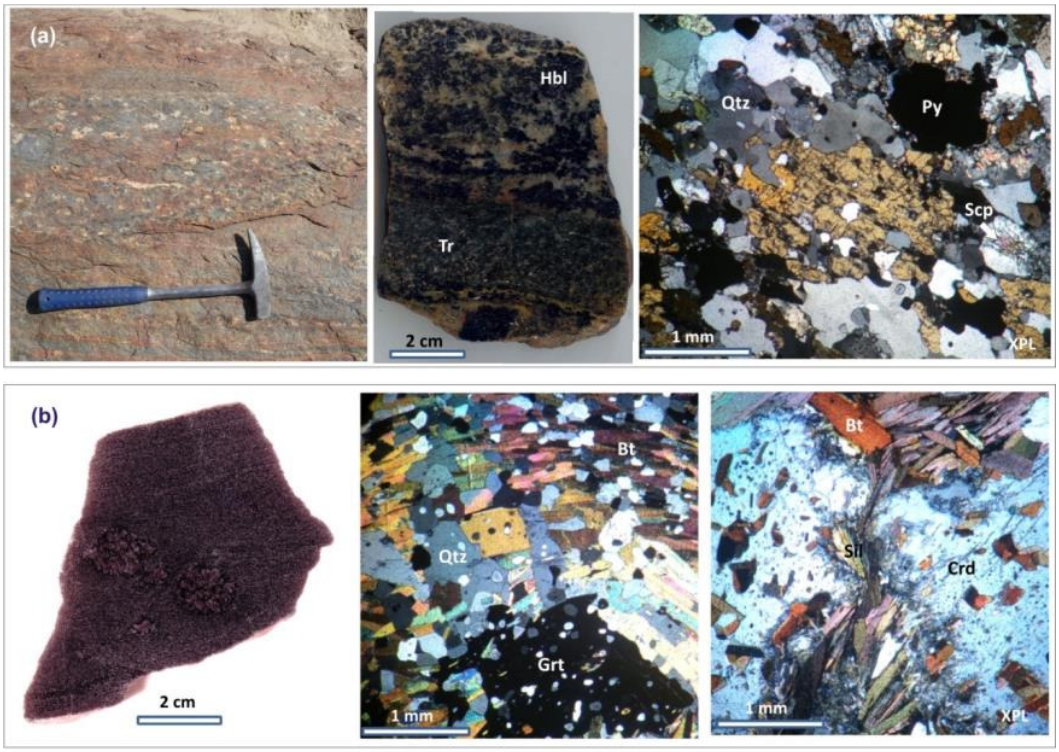


Figure 3.12. Lithologies of the Arandis Formation. (a) calc-silicate gneiss in outcrop (left) from the Karub Member at Z19 and 20008980 (middle) with corresponding thin section (right), a pyrrhotite-scapolite-tremolite-quartz gneiss also from the Z19 area; (b) Okawoyo Member biotite schist RPS011 in hand specimen and thin section (left, middle), a garnet-biotite-quartz schist from Panner Gorge showing biotite wrapping around pre-tectonic garnet poikiloblasts, and thin section of RSS060 (right) from the Khan River, a sillimanite-plagioclase-biotite-quartz-cordierite schist. PPL – plain polarised light, XPL – cross polarised light. For an explanation of mineral abbreviations refer to Appendix I.

3.4.6 Karibib Formation

Previous Work

In Chapter 1.2.2 the Karibib Formation was introduced as a marble-calc-silicate-dominant package occurring across the NZ and sCZ exhibiting considerable facies changes. Only the upper two members of three-member formation occurring in the nCZ, the Otjongeama Member and the upper Arises River Member, extend southwards into the sCZ (as far as 10 km south of Goanikontes – Miller, 2008). The Onguati Member is described as an uppermost member confined to the northern edge of sCZ (Badenhorst, 1992).

The Karibib Formation is not well described in the project area. In the wider area Lehtonen *et al.* (1993, 1996) describe the Otjongeama Member as a <10 m to >200 m thick marble with 1-5 cm thick calc-silicate interlayers (ribbon marble). The overlying Arises River Member is a pure calcitic marble up to 200 m thick that forms

resistant topographic highs, commonly graphitic and very coarse-grained. The uppermost Onguati Member consists of thinly interlayered calc-silicate and marble beds with minor schist up to 150 m thick (Lehtonen *et al.*, 1993, 1996), where according to Miller (2008) the schist layers represent interfingering of the Kuiseb Formation schist. West of Usakos Miller (2008) notes that thickness and lithology of the Karibib Formation is highly variable along strike, whilst in the confluence area of the Khan and Swakop rivers the formation consists of white dolomite with a locally present upper zone of grey limestone and dolomite.

South of the SJ pit, Laberge (2008b) mapped a medium- to coarse-grained marble occurring as numerous lenses generally 20-80 m thick but up to 170 m thick with locally megacrystic light-grey calcite crystals up to 30 cm in size. Laberge (2008b) describes the uppermost unit of the Karibib Formation in this area as fine- to medium-grained hornblende-biotite-quartz-plagioclase gneiss with amphibolite and green 1-5 cm thick calc-silicate bands.

Smith (1965) notes marbles of the Karibib Formation to be predominantly dolomitic with quartz as a major constituent and accessory tremolite, graphite, forsterite (and associated serpentine) and diopside. Very fine-grained, chert-like, calc-silicate intercalations consist of carbonate, quartz, feldspar, biotite, tremolite, diopside, scapolite and wollastonite with accessory sphene, apatite, graphite and sulphides. Thinly banded or thickly bedded intercalations of garnet- or cordierite-porphyroblastic (or quartz-biotite glomeroporphyroblastic) biotite-schist is dominantly an amphibole-biotite-plagioclase-K-feldspar-quartz schist with accessory zircon, apatite, sphene, carbonate, garnet, rutile, muscovite, scapolite, magnetite and pyroxene. Marbles mapped as Karibib Formation on the eastern margin of the Ida Dome have been re-interpreted as Rössing Formation by Longridge (2012; Chapter 3.3.3).

This Work

The expression of the Karibib Formation in outcrop and on remote sensing imagery is similar to the Rössing Formation. M.N.F. hyperspectral imagery is useful in tracing the numerous members which can be laterally continuous, albeit tectonically removed (boudinaged) in places. A critical difference of the Karibib Formation is the presence of an extensive dolomitic marble member (Figure 3.8). This bed forms some of the highest relief in the area and some particularly impressive outcrops within the Khan River (Figure 2.19).

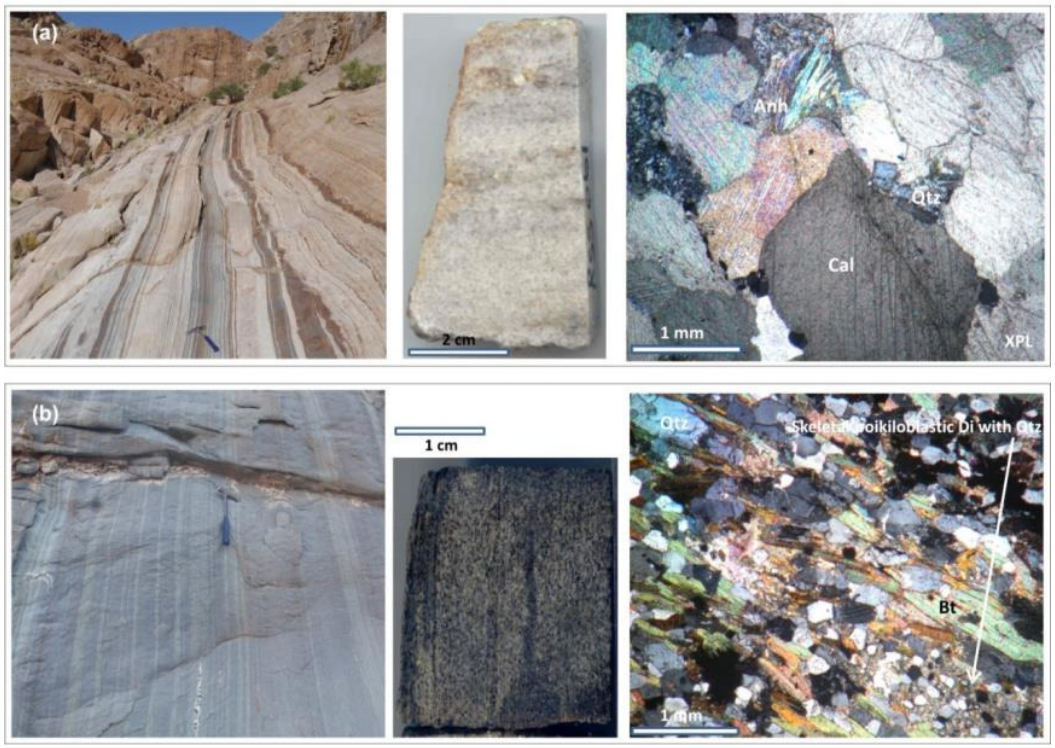


Figure 3.13. Lithologies of the Karibib Formation. (a) marble of the Otjongeama Member with calc-silicate interbeds at Z19 (left), RSS061 from the Khan River (middle), a graphitic calcitic marble from the same unit with corresponding thin section (right); (b) biotite gneiss in outcrop in the Khan River (left), in hand specimen and thin section (middle, right) of RSS063, a diopside-K-feldspar-biotite-quartz gneiss from the same location. PPL – plain polarised light, XPL – cross polarised light. For an explanation of mineral abbreviations refer to Appendix I.

A five member stratigraphy is present in the Karibib Formation of which units I, II and IV can be correlated to the stratigraphy described by Lehtonen *et al*. (1993, 1996) above (Table 3.1). The first three members of the sequence are marble beds each with distinct features that can be correlated across the mapping area. A basal calcitic marble containing centimetric-scale calc-silicate interbeds, is the 'ribbon marble' of the Otjongeama Member of Lehtonen *et al*. (1993, 1996; Figure 3.13; RSS061). The next marble is a massive dolomitic marble that can be easily traced on hyperspectral imagery (Figure 3.8) and is correlated with the Arises River Member of Lehtonen *et al*. (1993, 1996; note however that these authors describe this as a calcitic marble). An upper quartz-calcite marble that is present intermittently in the Khan River area is a characteristically grey colour but is not resolved at the scale of the appended map (RSS069; Table 3.1). Overlying the marble members, an undifferentiated mixed calc-silicate-marble-schist-meta-arkose sequence is present locally and is correlated with the Onguati Member of Lehtonen *et al*. (1993, 1996). A sample of meta-arkose sampled from this package is a granoblastic biotite-quartz-K-feldspar meta-arkose

(RSS062). Finally the uppermost unit of the Karibib Formation commonly present in the area is a granoblastic diopside-K-feldspar-biotite-quartz gneiss (sample RSS063; Figure 3.13b), which is the same as the medium-grained hornblende-biotite-quartz-plagioclase gneiss with amphibolite and calc-silicate bands described by Laberge (2008b). This unit has not been described in any publications reviewed. A notable feature within the biotite gneiss is the effects of regional attenuation visible as boudins occurring at a map scale on the limbs of the Welwitschia syncline.

3.4.7 Kuiseb Formation

Previous Work

The Kuiseb Formation is a thick monotonous package of dominantly pelitic schist forming the uppermost unit of the Damaran sequence (Chapter 1.2.2). The Kuiseb Formation is not documented in detail in the immediate project area. Smith (1965) describes the formation as consisting largely of fine- to coarse-grained, thin to thickly and massively bedded, biotite-rich quartzofeldspathic schist dominantly as biotite-plagioclase-K-feldspar-quartz schist with accessory apatite and zircon. Some beds are cordierite-, garnet-, amphibole- or sillimanite-porphyroblastic and these minerals increase in abundance west of Karibib (Miller, 2008). Towards the coast the schist shows a westward coarsening of grain size and becomes locally gneissic as metamorphic grade increases. Migmatites have formed from both partial melting and injection of granite veins around intrusions and where cordierite and garnet are particularly abundant in granulite facies the schist has a composition of kinzigite[6] (Jung *et al.*, 1999; Miller 2008).

South of the SJ open pit in the area of the Khan River the Kuiseb Formation is a monotonous sequence of medium-grained cordierite-porphyroblastic cordierite-garnet-biotite-quartz-plagioclase schist showing local migmatitic segregations containing quartz-K-feldspar-plagioclase-garnet-biotite (Laberge, 2008b). Cordierite is pinitised and accessory minerals include zircon, monazite, graphite, pyrite and chalcopyrite (Cuney, 1980b). Cross-bedding and graded bedding are locally preserved along the Khan River (Lehtonen *et al.*, 1993, 1996). More regionally, Smith (1965) notes that thick and thinly bedded units alternate, and porphryoblasts can also be hornblende or sillimanite knots.

[6] Kinzigite is a 'coarse-grained metamorphic rock of pelitic composition occurring in the granulite facies. Essential minerals are garnet and biotite, with which occur varying amounts of quartz, K-feldspar, oligoclase, muscovite, cordierite, and sillimanite. The name is from Kinzig, Schwarzwald, Germany' (http://www.mindat.org/glossary/kinzigite).

This Work

The Kuiseb Formation cordierite schist is readily identified for the purposes of interpretation due to its stratigraphic position and it is also spectrally distinct on hyperspectral imagery (e.g. Figure 3.1). Two samples are shown in the chapter on metamorphism in Figure 5.3. Cordierite is pre-tectonic and pinitised. The only compositional variation noted in this formation is in the general distribution of cordierite ± garnet, with the increased abundance of these minerals indicating more pelitic beds. The cordierite schist often exhibits tension gashes filled by quartz-feldspar leucosomes.

3.5 Superficial Sediments

Relatively recent superficial sediments occur around the periphery of the mapped area, consisting of consolidated calcrete river terrace deposits and unconsolidated alluvium, eluvium and aeolian sediment (Smith, 1965).

3.6 Summary and Discussion

An updated description of the stratigraphy of Damaran-aged metasediments in the Rössing area based on all work completed to date in the Rössing area has been presented above and in Table 3.1. This includes additional detail from this work particularly in formations overlying the Rössing Formation and those in areas not covered by previous detailed geological mapping. Observations from field traverses combined with interpretation of multiple geoscientific data layers (Chapter 2) has produced a geological map that extends the mapped stratigraphy of the immediate Rössing Mine throughout the mine lease and beyond. Extending the mapped stratigraphy also facilitates description of structure, metamorphism and mineralisation covered in subsequent chapters, and, in particular, the description of intrusive rock types (also summarised in Table 3.1) which is covered in Chapter 6.

The general twofold stratigraphy apparent within the Abbabis Metamorphic Complex compiled from Gevers (1931), Smith (1965), Brandt (1987), Marlow (1981), Sawyer (1976, 1979), Bunting (1977), Downing (1982, 1983), Jacob (1974), Barnes (1981) and Longridge (2012) is consistent with the regional geological mapping of Lehtonen *et al.* (1993, 1996). This consists of a lower paragneiss and orthogneiss unit and upper metasedimentary unit, respectively the Tsawisis and Naob Formations of the Abbabis Inlier and Lower and Upper Tumas River Formation of the Tumas Inlier and

Swaartbank areas. Within the project area meta-arkose (paragneiss) with (possible) metabasites are interpreted to be intruded by granitic orthogneiss. This may be analogous to the lower part of the A.M.C. described by Brandt (1987) as the Tsawisis Formation of the Abbabis Inlier and respectively the Narubis Granitoid Complex that intrudes it. This would also be consistent with the observations of Longridge (2012) for the nearby Palmenhorst Dome where only the lower part of the A.M.C. is preserved. Identification of the A.M.C. is assisted by reference to high uranium and thorium signatures in airborne radiometric data. Spivey *et al.* (2010) note the A.M.C. can be locally strongly anomalous in uranium concentrations. This was a feature also noted in this study where up to 15 ppm U occurs within anomalous zones of basement identified in airborne radiometric data. Where alaskites intrude stratigraphy proximal to the A.M.C. they commonly inherit strong thorium contents. The A.M.C is also readily distinguishable on hyperspectral imagery and this imagery could be used in the wider area to map units in relative detail. Map relations show that in the area northwest of the tailings dam (the Arandis Airport area) the Damaran metasedimentary sequence is in sheared contact with the A.M.C. with units structurally removed; the contact is folded indicating shearing occurred relatively early in the deformational history (Chapter 4).

In this study, the Etusis Formation has been clearly divided into a lower meta-arkose and upper biotite gneiss, a stratigraphy that is readily observable on 108-26-2 hyperspectral imagery (e.g. Figures 1.2, 2.11, 3.4). This is supported by both field observations and structural interpretations. Previous descriptions of the Etusis Formation stratigraphy in the SJ Dome area (Berning *et al.*, 1976; Berning, 1986; Oliver and Kinnaird, 1996; are partly erroneous either due to the misinterpretation of biotite gneiss as an additional member where it is infolded into the central part of the dome (e.g. Figure 4.2), or due to the incorporation of the lower part of the Khan Formation into this formation. The text of Berning *et al.* (1976) describing a two member stratigraphy is consistent with this work. Calc-silicate beds noted in the SJ Dome area may relate to discontinuous marble beds interpreted from hyperspectral imagery in the Nose Structure area and shown on the appended map, and presumably reflect temporally and spatially restricted carbonate influx into a predominantly siliciclastic sequence. The interpretation of Smith (1965) that the SJ Dome is cored by red gneissic granite is not, in accordance with subsequent workers cited above, and is supported here. As per the observations of Oliver and Kinnaird (1996), sedimentary structures are commonly preserved in this area. The observation that the meta-arkose has a similar U-Th-enriched response on ternary radiometric

imagery (Figure 2.3a) to that of the A.M.C. suggests that these sediments are at least in part derived from the latter. Area-wide structural interpretations (Chapter 4, sections on appended map) indicate that the SJ domal structure is not overturned and hence the major stratigraphic units are also considered to be right-way-up, in accordance with the outcrop-scale interpretations of Oliver and Kinnaird (1996). 'Blebby' textured quartz is a commonly observed feature of both members of the Etusis Formation in thin section. It is considered to represent a partial melting texture, and is consistent with the locally migmatitic and agmatitic textures observable in outcrop, particularly in the biotite gneiss.

Where it is best developed, the Khan Formation (and Rössing Formation) stratigraphy outlined is essentially the same as that described by Nash (1971). Nash's scheme remains an appropriate one for the immediate Rössing mining area however beyond this mapping shows that the Khan Formation is less lithologically variable. Additional detail of mineralogy has been added to the descriptions of Nash (1971) and rock names modified within the Khan Formation. Migmatitic textures are noted throughout, in agreement with previous workers and these are particularly well-developed in the more quartz-rich clinopyroxene granofels unit where the mottled texture is interpreted to consist of restitic mafic phases. The fact that the Khan Formation (and Rössing Formation) is best developed in the immediate Rössing area, laterally passing outward into monotonous clinopyroxene gneiss (± a middle granofels member), is perhaps noteworthy. The 'basal conglomerate' mapped by Mestres-Ridge (1992) in the Khan Formation of the SH area was sampled for petrography by the author. The mineralogy of this rock is identical to that of the calc-silicate rock of Chapter 5.3.3 where this is discussed separately. Although the protolith to this rock type in the SH area may well have been a conglomerate, it is unlikely to be a basal unit within the Khan Formation given its position near the contact with the Rössing Formation. It is likely to be the same polymict conglomerate noted in the upper clinopyroxene gneiss at the south end of Panner Gorge, albeit metasomatically altered (see Chapter 5.3.3). Magnetite appears to show an upward increase in the Khan Formation and may be present in significant amounts in the upper clinopyroxene gneiss. The intercalation of marble units at the top of the biotite gneiss with bedding-conformable amphibolite horizons supports the interpretation by Nash (1971) that this is a para-amphibolite sequence (i.e. intercalated shale-limestone). However given that acid metavolcanics occur at the top of the Nosib Group immediately north of the Okahandja Lineament southwest of Karibib

(Downing, 1982; de Kock, 1989) the possibility that some of this unit could represent metavolcanics cannot be precluded.

No evidence has been noted in the mapping area for an unconformity between the upper Nosib Group (Khan Formation) and lowermost Swakop Group (Rössing Formation). This is in agreement with the conformable or paraconformable contact interpreted by Nash (1971) but disagrees with the regional unconformity interpreted by Smith (1965) and Jacob *et al*. (1986). Certainly the presence of intercalated marble lenses in the uppermost Khan Formation supports a conformable and interfingering contact. The Rössing Formation stratigraphy of Nash (1971) is still applicable to the immediate Rössing Mine area, however away from here it is a highly variable package. Nonetheless from regional descriptions individual units may be correlatable where presumably basinal conditions may have been similar. This mapping has shown that calcitic marbles at the base of the formation are variably dolomitised and feldspathic quartzites, which locally dominate the succession, may contain significant pyrite ± pyrrhotite. Oxidation of these sulphides results in development of jarosite which can be readily mapped on hyperspectral imagery. Detailed mineralogy and migmatitic textures in the Rössing Formation units are discussed in Chapter 5.

No unconformity has been noted between the Rössing and Chuos Formations as documented by other workers (Jacob *et al*., 1986; Henry, 1992; Nex, 1997*).* However, in the project area the contact is obscured by recent cover. Units overlying the Rössing Formation have been described in more detail than previously as very little detailed mapping has been completed beyond the SJ area until recently. Hyperspectral imagery products and ground truthing of this data have permitted the Chuos Formation to be divided into three distinct diamictite-dominant facies which have a potassic nature in thin section. In outcrop the facies changes are manifested variations in ferro-aluminous mineral abundance (with a general upward increase in iron content) and concomitant changes in clast size and abundance. The local development of iron formation, metamorphosed to itabirite, in the upper facies presumably occurred where iron concentrations were greatest and such units are readily traceable on airborne magnetic data.

Within the Arandis Formation a three member stratigraphy has been described and correlated with the first three members identified by Lehtonen *et al*. (1993, 1996). The uppermost Oberwasser Member has not been identified here. These members

are spectrally distinct particularly on Minimum Noise Fraction transform and iron oxide (jarosite) end member hyperspectral imagery which has facilitated mapping their detailed distribution. The mapping shows that members or locally the entire formation can be commonly missing from the sequence. The absence of the Oberwasser Member and the Ghaub Formation (see Chapter 1.2.2 and Table 3.1) may indicate a period of non-deposition. However, no angular unconformity as noted regionally by Sawyer (1981), is observable at the base of the Karibib Formation. Within the Karibib Formation a five-member stratigraphy has been described of which three members have been correlated with those of Lehtonen *et al*. (1993, 1996). In contrast, these authors describe the Arises River Member as a calcitic marble, whereas in the mapping area it is dolomitic as shown on hyperspectral imagery and demonstrably so in the field. The well-defined sedimentary contacts and lateral continuity of this member demonstrate that dolomite is a primary sedimentary feature. The presence of dolomite in the Karibib Formation has also been noted by Miller (2008) in the confluence area of the Khan and Swakop rivers.

It is worth noting from the descriptions above that three of the Damaran formations show an upward increase in iron content culminating in either the presence of abundant visible magnetite (the Chuos and to a lesser extent Khan Formations) or iron sulphide (Rössing Formation). The Arandis Formation is also relatively iron-enriched. These semi-cyclic iron trends in both siliciclastic and chemical sediments may relate at least in part to periods of volcanism in the region. A further notable feature in the distribution of stratigraphic units is the presence of significant thickness and stratigraphic changes across major fold hinges – these features are discussed in Chapter 4.

Chapter 4: Structure

4.1 Introduction

The structural characteristics of the Central Zone were introduced in Chapters 1.2 and 3. The sCZ is interpreted as the root zone of the active continental margin of the Congo Craton which overthrust the Kalahari Craton during Damaran-age collisional orogenesis. Polyphase folding of up to four episodes (D_1-D_4), faulting and thrusting accompanied oblique collision and uplift of the sCZ and coincided with the formation of dome structures of probable D_3 age with a northeast elongation, for which numerous mechanisms have been proposed. High grade metamorphism and voluminous magmatism accompanied and immediately followed deformation. The sCZ is bound by major northeast-trending lineaments and crossed by north-northeast-trending lineaments including the Welwitschia Lineament which is spatially related to most uraniferous alaskite deposits including Rössing and Rössing South (Chapter 1.2.3 and references therein).

4.2 Previous Work in the Project Area

Interpreted pre-Damaran fabrics have been noted in basement gneisses of the Ida Dome by Longridge (2012) and in the Nose Structure anticline by Poli (1997) but not in the immediate mapping area. A synthesis of documented Damaran-age structures in the wider district, including details from the Rössing area is presented in Table 4.1. A summary of major structural elements of the Rössing area according to previous workers is shown in Figure 4.1.

Original bedding (S_0) in the Rössing area is defined by relict heavy mineral layering in quartzites (meta-arkoses in this study) of the Etusis Formation and as planar bedding in marbles and pyritic quartzites in the Rössing Formation (Basson and Greenway, 2004). Nash (1971) identified schistose and migmatitic S_1-S_2 fabrics in metasediments, however these are noted to be pervasively replaced by a later S_3 gneissosity to schistosity (dependant on the proportion of phyllosilicates; Nash, 1971; Basson and Greenway, 2004). Oliver and Kinnaird (1996) interpreted L_1 lineations defined by the elongation of quartz, plagioclase, K-feldspar aggregates and lepidoblastic biotite in the Etusis Formation of the Rössing SJ Dome. S_4 is expressed as an axial planar foliation associated with small isolated north-northeast-trending folds (Nash, 1971). These fabrics correlate to D_{1-4} identified in the CZ as described in Chapter 1.2.3.

Table 4.1. Summary of deformation features of the Rössing and wider area from previous work. Some assumptions are made in the correlation of deformation events of different workers where these are confident (e.g. that the northeast-trending F_2 structures of Nash (1971) equate to F_3 of other workers, due to the fact that F_1 structures were not identified in the area that Nash mapped.

Deformation	Planar features & lineations	Ductile features	Brittle features
D_1	S_1 and S_2 laminar foliation in pelites, migmatitic banding in psammites to semi-pelites (e.g. Nash, 1971), L_1 mineral lineations (Oliver & Kinnaird, 1996), L-S tectonites of Poli (1997)	F_1 folds: possibly SW-verging; rootless isoclinal intrafolial folds (Longridge, 2012); Stage 1 gentle dome formation of Poli (1997)	
D_2		F_2 possibly NW-trending SW-verging folds (Smith, 1965; Coward, 1983); infolding of pre-Damaran and Damaran rocks, development of recumbent folds and thrusts (Barnes, 1981); km-scale isoclinal recumbent to shallow N to NW-dipping (generally E-W trending) folds, shear zones, conjugate shear bands, NE- to SW-plunging stretching lineations (Longridge, 2012); Stage 2 main dome formation of Poli (1997)	
D_3	S_3 schistosity to gneissosity (Basson & Greenway, 2004)	F_3 folds: upright to SE-ESE-verging, NE-plunging, mostly coaxial with F_{1-2}, fold interference structures developed where they are not (Smith, 1965; Coward, 1983; Longridge, 2012); dome formation considered to occur here by most workers; similar folds in marbles of Swakop Group and concentric folds in Nosib Group (Smith, 1965); stress focused into basement-cover contact producing mylonites (Poli, 1997) and major detachment at basement-cover interface (Nose Structure area, Poli & Oliver, 2001) ramping through stratigraphy into the Nosib Group at the SJ Dome (Oliver & Kinnaird, 1996) and Goanikontes (Nex et al., 2001a); dextral shear geometries in tension gashes at Rossing SK (Laberge, 2008a)	Upright faults in high strain areas (Barnes, 1981)
D_4	Axial planar foliation (S_4) in small folds (Nash, 1971);	Rotation into NNE trend, e.g. Rössing Dome axis orientation and 'Welwitschia Trend' (Corner, 1981; Basson & Greenway, 2004); inferred NNE-trending left lateral shears cross-cutting and re-orienting NE-trending F_3 folds, NNE sinistral transtensional ladder veins (Anderson & Nash, 1997); N- to NW-trending folds of Smith (1965) and Barnes (1981 - gentle, upright folds) and E-W trending N-verging folds of Coward (1983) and Nash (1971) where quartz veins intrude axial planes; SE-directed overturning of F_3 folds (Anderson & Nash, 1997)	NNE-oriented sinistral strike-slip and thrust faults (Anderson & Nash, 1997); N-S to NNW-SSE dominantly sinistral faults, NW-SE dominantly dextral faults (Laberge, 2008a)

Ductile structures in the area consist of fold and transtensional (shear) to extensional structures. Fold style generally follows the regional pattern of elongate synforms and antiforms trending northeast-southwest (Smith, 1965). As noted in Chapter 1.2.3 F_1 and F_2 in the sCZ generally cannot be distinguished and the orientation of F_1 folds are speculative, however the outcrop of the Khan Formation across Rössing Mountain west of the project area may demarcate an F_1 fold axial trace (Smith, 1965; Miller, 2008). Rootless isoclinal intrafolial folds in Damaran metasediments around the Ida and Palmenhorst domes are interpreted as F_1 structures by Longridge (2012). In the lower Khan River area, Smith (1965) described three fold trends: *(a)* an early northwest trend (F_1 or F_2 of subsequent workers), *(b)* a later dominant northeast trend (F_3 of subsequent workers), and *(c)* a latest northwest trend, necessarily F_4 of other workers and coincident with the same northwest-southeast latest fold trend noted by Nash (1971) in the southeast and southwest parts of the SJ area. In most

cases $F_{1/2}$ and F_3 are coaxial, however where they are not, complex fold interference structures occur. The fold interference structures show consistent plunges to the northeast, a feature attributed by Smith (1965) to the original northeast attitude of the earliest fold axial planes. Smith (1965) favoured the origin of the interference structures as being due to opposing stress fields during D_1-D_2. Conversely Oliver (1994), Poli (1997) and Poli and Oliver (2001) propose a model of single-phase orogen-normal constrictional deformation to account for the relationship of folds, domes, foliation, and shear zones (introduced in Chapter 1.2.3; Table 4.1). According to these workers, the main southwest-vergent dome formation occurred during 'D_2' of other workers which was followed by deformation at the basement-cover contact during 'D_3' and the formation of the Khan River Detachment (Figure 4.1), a structure proposed by Oliver (1994) on the basis of the presence of a major L-S tectonite, and suggested to represent a major low-angle extensional shear zone. This shear zone was interpreted by Oliver and Kinnaird (1996) to ramp through the stratigraphy to the northeast where is occurs as the 'Rössing Shear Zone' truncating the Etusis Formation at the Rössing-SJ Dome. Nex *et al.* (2001a) extrapolate the same mid-crustal high strain zone to the Goanikontes area where it is proposed to comprise a significantly attenuated sequence of Etusis through to Chuos Formation characterised by L-tectonites and constrictional deformation. The timing of deformation in the high strain zone is considered to post-date M_1 metamorphism and constrained between 534 ± 7 Ma (age of red foliated granites within this zone at Goanikontes) and 508 ± 2 Ma (U-Pb ages from mineralised alaskites cross-cutting the high strain zone (Briqueu *et al*., 1980; Nex *et al*., 2001b). In contrast Longridge (2012) interprets multiple shear zone development in the same area of the Khan River Detachment as having developed during D_2, where multiple shear zones evidenced by sheared out fold limbs, are localised on the upright lower limbs of south-vergent F_2 folds. Corresponding overturned upper limbs show the effects of attenuation.

In the recent structural study of Longridge (2012; Table 4.1) the Ida and southern Palmenhorst domes (Figure 1.8) are interpreted to result from F_2 and F_3 fold interference that exhibit type 2 patterns of Ramsay (1967). The folds consist of kilometre-scale recumbent to shallow north to northwest-dipping (generally east-west trending) F_2 folds and upright to steeply west to northwest-dipping (northeast-southwest trending) F_3 folds. Longridge (2012) concludes that D_2 was the most intense deformational phase resulting from intense south southeast-verging shearing and forming most meso-scale structures in the area. These comprise tight to isoclinal

folds, ductile shear zones, conjugate shear bands and a northeast- to southwest-plunging mineral stretching lineation. Measurements of the latter two structures consistently indicate orogen-parallel northeast-southwest orientated extension during D_2 in conjunction with orogen-normal southeast-vergent constriction. Longridge (op. cit.) places D_2 deformation between 520-510 Ma based on U-Pb geochronology of syn-D_2 grey granite, garnet-bearing leucogranites and anatectic leucosomes localised in D_2 shear zones. The garnet-bearing leucogranites are considered by Longridge (op. cit) as being the product of partial melting of pelitic metasediments at peak metamorphism. D_3 formed kilometre-scale gentle to upright northeast-plunging folds with southeast to east-southeast vergence. Longridge (2012) notes that within the Ida-Palmenhorst dome area D_2-D_3 fold interference rarely produces interference structures observable at outcrop scale. Granite sheets intrude axial planes of F_2 folds and anatectic leucosomes are axial planar, whilst east of the Ida Dome uraniferous alaskite emplacement appears to be localised in the core of anticlinal F_3 folds.

Different metasedimentary units show markedly different deformation styles. For example the more competent rocks of the Khan and Etusis Formations show concentric (flexure) folds whereas less competent marbles of the Rössing and Karibib Formations show folding of a similar style with attenuated limbs hosting more competent boudinaged lithologies (Smith, 1965; Nash, 1971; Berning *et al.,* 1976). Blackening of marbles along the axial planes of minor folds is due to the distortion of calcite lamellae within these zones (Nash, 1971). Smith (1965) noted that the area is remarkably free of large-scale faulting, indicative of rocks deformed in a plastic state. Northeast-oriented shear deformation is evidenced by the presence of dextral shear deformation geometries at Rössing SK (Laberge, 2008a).

Around the Rössing-SJ Dome bedding and foliation dip generally outwards (Oliver and Kinnaird, 1996). Accordingly the axial plane of the SJ synclinorium dips to the south however the next major fold structures to the south, the Camp Anticline and Welwitschia Syncline, exhibit regional overturning that Anderson and Nash (1997) attribute to D_4 modification (Figure 4.1). D_4 north-northeast oriented sinistral strike-slip and thrust faulting is noted over the wider Rössing area by the same workers to cut across and re-orientate east-northeast-trending folds; these workers interpret the presence of a major sinistral shear zone passing through the Rössing SJ area, south of which, southeast-vergent thrusting and overturning of folds contrasts with the structural style to the north. Such shear zones frequently occur as sinistral shear couples controlling the emplacement of alaskite ladder vein arrays.

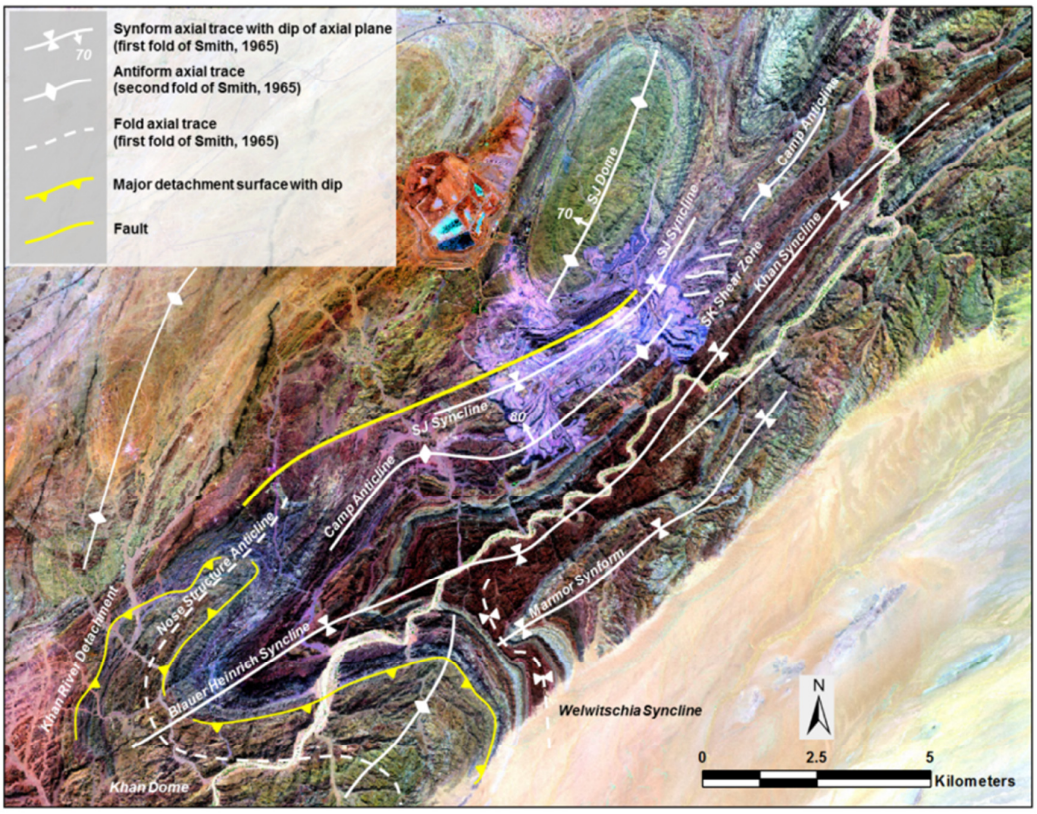


Figure 4.1. Selected structural elements in the Rössing area interpreted by previous workers including Smith (1965), Anderson and Nash (1997) and Oliver (1994). See text for details. Base image is hyperspectral line data with RGB band combinations 108-26-2 (equivalent to Landsat bands 7-4-1). Figure is centred on 505000 mE, 7511000 mN.

The north-northeast-trending Welwitschia Lineament of Corner (1981; Figures 1.5 and 1.8) is interpreted by Anderson and Nash (1997) as a series of en-echelon sinistral strike slip faults associated with the post-D_3 evolution of the Damara Belt. Within this the Rössing alaskites are associated with a thrust jog located on one such major D_4 sinistral fault. Basson and Greenway (2004) interpret late-tectonic anti-clockwise rotation of the SJ Dome into a north-northeast-trending D_4 trend with concomitant sinistral displacement along D_4 structures and southward dome impingement. This facilitated emplacement of the SJ uraniferous alaskites into a dense fault network within the upper Khan and lower Rössing Formations. Berning *et al.* (1973) note the presence of transverse oblique-slip faults with displacements ranging from very minor to >45 m, younger than the F_3 folds and SJ alaskites but older than dolerite dykes, indicating at least one phase of post-alaskite emplacement faulting at SJ.

Laberge (2008a) notes that a fault breccia in the southern limb of the SK anticlinal shear zone within the upper Khan Formation possibly represents a major bounding

fault that may also be present on the northern limb of this structure. The same author describes late brittle faulting occurring as either north to north-northwest dominantly sinistral displacements or northwest-orientated dextral faults displacements, post-dating alaskite emplacement. The former fault orientations can be associated with calc-silicate replacement (Chapter 5.3.3). Jointing is developed throughout the SJ area in both metasediments and alaskites with fracture orientations principally normal to D_3 (Nash, 1971; Berning, 1986).

4.3 This Work

A summary of major structures in the mapping area based on both previous work and this project is shown in Figure 4.2 (contrast Figure 4.1).

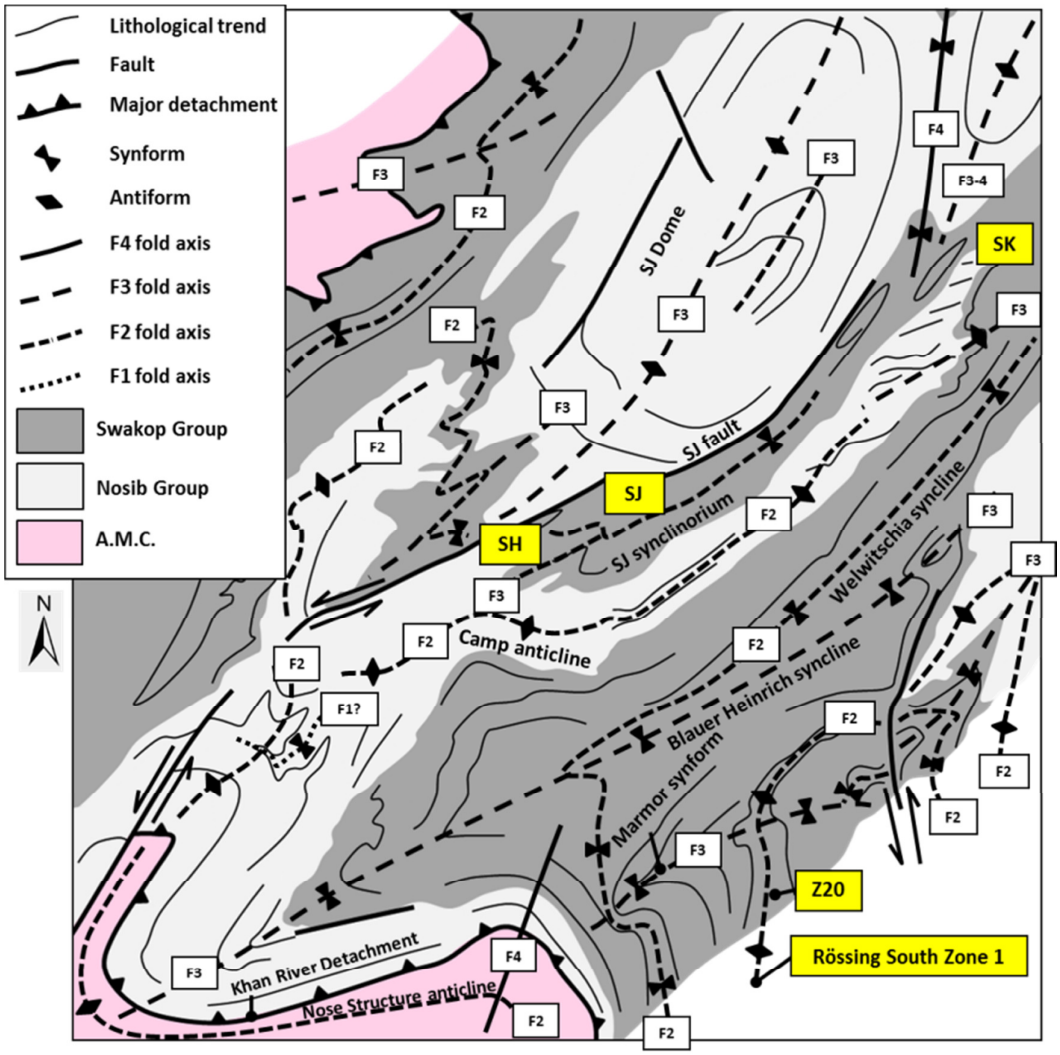


Figure 4.2. Selected structural elements of the Rössing area incorporated from previous work (Figure 4.1 and references therein) with modifications and additional detail added from this mapping. The location of the figure is coincident to the referenced area shown on the map in Appendix II. Figure is centred on 505000 mE, 7511000 mN.

4.3.1 Planar and Lineation Structures

The distribution of planar structures mapped as S_0 (bedding) and S_1 (first cleavage or foliation) is shown on the map in Appendix II. This data has been compiled from all known work (see previous work Chapter 2.5.1) including data from this project. Bedding (S_0) at a regional scale in the mapped area is defined by planar contacts between member-scale, mineralogically distinct units, where marble bed contacts in the carbonate-bearing formations are the most readily identifiable S_0 structures at outcrop scale. Locally bedding is preserved as relict heavy mineral layering in quartzites of the Etusis Formation. Subsequently developed schistose, gneissic and migmatitic fabrics have been assigned S_1-S_4 by previous workers (Chapter 4.2). No attempt has been made to refine this here. In this study, structural data compiled across the mapping area is reviewed where sufficient measurements are coincident with major fold structures resolved on the geology map in order to determine fold orientations.

Examples of planar and lineation structures recorded during field traversing are shown in Figure 4.3. Moderately northeast plunging bedding-cleaving intersection lineations (Figure 4.3 c, d) noted within the Marmor synform area share the same plunge orientation as F_3 folds in the area, (Appendix II map stereograms, Figure 4.4, both showing Marmor synform S_0-S_1 data).

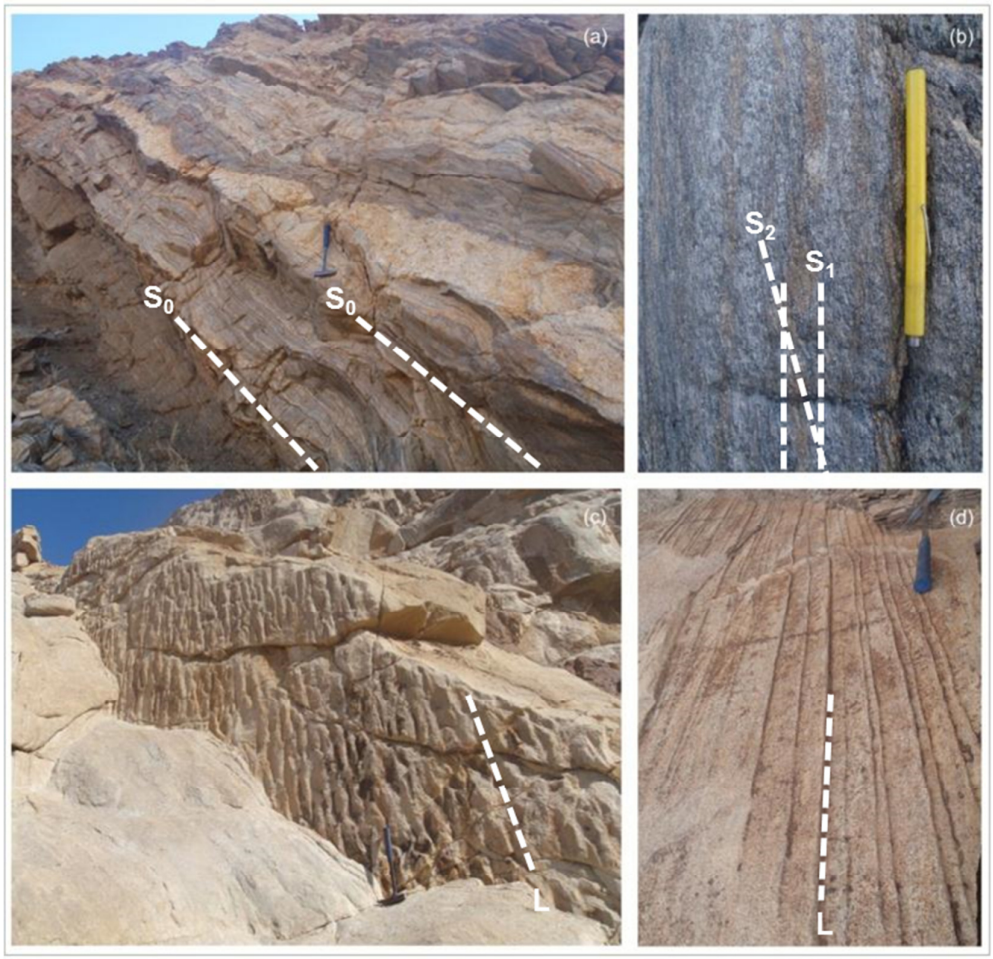


Figure 4.3. Examples of planar and lineation fabrics developed in the Damara succession. (a) bedding (S_0) in quartzo-feldspathic gneisses of the Rössing Formation on the north margin of the Rössing SJ Dome, defined by sub-metric compositional changes in beds, between which gneissosity is developed overprinting original sedimentary features. (b) development of local gneissic fabric (S_1) in Kuiseb cordierite schist of the Khan River with cross-cutting second cleavage (S_2) at a shallow angle to the gneissosity. (c) Karibib marble bedding contact in Panner Gorge showing a crudely developed and steeply plunging bedding-cleavage intersection lineation (L), better defined in the outcrop shown in (d) from the same general locality.

4.3.2 Ductile Structures

The interpreted axial traces and sequence of folding derived from review of this mapping is shown in Figure 4.2 together with the names of these structures taken from earlier work in the area. S_0-S_1 data density is greatest over the Rössing SH-SJ-SK area and the Marmor synform of the Z19-Z20 area. This data is shown on the stereograms of the appended map and in Figure 4.4. Where point structural measurements are scarcer major fold relationships are still broadly deducible from the detailed mapping of stratigraphy as shown for the area east of Z20 in Figure 4.5. Three distinct fold generations have been distinguished in the area largely from mapping and these are respectively assigned F_2, F_3, and F_4. The earliest folds form

the major meso-scale anticline-syncline trends across the area. These include the Nose Structure anticline, SJ synclinorium, Camp anticline, and Welwitschia syncline (Figure 4.2). The Nose Structure anticline was interpreted as an F_2 structure in the spatially adjacent detailed structural-tectonic study of Longridge (2012) where this underpins the nomenclature of fold generations in this study. As per the study of Longridge (2012) no earlier fold structures can be confidently identified from this mapping, however the presence of a hook structure folded into the hinge zone of the Nose Structure may represent an F_1 fold (Figure 4.2). The mapped extent of the Nose Structure F_2 fold indicates that the original orientation of F_2 may have been approximately east-west with a moderately north-dipping axial plane, reflected by the moderate northeast plunge of the majority of F_3 folds. This F_2 attitude is consistent with the conclusions of Longridge (2012). Across the area, F_2 folds have been variably reworked into northeast-southwest trending doubly plunging F_2-F_3 interference structures where the degree of rotation of the original F_2 fold axial planes controls the geometry of the resulting interference structures. On the southeast side of the SJ Dome the SJ synclinorium, Camp anticline and the northeast segment of the Welwitschia syncline, a series of close to tight anticline-synclines have formed where, at a map scale, F_2 fold axial planes have been rotated to the northeast and D_3 modification has been coaxial to slightly oblique to the original F_2 fold axes (Figures 4.2, 4.4 and Figure 7.2). In detail, as demonstrated by the outcrop patterns of Rössing Formation units in the SJ area there are zones where F_2 fold axis rotation has not occurred and internal type 1 (of Ramsay, 1967) dome-shaped, and type 2 mushroom-shaped fold interference structures occur. Plunges range from subhorizontal across major interference structures to moderately northeast-southwest plunging F_3 folds on the limbs of major F_2 structures (Figure 4.4). Local overturning on the limbs of F_2 folds is considered to result from F_2-F_3 fold interference.

More pronounced examples of type 1 ‘dome and basin’ structures include respectively the Rössing SJ Dome itself and the doubly-plunging syncline to the southwest of the dome. In the case of the SJ Dome there is insufficient structural data to resolve its detailed geometry, however the available data and mapping shows that the stratigraphy is right-way-up on all sides of the dome and that the northwest and southeast limbs form a close to tight upright, subhorizontal structure similar to the reworked F_2 folds to the southeast.

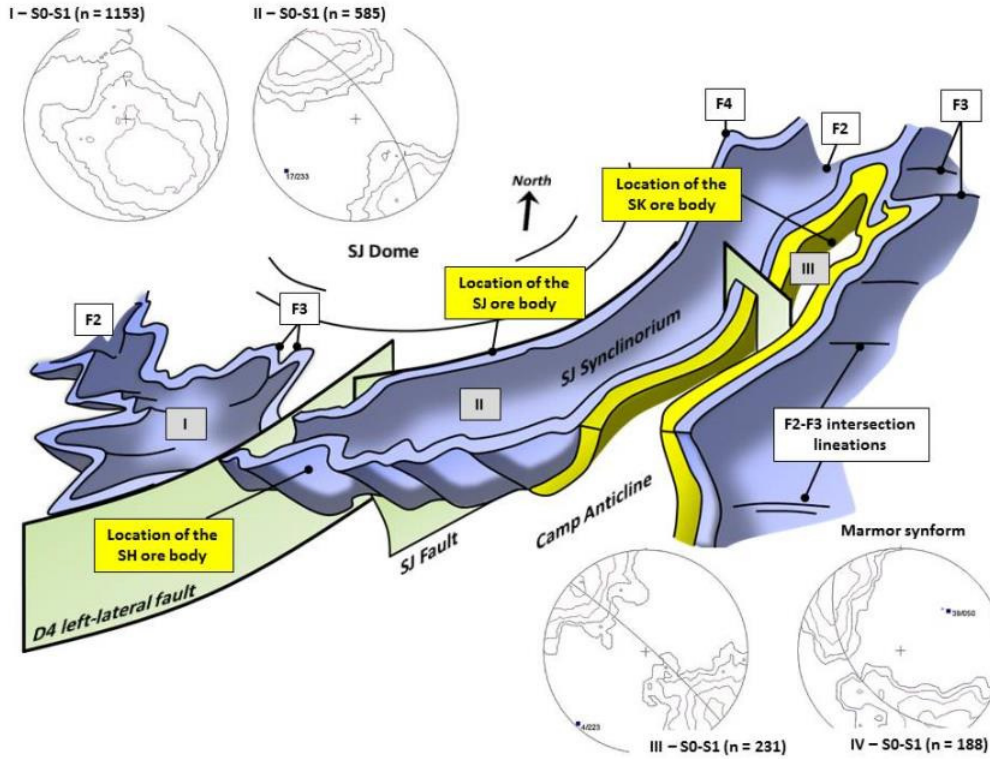


Figure 4.4. Fold interference relationships in the SH-SJ-SK area as determined from compilation of structural data. F_2 fold axes (cf. Figure 4.2) are reworked into northeast-southwest doubly plunging and sub-horizontal F_2-F_3 interference structures that wrap around the SJ Dome (areas I, II, III and corresponding stereograms). Area I northwest of SH forms a subhorizontal doubly plunging basin-shaped syncline. Area II (SJ area) plunges gently southwest. Area III (SK area) is likely doubly plunging given the anticlinal fold closure to the northeast, with measurements indicating a gentle plunge southwest. Individual F_3 folds on the limbs of the F_2 structures predominantly plunge moderately northeast – an example is shown from S_0-S_1 data from the F_3 Marmor synform (stereogram IV) to the south of this area. See also appended map for location of structural data. Note the presence of late left-lateral and locally right-lateral faulting. Yellow = top of the Khan Formation, blue = base of the Rössing Formation.

The interior of the SJ Dome is composed of Etusis Formation meta-arkose however an F_2-F_3 fold interference structure infolds the upper biotite gneiss member into the eastern half of the dome core where the 'V-shape' surface expression of this unit suggests this area plunges gently southwest (Figure 4.4 and appended map). The basin-shaped interference structure southwest of the dome is upright and horizontal (stereogram I of Figure 4.4). The doubly-plunging nature of this structure and the Rössing SJ Dome reflect the original east-west to northwest-southeast trending axial planes of F_2 folds.

The moderately northeast plunging F_3 Marmor synform and the parallel Blauer Heinrich syncline (actually a synform) are obliquely superimposed on the major F_2 Nose Structure and Welwitschia syncline forming type 3 fold interference of Ramsay

(1967). The same pattern is present in the area northeast of Z20 and south of Z17 as shown in Figure 4.5 where this interference structure is further complicated by a left-lateral D_4 fault offsetting the closure of the F_2 syncline by a distance of approximately 600 m. A further example of a type 3 'hook' structure is superimposed on the northeast limb of the Camp anticline in the SK area of (see Figure 7.2c, Chapter 7). The fold interference relationships described here facilitate the structural setting of the SH, SJ and SK, Z20-Z17 and Rössing South mineralised intrusions and this is discussed in more detail in Chapter 7.

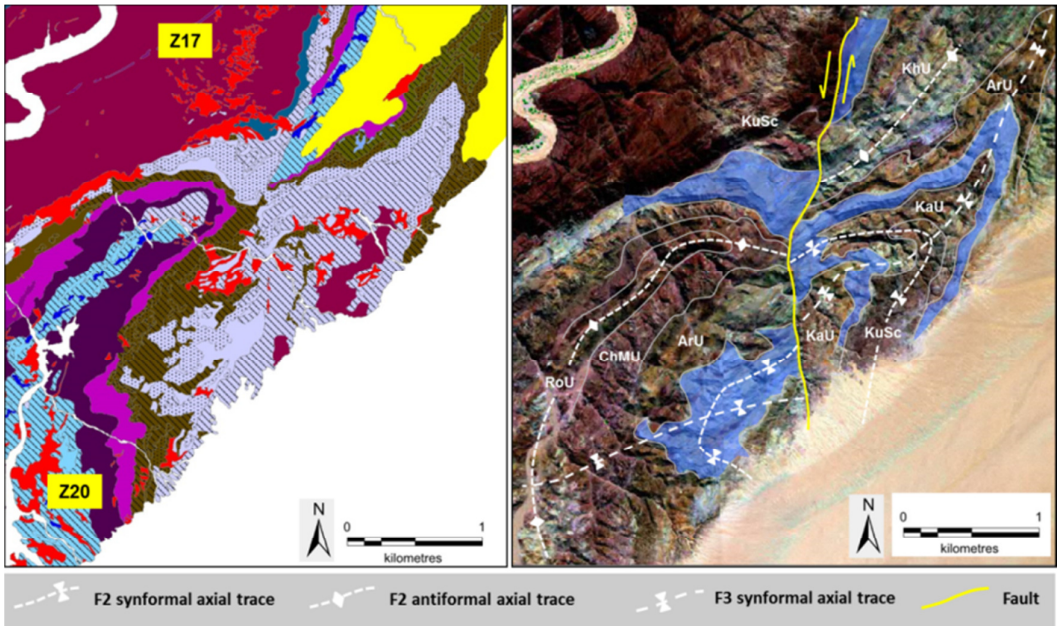


Figure 4.5. Left – lithological interpretation of the area northeast of the Z20 anomaly and Rössing South Zone 1 as per the attached map. Right – structural interpretation that uses marble of the Karibib Formation (blue) to highlight a type 3 fold interference structure comprising F_3 folds superimposed on earlier F_2 structures; the geology is further complicated by the presence of a left-lateral D_4 fault offsetting the closure of the central F_2 syncline by a distance of approximately 600 m. Base image is hyperspectral line data with RGB band combinations 108-26-2 (equivalent to Landsat bands 7-4-1). See Figure 4.2 for location. KhU – undifferentiated Khan Formation; RoU – undifferentiated Rössing Formation; ChMU – undifferentiated Chuos Formation diamictite; ArU – undifferentiated Arandis Formation; KaU – undifferentiated Karibib Formation; KuSc – Kuiseb Formation schist. Figure is centred on 508000 mE, 7509000 mN.

The identification of F_4 folding is restricted to the area immediately east of the Rössing SJ Dome where F_3 folds superimposed on F_2 are in turn affected by minor north-northeast trending folds (Figure 4.2).

Tectonic attenuation of stratigraphy can be seen at a map scale on the limbs of F_2 folds. More competent stratigraphic units commonly occur as 'mega-boudins' whilst carbonate units tend to be more attenuated. Map examples of mega-boudins can be

seen in the biotite gneiss member of the Karibib Formation on the limbs of the Welwitschia syncline. At outcrop scale the lowermost member of the Karibib Formation shows the same effects where calc-silicate bands within marble are often intensely boudinaged. Within the hinge zone of the F_3 Marmor synform such structures are refolded demonstrating pre-D_3 development (Figure 4.7c,d).



Figure 4.6. Fold styles at outcrop scale. (a) typical interference folding in a mixed sequence of the Rössing Formation within the hinge zone of the Blauer Heinrich syncline in the lower part of Khan Mine Gorge, with Khan Formation gneisses forming the prominent high relief in the background. (b) single early alaskitic vein in Chuos Formation diamictite at Z19 showing the effects of extreme shortening. (c) upright, open chevron style folds developed in Karibib Formation marble in the Khan River valley, locally exhibiting dextral displacements along planes parallel to the fold axes. (d) Fold interference patterns in Kuiseb Formation cordierite schist near Z19. (e) and (f) concentric folds in early alaskite intruding the Chuos Formation in Panner Gorge and Khan Formation northeast of the mapped area respectively. These are probably A type alaskites of Nex (1997).

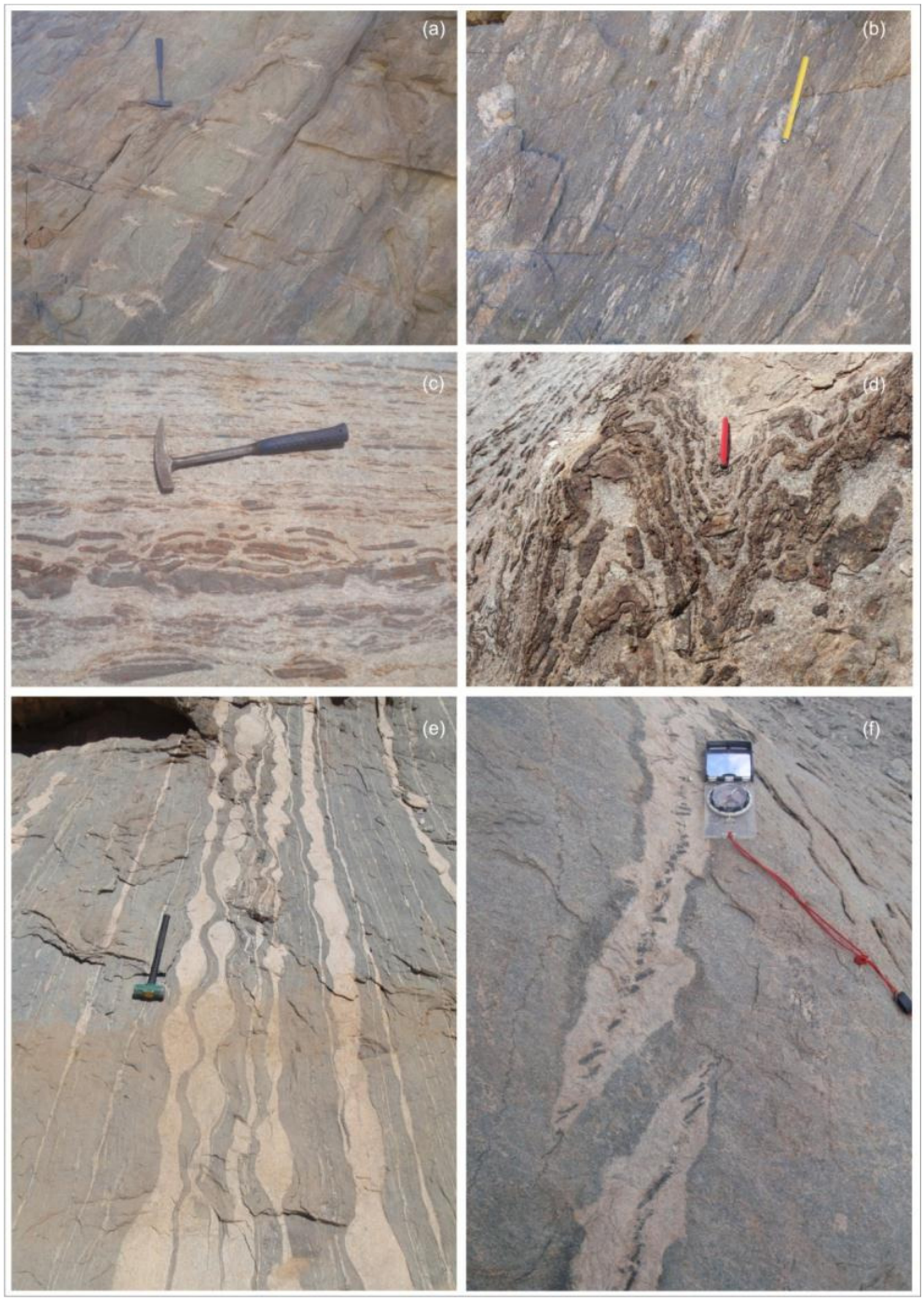


Figure 4.7. Examples of structural attenuation in outcrop. (a) leucosomal tension gashes developed perpendicular to gneissosity in Khan Formation gneisses near SH. (b) pebbles elongated parallel to schistosity in diamictite of the Chuos Formation. (c) boudinaged calc-silicate beds in Karibib Formation marble at Z19. (d) as per (c), but within the hinge zone of northeast-plunging Marmor Synform closure southwest of Z19, demonstrating that boudinage in this case predates F_3 folding. (e) boudinaged sheeted alaskites in the Khan Formation, Khan River valley. These are probably A type alaskites of Nex (1997). (f) migmatitic hornblende melanosomal and quartzo-feldspathic leucosomal segregations in Khan Formation gneisses of Panner Gorge. The migmatite textures have been boudinaged and subsequently compressed along a plane perpendicular to the gneissosity producing a 'domino structure' in the hornblende melanosome.

Extensional zones along F_2 fold limbs and hinges also appear to be locally exploited by voluminous alaskite intrusions, such as in the closure of the Nose Structure and in the Khan Copper Mine area where these intrusions are deformed by northeast trending F_3 folds. Other effects of ductile tectonic attenuation and/or shear observable at outcrop scale include, boudinage of early alaskite sheets (Figure 4.7e), stretching of pebbles in metasediments (Figure 4.7b), attenuation of partial melt melanosomes (Figure 4.7f), and development of leucosomal tension gashes. Relative timing has not been constrained for these other features however tension gashes clearly postdate development of the main gneissosity. A component of tectonic thinning during D_3 can also be inferred from the thickening of stratigraphy into F_3 similar fold hinges such as the Blauer Heinrich syncline where this must have been accommodated by thinning in F_3 fold limbs. Rapid variations in both thickness and lithology across major fold hinges may reflect original sedimentation across active basin margin faults of the kind interpreted by Miller (2008) for the deposition of the Nosib Group in half grabens (Alasdaire Pope, pers. comm.). An example of this is the thickness and stratigraphic variability across the F_2 Camp anticline in the SK area.

At least one phase of shear deformation predated D_3 as evidenced by the sheared contact between A.M.C. basement and Damaran metasediments in the area around Arandis Airport. The Rössing Formation in this area lies directly on basement and the contact zone is deformed by northeast trending F_3 folds. It seems likely that shear deformation between the Damaran sequence and basement to the southeast in the Nose Structure, termed the Khan River Detachment by Oliver (1994; Chapter 4.2), would have been contemporaneous to this. Late D_3 to D_4 shear is apparent from the presence of north-northeast oriented en-echelon uraniferous alaskites showing tension gash morphologies in the SK area. Here the shear sense as noted by Laberge (2008a) is dextral and map relationships show that the alaskites cut across F_2-F_3 fold interference structures (see Figure 7.2c) and occur in a north-northeast trending zone that is oblique to the northeast F_3 fold trend in the same area. Map relationships suggest that a north-northeast trending swarm of barren alaskites at Z17 also cut across F_3 folds. On this basis and as will be further discussed in Chapter 7, late-tectonic alaskites in the area are suggested to have been emplaced into late north-northeast oriented throughgoing shear zones that developed during D_4.

4.3.3 Brittle Structures

Brittle faulting in the area consists of regional fault zones where individual structures within these generally appear to be laterally discontinuous. Map relations show these faults which range in orientation from northeast-, through north-northeast-, to northwest-trending, record latest predominantly sinistral offsets of up to 1200 m (see Appendix II map inset of Nose Structure Anticline at 1:30 000, and Figure 4.2). The majority of these faults are interpreted as having being active during D_4 as in many cases they disrupt F_3 folds or F_2-F_3 fold interference structures (e.g. Figure 4.4). However, a number of faults trending parallel to the D_3 trend, notably in the SJ pit where mining has well-exposed fault planes such as the SJ Fault, kinematic indicators demonstrate multiple senses of thrust and normal movements on such structures (Alasdaire Pope, pers. comm.) where at least some of these presumably predate the latest D_4 movements. Sinistral movement on the F_4 fault that displaces the Nose Structure and the area of Rössing Formation around SH either appears to have either been accommodated by ductile deformation in the Khan Copper Mine area, as there is no apparent significant offset of Khan Formation units in the latter area. At the scale of the attached map there are no obvious significant brittle displacements of late alaskite intrusions.

Joint orientations recorded over the SJ pre-mining surface from both metasediments and alaskites (Nash, 1971; Berning, 1986), pre-tailings area substrate and Panner Gorge as shown on the map in Appendix II and rose diagrams therein (Harris *et al*., 1993, 1994; Jacob *et al*., 1997; Jacob and Kerber, 1997), show a dominant north northwest-south southeast trend indicating development during D_3, transverse to F_3 fold axial planes and parallel to the principal stress orientation. Such joints would have facilitated the development of D_4 faults described above, as the principal stress orientation changed between D_3 and D_4. Such dense jointing would have dramatically increased permeability and hence played a crucial role in the supergene enrichment of primary uranium mineralisation.

4.4 Summary and Discussion

Mapping in the area has constrained three geometrically distinct fold generations (F_2-F_4) and geometries of some major F_2 and F_3 fold relationships have been determined through interrogation of point S_0-S_1 data compiled during this project. F_1 folds have not been confidently identified in this area but are inferred from regional studies in the CZ including that of Longridge (2012) whose study underpins the nomenclature of the fold phases F_2-F_4 discussed here. The original orientation of F_2 axial planes were

east-west to west-northwest-east-southeast trending, moderately north dipping, consisting of close to isoclinal folds. In the area of the Rössing SJ Dome these have been refolded into northeast-southwest doubly plunging type 1 (dome and basin) F_2-F_3 fold interference structures. Overturning of major F_2 fold structures in the southeast of this area is not attributed to D_4 modification as suggested by Anderson and Nash (1997) but to F_2-F_3 fold interference (Figure 4.4). In the southeast of the mapped area, type 3 (hook-shaped) fold interference of Ramsay (1967) dominates. Type 3 refolds have straight first hinges and folded first axial planes, in contrast to type 2 refolds which are typified by both the first hinges and axial planes being folded.

Superimposition of F_2 and F_3 producing fold interference is in agreement with the study of Longridge (2012) for the Palmenhorst Dome. However the variety of F_2-F_3 fold interference structures present (types 1 and 3 of Ramsay, 1967) must reflect varying F_2 fold axial plane attitudes, since F_3 fold axial plane orientations can be seen from Figure 4.2 to be constant. Differing F_2 fold axial plane orientations could be due to either (i) the presence of F_1 folding that has not been recognised or (ii) progressive deformation of the sort proposed by Oliver (1994) and Poli and Oliver (2001) involving transpressive rotation and refolding of early fold phases by later ones. F_2 in this study is correlated with Smith's F_1 (1965; Chapter 4.2) and F_3 with Smith's F_2. The latest northwest fold trend identified by Smith (1965) and Nash (1971) is not well understood by the current author. This trend is apparent on the attached map as kinks occurring on the limbs of refolded F_2 structures. These trends could also result from progressive deformation between F_2 and F_3. A minor phase of north-northeast oriented F_4 folding is considered essentially as a continuum of D_3 deformation into D_4 where the principal stress axes rotated from northwest-southeast to west northwest-east southeast.

Pre-D_3 attenuation of stratigraphy is evidenced by map- and outcrop-scale boudinage structures on F_2 fold limbs and this was likely to have been accompanied by alaskite intrusion. Pre-D_3 alaskites can be interpreted where they are folded by F_3 folds (e.g. Khan Copper Mine intrusion) or F_2-F_3 fold interference structures (e.g. Rössing SJ Dome). Thickness and stratigraphic changes across major fold structures are considered largely to result from D_2-D_3 ductile attenuation and boudinage combined with fold interference, as opposed to indicating the presence of early extensional faults as suggested by Alasdaire Pope (pers. comm.), although rapid lateral stratigraphic changes particularly in the Rössing Formation have been described in

Chapter 3. Shear deformation of the basement-cover zone is demonstrably pre-D_3 in age as it is folded by F_3 folds in the northwest of the mapped area. Such deformation would also have been focussed into the Nose Structure basement-cover contact named the Khan River Detachment by Oliver (1994; Figure 4.2) who suggest timing of deformation to be D_3. There is no evidence for this shear zone ramping through stratigraphy to the Rössing SJ Dome area as proposed by Oliver and Kinnaird (1996). Since no definitive D_1 structures are recognised in the project area the timing of this extensional and shear deformation is therefore in general agreement with that proposed by Longridge (2012) for shear structures at the basement-cover interface and northeast and southwest stretching lineations within the Palmenhorst Dome area as representing D_2 deformation. Based on field measurements of the attitude of overlying Damaran metasediments, the orientation of the basement cover shear plane in Figure 4.2 is drawn opposite to that shown by Poli and Oliver (2001), i.e. this contact in both the Khan River and Arandis Airport area inliers is interpreted to be right-way-up rather than overturned or overthrust.

D_4 transtensional deformation is suggested by the presence of north-northeast aligned zones of both barren and uraniferous alaskites that appear to be largely undeformed and cross-cut F_3 folds or F_2-F_3 fold interference structures (SK, Z17, possibly Z20-Rössing South). This is discussed further in Chapter 7 and represents a refinement of the model proposed by Anderson and Nash (1997) and Basson and Greenway (2004) of uraniferous alaskites at Rössing SJ intruding a major sinistral D_4 fault or fault zone. The interpretation presented here, primarily based on map observations, is that uraniferous (and barren) alaskite intrusion accompanied the development of post-D_3 to early D_4 north-northeast Welwitschia trend district-scale throughgoing shear zones and was focused into sites where these coincided with D_2-D_3 dilational parts of fold interference structures. D_4 brittle deformation accompanied the dome rotation described by Basson and Greenway (2004) and offset earlier ductile structures. Such faults record a maximum sinistral displacement of 1200 m as seen in the Nose Structure anticline (inset of attached map). Brittle offset of grade zones is a feature of the Rössing SJ deposit (Alasdaire Pope, pers. comm.). In addition minor predominantly north to north-northwest sinistral but locally northwest dextral displacements of alaskites in the SJ and SK areas that do not affect Mesozoic dolerite dykes have been respectively described by Berning *et al*. (1973) and Laberge (2008a). These faults are generally not resolved at the scale of this mapping, but suggest that D_4 brittle deformation postdated alaskite intrusion. Some late faults are associated with calc-silicate replacement as noted by Laberge (2008a).

The development of a fracture network normal to the F_3 trend (rose diagrams on Appendix II) presumably facilitated F_4 fault development and would have subsequently significantly enhanced the supergene enrichment process of the Rössing SJ orebody, discussed in Chapter 7.

Chapter 5: Metamorphism

5.1 Introduction

Metamorphism in the wider CZ was introduced in Chapter 1.2.4. Two high-grade metamorphic pulses have been recognised in the CZ of the Damaran Orogen, within which interpreted P-T data suggests a pressure decrease consistent with that seen in the SZ and SMZ (Nash, 1971; Kasch, 1983; Puhan, 1983; Masberg *et al*., 1992; Nex *et al*., 2001b; Goscombe *et al*., 2004). There is significant disagreement in the literature with regards to the timing of these events, however peak M_2 metamorphism seems well-constrained to between 520-504 Ma (Nex *et al*., 2001b; Jung and Mezger, 2003; Ward *et al*., 2008; Longridge, 2012). The recent study of Longridge (2012) suggests that M_2 metamorphism accompanied D_2 deformation (Table 1.1), however other workers (e.g. Nex *et al*., 2001b) have assigned peak M_2 conditions to post-D_3 deformation. These metamorphic pulses were contemporaneous with voluminous syn- to post-tectonic granitic plutonism (Chapter 1.2.5 and Chapter 6).

5.2 Previous Work in the Project Area

The study of Nash (1971) represents the most detailed metamorphic petrological study in the immediate Rössing area. From petrographic relationships Nash (1971) distinguished psammitic, basic, pelitic and carbonate compositional groups within the Damaran metasedimentary sequence as described in Chapter 3. A paragenesis of selected minerals summarised from review of the various diagrams and text of Nash (1971) is shown in Figure 5.1. Despite Nash's distinction of a 'basic group' of gneisses in the Khan Formation as suggested by major element geochemistry, Nash attributed a sedimentary protolith to these gneisses based on the regional mapping of Smith (1965). Nash interpreted three metamorphic pulses consisting of two phases of upper amphibolite facies metamorphism and migmatisation (M_1 and M_2) and a third M_3 phase of retrograde metamorphism that is less widely discernible. Nash (1971) related these metamorphic pulses to three deformational episodes which are correlated to D_{1-2}, D_3, and D_4 respectively in this thesis (Chapter 4; Figure 5.1; the first two correlations seem quite clear whilst the latter is tentative). According to Nash (1971, 1972) within the Khan Formation the growth of clinopyroxene, plagioclase and andradite in 'basic' gneisses and growth of muscovite, staurolite, biotite and K-feldspar in metapelites is attributable to M_1. Clinopyroxene and andraditic garnet are seen in inclusions in early migmatitic segregations. Nash also interprets the presence of relict tremolite in marbles with diopside and forsterite to indicate relatively high pressures (+6 kbar) during M_1.

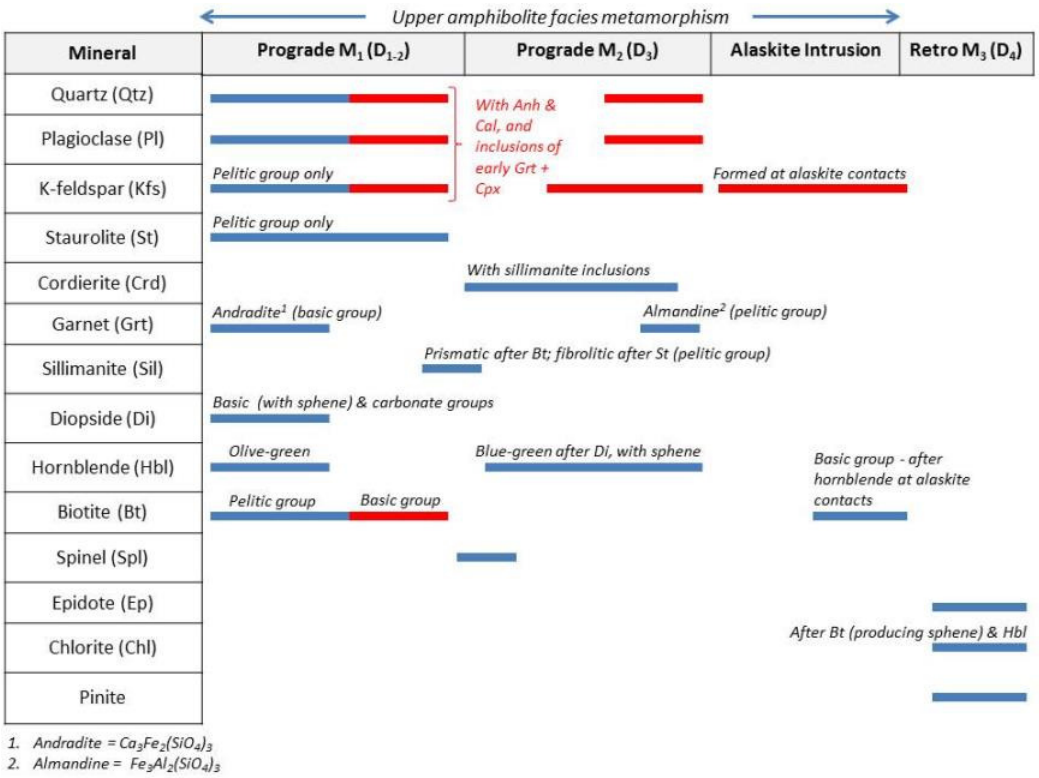


Figure 5.1. Diagram showing the paragenesis of selected minerals compiled from Nash (1971) shown as blue bars and occurring within four compositional groups (psammitic, basic, pelitic and carbonate groups). The current author's correlation of M_1 and M_2 with regional D_{1-2} and D_3 events respectively is clear from Nash's description, however in the case of correlating M_3 with D_4 this is tentative. Note that Nash (1971) interprets two phases of migmatisation during both prograde M_1 and M_2 pulses, where the resulting partial melt material is shown as red bars. An explanation to mineral abbreviations is provided in the left column and in Appendix I.

M_2 (syn-D_3) caused shear banding, growth of hornblende at the expense of clinopyroxene in Khan Formation gneisses, and growth of cordierite in metapelites (Nash, 1971). Smith (1965) interpreted F_3 folding (his second fold generation) to have produced axial-planar biotite in F_3 folds, where this post-dates at least one phase of amphibole formation as shown by the boudinaged nature of amphibolite bands. The presence of random mineral orientations in Khan Formation gneisses and porphryoblasts in Rössing Formation biotite schists, is interpreted by Smith as being indicative that the latest prograde (M_2) metamorphism outlasted major fold movements. The effects of partial melting are apparent throughout the stratigraphy as migmatitic and locally agmatitic textures as described throughout Chapter 3. These include quartz-feldspar leucosomes commonly within tension gashes and mafic phases in boudinaged melanosomes. Nash (1971) directly attributed granite formation to these textures.

According to Nash (1971) critical metamorphic assemblages indicate M_1 temperatures of ~700˚ C and pressures of 6-8 Kb, conditions corresponding to upper amphibolite facies Barrovian-type metamorphism. The presence of cordierite in rocks of appropriate composition indicate temperatures of ~675-750˚ C at lower pressures of 3-5 Kb attained during metamorphism at a higher crustal level during M_2 (Nash, 1971). In the Rössing-SJ Dome area, the lack of muscovite and presence of biotite + quartz + K-feldspar in pelites and migmatitic partial melts is an assemblage noted by Oliver and Kinnaird (1996) to require temperatures of >730º C. In the more calcic clinopyroxene-rich Khan Formation gneisses, the absence of orthopyroxene also suggests that the metamorphic grade is below the onset of granulite facies, where orthopyroxene would form from clinopyroxene + quartz at temperatures >780˚ C (Laberge, 2008b; Oliver and Kinnaird, 1996).

Ward *et al.* (2008) describe lens-shaped alaskite leucosomes within the Kuiseb Formation of the project area, developed at high angles to a regional stretching lineation defined by elongate moderate to steeply, northeast-plunging elongate cordierite porphyroblasts, and within which biotite underwent incongruent melting via the reaction:

$$\text{Biotite} + \text{Qtz} + \text{Pl} + H_2O \leftrightarrow \text{melt} + \text{garnet} + \text{cordierite}$$

Within these leucosomes garnet is typical as large (up to 12 cm) poikiloblasts whilst cordierite has nucleated on pre-existing crystals within the bounding gneiss. Thermobarometry applied to the anatectic assemblage yields low-temperature, granulite-facies peak conditions of 750 ℃ and 0.5 GPa (5 kbar) where the relatively low temperature indicates water must have been present in facilitating partial melting in these dilational zones.

Further afield microprobe analysis of garnets of Chuos Formation schist by Nex *et al.* (2001b) at Goanikontes show these to be dominantly almandine ($Fe_3Al_2(SiO_4)$. These workers interpret mineral growth stages as follows:

Earliest cordierite porphyroblasts – spinel-sillimanite symplectites – biotite and cordierite overgrowth with first fibrolite – garnet (overgrowing biotite foliation) – latest second generation fibrolitic sillimanite.

These authors note that early cordierite porphyroblasts may have formed by breakdown of earlier staurolite and/or andalusite which would be consistent with the interpretation of Jacob (1974) for the area of the lower Swakop River. Partial melting was contemporaneous with late garnet growth and reflects the M_2 thermal metamorphic overprint.

Skarn bodies ranging in size from a few centimetres to several metres are widespread, consisting of any of wollastonite, diopside, grossular garnet, tremolite, and scapolite with variable amounts of calcite, quartz, titanite (sphene) and apatite (Nash, 1971; Nex *et al.*, 2002). A study by Mbangula (2007) of skarn bodies in the SH and SJ area has demonstrated that these are not significantly uranium-enriched, in contrast to skarns in the Ida Dome area (e.g. Freemantle, 2012).

'Calc-silicate' bodies have been mapped and described in the SK area and south of the SJ area by Laberge (2008a, 2008b); these are described as pale-green, fine-grained and granoblastic, locally cross-cutting and exhibiting massive, conglomeratic or brecciated textures suggestive of a replacement origin. Field observations indicate that this rock type pre-dates at least some alaskite emplacement but may also be associated with late northwest to north-northwest striking faults (Laberge, 2008a; 2008b).

5.3 This Work

5.3.1 Mineral Parageneses

In the study of Nash (1971) minerals are described as compositional paragenetic associations comprising psammitic, basic, pelitic, and carbonate groups with the addition here of a fifth calc-silicate group.

Psammitic Association

Meta-psammites in the area consist of metamorphosed arkoses of the A.M.C., Etusis, Rössing and Karibib Formations, biotite gneiss of the Etusis Formation, and Facies I (psammitic diamictite) of the Chuos Formation. Throughout these lithologies the major constituent minerals generally comprise:

Quartz + K-feldspar ± plagioclase ± biotite ± tremolite ± muscovite ± tourmaline

Locally sillimanite has been noted in Etusis Formation meta-arkose. Migmatitic and locally agmatitic textures are common throughout the Etusis Formation meta-

psammites and occasionally within Chuos Formation Facies I (Figure 5.2d and f). The dominantly potassic nature of the meta-psammites and presence of migmatitic leucosomes of similar composition to alaskite intrusions throughout the area is considered by the author to strongly suggest a direct relationship between partial melting of meta-psammites and alaskite generation, as suggested by Nash (1971).

Basic Association

Although gneisses of the Khan Formation are likely to be of siliciclastic origin (Chapter 1.2.2), their feldspar-dominant (± amphibole) mineralogy comprising generally <20% quartz renders them mineralogically similar to basic igneous rocks for the purposes of discussion. Also included within this group are the 'basic gneisses' of the A.M.C. described in Chapter 3.2. This association is generally characterised by:

Plagioclase + quartz ± amphibole (as tremolite or hornblende) ± K-feldspar ± biotite ± diopside ± garnet

Epidote and chlorite commonly occur in this group as retrograde alteration products after garnet and pyroxene respectively. Tremolite appears to be more common to the clinopyroxene gneiss unit whilst tremolite and hornblende both occur in the clinopyroxene granofels and biotite gneiss units of the Khan Formation, presumably indicative of the increased availability of iron in the original sedimentary beds of the latter to form hornblende.

The clinopyroxene granofels of the Khan Formation is the most siliceous unit (locally up to 50% quartz) in this group and accordingly textures attributed to partial melting processes are mostly frequently observed in this unit. The mottled texture of this unit ('*mottled gneiss*' in the Rössing Mine stratigraphy) is interpreted as a migmatitic texture where ferromagnesian minerals form restites and quartz-feldspar aggregates represent migmatitic leucosomes. Demonstrably early migmatitic melanosomes are also a frequent feature constituting deformed hornblende and/or diopside lenses (Figure 5.2e).



Figure 5.2. Effects of metamorphism on units of the Damara succession. (a) cordierite porphyroblasts in cordierite gneiss of the Rössing Formation, SK, slightly elongated into the plane of gneissosity. (b) 'wollastonitised' marble unit of the Rössing Formation, southwest of the tailings area. (c) pegmatitic leucosomal partial melt development in a tension gash formed in Khan Formation gneiss near SH (see also Figure 4.7a). (d) alaskitic, migmatitic leucosomes in Chuos Formation diamictite at Z19. (e) early hornblende migmatitic melanosome in Khan Formation gneiss, Panner Gorge, that has experienced attenuation (leucosomal tension gashes) followed by folding. (f) migmatitic biotite gneiss of the Etusis Formation of the SJ Dome where the leucosome is an alaskitic composition.

Pelitic Association

The pelitic association reflects metamorphism of pelitic to semi-pelitic (i.e. argillaceous) sediments represented by biotite-cordierite gneiss of the Rössing Formation, diamictites of facies II and III of the Chuos Formation, biotite schist and biotite gneiss of the Karibib Formation, and cordierite schist of the Kuiseb Formation. The association most frequently consists of:

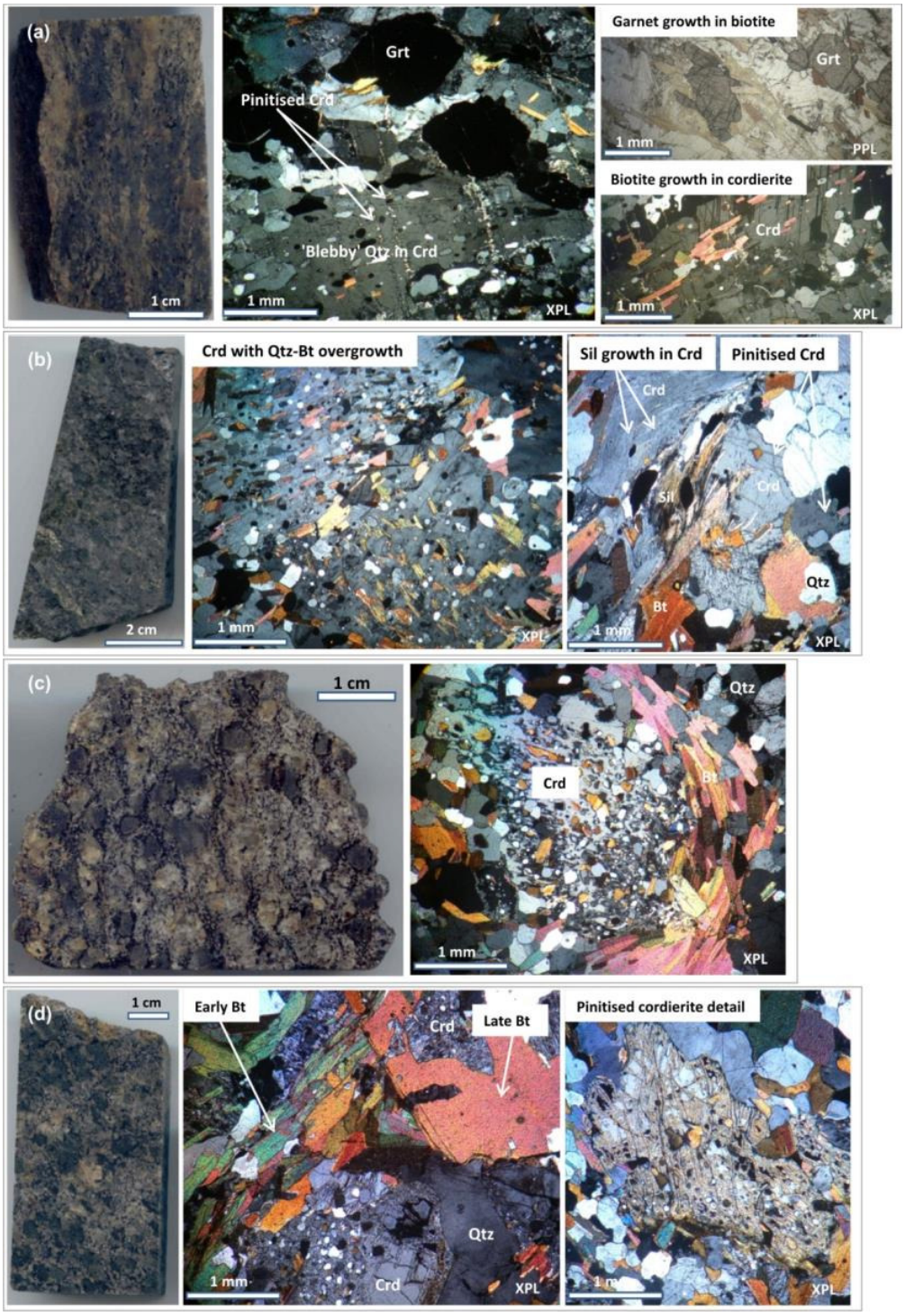


Figure 5.3. Textures and mineral parageneses within metapelites in hand specimen and thin section. (a) RSS036, Grt-Bt-Qtz-cordierite gneiss, Rössing Formation, exhibiting late garnet growth in early biotite bands, and late biotite growth in early cordierite; (b) RSS086, Py-Sil-Crd-Bt-Qtz-K-Fsp gneiss, Rössing Formation, showing late quartz, biotite and sillimanite overgrowing early cordierite; (c) RSS064, Pl-Qtz-Bt-Crd schist, Kuiseb Formation, showing early cordierite porphyroblasts enclosed by early biotite and late quartz-biotite overgrowing cordierite; (d) K-Fsp-Bt-Qtz-Crd schist, Kuiseb Formation, exhibiting both early and late biotite stages. PPL – plain polarised light, XPL – cross polarised light. For an explanation of mineral abbreviations refer to Appendix I.

Quartz + biotite + cordierite ± K-feldspar ± plagioclase ± sillimanite ± garnet ± hornblende

Textures indicating a general paragenetic mineral sequence within metapelites are shown in Figure 5.3. In contrast to the paragenesis of Nash (1971, Figure 5.1), cordierite is considered to have formed relatively early in the sequence, as evidenced by the pre- to syn-tectonic fabrics exhibited by porphyroblasts which are overgrown by later phases. Cordierite is overgrown by late quartz and biotite with subsequent retrograde pinitisation. Biotite shows both early and late growth stages with the latest phase occasionally overgrown by latest sillimanite. Migmatisation in these lithologies is most marked in the Rössing Formation biotite-cordierite gneiss where quartzo-feldspathic leucosomes are a characteristic texture (Figure 3.9c). Textural review of metapelites indicates a general paragenesis of earliest cordierite – biotite – almandine garnet – biotite – latest sillimanite.

Carbonate Association

The carbonate association encompasses predominantly marbles of the Rössing and Karibib Formations, however marbles of the Etusis and Chuos Formations are also included here, albeit not studied. The association comprises:

Carbonate (calcite or dolomite) ± quartz ± forsterite ± diopside ± tremolite ± phlogopite ± graphite ± sulphide (as pyrite or pyrrhotite)

Both chondrodite and pleonaste were also included here by Nash (1971) but not identified during this study. The carbonate species is usually calcite, however dolomitisation particularly at the base of the Rössing Formation has been noted above, whereas dolomitic marble of the Karibib Formation is a primary sedimentary feature (see Chapter 3.3.6 and 3.5).

Calc-silicate Association

The calc-silicate association relates to mineralogical assemblages interpreted as resulting from metamorphism of marls. Calc-silicate gneisses constitute mapped units of the Arandis Formation whilst calc-silicate beds occur throughout the same formation including most prominently within calcitic marble producing a 'ribbon marble' (Figure 3.13a). The assemblage here determined from calc-silicate gneiss samples comprises:

Amphibole (tremolite or hornblende) + quartz ± scapolite ± pyrrhotite

A second calc-silicate assemblage is described in Chapter 5.3.3 and is interpreted as a fault-related rock of a replacement nature. It is ubiquitously characterised by the assemblage:

Quartz + tremolite + plagioclase ± diopside

The common occurrence of tremolite throughout both associations may be indicative of either a dolomitic marl protolith (in the case of the calc-silicate gneisses of the Arandis Formation) or magnesium-bearing fluids (in the case of calc-silicate replacement).

5.3.2 Skarn Development

A study of skarns has not been a focus of this project and the assemblages have been well described by previous work (Nash, 1971; Mbangula, 2007; Chapter 5.2). A notable feature occurring particularly to the west of the mapped area is the presence of completely wollastonitised marble beds which form prominent resistant outcrops. Wollastonite generally forms through decarbonation of calcite in the presence of quartz at very high temperatures and low pressures in contact metamorphic aureoles. However, in regionally metamorphosed rocks the temperature stability range of this mineral may be significantly lowered if water infiltration from adjacent schists flushes away CO_2 (Yardley, 1989). This may help explain why wollastonitised marbles do not appear to be associated with any specific intrusive – this is true to say of many skarn assemblages in the project area where these may also result from regional heat flow induced by voluminous intrusive activity during regional metamorphism (Judith Kinnaird, pers. comm.). Quartz-tremolite-plagioclase calc-silicate rock formation (Chapter 5.3.3) is interpreted as a replacive calc-silicate assemblage that may relate to this process, but is discussed separately below.

5.3.3 Calc-silicate Rock

This unit occurs southwest of Dome Gorge on the southern limb of the Camp anticline cross-cutting the Khan through to Karibib Formations and also in the SK area within the Khan Formation biotite gneiss, where it was first mapped by Laberge (2008a, 2008b). It is described separately from the calc-silicate association noted in Chapter 5.3.1 as the mineral assemblage does not necessarily relate to that of the protolith given that it is interpreted as a replacive unit. The unit was sampled in the

area south of SJ in order to constrain its genesis (Figure 5.4). Field observations and map relations show that the calc-silicate rock predates the alaskite bodies which intrude it. Sample RSS067 from this area is a fine-grained massive textured rock composed of quartz-tremolite-plagioclase. Sample RSS068 is a clast-rich quartz-tremolite-plagioclase breccia with tremolite-plagioclase clasts in a tremolite-rich matrix.

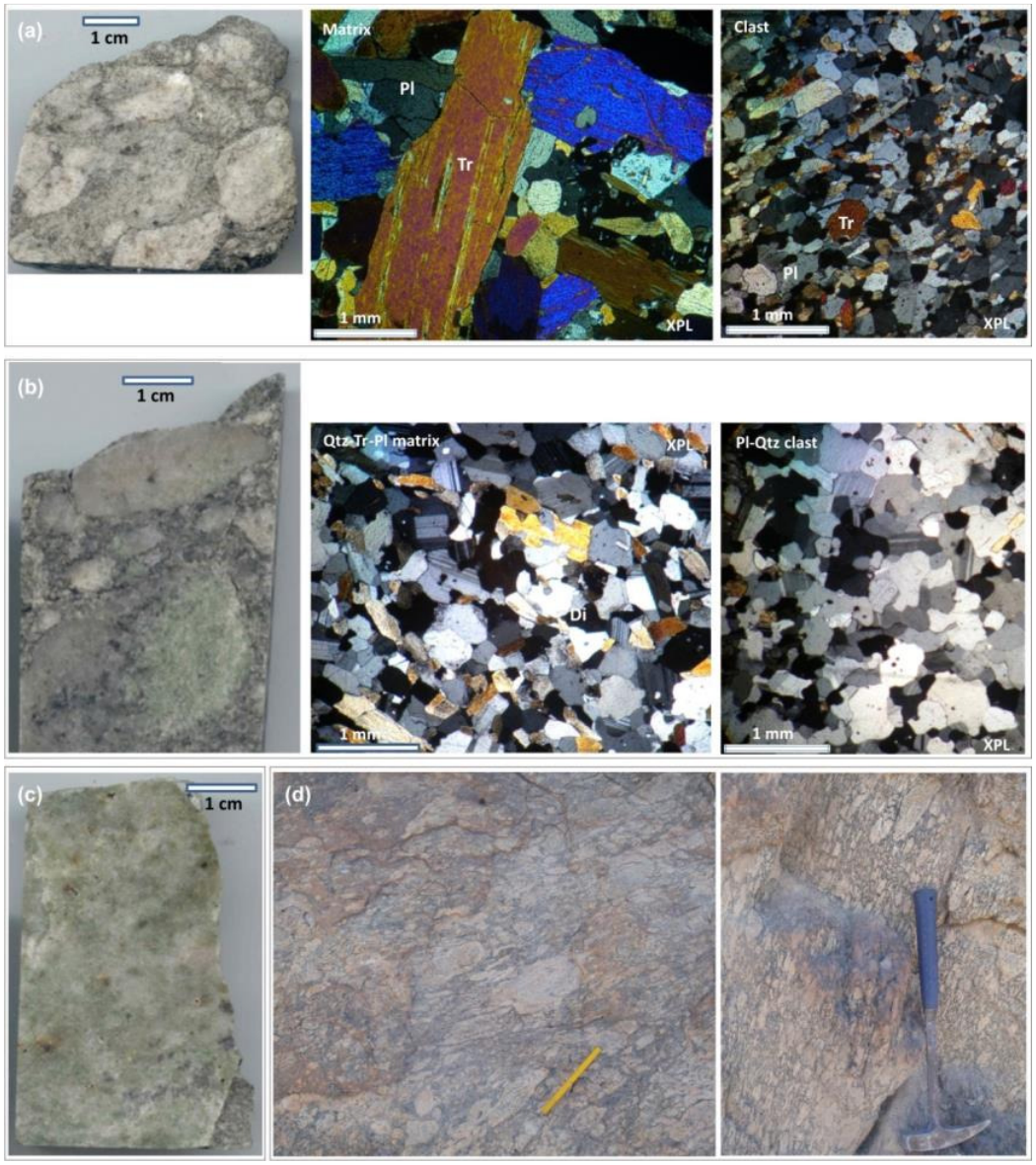


Figure 5.4. Calc-silicate rock exhibiting characteristic quartz-tremolite-plagioclase mineralogy. (a) RSS068 in hand specimen (left) and thin section (middle and right showing matrix and clast respectively), from southwest of Dome Gorge; (b) diopside-bearing RSS030 from SH hand specimen (left) and thin section (middle and right showing matrix and clast respectively); (c) RSS067 from southwest of Dome Gorge, exhibiting a fine-grained massive texture; (d) outcropping matrix-supported calc-silicate breccia from Panner Gorge. PPL – plain polarised light, XPL – cross polarised light. For an explanation of mineral abbreviations refer to Appendix I.

Mapping in the Panner Gorge area during this study delineated a similar lithology. A quartz-tremolite-plagioclase breccia outcrops within a 2000 x 400 m zone from SH and to the west, occurring within both the clinopyroxene granofels and overlying biotite gneiss of the Khan Formation. This indirectly suggests this unit may be cross-cutting in nature. In the field, the calc-silicate rock is observed to consist predominantly of rounded to angular quartzo-feldspathic clasts in a matrix of dark green tremolite (Figure 5.3). However, in places this texture appears to display a reverse relationship with apparent tremolite clasts set in a quartzo-feldspathic matrix. Conglomeratic textures are most frequent within this unit, however angular breccia textures occur in areas of lower strain. Assemblages observed in thin section from the Panner Gorge area are diopside-tremolite-quartz-plagioclase, quartz-tremolite-plagioclase, tremolite-quartz-plagioclase and tremolite-plagioclase-quartz (RSS030, RPS012, RPS014, RPS015, RPS044, and RPS016). Textures are typically granoblastic and commonly display late quartz leucosomes. In areas of high strain, this lithology may look gneissic, however the quartz-tremolite-plagioclase mineral assemblage seems to be fairly unique and diagnostic regardless of texture. A similar lithology has been intersected in deep drilling under the SJ pit (Rössing mine staff, pers. comm.). In Panner Gorge, the calc-silicate rock shows agmatitic textures where it is intruded and brecciated by alaskite, supporting an early phase of development relative to the alaskites. However this rock may also be spatially associated with late northwest to north-northwest striking faults (Laberge, 2008a; 2008b). The consistent mineralogy displayed by this unit across a range of textures is indicative of a replacement origin associated with faulting as interpreted by Laberge (2008a, 2008b) where brecciation may have accompanied calc-silicate replacement.

5.4 Summary and Discussion

A detailed metamorphic petrological study has fallen beyond the scope of this project. However, numerous field observations and petrographic review of samples permits a tentatively revised paragenesis of metamorphic events building on the study of Nash (1971; Figure 5.5). Mineral assemblages have been split into the same psammitic, basic, pelitic and carbonate compositional groups of Nash (1971) with the addition of a fifth calc-silicate group interpreted as metamorphosed magnesian marls. Within the first four groups the mineral assemblages are essentially the similar to those reported by Nash (1971) but are represented by a wider transect of stratigraphy to include the formations above the Rössing Formation. The assemblages have been extended to include ancillary minerals beyond some of

those described by Nash (1971). Little attempt has been made to separate paragenetic sequences within each group or establish detailed P-T interpretations from phase equilibria within these. However textural review of metapelites indicates a general sequence of earliest cordierite – biotite – almandine garnet – biotite – latest sillimanite, in contrast to the interpreted sequence of Nash (1971; Figure 5.1). Note that Ward *et al.* (2008) also describe late cordierite (above).

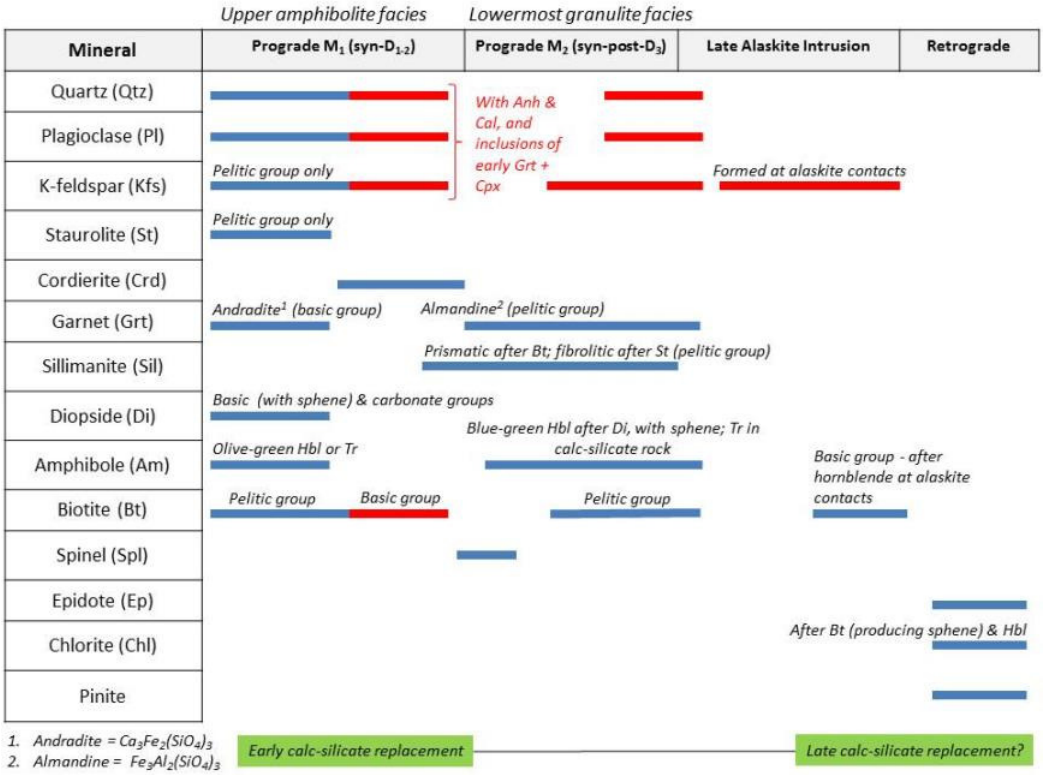


Figure 5.5. Diagram showing a revised mineral paragenesis after Nash (1971) with additional observations from this project. These include the presence of cordierite and almandine garnet earlier than that interpreted by Nash, and pulses of calc-silicate replacement (± brecciation) associated with faulting. The mineral assemblage suggests that M_2 reached lowermost granulite facies metamorphism (Figure 5.6). An explanation to mineral abbreviations where not given in the figure is shown in Appendix I.

The pelitic group provides the most useful index minerals for assessing peak metamorphic conditions in the Rössing area which is indicated in Figure 5.5. The general paragenetic sequence noted above is broadly consistent with the description of Nex *et al.* (2001b) for Chuos Formation metapelites at Goanikontes. This sequence has not been related to temporally-constrained structural fabrics, however it is considered likely here that pre-tectonic cordierite textures originate from pre-D_3 deformation. Intensely elongated cordierite porphyroblasts within the Blauer Heinrich syncline plunge moderately to the northeast where such northeast- (and southwest-)

plunging stretching lineations are assigned by Longridge (2012) to D_2 deformation (Chapter 4.2). Lens-shaped alaskite leucosomes with an associated granulite facies mineral assemblage studied by Ward *et al.* (2008) in the project area, cross cut this lineation, hence an interpretation that peak metamorphism post-dates D_2 deformation is merited, but is at variance with Longridge's (2012) interpretation that peak M_2 metamorphism was contemporaneous with D_2 deformation. Longridge's interpretation is based on U-Pb geochronology of garnet-bearing leucogranites deformed by F_2 folds. The late assemblage described here including sillimanite + almandine supports the conclusions of Ward *et al.* (2008) that lowermost granulite facies metamorphism was reached during M_2 (Figure 5.6). The staurolite identified by Nash (1971) forming the basis for his higher pressure M_1 metamorphism was not noted during this study. Mapping observations from this study support the late timing of alaskite intrusion in the Khan River area studied by Ward *et al.* (2008) where a north-northeast oriented swarm of alaskites in the area of the Z17 anomaly appear to clearly cut across the hinge zone of the F_3 Blauer Heinrich syncline (Figure 7.4). Based on the fact that latest biotite and/or sillimanite in thin section show no preferred orientation, and that there are numerous examples of alaskite intrusions that cross-cut F_3 structures in the project area, it is inferred that M_2 temperatures suitable to sustain sillimanite growth, partial melting and alaskite generation must have outlasted D_3 deformation. This is in agreement with the assertions of both Nash (1971) and Nex *et al.,* (2001b). Partial melting of potassic meta-psammites is considered to be responsible for the generation of the bulk of alaskitic melts generated throughout M_1-M_2. Despite the presence of lower metamorphic grade, retrograde assemblages that include chlorite and epidote, Nash's M_3 retrograde metamorphism is not supported here as a definable metamorphic pulse.

Quartz-tremolite-plagioclase ± diopside calc-silicate rock occurs as both early replacive bodies intruded by alaskite and it is associated with F_4 faults. This unit is therefore unlikely to relate to metasomatic alteration producing oxidation halos in E type alaskites, attributed to mobilisation of fluids during the Cretaceous (e.g. Freemantle, 2012; Corner, 1981, 1983; Chapter 6).

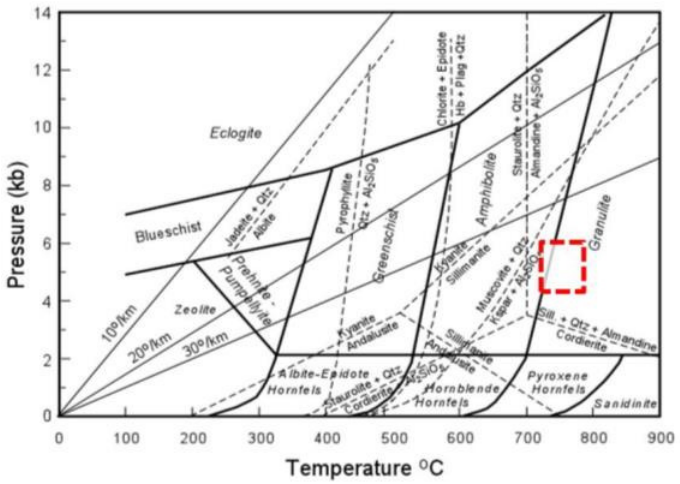


Figure 5.6. Temperature pressure mineral stability plot showing the approximate position of peak metamorphic assemblages in the Rössing area (red box) based on pelitic mineral paragenesis from Nash (1971) and this study, and thermobarometry of cordierite-bearing anatectic assemblages in Kuiseb schists of the project area indicating peak conditions of 750 °C and 5 kbar in the study of Ward et al. (2008).

Chapter 6: Plutonism

6.1 Introduction

Regional plutonism across the Central Zone was reviewed in Chapter 1.2.5. The Damaran Plutonic Suite is dominated by intrusions of granitic composition which formed contemporaneous to upper amphibolite to granulite facies metamorphism in the sCZ, possibly in response to syn- to post-tectonic orogenic decompression (e.g. Nex *et al*., 2001b). Brandt (1985) classified this suite into Salem granites, red inhomogeneous granites, red and grey homogeneous granites, post tectonic granites and alaskite (described as various types of leucogranites by other workers). The Goas Intrusive Suite of Lehtonen *et al.* (1995) forms a less volumetrically significant basic suite of magmatism. Within the Rössing area granitic magmatism is dominated by sheeted alaskite intrusions. Whilst the petrology of the alaskites in the immediate Rössing mine area have been the focus of numerous petrological and metallurgical studies (e.g. Marshall, 1973; Hiemstra, 1967, 1971; Cuney, 1980a, 1980b; Bowden *et al*., 1995; Herd, 1996; Kinnaird, 2005), intrusives in the wider mine lease area have not been well-studied, and there has been no attempt to classify these according to detailed petrological and structural criteria as completed at Goanikontes by Nex (1996) and subsequently extrapolated to other uranium deposits by Freemantle (2012). Whilst it is not the intention of this study to complete such a classification, correlations are made between alaskite subtypes noted through the course of this study and the classification scheme of Nex (1996).

6.2 Previous Work in the Project Area

Intrusives pre-dating Alaskites

Within the Ababbis Metamorphic Complex numerously documented amphibolite dykes have been generally regarded to be of pre-Damaran age (Smith, 1965; Steven, 1994; Barnes, 1981; Marlow, 1981; Brandt, 1987; Chapter 3.2) and hence may represent the oldest intrusions in the study area. In the area of the Ida and Palmenhorst domes, Longridge (2012) describes these as varying in width from decimetres to several metres, of basaltic composition and usually cross-cutting the pre-Damaran fabric present in the basement gneisses. These are commonly deformed into parallelism with the regional fabric during Damaran deformation, or where this is less intense they are folded into open to tight F_2 folds. Longridge (2012) has demonstrated that the amphibolites yield both Abbabis (~2 Ga) and Damaran ages (557 Ma; Chapter 1.2.5) where in the latter case, major element similarities

exist between these amphibolites and mafic rocks of the early Damaran Goas Intrusive Suite of Lehtonen *et al.* (1995; Chapter 1.2.5). In the SJ pit area massive, discontinuous, streaked-out bodies of coarse-grained amphibolite occur within the clinopyroxene-garnet ('mottled') gneiss of the Khan Formation both in the northwest prong area and further east below the pre-mining surface (Berning et al., 1976; Kerr, 1990; Nex *et al.*, 2002); Nash (1971), on the basis of major element geochemistry, interpreted these as orthoamphibolites. Smith (1965) describes regional occurrences of ring dyke-like outcrops of coarse-grained hornblendite that predate alaskite intrusions that may or may not be related. To the north of the SJ Dome an extensive batholith of biotite granite is considered to be of the Damaran-age Salem suite by Smith (1965). Smith describes the Salem granites as being biotite-rich, generally foliated and including both porphyritic and non-porphyritic varieties. Textures may be igneous or gneissose with subhedral to euhedral K-feldspar phenocrysts (or porphryoblasts) which range from being unorientated to strongly orientated. Red biotite granite, noted to intrude Karibib Formation northwest of the tailings dam, is also interpreted by Jacob and Kerber (1997) to be of Damaran age. Outcrops of red and grey biotite granite have been mapped by Oliver and Kinnaird (1996) across the SJ Dome.

Alaskites in the Wider Area

At Goanikontes Nex (1997) and Nex *et al.* (2001a) on the basis of structural and mineralogical characteristics defined six alaskite sub-types designated A-F where uranium mineralisation was interpreted to be associated with post-D_3 types D and E; this scheme was subsequently modified by Freemantle (2012) based on the study of the Valencia, Goanikontes and Ida Dome area deposits (Table 6.1). Nex *et al.* (2001a) note that type A alaskites are low in high field strength elements. Type B are highly peraluminous where fractured garnets reflect both post-emplacement deformation and radioactive inclusions (Nex *et al.*, 2001a; Freemantle, 2012). Type C alaskites are commonly magnetite- ± diopside- ± titanite-bearing where they intrude the Khan Formation or tourmaline-bearing higher in the stratigraphy (Freemantle, 2012). Type D sheets have consistently higher fluid content than other alaskites and also the highest uranium content (Nex *et al.*, 2001a). The biotite-rich grey cores of oxidation halos (originally described by Corner and Henthorn, (1978) in type E alaskites are geochemically indistinct from the rest of the intrusive body and hence do not likely represent xenoliths. The oxidation halos are common to the Rössing, Goanikontes and Ida Dome areas, and occur in both mineralised and barren alaskites (Freemantle, 2012). Freemantle (2012) interprets type E alaskite oxidation

halos to be altered type D or magnetite-bearing type C alaskites where palaeomagnetic studies of Corner (1981, 1983) indicate that such metasomatic alteration relates to Cretaceous fluid mobilisation; Basson and Greenway (2004) interpreted a similar mode of origin for such textures occurring in alaskites of the Rössing SJ open pit. Freemantle (2012) elaborated on the scheme of Nex (1997) to include subdivisions of the sixfold classification scheme based on accessory mineralogy. Freemantle notes that type C 'sheeted leucogranite' is the most frequent alaskite phase across all deposits studied with accessory-free, magnetite- and tourmaline-bearing sub-types distinguished. The magnetite-bearing C-type alaskites are hosted primarily by the Khan Formation whilst tourmaline-bearing C-types occur within the Swakop Group. Freemantle (2012) considers magnetite to be of both primary (magmatic) and assimilated (host metasediment) origin.

In the area of the Palmenhorst and Ida Domes, Longridge (2012) identified pre-D_3 sheeted granite sheets consisting of quartz-feldspar-magnetite pegmatite and anatectic garnet (± cordierite) leucogranite generally intruding the Khan and Rössing Formations respectively, and uraniferous leucogranites which intrude axial planar to F_3 anticlines. Longridge correlates the former two sub-types with C type and B type respectively of Nex (1997) and the latter are interpreted as being syn-tectonic to D_3 and equivalent to the D type leucogranites of Nex (1997). Minor pink pegmatitic leucogranites are comparable to F type leucogranites of Nex (1997). However, structural relationships indicate these are affected by D_2 extension rather than being post-D_3 as interpreted by Nex (1997). The anatectic (garnet- and cordierite-bearing) leucogranites show a close spatial association with partially melted metapelitic rocks of the Rössing or Chuos Formations and are analogous to anatectic leucosomes in Kuiseb Formation schists in the Blauer Heinrich syncline (Figure 4.2) described by Ward *et al.* (2008) and Kisters *et al.* (2009). These contain large poikiloblastic peritectic garnets and are seen occupying extensional fractures subparallel to the regional northeast-southwest D_2 extension direction.

Table 6.1. Sheeted leucogranite (alaskite) classification scheme of Nex (1997) and Nex et al. (2001a), modified after the latter to include the observations of Basson and Greenway (2004) at Rössing, Longridge (2012) at the Ida and Palmenhorst Domes and Freemantle (2012) at the Valencia, Goanikontes and Ida Dome area deposits. Note types 'D' and 'E' are variably uranium mineralised with types D-E-F interpreted to have been emplaced syn- to post-D_3 by all those cited above.

Type	Structural features	Mineralogical features	Comment
A	Irregular form, bedding parallel, weak foliation, boundinaged and folded (often ptygmatically) by D_3 of Nex (1997) and Basson & Greenway (2004)	Pale pink to white, fine to medium grain size, homogeneous saccharoidal texture	Present at Valencia, Goanikontes, Rössing Dome
B	Weakly foliated, frequently boundinaged and occasionally folded by D_3 of Nex (1997)	White or light pink, fine to pegmatitic grain size although commonly medium-grained, typically garnetiferous ± cordierite-bearing, infrequent abundant biotite and tourmaline	Present at Valencia, Ida Dome, Goanikontes, Rössing Dome; anatectic garnet (± cordierite) leucogranite of Longridge (2012)
C	Occasionally boudinaged, occurs in F_3 fold flexures of Nex (1997), bedding parallel	White to pink, medium to pegmatitic grain size, hypersolvus with interstitial clear quartz, magnetite, ilmenite and tourmaline	Present throughout Central Zone, Rössing Dome, magnetite-bearing varieties at Ida Dome, Valancia Goanikontes and Hildenhof, tourmaline-bearing varieties at Valencia & Ida Dome; quartz-feldspar-magnetite pegmatite of Longridge (2012)
D	Irregular and anastomosing; syn- to post-D_3 according to Nex (1997) & Longridge (2012), D_4 according to Basson & Greenway (2004) at Rössing	White, medium to coarse-grained, granular texture, white feldspar with characteristic smoky quartz, uraniferous	Present at Valencia, Ida Dome, Goanikontes, Rössing; uraniferous leucogranite of Longridge (2012)
E	Generally tabular, occasionally bifurcating generally emplaced parallel to the prominent gneissosity	Extremely variable colour and grain size, contain 'oxidation haloes', high biotite content and smoky quartz, uraniferous; Basson & Greenway (2004) and Freemantle (2012) interpret these as metasomatically-altered type D or magnetite-bearing type C alaskites	Present at Rössing SJ, Goanikontes, Hildenhof, Ida Dome
F	Tabular with straight parallel sides, cross-cuts all structural features	Distinctive red colour, coarse to pegmatitic grain size, pink perthitic feldspar and milky coloured quartz	Present at Valencia, Ida Dome, Goanikontes, SE of Rössing mine

Alaskites in the Rössing Mine Area

Pre- to post-tectonic uranium-bearing and barren, variably pegmatitic alaskites form generally sheeted banding-parallel intrusions throughout the area (Smith, 1965; Berning, 1986). Sheets vary in width from several centimetres to >100 m across with larger sheets which may be composite intrusions showing mineralogical, textural and colour banding (Berning, 1986; Nex *et a*l., 2002). Colours range from white through cream to grey or pink and sheets are texturally variable ranging from granophyric, porphyritic, aplitic and fine-grained to pegmatitic (Nex *et al*., 2002). Alaskite composition in the SJ area ranges from granodiorite to alkali-feldspar granite whilst only the latter is present at SH (e.g. Nex *et al*., 2002). The majority of alaskites are weakly metaluminous but may also be peralkaline or peraluminous (Herd, 1996). According to Bowden *et al.* (1995) the majority of alaskites intruding cover rocks in the Rössing Mine area can be regarded as fractionated I/S type granites. Intrusions may be locally plug-like (e.g. SH) or form discordant sub-vertical dykes (SK; Chapter 7.2.1). In the larger area Smith (1965) describes alaskites which are *(a)* folded by $F_{1/2}$

folds, *(b)* intruding F_3 fold axial zones or *(c)* intruding into tension zones and faults cross-cutting all fold structures. In the SJ area, alaskite emplacement is strongly controlled by D_3 structures with bodies commonly intruding the axial zones of F_3 folds or emplaced into northeast- northwest-trending fractures (Berning *et al.*, 1976; Nash, 1971). Alaskite emplacement in the SJ area took place during the closing stages of D_3 (M_2), where massive xenoliths of country rock completely engulfed by alaskite show no dip/strike rotation indicative of passive intrusion (Berning *et al.*, 1976; Nash, 1971). Nex *et al.* (2002) observe that it is difficult to distinguish alaskite subtypes at Rössing SJ due to the predominantly sub-parallel nature of sheets. According to Basson and Greenway (2004) all six alaskite types identified at Goanikontes by Nex *et al*. (2001a; Chapter 1.2.5 and Table 1.4) are present at Rössing with uranium mineralisation hosted by post-D_3 types D and E. Abraham (2009) correlated types B through to E with alaskite samples from the SK area.

Early mineralogical work on alaskites of the SJ area by Marshall (1973) and Hiemstra (1967, 1971) showed these rocks to consist of microcline and microcline-perthite (30-40%), albite-oligoclase (<5-20%), quartz (40-60%), biotite (<5%) and up to 5% montmorillonite. HCl effervescence of nearly all samples investigated indicates widespread but minor calcite. Notable effects of weathering are the development of montmorillonite, iron oxides, alteration of biotite to chlorite, and development of secondary uranium minerals in mineralised alaskite. Accessory minerals are diverse and include allanite, anatase, apatite, bornite, chalcopyrite, chlorite, columbite, covellite, epidote, fluorite, galena, garnet, hematite, hornblende, ilmenite, magnetite, marcasite, microlite, molybdenite, monazite, powellite, pyrite, pyrrhotite, sphalerite, sphene, topaz, rutile, xenotime, zircon as well as the primary and secondary uranium phases detailed in Chapter 7.2.1 (Hiemstra, 1967, 1971; Marshall, 1973; Nex *et al.*, 2002). The presence of hexagonal quartz in pegmatitic alaskites is interpreted by Nex *et al.* (2002) as pseudomorphs of α-quartz after β-quartz, indicating substantial recrystallisation has not taken place. Accessory mineralogy of alaskite intrusions is frequently dependent on country rock lithology, for example where alaskites intrude mafic lithologies ferromagnesian minerals such as biotite-chlorite, ilmenite and hornblende form along contacts implying country rock-magma interaction (Nash, 1971; Nex *et al.*, 2002). Laberge (2008a, 2008b) notes accessory mineralogy of alaskites intruding the Swakop Group in the area south of SK-SJ south may consist of rare garnet in those intruding the Rössing Formation, whilst in the Chuos Formation and overlying stratigraphy alaskites may contain black tourmaline (c.f. observations of Freemantle, 2012, in the wider district). Even though there is at least

some host rock control on alaskite accessory mineralogy, there appears to be no such control on alaskite geochemistry (Nex *et al*., 2002). Skarn minerals have also developed in contact zones and in marginal zones of the intrusions (Nex *et. al*., 2002; Chapter 5.3.2). The available geochronological data suggests alaskite intrusion at Rössing and in the wider district spanned 520-510 Ma with the intrusion of uraniferous alaskites around 510-508 Ma. No reliable U-Pb ages are known to exist for the Rössing deposit (Chapter 1.2.5 and Table 1.3).

Origin of Alaskite

The origin of alaskitic melts has been ascribed to either representing end products of fractional crystallisation of a large magma reservoir, or to partial melting of underlying metamorphic rocks, or a combination of both (Nash, 1971; Jacob, 1974; Berning *et al*., 1976; Cuney, 1980b; Bowden *et al*., 1995). Smith (1965) points out the pegmatitic nature of many bodies and notes that the concentration of pegmatitic granites below marble horizons indicates 'damming up' of volatile constituents promoting the concentration of silica and alkalis. Berning *et al.* (1976) postulate a metasomatic origin of alaskites involving granitising fluid saturating and replacing already migmatised country rock giving rise to the textural banding in alaskites concordant to the host lithologies.

Intrusives post-dating Alaskites

The most recent igneous activity in the area is represented by narrow generally sub-vertical dolerite dykes of Karoo age (Smith, 1965). Regionally the dykes follow one of two trends, the north-northeast D_4 trend of Corner (1981) and Basson and Greenway (2004), and east-northeast. Microscopically these are olivine-bearing dolerites.

6.3 This Work

Due to granitoid plutonic rocks being spectrally indistinct on remote sensing data these have not been separated on the appended map. They consist of early quartz diorite, and (predominantly) alaskite. Separating these lithologies will require ground-truthing all mapped outcrops in the field (this is recommended but has been beyond the scope of this project). Narrow, sub-vertical dolerite dykes of Karoo age (Smith, 1965) form the most recent activity in the area.

6.3.1 Biotite Quartz Diorite

Biotite-bearing quartz diorite bodies only occur northwest of the SJ Dome and tailings area at the stratigraphic level of the Chuos Formation. An identical intrusive, locally

plagioclase-porphyritic, was sampled to the northeast of the mapped area on the Valencia access road (Figure 6.1a) where a thin section review shows this to be a biotite-bearing quartz diorite (RSS070). The quartz diorite shows alignment of constituent grains indicating a pre- to syn-tectonic timing of emplacement and hence could represent some of the earliest intrusions in the area. Salem granites occurring north of the mapped area are described by Smith (1965) as being K-feldspar-porphyritic and are therefore unlikely to relate to these quartz diorites.

6.3.2 Alaskite

Alaskites are by far the most common intrusive throughout the mapped area, intruding the entire stratigraphic sequence but notably absent (or infrequent) within the A.M.C. Their field morphology and mineralogy has been well described through previous work (Chapter 6.2) and features are also summarised in Table 3.1. Through review of the alaskite classification of Nex (1997) and Freemantle (2012) the alaskites observed in the Rössing area and described here can be broadly placed within these classifications. Intrusions are generally sheeted, concordant bodies, but are locally discordant and can form plug-like bodies as at SH or sub-vertical dykes filling tension gashes in shear zones as at SK (Chapter 7). Particularly voluminous intrusions occur at a number of stratigraphic horizons: at the contact between the A.M.C. and Damaran succession in the northwest of the area; at the contact of the meta-arkose and biotite gneiss of the Etusis Formation around the SJ Dome (Figure 6.2a) where the sheeted intrusives are clearly folded by the dome structure and are hence pre-D_3 doming; throughout the Khan Formation and particularly within the clinopyroxene granofels where alaskites may commonly be mineralised well beyond the SH-SJ-SK area; at the contact of the Khan and Rössing Formations where the intrusions are frequently mineralised and ore bodies may occur, with only locally voluminous alaskite 'swarms' occurring above this stratigraphic horizon. Petrography on some 36 sampled alaskite bodies during this study (Figures 6.1, 6.2, 6.3) is broadly in agreement with work conducted previously and this is summarised below. Alaskite types B, C, D and E of Nex (1997) can be confidently identified in this area, and to a lesser extent types A and F. Those sampled include early barren B type, barren C type, and mineralised D and E types, all of which show significant ranges of composition, texture, and in the case of C-E types scale (up to >100m across). They exhibit a temporal range of emplacement with both early deformed phases (A-C) and later intrusions which from map relations can be clearly seen to truncate F_3 (northeast-trending) fold axes and intrude late conjugate northeast- and northwest-trending fractures (D type).

Early Barren Alaskites (Type A of Nex, 1997)

Although not sampled, the earliest alaskite intrusions seen in the area are equated to A type intrusions of Nex (1997). They are typically small-scale intrusions that do not exhibit a macroscopically observable accessory mineralogy and are either intensely folded or boudinaged. Examples of these alaskites are shown in Figures 4.6b, 4.6e, 4.6f and 4.7e.

Early Barren, Biotite-garnet-bearing Alaskites (Type B of Nex, 1997)

Biotite-garnet sheeted alaskites (biotite-garnet granite on the appended map and Table 3.1) occur west of the mine tailings and in the Panner Gorge-SH area (Figure 6.1b). They are generally medium-grained and are predominantly syenogranite in composition (RPS034, RPS035, RPS037, RPS060, RPS065, RSS039) however monzogranite (RPS049, RPS070) and alkali feldspar granite (RPS069) also occur. The medium-grain size seems diagnostic however these are locally pegmatitic and fine- to medium-grained biotite and/or garnet is present; the latter tend to be rounded, red, skeletal and probably almandine porphyroblastic garnets. Sillimanite is locally present. The metamorphic mineral assemblages, commonly foliated textures and presence of cross-cutting pegmatites suggest this suite intruded early in the tectono-thermal history of the area. These B type intrusions are never seen to be enriched in uranium hence it is important to understand their distribution. Outcrops of red and grey biotite granite mapped by Oliver and Kinnaird (1996) across the SJ Dome are likely to be biotite-garnet granites.

Early, Generally Barren, Accessory-bearing Alaskites (Type C of Nex, 1997)

These alaskites are generally deformed by F_3 folds or F_2-F_3 interference folding (Chapter 4) and exhibit a large range of accessory minerals of which the more dominant are clearly controlled by the mineralogy of the host lithology (Figure 6.2). Those intruding the Etusis Formation tend to be ilmenite-bearing and in the Khan Formation ilmenite- or magnetite-bearing, reflecting the accessory opaque mineralogy of the metasediments as described in Chapter 3. Abundant coarse-grained diopside and hornblende, where these alaskites intrude the Khan Formation, is also a common feature and these ubiquitously exhibit pink K-feldspar (Figure 6.2d). Higher up in the stratigraphy, in more mixed carbonate-bearing sequences, tourmaline appears as a common accessory mineral, presumably as a function of more volatile material contributing to the melt. Magnetite is again common to C type alaskites in the Chuos Formation.



Figure 6.1. Features of various types of intrusions (a) Outcrop of plagioclase-porphyritic, foliated quartz diorite on Valencia access road (left), corresponding RSS070 (middle) and thin section (right); (b) medium-grained biotite-bearing alaskite as a foliated example outcropping on the track to Panner Gorge (centre left), RPS065, a biotite syenogranite in hand specimen (centre) and thin section (centre right) all of which are equated to B type alaskites (or 'leucogranites' – strictly these are biotite granites) of Nex (1996); (c) outcropping B-type alaskite on the mine access road, cut by a narrow pegmatite dyke (bottom left – this may be an F type of Nex 1996), a garnet syenogranite RPS035 (bottom centre) and corresponding thin section illustrating typical fractured garnet porphyroblast morphology (bottom right). PPL – plain polarised light, XPL – cross polarised light. For an explanation of mineral abbreviations refer to Appendix I.

C type alaskite compositions estimated from polished slabs and thin sections cover a spectrum from alkali feldspar granite (RSS065, RSS090, RSS092), syenogranite (RSS041) and quartz syenite (RPS075, RSS010, RSS017, RSS019) through to monzogranite (RSS073, RSS094). K-feldspar is generally either as perthite or microcline or a combination of both. Weak clay alteration of feldspars and chlorite alteration of biotite is common.

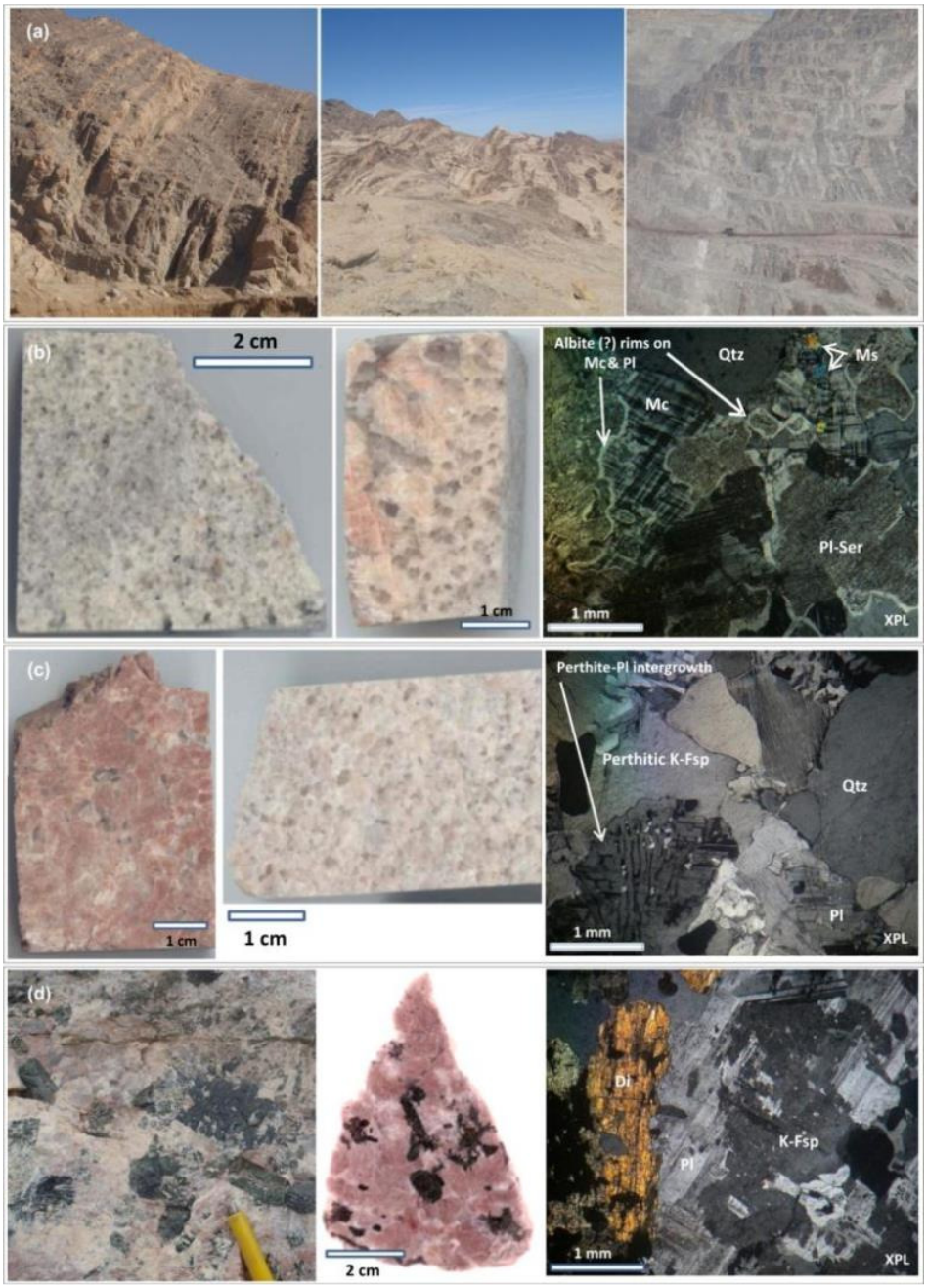


Figure 6.2. Examples of textural and mineralogical variability in barren alaskites equated to the C type of Nex (1997) (a) examples of outcrop style of C type alaskites at the eastern side of the SJ Dome intruding the upper part of the Etusis Formation biotite gneiss (left, note person for scale), looking southwest across the RA anomaly where alaskites can be weakly mineralised (middle), and (right), the north wall of the SJ open pit where alaskites are visibly deformed. (b) hand specimen RSS073 of quartz syenite from Panner Gorge (left), alkali feldspar granite sample RSS090 from SK drill hole SK07D13 (middle) and corresponding thin section (right). (c) quartz syenite RSS017 from the west side of the SJ Dome intruding the Khan Formation (left), quartz syenite RSS019 intruding the Etusis Formation 400 m from RSS017 (middle) and corresponding thin section (right). (d) characteristic pink diopside-hornblende-bearing quartz syenite only noted to occur in the Khan Formation in outcrop west of the SJ Dome (left) and corresponding sample RPS075 (middle) and thin section (right). PPL – plain polarised light, XPL – cross polarised light. For an explanation of mineral abbreviations refer to Appendix I.

C type alaskites may be very locally mineralised, for example in the area of the RA anomaly (for location see Figure 7.1 and appended map), particularly towards contacts with country rock. Examples of major occurrences of C type alaskites include the Rössing SJ Dome and RA anomaly areas where in both cases map relations show these to be deformed by F_3 folds or F_2-F_3 interference folding. West of the RA anomaly, the Khan Copper Mine (Chapter 7.3) is spatially associated with deformed C type alaskites.

Late, Generally Mineralised Alaskites (Type D-E of Nex, 1997)

These alaskites which are correlated with D and E types of Nex (1997) are often (but not always) demonstrably paragenetically late as discernible from map relations. Where mineralised, they ubiquitously exhibit distinct smoky quartz (Figure 6.3). They show the same range of compositions as their non-mineralised counterparts from alkali feldspar granite (RPS005, RPS006, RPS048, RSS089), syenogranite (RPS066, RSS002, RSS005, RSS024, RSS025, RSS093, RSS097) and quartz syenite (RPS047, RSS003) through to monzogranite (RSS099) and additionally granodiorite (RSS022, RSS098). K-feldspar occurs generally as microcline-perthite. Weak clay alteration of feldspars (infrared spectral analyses indicate this is predominantly montmorillonite) is a frequent feature together with chloritisation of accessory biotite which may locally be strong. The alteration present may be hydrothermal in origin but is not macroscopically manifested in hand specimen, and hence is probably unrelated to any significant mineralising process. Locally, these alaskites may be fluorite- and sillimanite-bearing (e.g. RPS047 from the SJ Pit). The SH main plug of alaskite shows a syenogranite composition and locally appears to cross-cut earlier mineralised alaskite bodies such as granodiorite sample RSS022. As per the C type alaskites, a less macroscopically obvious accessory mineralogy is dependent on the host lithology within uraniferous alaskites of the SJ pit. This relationship has direct implications on downstream processing whereby alaskite in the Rössing Formation inherited the acid-producing sulphide phases found therein. Iron oxide staining as ‘oxidation halos’ of the kind described by Corner and Henthorn (1978; see Section 6.2) is, in agreement with Freemantle (2012), is considered to be related to modification of type D alaskites. It is inferred from map relations that late alaskite intrusions that are probably contemporaneous with intrusion of D type mineralised bodies may be barren, as in the case of the Z17 area where map relations suggest these together with mineralised alaskite at Z20-Rössing South appear to be part of a larger north-northeast trending zone of alaskites (see Chapter 7 and Figure 7.3).

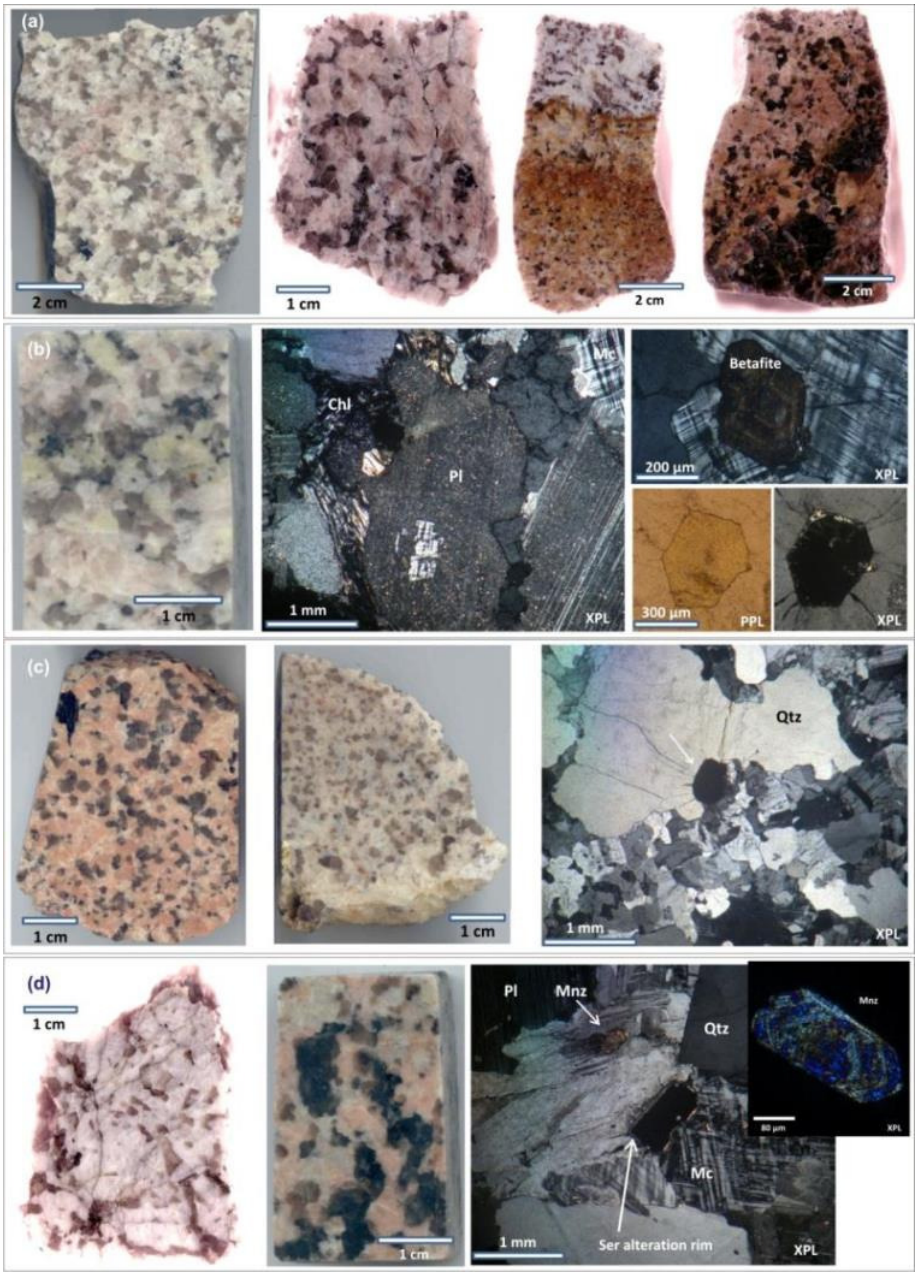


Figure 6.3. Examples of textural and mineralogical variability in uraniferous alaskites equated to the D and E types of Nex (1997). (a) examples of hand specimens from the SJ Pit from left to right: granodiorite D type RSS098, alkali feldspar granite D type RPS048 from the Trolley 10 area, quartz syenite E type RSS003 from Phase 2 exhibiting an iron oxide 'front' where this fills fracture planes, and ilmenite-bearing syenogranite E type RSS005 from Phase 2. (b) SJ Pit syenogranite RSS097 D type in hand specimen (left) and thin section (middle, right) showing typical minor clay alteration of plagioclase and strong chloritisation of biotite, and betafite detail shown on the three right hand images (c) syenogranite RSS025 D type from the SH alaskite plug (left) which appears in the field to cross-cut granodiorite RSS022 D type (middle, right – note betafite indicated by arrow). (d) alkali feldspar granite RPS005 D type from the northeastern extremity of Z19 (left), syenogranite RSS093 D type from SK drill hole SK07D041 in hand specimen (middle) illustrating the smokiness of the quartz and thin section (right) showing an opaque phase with a clay alteration rim and euhedral monazite zonation detail. PPL – plain polarised light, XPL – cross polarised light. For an explanation of mineral abbreviations refer to Appendix I.

Strongly pegmatitic and typically tourmaline- ± garnet-bearing granitic sheets occur frequently from the top of Panner Gorge toward Arandis Airport (i.e. west of the SJ Dome), together with the demonstrably earlier medium-grained biotite-garnet-bearing B type alaskites (Figure 6.1b). These may be tentatively correlated with the F type intrusions of Nex (1997) that exhibit the same grain size variation and characteristic milky-white quartz.

6.3.3 Dolerite

Plutonic bodies of dolerite occurs as narrow, north- to northeast-trending, late sub-vertical dykes throughout the area, cross-cutting all other structural features and north to northeast. Sample RPS056 from the SJ Dome shows notable spherulitic textures (Figure 6.4). Sample RSS048 from the hinge zone of the Blauer Heinrich syncline is plagioclase-phyric and contains appreciable ilmenite.



Figure 6.4. Dolerite samples. (a) RPS056 from the SJ Dome showing spherulitic textures (right). Spherulites are generally microcrystalline to cryptocrystalline intergrowths of quartz, calcite and other phases. (b) RSS048 sampled from a series of dolerite dykes that intrude the hinge zone of the Blauer Heinrich syncline, in this case from the lower section of the Khan Mine Gorge where it can be seen to be a plagioclase-phyric ilmenite-bearing dolerite. PPL – plain polarised light, XPL – cross polarised light. For an explanation of mineral abbreviations refer to Appendix I.

6.4 Summary and Discussion

Plutonic rocks in the project area have been described in the context of previous work in the Rössing and wider area. These lithologies are dominated by a variety of alaskite types with subordinate earlier biotite quartz diorite intrusions and late dolerite dykes. Detailed descriptions of alaskite intrusions have been compiled from numerous mineralogy reports and together with the petrography work conducted here, do not add significantly to the historical work. However previous work has focused on description of uranium-mineralised alaskites whereas this study has described alaskites and other intrusions from across the wider area. This has allowed correlations with varying confidence of alaskite types to be made with classifications of other workers, specifically that of Nex (1997) from the nearby Goanikontes deposit.

Red biotite granite in the tailings dam area, noted by Jacob and Kerber (1997) as intruding the Karibib Formation, may be similar to that in the Abbabis Metamorphic Complex nearby (Chapter 3.2 and Figure 3.2d). More fieldwork would be required to understand whether these could be the same unit. In the same general area, quartz diorite described in Chapter 6.3.1 could equate with the Goas Suite of Lehtonen *et al.* (1995) however these outcrops have received scant attention during this study making this correlation tentative at best. Additional fieldwork, sampling, major element geochemistry and geochronology would be required to correlate these units with confidence.

The alaskite descriptions presented here can broadly be equated with those of Nex (1996), however with varying confidence. Garnet- biotite-bearing sheeted alaskites can be confidently correlated with Nex's (1997) type B leucogranites and are predominantly syenogranite in composition and never mineralised. In terms of petrology these are neither alaskites nor leucogranites but the term alaskite is maintained here for simplicity. The observed distribution of type B alaskites mostly within the Rössing and Chuos Formations in the Panner Gorge area supports the assertion of Longridge (2012) that these represent anatectic products of partially melted metapelitic rocks of these two formations, analogous to the anatectic leucosomes in Kuiseb Formation schists in the Blauer Heinrich syncline (Figure 4.2) described by Ward *et al.* (2008) and Kisters *et al.* (2009).

Within the Rössing area alaskites confidently correlated with type C leucogranites of Nex (1997) form the most common alaskite type. This is consistent with the

observations of Freemantle (2012) across other deposits. However it should be borne in mind that non-mineralised type D alaskites probably exist in sections of stratigraphy that are not conducive to uranium mineralisation such as within the Kuiseb Formation of the Z17 area, where they may be difficult to distinguish from type C alaskites, however the latter are usually magnetite or tourmaline bearing. Map relations in this area suggest these alaskites together with those of the Z20-Rössing South area form a zone of north-northeast trending intrusions that cut across both F_2 and F_3 fold axes (Chapter 7.2.2, Figure 7.4). The stratigraphic control on accessory mineralogy consistently exhibited between alaskite types B and C (garnet and biotite in the former, ilmenite, magnetite, diopside, hornblende and tourmaline in the latter) strongly indicates that these are at least partly derived from partial melting or assimilation of the Damaran metasedimentary succession. The bulk volume of alaskite melt is considered to be derived from partial melting of potassic siliciclastic units from within the A.M.C, Etusis, Khan and Chuos Formation where these show the most pronounced migmatitic textures (Chapters 3 and 5).

Type D alaskites are demonstrably late in the sequence of intrusions as can be surmised from previous descriptions (principally Berning *et al*., 1976; Nash, 1971) and map relations clearly evident in the attached map compilation. These cross-cut the axial zones of F_3 folds and in the SJ area are emplaced as complex undeformed networks into conjugate fractures. As discussed in Chapter 4.4.4, uranium-bearing alaskite intrusions appear to have largely postdated significant D_4 lateral faulting, however some minor D_4 movements have outlasted the intrusions. Type E alaskites of Nex (1997) as a distinct sub-type are not supported here and, as per the interpretation of Freemantle (2012), these probably represent alteration of type D or earlier intrusions.

The observation by Basson and Greenway (2004) that all six alaskite types identified by Nex (1997) at Goanikontes are present in the Rössing area is generally supported however the specific observations leading to this conclusion appear somewhat different. Very few of the features described by these authors were observed.

Alteration in both barren and mineralised alaskites is a weak feature that is not considered to relate to any major (i.e. hydrothermal) mineralising process, as discussed next in Chapter 7. Sub-vertical, narrow olivine-bearing dolerites are a common but minor intrusive constituent throughout the area and are generally seen to intrude F_3 fold axial zones.

Chapter 7: Mineralisation

7.1 Introduction

Mineralisation associated with pegmatites and alaskites occurring within the CZ of the Damara Belt was introduced in Chapter 1.2.6., including a summary of the geology and controls of alaskite-hosted uranium mineralisation of the sCZ as presently understood. Grade-tonnage data of the more important deposits was presented. Uranium mineralisation predominantly as uraninite is considered to be associated with syn- to post D_3 alaskites (type D and E of the scheme of Nex, 1996) that have intruded at the level of the Khan and Rössing Formations where redox contrasts and the presence of carbonate and/or sulphides may have facilitated deposition of uranium. Structural controls cited include D_3-D_4 ductile to brittle transition and development of north-northeast oriented (Welwitschia trend) faults and/or shears. Development of secondary uranium oxides contribute significantly to the overall uranium budget. Despite the low uranium grade, Rössing SJ has been a world-class uranium source due to its size and low cost extraction methodology of uranium oxide. In the southern extremity of the project area the northern extent of the recently discovered Rössing South (more recently renamed to the Husab Project) deposits occurs in the Z20 area. In addition the Khan Copper Mine in the west of the project area has played an important role in historical copper production in Namibia.

7.2 Uranium

7.2.1 Previous Work in the Project Area

Exploration

The location of the various radiometric anomalies associated with uraniferous alaskites identified during early Anglo American and Rio Tinto exploration in the Rössing area are shown in Figure 7.1. These are discussed throughout this chapter. Berning (1986) provides an account of the exploration history of the area which is briefly summarised as follows. Dr E. Reuning in 1910 was the first to note the presence of radioactive minerals in the area in the form of heliodore in a pegmatite near Rössing Mountain. Subsequent discoveries of radioactive minerals including that by Captain Louw in 1928 led to the formation of the Louw Syndicate in 1954 which obtained a prospecting license and entered into an option agreement with the Anglo American Prospecting Company. A number of radiometric anomalies were subsequently defined of which the most promising (due to the recognition of uraninite) was the SJ anomaly. Drill testing and underground development led to a negative assessment of the deposit by Anglo American on the basis of the low grade.

Rio Tinto South Africa Limited subsequently executed an agreement with the Louw Syndicate and between 1966-1973, through further work including airborne and ground radiometric surveys, geological mapping, drilling and bulk sampling, confirmed that the SJ ore body was commercially viable as a large, low grade open pit operation.

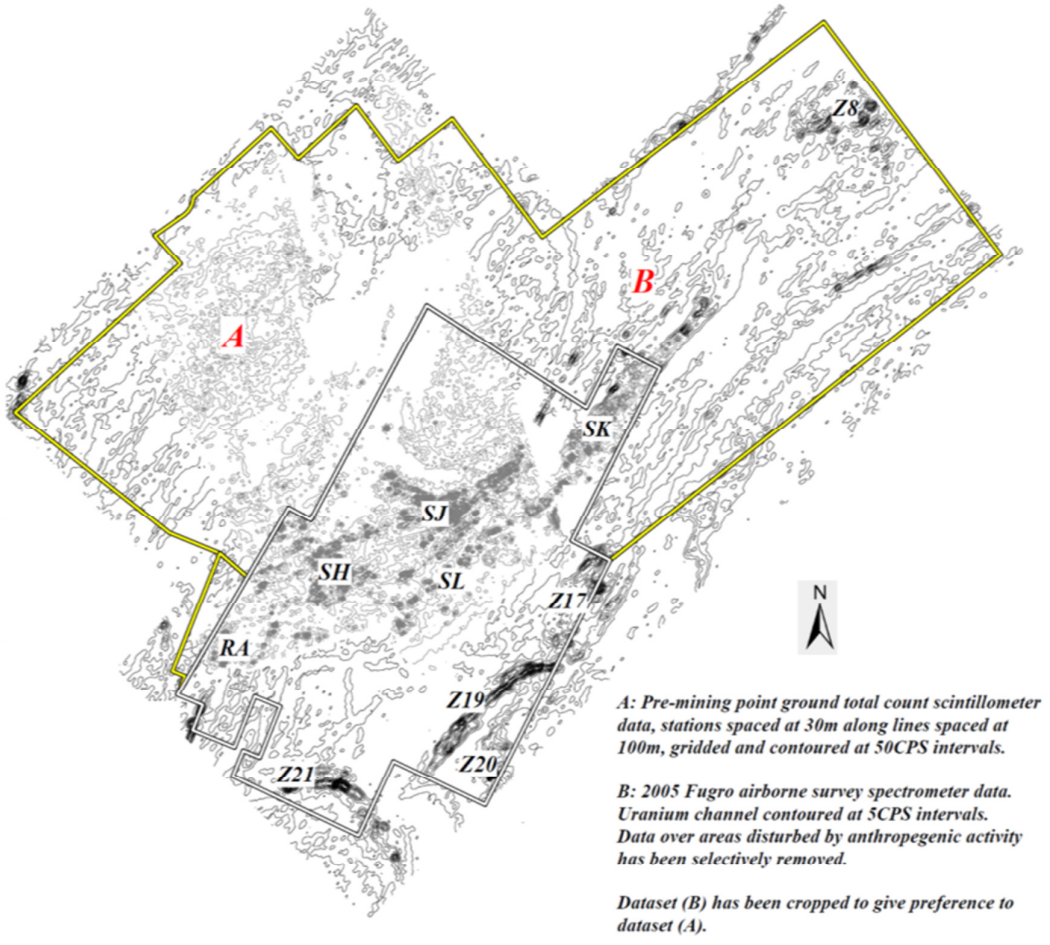


Figure 7.1. Location of radiometric anomalies within the Rössing mine lease ML28 shown on contoured radiometric data compiled as part of this project (see inset and Chapter 2.2 for explanation). Figure is centred on 506000 mE, 7516000 mN.

Further anomalies in the area, particularly SK and SH, but also Z19, Z21 and RA have since been investigated and drill tested during various campaigns over the decades (numerous Rio Tinto and Rössing Uranium Ltd. internal reports). Despite this, the geological setting of all but the SJ, SK and SH areas are poorly documented, and even in these areas some features are not well described. A recent review of historical work and reassessment of these anomalies is given by Scott and Northam (2005). The most recent exploration in the mining lease at the Z20 anomaly was

generated from the results of this project where evaluation drilling at the time of writing has delineated a 54 Kt U_3O_8 indicated and inferred resource (Table 1.6).

Uranium Mineralisation

The Rössing SJ uraniferous alaskites are situated along the northern limb of the SJ Synclinorium developed between the SJ Dome and the Khan River to the south (Berning *et al*, 1976; Berning, 1986). Completely barren or sparsely mineralised alaskites are widespread beyond the limits of the ore body. Alaskite in the lower and upper clinopyroxene-amphibole gneiss of the Khan Formation forms regular dykes parallel to banding, whereas alaskite present in the clinopyroxene-garnet gneiss assumes a more massive habit. In many localities alaskite dykes are described as being emplaced along the axial planes of F_3 folds and within northeast- and northwest-trending conjugate fractures (e.g. Berning *et al*, 1976; Berning, 1986; this is supported by map relations shown in Appendix II). The bulk of economic mineralisation is contained in alaskite preferentially emplaced into the clinopyroxene-garnet gneiss in the northern part of the deposit, and into the amphibole-biotite schist and lower marble and cordierite gneiss units of the Khan and Rössing Formations in the southern part of the deposit (see attached map and total count scintillometer data). These ore zones merge to the east due to steepening dips and thinning of strata, and also plunges to the east resulting in shallow keels of mineralised bodies to the extreme west and blind mineralisation to the extreme east of the ore body. The highest uranium grades are associated with biotite-rich selvages of alaskite, in dykes or veins emanating from larger bodies, in alaskite emplaced along the axial planes of folds, and in areas where alaskite has replaced amphibolite (Berning *et al*, 1976; Berning, 1986). Uranium-bearing phases at the SJ deposit are represented by approximately 55% uraninite, <5% betafite and 40% secondary minerals (Hiemstra and Beukes, 1969; Berning, 1986; Kinnaird, 2005). Uranium grades are highly variable between different alaskite sheets (e.g. Nex *et al.*, 2002). The emplacement of such large volumes of post D_3 alaskite in the region of the Khan-Rössing Formation contact at SJ may have been facilitated by competency contrasts between the Khan and Rössing Formations and/or post-D_3 dome rotation (Nash, 1971; Basson and Greenway, 2004; Chapter 4).

Primary uranium- and/or thorium-bearing phases at SJ include uraninite, betafite, brannerite, and thorite whilst secondary phases include gummite, betauranophane, uranophane, torbernite, metatorbernite, carnotite, metahaiweeite thorogumite and rössingite (Hiemstra, 1967, 1971; Marshall, 1973; Kinnaird, 1995; Nex *et al.*, 2002).

Secondary uranium minerals in alaskite and country rock constitute around 40% of the radioactive minerals present (but only 10% in the case of alaskite only – Kinnaird, 2005) and these are commonly visible as yellow-green coatings in fractures. Uraninite constitutes 55% and is associated with zircon, hematite and pyrite, occurring at grain boundaries and as feldspar inclusions with 70-90% of all grains falling in the size range 70-200 microns. High uranium grades are associated with smoky quartz and milky white feldspar. Low uranium grades are associated with clear quartz, graphic textures and red or pink feldspars. Mineralised alaskites intruding the Khan Formation are characterised by accessory hematite (dominant), magnetite and pyrite, with a low primary to secondary uranium mineral ratio, altered uraninite and deeper extent of secondary mineral development than those intruding the Rössing Formation. Alaskites intruding the Rössing Formation are characterised by accessory pyrite (dominant), pyrrhotite, chalcopyrite and limonite, a high primary to secondary uranium mineral ratio, fresh but fractured uraninite and shallower development of secondary uranium phases (Marshall, 1973; Hiemstra, 1968, 1971). The presence of samarskite at SJ has been noted by Beukes and Hiemstra (1969).

At SK, sub-vertical en-echelon alaskite dykes intrude the hinge zone of a major anticline exposing the Khan Formation (the Camp anticline, Chapter 4, Figure 4.2). The en-echelon arrangement of dykes indicate intrusion into tension gashes formed in a dextral shear zone (Laberge, 2008a), supported by the observation of quartz-filled tension gashes showing the same geometry at outcrop scale (Abraham, 2009). Pope (2008) suggests that the significantly differing basal Rössing Formation stratigraphy either side of the SK anticline may indicate the presence of a syn-sedimentary structure that influenced the evolution of the shear zone.

The SH anomaly consists of a 500 m x 200 m NW-SE oriented alaskite plug of alkali feldspar granite composition that has intruded an antiformal axial zone in the north and a synformal axial zone in the south, with sheeted apophyses extending into the surrounding metasedimentary sequence (Mestres-Ridge, 1992; Nex *et al*., 2002; Figure 2.18). The uranium mineralogy consists almost exclusively of brown and yellow betafite (a refractory pyrochlore group mineral), of which >90% of grains are >0.14mm, but with minor uraninite and secondary metahaiweeite and uranophane largely on joint planes (Hiemstra and van Huyssteen, 1969; Reynolds, 1975; Kinnaird, 2005). Uraninite is present in greater proportions in apophyses that extend into country rocks (Nex *et al*., 2002). The presence of Nb and Ti with U in geochemical assays may be used as an indicator of the presence of betafite,

however care should be taken as other Nb-bearing phases may be present such as ilmenite, rutile and columbite (Herd, 1996; Nex *et al*., 2002). Mestres-Ridge (1994, geological map of Figure 2.18) noted textural trends associated with betafite distribution, with betafite generally not present in early euhedral or late quench (graphic) textures. Similar associations have been noted by Ratcliffe (1992) in the SK area. The presence of chert veins containing betauranophane in the SH area are analogous to veins in the Goanikontes area which occur along faults offsetting Karoo-age dolerite dykes (Nex *et al*., 2002).

Genesis

First order controls on the genesis of alaskite-hosted uranium deposits in the Rössing district were presented in Chapter 1.2.6. The following applies only to the Rössing deposits. Berning *et al.* (1976) proposed that reduction of U^{6+} and precipitation of U^{4+} in uraniferous alaskites could be facilitated by the assimilation of basic country rock by an acid magma, whilst Kerr (1990) suggested that the assimilation of Fe^{2+}, S or C derived from the Rössing Formation lower marble member may have also have facilitated this process. Hydrothermal processes have been variously cited as a mechanism for a component of uranium mineralisation at Rössing and have been documented at other deposits (Freemantle, 2012; Chapter 1.2.6). Kerr (1990) proposed that alaskite-country rock contact zones may have undergone alteration by low temperature potassic (± earlier sodic) fluids with significant CO_2 content. Sub-solidus fluid alteration is indicated by albite rims on quartz, biotite and plagioclase alteration, development of patch-perthite textures and enriched LREE profiles of alaskite samples (Kerr, 1990). Post-magmatic metasomatic albitisation of alaskites is also suggested to have occurred at SH by Mestres-Ridge (1994). According to Bowden *et al.* (1995) a component of hydrothermal uranium mineralisation at Rössing is evidenced by unusually low concentrations of thorium and rare earth elements in uraninite (see Rich *et al*., 1977), disequilibrium mineral assemblages in alaskite sheets, formation of Cu-Fe-Mo-As-S ore minerals associated with the formation of betafite and highly ordered alkali feldspars in alaskite sheets with triclinicities close to 1. Due to the low mobility of thorium in both hydrothermal and supergene environments, low Th/U ratios associated with uraniferous alaskites at Rössing are considered by Bowden *et al*. (1995) to be due to successive concentrations of uranium relative to thorium consisting of 1) primary magmatic mineralisation, 2) hydrothermal redistribution and 3) supergene enrichment producing secondary uranium phases. Recent mineralogical work on Rössing SJ alaskite samples by Ryan (2010) supports the presence of two uraninite phases. Quantitative

geochemical analysis via automated energy dispersive spectrometry shows the later phase to be significantly depleted in Th and Y relative to the first phase, indicative of remobilisation by either hydrothermal or meteoric fluids. A hydrothermal overprint is consistent with high total fluids and H_20 abundances in fluid inclusions observed by Nex *et al.* (2002) at SJ compared with SH (a feature also noted within type D mineralised alaskites at Goanikontes by Nex *et al.*, 2001a). Nex *et al.* (2001a) suggest such hydrothermal modification at Rössing SJ may have contributed significantly to the overall uranium budget. At Rössing South, magnetite and pyrite rims on uraninite are interpreted as hydrothermal in origin by Freemantle (2012), whilst the same author cites quartz, fluorite, K-feldspar, chlorite and secondary uranium phases as being present as alteration products in other deposits in the district (Chapter 1.2.6). Wilson (1975) proposed that uranium enrichment in Rössing alaskites could at least in part due to the presence and assimilation of uraniferous amphibole schist (the protolith of which Wilson interprets to be a pyritic shale) into rising alaskitic magma.

Major and trace element geochemistry have failed to distinguish between the alaskite geochemistry of the SH and SJ areas (e.g. Cuney, 1980a, 1980b; Herd, 1996). SJ alaskites are more metaluminous compared to those at SH, however this may be due to the presence of secondary calcite (Herd, 1996). The controls on the formation of betafite over uraninite are not well constrained. Mestres-Ridge (1994) suggested that the more mafic composition of assimilated country rock at SH may play a role. SJ and SH alaskites exhibit differing fluid inclusion geochemistry with SJ inclusions showing higher H_2O/CO_2 ratios and total fluid content, where relatively elevated CO_2 at SH due to proximity to carbonates coupled with the presence of Nb may have favoured the formation of betafite (Herd, 1996; Nex *et al.*, 2002). Conversely at SJ, the sub-vertical nature of alaskites may have resulted in greater fluid flux (rather than retention) at SJ (Nex *et al.*, 2002). Herd and Kinnaird (pers. comm.) concluded that betafite tends to occur where alaskite has intruded the cores of antiformal structures, amphibolite or areas with thick overlying marbles where in all cases fluid loss is proposed to have been inhibited. One such example is proposed by Abraham (2009) where the relative lack of betafite around the synclinal SK4 anomaly contrasts within the larger anticlinal SK anomaly area where betafite tends to predominate.

7.2.2 This Work

Features of mineralisation described in this study are mostly those identified from map relations. The petrographic features of both barren and uraniferous alaskites reviewed during this study were presented in Chapter 6 and a summary of the extensive metallurgical and other studies pertinent to uraniferous alaskite petrology was presented in Chapter 7.2. Observations and petrographic review of alaskite throughout the area has allowed intrusion types to be equated with the classification scheme of Nex (1996), where post-D_3 type D-E alaskite hosts uranium mineralisation in the area (Chapter 6). Type C alaskites may be weakly mineralised whilst type E are considered to be iron oxide-altered variants of type D. Type D and E alaskites show clay (predominantly montmorillonite) alteration of feldspars and chlorite alteration of biotite. Compositions sampled range from alkali feldspar granite, syenogranite, quartz syenite through to monzogranite and granodiorite.

Geological map compilation and interpretation combined with digitisation of pre-mining ground scintillometer survey data and integration with airborne radiometric data (Chapter 2.2) allows uranium mineralisation at all scales across the mining lease to be placed into detailed geological context. Figures 7.2 and 7.3 respectively show summary geological features of the SH-SJ-SK and Z20-Z19-Z17 areas as determined primarily from relationships evident on the appended map.

SH-SJ-SK

These deposits can conveniently be described together as all uranium mineralisation essentially occurs within the same large-scale fold interference structure and the deposits may have shared genetic features. Note that early barren (C type of Nex, 1997) and late uraniferous (D-E type) alaskites are broadly differentiated on Figure 7.2. The outcrop pattern around the entire dome delineates a series of meso-scale gently to moderately doubly-plunging F_2-F_3 type 1 (of Ramsay, 1967) fold interference structures across which smaller scale type 1 dome (e.g. northwest of SH), type 2 mushroom (e.g. southwest of SK) and type 3 hook (e.g. east of SK) satellite fold interference patterns occur (Chapter 4; Figure 4.5). Early C type alaskite intrusions, which may be weakly uranium-enriched around the Rössing SJ Dome (see total count scintillometer image of Figure 2.3), are folded by the interference structures, whilst late D-E type variably uranium-mineralised alaskites cut across the interference structures. The SH plug-like intrusion is a syenogranite D type alaskite that intrudes into a satellite F_2-F_3 fold interference 'buckle' that occurs on the southern limb of the SJ synclinorium at the contact of the Khan and Rössing

Formations (Figure 4.5). The syenogranite plug clearly truncates F_3 fold axes (Figure 3.4, Figure 7.2). The SK alaskites are emplaced into the axial zone of the F_2 Camp anticline and show dextral transtensional, en echelon geometries. It is important to note that in the SK area the north-northeast trending shear geometry cuts across F_2-F_3 interference folding and that the northeast trend of F_3 folds that are clearly oblique to the trend of the alaskites. The SK alaskites have therefore been emplaced into north-northeast trending tension gashes that are offset to and post-date F_3 folds. The north-northeast shear trend is oriented between the northeast D_3 trend and the strongly north-northeast trend of the SJ dome and adjacent F_4 folds, suggesting a post-D_3 to early D_4 relative timing of development. It can be postulated from map relations that the dextral tension gash morphology of the SK alaskites is not limited to this immediate area, but based on the outcrop pattern of late D-E type alaskites of Figure 7.2, may extend to include the SJ and SH alaskites forming a large-scale dilational zone as part of a major throughgoing north-northeast oriented shear zone (Figure 7.2d).

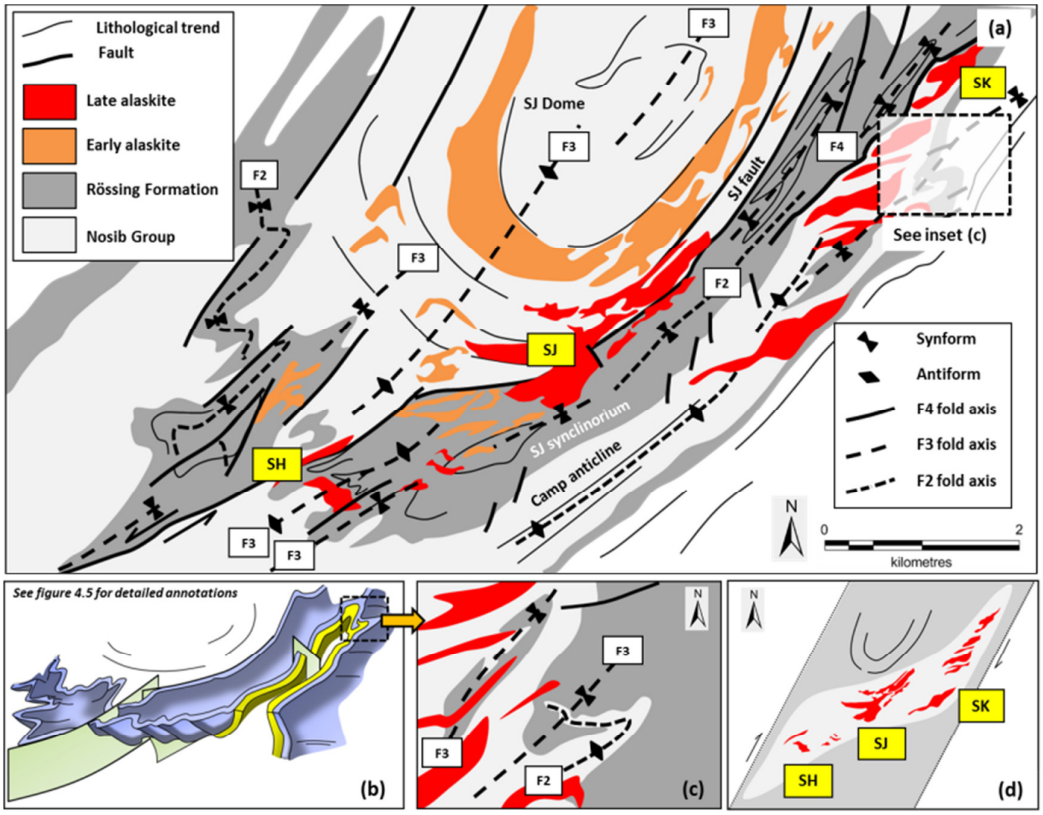


Figure 7.2. ***(a)*** *Summary geological map after the appended detailed map showing the geological setting of the SJ, SH and SK uraniferous alaskite bodies. Note that early barren (C type of Nex, 1997) and late uraniferous (D-E type) alaskites are broadly differentiated, where these are either folded by, or cross-cut F_3 folds, respectively.* ***(b)*** *3D sketch depicting fold interference structures in the area (see Figure 4.5 for detailed explanation).* ***(c)*** *Detail of an*

F_2-F_3 fold interference ('hook type') structure in the area highlighted in figures (a) and (b) – note the relationship of post-D_3 alaskites cutting across the interference structures. ***(d)*** *Possible structural model for the emplacement of uraniferous alaskites across SH-SJ-SK as part of a large dilational zone occupying a throughgoing post-D_3 to D_4 dextral shear zone. Figure is centred on 506000 mE, 7514000 mN.*

The latest deformation in this area consists of brittle dominantly sinistral faults where the largest lateral displacements are in the area immediately northwest of SH, offsetting the Rössing synclinorium as shown in Figure 7.2b. The highest uranium grades at SJ, evident from total count contour data of the pre-mining surface, occur around the amphibolite emplaced within the clinopyroxene granofels of the Khan Formation, and at the contacts of biotite-cordierite gneiss of the Rössing Formation.

Z20-Z19-Z17 (and Rössing South Zone 1)

Previously the Z20 radiometric anomaly has received little attention given its limited surface extent in an area where no geological mapping existed. Evaluation of the area in the context of the emerging Rössing South discovery during this study placed Z20 into geological context as the northern extension of Rössing South Zone 1. Subsequent drilling has delineated a 54 Kt U_3O_8 indicated and inferred resource (Table 1.6).

The stratigraphic and structural setting of the Z20 area can be largely unravelled by reference to adjacent map units and fold structures. Fold interference northeast of Z20, as well as that affecting the Welwitschia syncline in the area of the Khan River to the west, consists of moderately to steeply east-dipping isoclinal F_2 folds, refolded into open to closed northeast trending F_3 folds, the axial planes of which plunge according to the original dip of the F_2 fold limbs (Chapter 4.3.2, Figures 4.2 and 4.5, Figure 7.3 below). The eponymous Rössing South anticline (Spivey *et al*. 2010) is one such F_2 fold that exposes units of the Rössing Formation flanked by Chuos Formation diamictites at its northern extremity in the Z20 area. The southern continuation of the Rössing South anticline under Namib Desert cover is taken from Spivey *et al*. (2010) where the kinks in the subcrop of the Zone 1 ore body delineate east-northeast trending F_3 folding superimposed on the F_2 fold axis. This interpretation contrasts with the comments of Spivey *et al.* (2010) that the Rössing South anticline results from F_4-F_3 fold interference (Chapter 1.2.6). Although contacts are poorly exposed (or unexposed) it is inferred that uraniferous alaskite forms late post-D_3 intrusions due to the apparent continuation of north-northeast oriented outcrops of late and largely barren alaskite intrusions cutting the Blauer Heinrich syncline fold axis of the Z17 area (Figure 7.3). The orientation of the trend of alaskite

intrusion (and the Rössing South Zone 1 ore body subcrop) is consistent with that seen in the Rössing SK area where intrusions demonstrably cut F_2-F_3 fold interference structures (see above). Therefore, as in the Rössing SH-SJ-SK area, uraniferous alaskites may be interpreted to intrude a transtensional throughgoing post-D_3 to D_4 shear zone where the outcrop of alaskites in the Z20 area is suggestive of a sinistral sense of shear. Juxtaposed against this in the Z19 area, uraniferous alaskites intrude the Arandis Formation and upwards into the Karibib Formation in the northeast where they have breached the intensely boudinaged marble members (Figure 7.3).

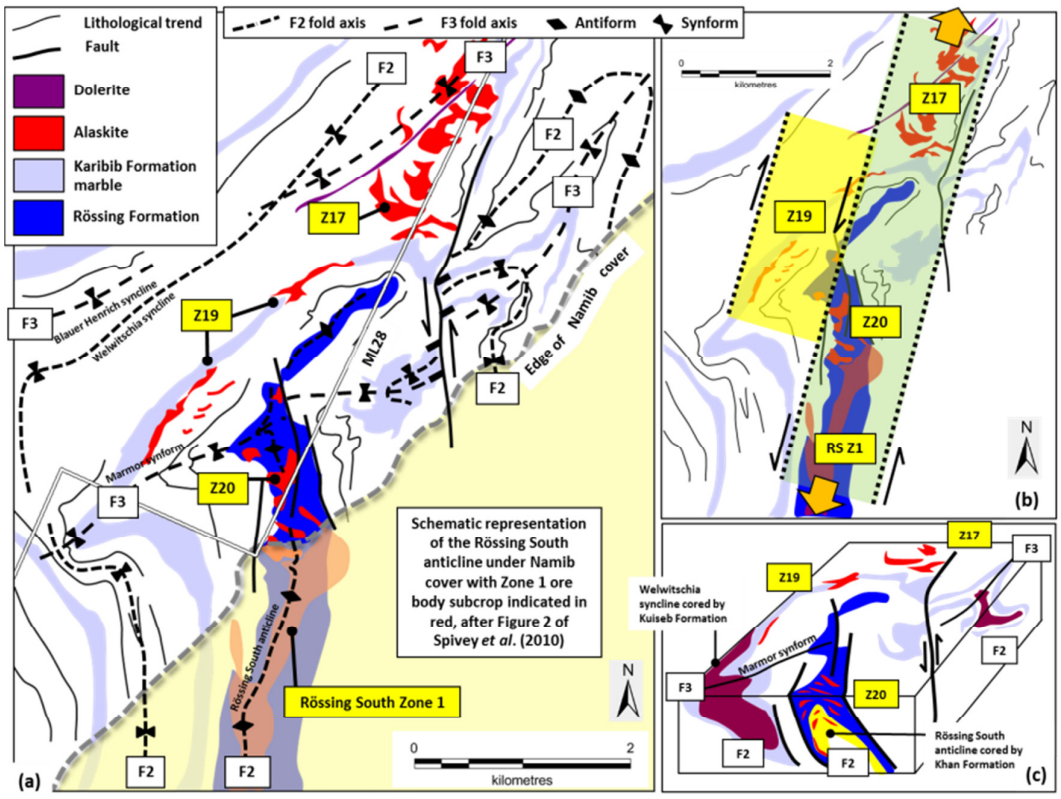


Figure 7.3. ***(a)*** *Simplified geological setting and major structures in the Z20-Z19-Z17 (and Rössing South Zone 1) area. Major early isoclinal F_2 folds comprising the Rössing South anticline and Welwitschia anticline are refolded into upright northeast-plunging F_3 folds that include the Marmor synform, Blauer Heinrich syncline (see Figure 4.2) and the complex interference structure northeast of Z20 (see Figure 4.4 for detail); the fold interference structure has subsequently been disrupted by left-lateral north-northeast oriented strike slip movements (D_4 sinistral faults). The locations of uraniferous alaskites are shown, including the subcrop of Rössing South Zone 1 under Namib cover taken from Figure 2 of Spivey et al. (2010).* ***(b)*** *Interpretation of district-scale mode of emplacement of uraniferous alaskites into syn- to post through-going north-northeast oriented transtensional zones that probably predate D_4 sinistral faulting, controlling emplacement of alaskites at Rössing South, Z20, Z17 and Z19.* ***(c)*** *Simple 3D block diagram of the area shown in Figure 7.3a illustrating the relationship between major folds and faults. Bedding parallel faults at the Rössing and Karibib Formation contacts are likely to have been early structures that formed during $D_{1\text{-}2}$ and were subsequently reactivated. Figure is centred on 507000 mE, 7508000 mN.*

Lithological trends in the Z19 area appear to indicate a dextral shear sense, which suggests the presence of multiple shear blocks with opposing senses of shear between individual blocks (Figure 7.3b). From map relations it is apparent that the most anomalous areas of uranium mineralisation in the southwest part of Z19 appear to be associated with pyrrhotite-bearing calc-silicate gneiss. The latest deformation in the area is characterised by D_4 north-northeast-south-southwest through north-south to north-northwest-south-southeast left lateral faulting.

7.3 Copper

Smith (1965) and Schneider and Seeger (1992) provide a synthesis of documentation of the Khan Copper Mine, situated at the western extremity of the mapped area in the eponymous Khan Mine Gorge (Figure 1.2). This is paraphrased in the next paragraph.

Discovered in 1905, the mine was operated from 1914-18 by Kupfergrube-Gesellschaft with 32,454 tons of ore milled from 1915-1918, with a second period of production from 1964-75 producing a total of 4,962 tons of recovered copper. Production grade ore during the first period was 3.87% Cu and concentrates also contained 159.3 g/t Ag and 0.99 g/t Au, plus 0.146% selenium and tellurium. The copper occurs in association with a 'pegmatite' (alaskite) concordantly emplaced into thick-bedded Khan Formation gneisses and has an average width of 1 m, strike length of 300 m, and down-dip extension >200 m, dipping 45-70º to the northwest. Sulphides (predominantly bornite) are concentrated in the northern and southern parts of the alaskite. The paragenetic sequence of the primary ore minerals is sphalerite, chalcopyrite, bornite, chalcocite and malachite. Ore minerals fill interstices and replace locally brecciated skarn. The skarn-pegmatite transition zone was exceptionally high grade. The folded nature of the mineralised alaskite and its position in necks between boudinaged amphibolite bands indicates a syn-tectonic timing of emplacement. The calc-silicate gangue mineralogy is suggestive of a partially metasomatic origin. Copper mineralisation is present at a number of localities at this stratigraphic horizon, for example at Valencia and Ida Dome indicating an original sedimentary control on copper deposition.

The pegmatitic alaskite contains large crystal of green diopside and hornblende up to 1 m in length (Ramdohr, 1938; Söhnge, 1939) which Miller (2008) attributes to a metasomatic origin. Kinny *et al.* (1994) dated sphene from a Khan Mine pegmatite at 518 ± 2 Ma. Copper showings occur elsewhere in the Khan Formation of the district

including at the Ida Mine (Chapter 1.2.6). Freemantle (2012) noted that alaskites of the Ida Dome and Valencia can contain significant amounts of iron, copper (up to 2100 ppm Cu), nickel (up to 250 ppm Ni), lead and zinc (up to 170 ppm Pb, Zn) and molybdenum (up to 170 ppm Mo) sulphides. A pyrite-, pyrrhotite-, chalcopyrite-, bornite- and molybdenite-bearing schist described by Corvino and Pretorius (2013) between the Khan and Rössing or Karibib Formations at the Ida Dome is also likely to be the same horizon in the Khan Formation. This formation therefore appears enriched in polymetallic elements and copper showings at this horizon have been tentatively correlated with those of the Lower Roan Group of the copperbelt in Zamiba-DRC (e.g. Clifford, 1967; Nash, 1971).

Copper also occurs within sulphides in Rössing Formation pyritic quartzite where it has been targeted by exploration over the Arandis Grant during the late 1970s and early 1980s (Schneider and Seeger, 1992). From the attached map it can be observed that the larger (C type of Nex, 1997) intrusions of the Khan Copper Mine area are folded by F_3 folds and that the area is truncated by the same D_4 sinistral fault that displaces the Nose Structure anticline. No detailed work was undertaken in this area during the course of this project.

7.4 Summary and Discussion

This chapter has briefly presented the exploration history of the Rössing area and synthesised generations of mineralogy, academic and mapping reports to produce an updated description of uranium mineralisation in the area. Based on this literature compilation the mineralogy of host alaskites and ore has been described in some detail. Salient features have also been presented for the SJ, SK and SH ore bodies as determined from previous studies.

Mapping and geophysical data compilation, new geological map interpretations and review of map relations from this study has placed major occurrences of variably uranium mineralised alaskite intrusions into the late-tectonic evolution of the area. D_4 deformation is considered to have been progressive from D_3 involving gradual rotation of the principal stress axis from northwest-southeast to west-northwest-east-southeast where F_3 and F_4 fold axial planes respectively formed perpendicular to these orientations (Chapter 4). During the post-D_3 to early D_4 deformation stages north-northeast trending through-going shear zones are interpreted from mapped intrusive relationships to have developed in both the SH-SJ-SK and Z20-Z19-Z17 (and Rössing South Zone 1) areas. Alaskite swarms intruded these shear zones

where they cut dilational zones of doubly-plunging F_2-F_3 fold interference structures where uranium mineralisation is variably developed depending on the nature of the host stratigraphy. This was partly postdated by F_4 faulting that resulted in minor displacements of alaskite intrusions. Such shear zones at map scale appear to show both dextral (e.g. SK and wider area) and sinistral (more tentative, Z20 and wider area) senses of transtension and hence shear blocks may have existed with changes in sense of lateral displacement from one block to the next.

These conclusions are consistent with the observation by Corner (1981, 1983) that most uraniferous alaskites deposits are spatially associated with the latest D_4 north-northeast structural trend in the district. This was developed by the remote sensing interpretations of Anderson and Nash (1997) and further by detailed field observations of Basson and Greenway (2004) into a model whereby uraniferous alaskites were emplaced into dilational jogs within a zone north-northeast trending (Welwitschia trend) sinistral F_4 faults/shears that formed in response to north-south transpression. The features in the Rössing area are also consistent with observations of Nex (1997) and Longridge (2012) where uraniferous alaskites post-date D_3 structures in the southern Palmenhorst and Ida Domes.

Uraniferous alaskites (D-E type of Nex 1997) and to a lesser degree earlier (C type) barren alaskites show weak alteration features. Previous work at Rössing and other deposits in the district has highlighted the presence of hydrothermal alteration which has been cited by various workers as being a possible significant contributor to overall uranium grade. Despite recent studies at Rössing that support the presence of 'secondary' hydrothermal uraninite showing depleted Th relative to Y (Ryan, 2010), there is no textural or mineralogical evidence that supports the notion that hydrothermal processes have significantly enhanced the uranium grade at Rössing. Perthitic and albite rimming textures also noted during this study can be regarded as primary magmatic features. Minor clay alteration of feldspars and chlorite alteration of biotite is a common feature that may relate to low temperature hydrothermal modification (these could also be weathering and/or retrograde metamorphic features), however primary mineralogy and textures are preserved throughout both alaskite and country rock and such features would be inconsistent with any ore deposit owing a significant hydrothermal component to its genesis. The assertion of Bowden *et al*. (1995) is therefore considered reasonable that minor low temperature hydrothermal redistribution may have taken place. Such modification may also be responsible for the development of 'oxidation halos' or iron oxide staining seen in E

type alaskites which are considered to represent altered D types (Chapter 6). Subsequent enrichment by secondary uranium oxides is considered to relate to surficial processes where leached profiles have been described at Rössing South (Spivey *et al*., 2010) relating to downward leaching of uraninite which is presumably redeposited as oxide phases at depth. The most anomalous areas of uranium mineralisation throughout the area documented from previous work, and as can be determined from map relations, are associated with (i) biotite-rich selvages of alaskite, (ii) in alaskites emplaced along fold axial planes, (iii) in areas where alaskite has intruded amphibolite (iv) at contacts of biotite-cordierite gneiss of the Rössing Formation and (v) around pyrrhotite-bearing calc-silicate gneiss of the Arandis Formation.

The role of stratigraphy in controlling the presence and mineralogy of uranium mineralisation is considered to be important. Areas of basement rocks hosting highly anomalous uranium concentrations of up to 15 ppm have been noted in this study and also in the wider area by Spivey *et al.* (2010; Chapter 3.2). At a macroscopic and microscopic scale the accessory mineralogy of the vast majority of alaskites sampled can be related directly to the mineralogy of the host lithology, a feature that has been documented throughout Rössing mineralogy and mapping reports and noted by other workers in the district (e.g. Freemantle, 2012). Hence it is reasonable to infer that the uranium concentration and mineral speciation is also likely to be largely controlled by the nature of the original partial melt and any subsequent material that was entrained into this.

No conclusions can be drawn from this study as to why uranium has been focussed into only the latest alaskite intrusions as opposed to earlier ones – other workers have proposed mechanisms as summarised in Chapter 1.2.6. However, the latest timing of uraniferous alaskite emplacement is clear from the summary of deposit features set out in this chapter. In the district summary of Chapter 1.2.6 it was introduced that uplift associated with D_3 deformation may have brought into play a uranium-enriched source lithology that had not previously experienced melt extraction (see references therein). This scenario could be all the more plausible given the demonstrable origin of fold interference between F_2 and F_3 in the Rössing area where, coupled with the interaction of throughgoing shear zones, uranium-enriched portions of basement and/or cover in dilational zones may have been exposed to higher heat flow and partial melting processes during lowermost granulite facies metamorphism. Such process may have been further facilitated in the Rössing

area by the presence of a thick and highly variable stratigraphic sequence with carbonate and sulphide-bearing horizons which also appear to have played an important role on uranium deposition. The development of fractures predominantly normal to the F_3 fold trend must have been pivotal in secondary upgrading processes at the SJ deposit which were likely to be supergene related.

Based on the available historical information and on map relations the development of copper ore in a skarn zone associated with a pegmatite at the Khan Copper Mine is considered to relate to remobilisation of copper from a cupriferous horizon in the Khan Formation possibly associated with C type alaskite.

Chapter 8: Summary and Concluding Remarks

8.1 Project Summary

This project has seen the compilation of numerous geoscientific data layers: lithological and structural mapping, remote sensing, ground and airborne geophysical data and historical company reports. This has been complemented by the processing and interpretation of this plus additional data, most notably a suite of HyMap hyperspectral data products, underpinned by detailed field traverses and associated sampling, petrography and infrared spectroscopy. The resulting map and descriptions presented through the preceding chapters provide a geological synthesis of the Rössing area, and in particular elements of the stratigraphic and structural setting of alaskite-hosted uranium mineralisation in the Rössing area have been refined.

Detailed stratigraphic mapping of the mine lease area has been achieved by merging pre-existing maps and interpreting the above data. Minimum noise fraction, principal components and mineral end member processing products of HyMap hyperspectral data and aerial photography have been particularly useful interpretation aids. The review of historical mapping and reports, petrography and infrared spectroscopy have allowed these units to be described in some detail. The Proterozoic Abbabis Metamorphic Complex (A.M.C.) of the Rössing area has not been studied in detail. However, the metasedimentary (± metavolcanic) and orthogneiss units observed probably equate to Brandt's (1987) Tsawisis Formation and Narubis Granitoid Complex respectively of the Abbabis Inlier. The A.M.C. is characterised by anomalous (locally highly anomalous) uranium and thorium concentrations. Map relations demonstrate that the overlying Damaran sequence has a sheared contact with the basement that is itself folded. The Etusis Formation exhibits a two-fold stratigraphy consistent with the description of Berning *et al.* (1976) where the lower meta-arkose member shows an anomalous U-Th signature consistent with derivation from an A.M.C. hinterland. Within the area mapped Nash's (1971) Rössing mine stratigraphy of the Khan and Rössing Formations is only applicable to the immediate Rössing SH-SJ-SK area where these formations notably exhibit more lithological heterogeneity than seen elsewhere. Where they are present, lower marbles of the Rössing Formation have been demonstrated to be variably dolomitised. The Swakop Group conformably overlies the Nosib Group in the project area. This project (including compilation of previous mapping, e.g. Laberge 2008a, 2008b) has significantly refined the stratigraphy and mapped distribution of the Chuos, Arandis

and Karibib Formations. The Chuos Formation has been divided into three distinct diamictite-dominant facies showing a variety of clast size and frequency distributions. Iron formation as itabirite ± ferruginous quartzite at the top of the formation is mapped in the Arandis Airport area. The Arandis and Karibib Formations have been divided into a three and five member stratigraphy respectively and these units have been correlated with those of Lehtonen *et al*. (1993, 1996). No angular unconformity is present at the base of the Karibib Formation as described by Sawyer (1981) and de Kock (1989, 2001). However, the uppermost Oberwasser Member of the Arandis Formation (Lehtonen *et al*., 1993, 1996) and the overlying Ghaub Formation (see Chapter 1.2.2) are missing probably indicating a period of non-deposition. Dolomite is a primary sedimentary feature in the Karibib Formation as opposed to it being of replacement origin in the Rössing Formation. The presence of abundant iron oxides in the Khan and upper Chuos-Arandis Formations appears semi-cyclic and could plausibly relate to distal volcanic activity elsewhere in the basin.

Geological mapping and structural data compilation has allowed aspects of the structural geology of the area to be refined beyond that previously described. Three fold phases F_2-F_4 have been distinguished and correlated with the mapping of Longridge (2012) in the Palmenhorst Dome area immediately to the southwest. Superimposition of a northeast trending F_3 fold trend upon originally east-west to west-northwest-east-southeast trending F_2 folds has produced both type 1 dome and basin (e.g. Rössing SJ Dome) and type 3 hook (e.g. east of Z20) fold interference structures according to the classification of Ramsay (1967). The variation of fold interference structures produced may be due to an unresolved F_1 influence on F_2 axial plane orientation or to progressive deformation during D_3. Progressive deformation is attributed to the spectrum of fold orientations from D_3 (east-northeast to northeast) to D_4 (north-northeast). Significant pre- to syn-D_2 attenuation of stratigraphy is evidenced by boudinage and shear structures that are deformed by F_3 folds, including the basement-Damaran cover contact as noted above. Early barren alaskite (predominantly type C of Nex, 1997) intrusions exploit such extensional structures and these are also deformed by F_3 folds. Map relations support D_4 deformation spanning the timing of emplacement of uraniferous (and barren) alaskites, which may form north-northeast trending en echelon intrusions or swarms, cutting F_3 and earlier fold axes. Based on map relations these late intrusions are interpreted to have been emplaced into through going ductile shear zones particularly where these coincide with F_2-F_3 dilational interference structures. Map relations suggest post-C type alaskite intrusions were emplaced subsequent to major D_4 strike

slip movements as there are no significant displacements of these alaskite swarms. In contrast to early F_4 ductile rotation, minor folding, shear development and strike slip movements (maximum sinistral displacement of 1200 m), latest D_4 deformation was characterised by brittle faulting recording movements on the scale of meters.

The metamorphic petrology of the area remains largely unrefined beyond the original study of Nash (1971) as this has been somewhat beyond the scope of this project. However, an updated metamorphic paragenesis has been presented with a fifth calc-silicate association added to Nash's original compositional mineral groups. In contrast to the paragenesis of Nash (1971), cordierite appears early in the mineral paragenesis and cordierite stretching lineations deformed by F_3 folding are consistent with mineral lineations described by Longridge (2012) in the adjacent Palmenhorst Dome area which have been assigned to D_2 deformation. The presence of sillimanite + almandine late in the mineral paragenesis indicates that lowermost granulite facies metamorphism was reached during M_2 metamorphism. M_2 metamorphism continuing beyond D_3 deformation is supported by S_3-destructive biotite and sillimanite growth textures and the presence of post-D_3 alaskite swarms cutting F_3 structures. A partial melting origin for alaskite generation through melting of potassic meta-psammites as suggested by Nash (1971) and others is strongly evidenced by variably developed migmatitic textures both in outcrop and thin section throughout the stratigraphy, particularly visible within K-feldspar-rich psammitic units of the Etusis and Chuos Formations. Fault-related replacive calc-silicate rock occurs both early and late in the sequence of metamorphic events.

Intrusive igneous bodies consist of voluminous alaskite intrusions focused into dilational stratigraphic and structural zones with subordinate early biotite quartz diorite intrusions and volumetrically minor late dolerite dykes generally emplaced into F_3 fold axial planes. Alaskite subtypes have been equated to the scheme of Nex (1997) for the nearby Goanikontes deposit with the highest confidence for types B, C, D and E. However these, nor the subordinate quartz diorite bodies are distinguished from other intrusions on the appended map as they are not spectrally distinct in remote sensing data. Early and later alaskite intrusions can, however, be distinguished both by field and mapped structural relationships (see structural summary above). The clear stratigraphic control on alaskite accessory mineralogy described in this study and by other workers (e.g. Laberge, 2008a, 2008b; Freemantle, 2015) further supports a partial melting origin for alaskite generation beyond the evidence mentioned above. All alaskite subtypes are macroscopically

fresh and lack any visible hydrothermal alteration. Low to moderate temperature alteration assemblages evident in thin section and from infrared spectroscopy, including clay minerals, chlorite, epidote, and sericite, may be attributed to a combination of weak hydrothermal alteration, retrograde metamorphism and weathering.

Digitisation of pre-mining ground scintillometer and combination with airborne radiometric data as a contoured overlay to the detailed geological compilation and mapping means that for the first time all deposits and radiometric anomalies across the Rössing mining lease have been placed into geological context on one map. Summary descriptions have been made of the geological setting of mineralisation in the SH-SJ-SK and Z20-Z19-Z17 to Rössing South Zone 1 areas using all of the available information compiled in this project. In both areas mineralised alaskite intrusions are interpreted to relate to north-northeast directed through- going transtensional shear zones that developed during D_4 deformation, determined from the alignment of en echelon arrays and swarms of type D-E (of Nex, 1997) alaskites that cut F_3 folds (see structural geology summary above). In the Rössing SH-SJ-SK area uraniferous alaskites are emplaced across the southeastern limb of an elongate F_2-F_3 type 1 interference fold structure (the Rössing SJ Dome). Alaskite intrusion at SJ appears to have been particularly facilitated by a mapped northeast-southwest oriented F_4 strike slip fault zone that can be traced southwest through the Khan copper mine area and beyond into the Nose Structure (location shown on Figure 1.2). Sinistral displacements along this fault zone occurred immediately prior to uraniferous alaskite intrusion. The alaskites in this area cut F_2 folds, of which the Rössing synclinorium is an example, and F_3 folds that rework these. An example of the latter, is in the area of the SH syenogranite plug which intrudes an F_3 antiform superimposed on the Rössing synclinorium. In the SK area an en echelon array of uraniferous alaskites cut across both an F_2 anticline and a satellite F_2-F_3 type 3 hook fold interference structure. In the Z20-Z19-Z17 to Rössing South Zone 1 area alaskite swarms aligned to the north-northeast truncate F_2-F_3 fold interference and intrude throughout a large section of the Damaran-age stratigraphy. Alaskites through this zone are only strongly mineralised at certain stratigraphic horizons: within the Rössing Formation at Z20-Rössing South Zone 1 (this study; Spivey *et al*. 2010), within the Karibib Formation and locally the Arandis Formation at Z19. The Rössing South anticline is a F_2 fold where doming described by Spivey *et al.* (2010) is due to refolding by east-northeast F_3 folds and the original F_2 axial plane is rotated into a north-northeast D_4 trend. The realisation through the course of this mapping that the

Z20 area of the Rössing mine lease represented a geological continuity of Rössing South Zone 1 led to drill testing and ultimately the addition of a 54 Kt U_3O_8 resource to Rössing Uranium's mineral inventory.

A D_4 structural control on the intrusion of uraniferous alaskites is consistent with the interpretations of Corner (1981, 1983) relating the Welwitschia Lineament to alaskite-hosted uranium deposits of the sCZ and the subsequent work in the Rössing area by Anderson and Nash (1997) and Basson and Greenway (2004) which significantly refined this hypothesis. This project has advanced these models in particular to refine the stratigraphy and pre- to syn-mineral structural evolution of the area and provide map relationships to support these assertions. These demonstrate an earliest D_4 phase of faulting that disrupts F_2-F_3 structures and immediately predated uraniferous alaskite intrusion.

Based on the preceding text and related previous work in the project area this paragraph summarises the major outcomes of this project in advancing the understanding of alaskite-hosted uranium mineralisation in the Rössing area. Uranium-bearing alaskites in the Rössing area intruded during mid to late D_4 deformation at around 510 Ma during a transition from approximately north-south directed ductile (shears, minor folds and strike slip faulting) to brittle (minor faulting) deformation (Briqueu *et al*., 1980; Kröner, 1982; Basson and Greenway, 2004; this work). Field and petrographic observations from this and previous work show that migmatisation at upper amphibolite to lower granulite facies metamorphism of the Rössing area stratigraphy was particularly intense within potassic quartzo-feldspathic units, which may contain highly anomalous U-Th concentrations in the case of the A.M.C. (Nash, 1971; Spivey *et al*., 2010; this study) or inherit anomalous U-Th from weathering of an A.M.C. hinterland (Etusis Formation). D_3 deformation resulted in the development of complex F_2-F_3 fold interference structures including types 1 and 3 of Ramsay (1967) and provided dilational zones into which the latest alaskites were focused. These alaskites intrude throughout the Damaran-age stratigraphy within north-northeast trending D_4 transtensional shear zones and are volumetrically increased at Rössing SJ due to the coincidence of a northeast trending early D_4 fault zone with the Khan-Rössing Formation contact within one such shear zone. The uranium-bearing alaskites are only mineralised within the Khan, Rössing, Karibib and locally Arandis Formations with the economically significant uranium deposits hosted by the first two formations. The alaskite-hosted uranium deposits are considered to be strictly magmatic-supergene deposits by the author. A weak hydrothermal

overprint to the magmatic mineralisation is present (Bowden *et al.*, 1995; Ryan, 2010) however there is no evidence that supports a resultant increase in uranium grade. Supergene enrichment resulting in secondary uranium phases, on the other hand, is considered to have played a significant role in the economics of these deposits. This is supported by the presence of leached caps at Rössing South (Spivey *et al.*, 2010), and at Rössing SJ this would have been facilitated by the increase in permeability associated with F_3-normal jointing. Whilst this project has advanced the understanding of the geology of these uranium deposits, major aspects of the genesis of alaskite-hosted uranium deposits in Namibia require significant further research that has been beyond the scope of this work. These are particularly within the areas generating late stage uraniferous melts and the geochemical controls on magmatic uranium deposition.

8.2 Concluding Remarks

To date this project represents some of the most extensive detailed mapping and data integration within which is a globally significant uranium district, encompassing a number of economic to sub-economic deposits, including the world-class Rössing SJ deposit and the northern limits of the Rössing South ore bodies. This project has been greatly facilitated by the availability of HyMap hyperspectral data – data which is available across much of the uranium district and it is recommended that more studies utilise this resource in order to further the geological understanding of the area. The appended map fulfils the original purpose of this project – to provide Rössing Uranium Limited with a map from which to generate exploration targets across the Rössing mine lease. The geological mapping has highlighted the Z20 area as the northern continuation of Rössing South Zone 1 where subsequent drill testing has added signifant resources to the mine's uranium inventory. Fortuitously an opportunity was presented through the University of the Witwatersrand to refine and interpret the mapping well beyond the initial scope of work and this has been completed and documented within this thesis. This has notably resolved and built upon the stratigraphic systems of both regional mapping and previous work in the Rössing environs. The detailed structural relationships borne out of map interpretation have added new insights into the structural setting, control and timing of uraniferous alaskite emplacement in the Rossing area.

References

Abraham, I.M. 2009. *Geology and spatial distribution of uranium mineralisation in the SK anomaly area, Rössing area, Namibia.* M.Sc. dissertation, University of the Witwatersrand, Johannesburg, pp. 112.

Allsopp, H.L., Barton, E.S., Kröner, A., Welke, H.J. and Burger, A.J. 1983. Emplacement versus inherited isotopic age patterns: a Rb-Sr and U-Pb study of Salem-type granites in the central Damara Belt. *In*: Miller, R. McG. (Ed.). Evolution of the Damara Orogen of South West Africa/Namibia. *Geological Society of South Africa Special Publication,* **11,** 281-287.

Anderson, H., and Nash, C. 1997. Integrated lithostructural mapping of the Rössing area, Namibia using high resolution aeromagnetic, radiometric Landsat data and aerial photographs. *Exploration Geophysics*, **28,** 185–191.

Andreoli, M.A.G, Hart, R.J., Ashwal, L.D. and Coetzee, H. 2006. Correlations between U, Th content and metamorphic grade in the western Namaqualand Belt, South Africa, with implications for radioactive heating of the crust. *Journal of Petrology*, **47,** 1095-1118.

Badenhorst, F.P. 1992. *The lithostratigraphy of areas 2115 B and D in the Central Zone of the Damara Orogen, Namibia: with emphasis on facies changes and regional correlation.* Unpublished MSc thesis, University of Port Elizabeth, pp. 124.

Barnes, J.F.H. 1981. *Some aspects of the tectonic history of the Khan-Swakop region of the Damara Belt, Namibia*. Unpublished PhD thesis, University of Leeds, pp. 466.

Barnes, J.F.H. and Sawyer, E.W. 1980. An alternative model for the Damara mobile belt: ocean crust subduction and continental convergence. *Precambrian Research*, **13,** 297-336.

Basson, I.J., and Greenway, G. 2004. The Rössing uranium deposit: a product of late-kinematic localization of uraniferous granites in the Central Zone of the Damara Orogen, Namibia. Journal of African Earth Sciences, **38,** 413–435.

Bedell, R., 2004. Remote sensing in mineral exploration. *SEG Newsletter*, **58,** 1, 8-14. July 2004. Society of Economic Geologists.

Behr, H.J., Ahrendt, H., Porada, H., Rohrs, J. and Weber, K. 1983. Upper Proterozoic Playa and Sabkha Deposits in the Damara Orogen, SWA/Namiba. *In*: Miller, R. McG. (Ed.). Evolution of the Damara Orogen of South West Africa/ Namibia. *Geological Society of South Africa Special Publication* **11,** 1-20.

Berning, J., Cooke, R., Hiemstra, S.A, and Hoffman, U. 1976. The Rössing Uranium Deposit, South West Africa. *Economic Geology,* **71,** 351-368.

Berning, J. 1986. The Rössing uranium deposit, southwest Africa/Namibia. *In:* Anhaeusser, CR and Maske, S (Eds), *Mineral Deposits of Southern Africa*. **2,** 1819–1832. Geological Society of South Africa, Johannesburg.

Beukes, G.J.and Hiemstra, S.A. 1969. *A mineralogical analysis of two samples from the Rössing area.* Research report of the National Institute for Metallurgy, Johannesburg, South Africa.

Blaine, J.L. 1977. *Tectonic evolution of the Waldau Ridge structure and the Okahandja Lineament in part of the Central Damara Orogen, west of Okahandja, South West Africa.* Chamber of Mines, Precambrian Research Unit, University of Cape Town, Bulletin **21**.

Bowden, P., Herd, D. and Kinnaird, J.A. 1995. The significance of uranium and thorium concentrations in pegmatitic leucogranites (alaskites), Rössing Mine, Swakopmund, Namibia. *Communications of the Geological Survey of Namibia*, **10,** 43-49.

Brandt, R. 1985. Preliminary report on the stratigraphy of the Damara sequence and the geology and geochemistry of Damaran granites in an area between Walvis Bay and Karibib. *Communications of the Geological Survey of Southwest Africa/Namibia,* **1,** 31-43.

Brandt, R. 1987. A revised stratigraphy for the Abbabis Complex in the Abbabis Inlier, Namibia. *South African Journal of Geology*, **90,** 314-323.

Briqueu, L., Lancelot, J.P., Valois, J.P. and Walgenwitz, F. 1980. Géochronologie U-Pb et gènese d'un type de minéralisation uranifère: les alaskites de Goanikontes (Namibie) et leur encaissant. *Bulletin Centres Recherches Exploration – Production Elf Aquitaine*, **4,** 759-811.

Buhn, B., Okrusch, M., Woermann, E., Lehnert, K. and Hoernes, S. 1995. Metamorphic evolution of Neoproterozoic manganese formations and their country rocks at Otjosondu, Namibia. *Journal of Petrology*, **36(2),** 463-496.

Bunting, F.J.L. 1977. *Geology of part of the central Damara Belt around the Tumas River, South West Africa*. Unpublished M.Sc. thesis, Rhodes University, pp. 168.

Caballero, A. 2009. *Hyperspectral data processing, Rössing Uranium Mine district*. Internal consultant's report prepared for Rössing Uranium Limited, pp. 15.

Clifford, T.N. 1967. The Damaran Episode in the Upper Proterozoic-Lower Palaeozoic structural history of southern Africa. *Special Paper of the Geological Society of America*, **92**, pp. 100.

Corner, B., Henthorn, D.I., 1978. Results of a palaeomagnetic survey undertaken in the Damara mobile belt, South West Africa, with special reference to the magnetisation of the uraniferous pegmatitic granites. *Report PEL-260 Pelindaba*, Atomic Energy Board South Africa.

Corner, B. 1981. *An interpretation of the aeromagnetic data covering portions of the Damara Orogenic Belt with special reference to the occurrence of uraniferous granite*. PhD thesis, University of the Witwatersrand, Johannesburg, South Africa, pp. 115.

Corner, B. 1983. An interpretation of the aeromagnetic data covering the western portion of the Damara Orogen in South West Africa/Namibia. *Special Publication of the Geological Society of South Africa*, **11,** 339-354.

Corner, B. 2008. Crustal framework of Namibia derived from an integrated interpretation of geophysical and geological data. *In:* Miller, R. McG. *The Geology of Namibia* **1**, Ministry of Mines and Energy, Geological Survey, Windhoek, 2-1 – 2-19.

Corvino, A.F. and Pretorius, L.E. 2013. Uraniferous leucogranites south of Ida Dome, central Damara Belt, Namibia: morphology, distribution and mineralisation. Journal of African Earth Sciences, **80,** 60-73.

Coward, M.P., 1983. The tectonic history of the Damaran Belt. *In:* Miller, R.McG. (Ed.), *Evolution of the Damara Orogen of South West Africa*. Special Publication of the Geological Society of South Africa **11,** 409–421.

Cuney, M. 1980a. Preliminary results on the petrology and fluid inclusions studies of the Rössing uraniferous alaskites. *Transactions of the Geological Society of South Africa*, **83,** 39–45.

Cuney, M. 1980b. *Petrography, geochemistry and fluid inclusion studies of the Rössing alaskites and surrounding gneisses*. Attaché de Recherches au C.N.R.S. Cregu.

Cuney, M. 2009. The extreme diversity of uranium deposits. *Mineralium Deposita*, **44,** 3-9.

Dames and Moore. 1982. *Rössing Uranium Ltd, Geological map of mine area, Swakopmund, Namibia*. Photo-geological interpretation of the tailings dam area.

de Kock, G.S. 1989. *'n Geotektoniese studie van die Damara-orogeen in 'n gebied suidoos van Karibib, Suidwes-Afrika*. Unpublished PhD thesis, University of the Orange Free State, Bloemfontein, pp. 438.

de Kock, G.S., Eglington, B., Armstrong, R.A., Harmer, R.E. and Walraven, F. 2000. U-Pb and Pb-Pb ages of the Naauwpoort rhyolite, Kawakeup leptite and Okongava Diorite: implications for the onset of rifting and orogenesis in the Damara belt, Namibia. *Communications of the Geological Survey of Namibia*, Henno Martin Volume, 12, 81-88.

de Kock, G.S. 2001. A reappraisal of the Namibian Damara stratigraphy in part of the Southern Swakop Terrane and its implications to basin evolution. *South African Journal of Geology*, **104(2),** 115-136.

Downing, K.N. 1982. *The evolution of the Okahandja Lineament and its significance in Damaran tectonics (Namibia).* Unpublished Ph.D. thesis, University of Leeds, pp. 242.

Downing, K.N. 1983. The stratigraphy and palaeoenvironment of the Damara Sequence in the Okahandja Lineament area. *In*: Miller, R. McG. (Ed.). Evolution of the Damara Orogen of South West Africa/Namibia. *Geological Society of South Africa Special Publication* **11,** 37-41.

Downing, K.N. and Coward, M.P. 1981. The Okahandja Lineament and its significance for Damaran tectonics in Namibia*. Geologisch Rundschau*., **70,** 972-1000.

Freemantle, G. 2015. Petrographic, Mineralogical and Geochemical Characterisation of Granite-hosted Uranium Deposits of the Central Damara Orogen, Namibia. PhD in progress, University of the Witwatersrand.

Frimmel, H.E., Basei, M.S., and Gaucher, C. 2011. Neoproterozoic geodynamic evolution of SW-Gondwana: a southern African perspective. *International Journal of Earth Sciences*, **100,** 323-354.

Fugro, 2005. *Helicopter Borne Magnetic Horizontal Gradient (MIDAS™) and Radiometric Geophysical Survey over the Rössing Uranium Mine, in Western Namibia*. Logistics Report FCR 2344 for Rio Tinto Mining and Exploration Ltd, pp. 51.

Gevers, T.W. 1931. *The Fundamental Complex of western Damaraland, South West Africa.* Unpublished D. Sc. Thesis, University of Capetown, pp. 163.

Golder Associates, 1978. *Surface Geology of the SJ Area, Rössing Uranium Mine, Swakopmund, Namibia.* Geological Map of Golder Associates.

Goscombe B.D., Gray D. and Hand M. 2004. Variation in metamorphic style along the northern margin of the Damara Orogen, Namibia. *Journal of Petrology*, **45,** 1261-1295.

Gray, D. R., Foster, D. A., Maas, R., Spaggiari, C. V., Gregory, R. T., Goscombe, B. D. and Hoffmann, K. H. 2007. Continental growth and recycling by accretion of deformed turbidite fans and remnant ocean basins: examples from Neoproterozoic and Phanerozoic orogens. *In:* Hatcher, R. D., JR., Carlson, M. P., McBride, J. H. and Marti´Nez Catala, N. J. R. (eds), *The 4D Framework of Continental Crust*. Geological Society of America, Memoirs, doi: 10.1130/2007.1200(05).

Gray, D.R., Foster, D.A., Meert, J.G., Goscombe, B.D., Armstrong, R.A., Trouw, R.A.J. and Passchier, C.W. 2008. A Damara Orogen perspective on the assembly of southwestern Gondwana. *In:* Pankhurst, R.J., Trouw, R.A.J., Brito Neves, B.B. and De Wit, M.J. (Eds.). West Gondwana: Pre-Cenozoic correlations across the South Atlantic region. *Geological Society of London Special Publications, **294**,* 257-278.

Haack, U., Gohn, E. and Klein, J.A. 1980. Rb/Sr ages of granitic rocks along the middle reaches of the Omaruru River and the timing of orogenic events in the Damara Belt (Namibia). *Contributions to Mineralogy and Petrology*, **74,** 349-360.

Haack, U., Gohn, E., Hartmann, O., 1983. Radiogenic heat generation in Damaran rocks. In: Miller, R.McG (Ed.), *Evolution of the Damara Orogen of South West Africa/Namibia*. Special Publication of the Geological Society of South Africa, **11,** 225–232.

Hanson, R.E. 2003. Proterozoic geochronology and tectonic evolution of southern Africa. *In:* Yoshida, M., Windley, B.F., & Dasgupta, S. (Eds.). *Proterozoic East Gondwana: Supercontinent Assembly and Breakup*. Geological Society of London, Special Publication, **206,** 427-463.

Harris, R. Jacob, R.E. and Geology Honours Students. 1993. *Geology of the area around Panner Gorge, with reference to groundwater movement in the amphibole schist.* Mapping report of Rhodes University, Grahamstown, South Africa.

Harris, R. Jacob, R.E. and Geology Honours Students. 1994. *Geology of the area between the main tailings dam and Panner Gorge, Rössing Uranium Mine*. Mapping report of Rhodes University, Grahamstown, South Africa.

Hawkesworth, C.J., Gledhill, A., Roddick, J.C., Miller, R. McG. and Kröner, A. 1983. Rb/Sr geochronology and its bearing on models for the thermal evolution of the Damara orogenic belt, Namibia, *In*: Miller, R. McG. (Ed.). Evolution of the Damara Orogen of South West Africa/ Namibia. *Geological Society of South Africa Special Publication* **11,** 323-328.

Henry, G., Clendenin, C.W., Stannistreet, I.G., Maiden, K.J., 1990. Multiple detachment model for the early rifting stage of the Late Proterozoic Damara orogen in Namibia. *Geology* **18,** 67–71.

Henry, G. 1992. *The sedimentary evolution of the Damara Sequence in the lower Khan River valley, Namibia.* PhD thesis, University of the Witwatersrand, Johannesburg, South Africa, 1992, pp. 217.

Herd, D.A. 1996 *Geochemistry and mineralisation of alaskites in selected areas of the Rössing Uranium Mine, Namibia*. MSc thesis, University of St. Andrews, St Andrews.

Hiemstra, S.A. 1967. *Rössing: uranium prospect in South West Africa*. Research report of the National Institute for Metallurgy, Johannesburg, South Africa.

Hiemstra, S.A. 1968. *The determination of relative amounts of uraninite and secondary uranium-bearing minerals in nine samples from the underground workings at Rössing*. Research report of the National Institute for Metallurgy, Johannesburg, South Africa.

Hiemstra, S.A. 1971. *A review of the petrography and mineralogy of the alaskite ore body at Rössing, with special reference to extraction metallurgy.* Report of the National Institute for Metallurgy, Johannesburg, South Africa.

Hiemstra, S.A. and van Huyssteen, E. 1969. *Mineralogical investigation of the radioactive constituents of samples from boreholes in the SH area, Rössing.*

Research report of the National Institute for Metallurgy, Johannesburg, South Africa.

Hminady *et al.*, 1985. Proterozoic Crustal Evolution in Southwestern Africa. *Episodes* **8,** 236-244. Incomplete reference as cannot be located.

Hoffmann, K.-H., Constance, C. and Kohonen, J. 1994. Geological map 2314 – Kuiseb. *Geological Survey of Namibia*, Windhoek.

Hoffmann. P.F., Hawkins, D.P., Isachsen, C.E. and Bowring, S.A. 1996. Precise U-Pb zircon ages for early Damaran magmatism in the Summas Mountains and Welwitschia inlier, northern Damara belt, Namibia. *Communications of the Geological Survey of Namibia*, **11,** 47-52.

Hoffmann, K.-H.and Prave, A.R. 1996. A preliminary note on a revised subdivision and regional correlation of the Otavi Group based on glaciogenic diamictites and associated cap dolostones. *Communications of the Geological Survey of Namibia*, **11,** 77-82.

Hoffmann, K.-H., Condon, D.J., Bowring, S.A. and Crowley, J.L. 2004. U-Pb zircon date from the Neoproterozoic Ghaub Formation, Namibia: Constraints on Marinoan glaciation. *Geology*, **32,** 817-820.

Hoffmann, P.F. 2005. 28th DeBeers Alex Du Toit Memorial Lecture: On Cryogenian (Neoproterozoic) ice-sheet dynamics and the limitations of the glacial sedimentary record. *South African Journal of Geology*, **108,** 557-576.

Jacob, R.E. 1974. *Geology and metamorphic petrology of part of the Damara Orogen along the lower Swakop River, South West Africa*. Chamber of Mines, Precambrian Research Unit, University of Cape Town, Bulletin **17**, pp. 185.

Jacob, R.E., 1978. Granite genesis and associated mineralisation in part of the Central Damara Belt. In: Verwoerd, W.J. (Ed.), *Mineralisation in Metamorphic Terranes*. Geological Society of South Africa Special Publication, **4,** 417–432.

Jacob, R. E., Kroner, A. and Burger, A.J. 1978. Areal extent and first U-Pb age of the pre-Damaran Abbabis Complex in the central Damara belt of South West Africa (Namibia). *Geologisch Rundschau,* **67 (2),** 706-718.

Jacob, R.E., Snowden, P.A. and Bunting, F.J.L. 1983. Geology and structural development of the Tumas Basement Dome and its cover rocks. *Geological Society of South Africa Special Publication*, **11,** 157-172.

Jacob, R.E. Snowden, P.A. and Bunting, F.J.L. 1983. Geology and structural development of the Tumas basement dome and its cover rocks. *In*: Miller, R. McG. (Ed.). Evolution of the Damara Orogen of South West Africa/Namibia. *Geological Society of South Africa Special Publication,* **11,** 157-172.

Jacob, R.E., Corner, B.and Brynard, J.H. 1986. The regional geological and structural setting of the uraniferous granitic provinces of Southern Africa. *In:* Anhaeusser, C.R.and Maske, S. (Eds). *Mineral Deposits of Southern Africa.* **2,** 1819–1832. Geological Society of South Africa, Johannesburg.

Jacob, R.E., and Kerber, P. 1997. *Geology of the Area around the Main Tailings Dam, Rössing Uranium Mine.* Mapping report of Rhodes University, Grahamstown, South Africa.

Jacob, R.E. Moore, J.M. and Armstrong, R.A. 2000. Zircon and titanite age determination from igneous rocks in the Karibib District, Namibia: implications for Navachab vein-style gold mineralisation. *Communications of the Geological Survey of Namibia*, **12,** 157-166.

John, T., Schenk, V., Hasse, K., Scherer, E. and Tembo, F. 2003. Evidence for a Neoproterozoic ocean in south-central Africa from mid-oceanic-ridge-type geochemical signatures and pressure-temperature estimates of Zambian eclogites. *Geology*, **31,** 243-246.

Johnson, S.D., Poujol, M. and Kisters, A.F.M. 2006. Constraining the timing and migration of collisional tectonics in the Damara Belt, Namibia: U-Pb zircon ages for the syntectonic Salem-type Stinkbank granite. *South African Journal of Geology*, **109,** 427-440.

Jung, S. Hoernes, S., Masberg, P., and Hoffer, E. 1999. The petrogenesis of some migmatites and granite (central Damara Orogen, Namibia): evidence of disequilibrium melting, wall rock contamination and crystal fractionation. *Journal of Petrology*, **40,** 1241-1269.

Jung, S., Hoernes, S., and Mezger, K. 2002. Synorogenic melting of mafic lower crust: constraints from geochronology, petrology and Sr, Nd, Pb and O isotopic geochemistry of quartz diorites (Damara Orogen, Namibia). *Contributions to Mineralogy and Petrology***, 143**, 551-566.

Jung, S., and Mezger, K. 2003. Petrology of basement-dominated terranes: I. Regional metamorphic T-t from U-Pb monazite and Sm-Nd garnet geochronology (Central Damara Orogen, Namibia). *Chemical Geology*, **198,** 223-247.

Kasch, K.W. 1983. Regional P-T variations in the Damara Orogen with particular reference to early high-pressure metamorphism along the southern margin. *In:* Miller, R. McG, (Ed.) *Evolution of the Damara Orogen of South West Africa/Namibia*. Special Publication of the Geological Society of South Africa, **11**, 243-254.

Kerr, A.C. 1990. *The geochemistry of the Rössing Leucogranites and several associated metasediments, Rössing, Namibia*. Senior Honours Thesis, University of St Andrews, Scotland.

Kinnaird, J.A. 2005. *An investigation of the proportions of betafite, uraninite and secondary uranium minerals in SJ borehole core samples*. Report to Rössing Uranium Ltd, pp. 35.

Kinnaird, J.A. and Nex, P.A.M. 2007. A review of geological controls on uranium mineralisation in sheeted leucogranites within the Damara Orogen, Namibia. *Transactions of the Institute of Mining and Metallurgy (B, Applied Earth Science)*, **116,** (**2**) 69-85.

Kinny, P.D., McNaughton, N.J., Fanning., C.M. and Maas, R. 1994. 518 Ma sphene (titanite) from the Khan pegmatite, Namibia, Southwest Africa: a potential ion-microprobe standard. *Abstracts of the Eighth International Conference on*

geochronology, Cosmochronology and isotope geology. Berkely California US Geological Circular, 1107, 171.

Kisters, A.F.M., Jordaan, L.S., and Neumaier, K. 2004. Thrust-related dome structures in the Karibib district and the origin of orthogonal fabric domains in the south Central Zone of the pan-African Damara belt, Namibia. *Precambrian Research*, **133,** 283–303.

Kisters, A.F.M., Ward, R.A., Anthonissen, C.J., and Vietze, M.E., 2009. Melt segregation and far-field melt transfer in the mid-crust. *Journal of the Geological Society of London*, **166,** 905–918.

Klein, J. 1980a. The geology of area 2115A. Unpublished report and 100 000 map of the Geological Survey of Namibia, pp.69.

Klein, J. 1980b. Evolution of first generation folds in a marble unit (Damara Orogenic Belt, Namibia). *Geologische Rundschau*., **69,** 770-800.

Korzeb, S.L., Foord, E.E. and Lichte, F.E. 1997. The chemical evolution and paragenesis of uranium minerals from the Ruggles and Palermo granitic pegmatites, New Hampshire. *Canadian Mineralogist*, **35,** 135–144.

Kröner, A. 1982. Rb:Sr geochronology and tectonic evolution of the Pan-African Damara Belt of Namibia, southwestern Africa. *American Journal of Science*, **282,** 1471-1507.

Kroner, A., Retief, E.A., Compston, W., Jacob, R.E. and Burger, A.J. 1991. Single grain and conventional zircon dating of remobilised basement gneisses in the central Damara belt of Namibia. *South African Journal of Geology*, **94,** 379-387.

Kukla, C., Kramm, U., Kukla, P.A. and Okrusch, M., 1991. U–Pb monazite data relating to metamorphism and granite intrusion in the northwestern Khomas Trough, Damara Orogen, central Namibia. *Communications of the Geological Survey of Namibia*, **7,** 49–54.

Kukla, P. A. and Stanistreet, I. G. 1991. Record of the Damaran Khomas Hochland accretionary prism in central Namibia: refutation of an 'ensialic' origin of a Late Proterozoic orogenic belt. *Geology*, **19,** 473–476.

Laberge, J. 2008a. *Geological map of the SK Zone, Rössing Uranium Mine.* Rio Tinto Exploration Internal Report.

Laberge, J. 2008b. *Geological mapping between the SK Zone and the SJ Pit, Rössing Uranium Mine*. Rio Tinto Exploration Internal Report, pp. 16.

Lehtonen, M.I., Manninen, T.E.T. and Schrieber, U.M. 1993. *The geology of the area between the Khan River and the coast, and in the vicinity of Omdel Dam.* Mapping Report and Geochemical Study, Finnish-Namibian Geological Mapping and Maps Project, Windhoek, Namibia, 1993.

Lehtonen, M.I., Manninen, T.E.T. and Schrieber, U.M. 1995. Geological map sheet 2214 – Walvis Bay, 1:250 000. *Geological Survey of Namibia*.

Lehtonen, M.I., Manninen, T.E.T. and Schrieber, U.M. 1996. Report: lithostratigraphy of the area between the Swakop, Khan and lower Omaruru Rivers, Namibia Desert. *Communications of the Geological Survey of Namibia*, **11,** 65-76.

Lillesand, T.M., Kiefer, R.W., Chipman, J.W., 2008. *Remote Sensing and Image Interpretation*. Sixth edition. John Wiley and Sons, Inc, pp. 756.

Longridge, L. 2012. Tectonothermal evolution of the southwestern Central Zone, Damara Belt, Namibia. PhD thesis, University of the Witwatersrand, pp. 525.

Longridge, L., Gibson, R.L., Kinnaird, J.A. and Armstrong, R.A. 2008. Timing of deformation and granite emplacement in the central zone of the Damara Orogen, Namibia. *SEG Student Geocongress Abstract Volume*.

Manolakis, D., Marden, D., and Shaw, G.A. 2003. Hyperspectral image processing for automatic target detection applications. *Lincoln Laboratory Journal*, **14 (1),** 79-116.

Marlow, A.G.M. 1981. *Remobilisation and primary uranium genesis in the Damaran Orogenic Belt*. PhD thesis, University of Leeds, pp. 277.

Marlow, A. 1983. Geology and Rb-Sr geochronology of mineralised and radioactive granites and alaskites, Namibia. *In*: Miller, R. McG. (Ed.). Evolution of the Damara Orogen of South West Africa/Namibia. *Geological Society of South Africa Special Publication,* **11,** 289-268.

Marshall, C.G.A. 1973. *Rössing Uranium Limited – interim report on the mineralogical work done for and at Rössing during the period June 1967 to March 1973*. Rössing Uranium Ltd. internal report.

Masberg, H. P., Hoffer, E. and Hoernes, S. 1992. Microfabrics indicating granulite-facies metamorphism in the low-pressure central Damara Orogen, Namibia. *Precambrian Research,* **55,** 243–257.

Mbangula, N. 2007. *Uranium distribution and mineralogy of the skarns in the SJ area, Rössing Uranium Ltd.* M Eng Project Thesis, University of the Witwatersrand.

McDermott, F. 1986. *Granite petrogenesis and crustal evolution studies in the Damara Pan-African Orogenic Belt, Namibia*. Unpublished PhD thesis, Open University, Milton Keynes, England, pp. 303.

McDermott, F., Harris, N. B. W. and Hawkesworth, C. J. 1989. Crustal reworking in southern Africa: constraints from Sr–Nd isotope studies in Archaean to Pan-African terrains. *Tectonophysics*, **161,** 257–270.

McDermott, F., Harris, N. B. W. and Hawkesworth, C. J. 1996. Geochemical constraints on crustal anatexis: a case study from the Pan-African Damara granitoids of Namibia. *Contributions to Mineralogy and Petrology*, **123,** 406–423.

McDermott, F., Harris, N. B. W. and Hawkesworth, C. J. 2000. Geochemical constraints on the petrogenesis of Pan-African A-type granites in the Damara Belt, Namibia. *In*: Miller, R. M^{C}G. (ed.) Henno Martin Commemorative Volume. *Communications of the Geological Survey of Namibia*, **12,** 139–148.

Mestres-Ridge, D.A. 1991. *Preliminary Report on the Mapping and Sampling of the SH Anomaly.* Preliminary report to Rössing in conjunction with University of St. Andrews MSc thesis.

Mestres-Ridge, D.A. 1992. *An investigation into the controls on the distribution of betafite in the SH area, Rössing Uranium Mine, Namibia.* MSc thesis, University of St Andrews, Scotland, pp. 136.

Mestres-Ridge, D.A. 1994. *Metasomatic betafite genesis in alkaline granites of the Rössing Uranium Mine, Namibia*. Draft paper (for *Communications of the Geological Survey of Namibia*) communicated to R. Murphy, Chief Geologist, Rössing Mine, September 23rd 1994.

Miller, R.McG. 1974. The stratigraphic significance of the Naauwport Formation of east central Damaraland, South West Africa. *Transactions of the Geological Society of South Africa*, **77,** 363-367.

Miller, R.McG. 1979. The Okahandja Lineament, a fundamental tectonic boundary in the Damara Orogen of South West Africa/Namibia. *Transactions of the Geological Society of South Africa,* **82,** 349-361.

Miller, R.McG. 1983. The Pan-African Damara Orogen of South West Africa/Namibia. *In* Miller, R. McG. (Ed.). Evolution of the Damara Orogen of South West Africa/Namibia. *Geological Society of South Africa Special Publication* **11,** 431-515.

Miller, R.McG. 1992a. Mineral exploration targets in Namibia. *In* Miller, R. McG. *Mineral Resources of Namibia*, Ministry of Mines and Energy, Geological Survey of Namibia, Windhoek, **1.1,** 1-8.

Miller, R.McG. 1992b. Stratigraphy. *In*: Miller, R. McG. *Mineral Resources of Namibia*, Ministry of Mines and Energy, Geological Survey of Namibia, Windhoek, **1.2,** 1-22.

Miller, R.McG. (2008). Neoproterozoic and early Palaeozoic rocks of the Damara Orogen. *In* Miller, R. McG.*The Geology of Namibia* **2**, Ministry of Mines and Energy, Geological Survey, Windhoek, 1-410.

Miller, R.McG. and Grote, W. 1988. Geological map of the Damara Orogen, Namibia (scale 1:500 000). *Geological Survey of Namibia, Windhoek*.

Mouillac, J.L., Valois, J-P., and Walgenwitz, F. 1986. The Goanikontes Uranium Occurrence in South West Africa / Namibia. *In:* Anhaeusser, C.R., & Maske, S. (Eds.) *Mineral Deposits of Southern Africa.* Geological Society of South Africa, Johannesburg, 1833-1843.

Nash, C.R. 1971. Metamorphic petrology of the SJ area. Precambrian Research Unit, University of Cape Town, Cape Town, South Africa, Bulletin **9**, pp. 77.

Nash, C.R. 1972. Primary anhydrite in Precambrian gneisses from the Swakopmund District, South West Africa. *Contributions to Mineralogy and Petrology*, **36,** 27-32.

Nex, P. 1997. *Tectono-metamorphic setting and evolution of granitic sheets in the Goanikontes area, Namibia*. PhD thesis, University College Cork, National University of Ireland, pp. 322.

Nex, P., Kinnaird, J.A. and Oliver, G.J.H 2001a. Petrology, geochemistry and uranium mineralisation of post-collisional magmatism around Goanikontes, southern Central Zone, Damaran Orogen, Namibia. *Journal of African Earth Sciences,* **33,** 481-502.

Nex, P., Oliver, G.J.H and Kinnaird, J.A. 2001b. Spinel-bearing assemblages and P-T-t evolution of the Central Zone of the Damara Orogen, Namibia. *Journal of African Earth Sciences*, **32,**471-489.

Nex, P. A. M., Herd, D., and Kinnaird, J. 2002. Fluid extraction from quartz in sheeted leucogranites as a monitor to styles of uranium mineralisation: an example from the Rössing area, Namibia. *Geochemistry: Exploration, Environment, Analysis***,** **2**(1), 83-96.

Oliver, G.J.H. 1994. Mid-crustal detachment and domes in the Central Zone of the Damara Orogen, Namibia. *Journal of African Earth Sciences*, **19,** 331-344.

Oliver, G. J. H. 1995. The Central Zone of the Damara Orogen, Namibia as a deep metamorphic core complex. *Communications of the Geological Survey of Namibia*, **10,** 33–41.

Oliver, G.J.H. and Kinnaird, J.A. 1996. The Rössing SJ Dome, Central Zone, Damara Belt, Namibia: an example of mid-crustal extensional ramping. *Communications of the Geological Survey of Namibia*, **11,** 53–64.

Owen, G.J. 2011. *Geology of the Kranzberg syncline and emplacement controls of the Usakos pegmatite field, Damara Belt, Central Namibia*. University of Stellenbosch Ph.D. thesis, pp. 168.

Poli, L.C. 1997. *Mid-crustal geodynamics of the southern Central Zone, Damaran Orogen, Namibia*. PhD thesis (unpubl), University of St Andrews, UK, pp. 233.

Poli, L.C., and Oliver, G.J.H. 2001. Constrictional deformation in the Central Zone of the Damara Orogen Namibia. *Journal of African Earth Sciences*, **33,** 303-312.

Pope, A. 2008. *Structural Controls on Alaskite Intrusion and Uranium Mineralisation - Rössing District.* Kennecott Exploration Company Internal Memo.

Porada, H., 1979. The Damara-Ribeira orogen of the pan-African-Braziliano cycle in Namibia (Southwest Africa) and Brazil as interpreted in terms of continental collision. *Tectonophysics*, **57,** 237-265.

Porada, H. and Wittig, R. 1983. Turbidites and their significance for the geosynclinal evolution of the Damara Orogen, South West Africa/Namibia. *In* Miller, R. McG. (Ed.). Evolution of the Damara Orogen of South West Africa/Namibia. *Geological Society of South Africa Special Publication* **11,** 21-36.

Prave, A.R. 1996. Tale of three cratons: tectonostratigraphic anatomy of the Damara Orogen in northwestern Namibia and the assembly of Gondwana. *Geology*, **24,** 1115-1118.

Puhan, D. 1983. Temperature and pressure of metamorphism in the central Damara Orogen, *In:* Miller, R. McG, (Ed.) *Evolution of the Damara Orogen of South West*

Africa/Namibia. Special Publication of the Geological Society of South Africa, **11**, 219-224.

Ramdohr, P. 1938. Die Khan-Grube bei Arandis, Südwestafrika. *Zeitschrift fur Praktische Geologie*, **46,** (3), 41-50.

Ramsay, J.G. 1967. *Folding and Fracturing of Rocks.* McGraw-Hill, New York, pp. 568.

Ratcliffe, A. 1992. *A geochemical investigation into the location and structural chemistry of betafite, Rössing Uranium Mine, Swakopmund, Namibia*. Senior Honours Thesis, University of St Andrews, Scotland.

Reynolds, I.M. 1975. *A mineralogical and petrographic investigation of borehole cores from the SH area at Rössing.* Atomic Energy Board report by the National Institute for Metallurgy, South Africa.

Rich, R.A., Holland, H.D. and Petersen, U. 1977. *Hydrothermal Uranium Deposits*. Elsevier, Amsterdam, pp. 264.

Roesener, H. and Schreuder, C.P. 1994. Nuclear and Fossil Fuels-Uranium. *In* Miller, R. McG. *Mineral Resources of Namibia*, Ministry of Mines and Energy, Geological Survey of Namibia, Windhoek, **7.1,** 1-59.

Ryan, E. 2010. *Mineralogy of variable rock types from Rössing*. Rio Tinto Internal Memorandum, 26th October 2010, pp. 27.

Sawyer, E.W. 1976. The geology of an area south-east of Walvis Bay. Part 1: lithology, sedimentation and field relationships. *Open File Report, Geological Survey of Namibia*, **RG 3**.

Sawyer, E.W. 1979. Unpublished geological maps 2214 DD, 2215 CC. *Geological Survey of Namibia,* pp. 136.

Sawyer, E.W. 1981. Damaran structural and metamorphic geology of an area south-east of Walvis Bay, South West Africa/Namibia. *Memoirs of the Geological Survey of South West Africa,* **7**, pp. 83.

Schneider, G.I.C. and Seeger, K.G. 1992. Copper. *In*: *The Mineral Resources of Namibia*. Namibian Ministry of Mines and Energy, Geological Survey. 2.3 44 – 2.3 45.

Scott, B, and Northam, G, 2005. *Rössing near mine project, final report*. Rio Tinto Exploration Africa/Europe Region internal report.

Sharma, P.V. 1987. Magnetic method applied to mineral exploration. *Ore Geology Reviews*, **2,** 323-357.

Smith, D.A.M. 1965. The geology of the area around the Khan and Swakop Rivers in southwest Africa', *Southwest Africa Series, Memoir 3*, Geological Survey of South Africa, Pretoria, South Africa, pp. 113.

Söhnge, P.G. 1957. Paragenesis of the Khan pegmatite, South West Africa. *Transactions of the Geological Society of South Africa*, **42,** 23-34.

Spivey, M., Penkethman, A. and Culpan, N. 2010. Geology and Mineralisation of the Recently Discovered Rössing South Uranium Deposit, Namibia. *Society of Economic Geologists, Inc. Special Publication*, **15,** 729-746.

Spurr, J.E. 1900. Classification of igneous rocks according to composition. *American Geologist.* XXV, 229-230.

Stanistreet, I.G., Kukla, P.A. and Henry, G., 1991. Sedimentary basinal responses to a Late Precambian Wilson Cycle: the Damara Orogen and Nama Foreland, Namibia', *Journal of African Earth Sciences.* **13,** 141–156.

Steven, N. M. 1994. Note: Mafic dykes in the pre-Damara basement, south-east of Usakos, central Namibia. *Communications of the Geological Survey, Namibia* **9,** 92-95.

Tack, L., Williams, I. and Bowden, P. 2002. SHRIMP constraints on early post-collisional granitoids of the Ida Dome, central Damara (Pan African) Belt, western Namibia. *Abstracts of the 11th IAGOD Quadrennial Symposium and Geocongress, Windhoek, Namibia*. Geological Survey of Namibia.

Taranik, J.V. and Aslett, Z.L. 2009. Development of hyperspectral imaging for mineral exploration. *In:* Bedell, R., Crosta, A.P. and Grunsky, E. 2009. Remote sensing and spectral geology. *Reviews in Economic Geology*, **16,** 83-95.

Thiesson, R. 1986. Two-dimensional fold interference patterns. *Journal of Structural Geology,* **8,** (5), 563-573.

Trumbull, R. B., Reid, D. L., De Beer, C. H., Romer, R. L. 2007. Magmatism and continental breakup at the west margin of southern Africa: A geochemical comparison of dolerite dikes from NW Namibia and the Western Cape. *South African Journal of Geology*, **110,** 2-3, 477-502.

Ward, R., Stevens, G. and Kisters, A. 2008. Fluid and deformation induced partial melting and melt volumes in low-temperature granulite-facies metasediments, Damara Belt, Namibia. *Lithos*, **105,** 253-271.

Wegerhoff, N.A. 1973. *Geological map of proposed tailings dispersal and seepage control dam areas, 1:5000.* Rössing Uranium Ltd.

Wilson, R.G. 1975. *Rössing Uranium Deposit, Swakopmund, South West Africa.* Rio Tinto Internal Report, C.R.A. Exploration Pty. Ltd., pp. 14.

Yardley, B.W.D. 1989. *An Introduction to Metamorphic Petrology*. Longman, England, pp. 248.